Game Theoretic Models for Resource Sharing in Wireless Networks

A Thesis

Submitted to the Faculty

of

Drexel University

by

Ilaria Malanchini

in partial fulfillment of the

requirements for the degree

of

Doctor of Philosophy

December 2011

Dedications

I would like to dedicate this doctoral dissertation to my parents, Lauretta and Pier Luigi. Their love has been the strongest support for me. Without them, I would not be the person I am today. Thank you.

Acknowledgments

Foremost, I would like to express my sincere gratitude to my advisors, Prof. Matteo Cesana and Dr. Steven Weber, for the precious support during my Ph.D. study and research, for their patience, motivation, enthusiasm, and knowledge. Their guidance has been fundamental during these four years.

Besides my advisors, I would like to thank all the professors that have contributed to this work with valuable feedback, insightful comments, and suggestions: Prof. Antonio Capone, Prof. Nicola Gatti, Dr. John Walsh, Dr. Kapil Dandekar, Dr. Moshe Kam, Dr. Roger McCain and Prof. Patrick Maillè.

I would like to thank all my labmates from both the AntLab (in Milan) and the Drexel Network Modeling Laboratory (in Philadelphia).

I am deeply thankful to my parents, who have always supported me throughout all my academic career.

Last but not least, I would like to thank all my friends from all over the world, their support and friendship have been incredibly helpful for me and have made these years simply unforgettable.

Table of Contents

List of Tables

List of Figures

Abstract

Game Theoretic Models for Resource Sharing in Wireless Networks
Ilaria Malanchini
Dr. Steven Weber, Ph.D. and Dr. Matteo Cesana, Ph.D.

Wireless communications have been recently characterized by rapid proliferation of wireless networks, impressive growth of standard and technologies, evolution of the end-user terminals, and increasing demand in the wireless spectrum. New, more flexible schemes for the management of the available resources, from both the user and the network side, are necessary in order to improve the efficiency in the usage of the available resources.

This work aims at shedding light on the performance modeling of radio resource sharing/allocation situations. Since, in general, the quality of service perceived by a system (e.g., user, network) strictly depends on the behavior of the other entities, and the involved interactions are mainly competitive, this work introduces a framework based on non–cooperative game theoretic tools. Furthermore, non–cooperative game theory is suitable in distributed networks, where control and management are inherently decentralized.

First, we consider the case in which many users have to make decisions on which wireless access point to connect to. In this scenario, the quality perceived by the users mainly depends on the number of other users choosing the very same accessing opportunity. In this context, we also consider two–stage games where network make decisions on how to use the available resources, and users react to this selecting the network that maximizes their satisfaction. Then, we refer to the problem of spectrum sharing, where users directly compete for portions of the available spectrum. Finally, we provide a more complex model where the users utility function is based on the Shannon rate. The aim of this second part is to provide a better representation of the satisfaction perceived by the users, i.e., in terms of achievable throughput. Due to the complexity of the game model, we first provide a complete analytical analysis of the two–user case. Then, we extend the model to the N–user case. We mainly analyze this game through simulations. Finally, inspired by the results obtained numerically, we introduce stochastic geometry in the analysis of spectrum games in order to predict the performance of the game in large networks.

Chapter 1: Introduction

The impressive growth of standards and technologies for wireless communications has dramatically increased the opportunities for mobile users to connect anytime anywhere. End user equipment often comes with multiple radio interfaces featuring different communication standards, from short range (Zigbee, Bluetooth) to medium, long range ones (WiFi, WiMAX, 2G, LTE). Moreover, a given geographical area may be "covered" by multiple access network/technologies with different characteristics (bandwidth, access cost), even potentially run by different operators. As an example, 2G/3G cellular systems owned by big Tel–Co operators may provide geographical coverage side by side with multi–domain Wireless Local Area Networks (WLANs), and Wireless Mesh Networks (WMN) run by medium/small Wireless Internet Service Providers (WISPs).

Differently from the past when wireless connectivity was monopolized by a single operator/technology, the over–provisioning of access networks nowadays allows mobile users to choose among multiple access opportunities on the base of availability, cost and/or quality, eventually achieving a seamless, ubiquitous, and pervasive connectivity experience. To reach this ambitious goal, however, many technical challenges still have to be addressed in different fields. On the network side, signaling architectures are required to effectively support user's mobility among multiple networks and to manage the radio *resource allocation* process; on the user's side, effective techniques are required to discover and classify the multiple connectivity opportunities based on quality parameters (actual throughput, access delay, wireless interference level) to steer eventually the dynamic *selection of the best connectivity opportunity*. Furthermore, the increasing demand in wireless spectrum has shown that new, more flexible, spectrum management schemes are necessary to improve the efficiency in spectrum usage. In this context, users are allowed to exploit the available spectrum, taking decisions that are based on the current availability of different spectrum opportunities. The problem of *spectrum sharing* refers to the competition between users in accessing the available spectrum. Within this field, recent advancements in the field of software–defined radios allow the development spectrum–agile devices that can be programmed to operate on a wide spectrum range and tuned to any frequency band in that range with negligible delay. Resulting cognitive radios are able to sense a wide spectrum range, dynamically

classify spectrum blocks for data communications, and "intelligently" select the best spectrum opportunity.

The main goal of this thesis is to provide quantitative tools based on game theory to analyze all the aforementioned scenarios, that can be seen as different instances of the **resource sharing problem**. Namely, we analyze the problem of wireless network selection, that refers to the choice given to the end users to select the best wireless access network to connect to. We start off by addressing the network selection problem in the most common wireless access paradigm, that is the one based on access points (e.g., WiFi–based) operating as bridges between the wireless realm (connection to the users) and the wired one (connection to the Internet). However, this access paradigm may have both economical and technical shortcomings under some network scenarios; as an example, the capillary coverage of large metropolitan areas may require high capital investments for cabling up all the required wireless access points, or cabling itself may simply be impossible or externally constrained (e.g., historical buildings, etc.). To overcome the aforementioned limitations, the paradigm of Wireless Mesh Networking (WMN) has been widely recognized as a cost effective solution for providing wireless connectivity/access to mobile users [6, 7].

Regardless of the specific wireless access network (cellular, WLANs, WMNs), the user always has to make decisions on network association. Namely, network association refers to the dynamic and automatic choice of the best "connectivity opportunity", that is, the cellular base station in classical cellular systems, the access point in WiFi WLANs, and the mesh router in Wireless Mesh Networks (WMNs). In classical hot–spot–like access networks (e.g., WLAN), the access decision is (almost) completely driven by the quality of the "last–mile" link. Indeed, the users decide to associate with the WLAN hot–spot providing the "best" wireless link accounting for the Signal to Interference and Noise Ratio (SINR), the average load, the nominal data rate, etc. In contrast, in case the access network is a WMN, the user–perceived quality depends on the overall quality of the entire path towards the specific entry/exit mesh gateway; thus, the association to the specific mesh router in a WMNs should account for "global" quality parameters, other than only local ones.

The association process is intrinsically distributed (no coordination is allowed in the association phase), and competitive in that each user is willing to act to maximize the perceived quality. Moreover, the single association choice taken by a user impacts the quality of the other users. Roughly speaking, if a user uses a wireless resource (access point, wireless link, frequency band, etc.), it produces interference to all the other

users on the same resource. To this extent, it becomes natural to study such competitive dynamics resorting to non–cooperative game theoretical tools [8]. In this scenario, game theory is often used to model the competition among accessing users [9, 10]. An interesting overview on the potentials of game theory in the field of network selection is provided in [11]. Mittal *et al.* [10] resort to a non–cooperative game to model the association process to WiFi–based Access Points (APs). A comprehensive survey on this topic is provided in [11]. In particular, we model the problem of association in wireless networks (WiFi hot spots and WMNs) as a special case of *congestion game* [12] where each user acts selfishly to maximize the perceived quality of service.

While the first part of this thesis studies the dynamics among end users only further assuming the network resource allocation (i.e., frequency assignment, routing paths) as fixed, in the second part of this work we drop this assumption and bring networks/operators into the competition. In fact, in practical settings, it is reasonable to assume that each operator tries to maximize her own revenue (e.g., number of connected customers) changing the configuration of several parameters of the specific radio technology used for providing access. In this case, we assume that this configuration process corresponds to the selection of the "best" resource allocation. The problem of allocating frequency channels does exist in homogenous access scenarios [13, 14, 15], but also in heterogeneous wireless access networks where different technologies coexist [16]. Game theoretic approaches for studying the interaction of difference access networks are proposed in [9, 17, 18]. The aforementioned manuscripts focus on the single problem of resource allocation. Since however this problem is strictly related to the network selection problem, we consider them jointly. This leads to a *multi–leader/multi–follower two–stage game* where both users and networks compete in order to maximize/minimize specific utility/cost functions. In particular, end users may choose among multiple available access networks to get connectivity, and network operators may set their radio resources to provide connectivity. Namely, in the first stage the network operators (i.e., the leaders) play by choosing their resource allocation strategies, while in the second stage the users (i.e., the followers) play the network selection/association game.

The following and final part of the thesis studies the resource allocation problem from a slightly different point of view. The resources to be shared are no longer access networks but rather spectrum portions and

bands. Indeed, strongly motivated by the fact that current policies for use of available wireless spectrum are increasingly inadequate, we assume a flexible spectrum management between users and operators, and we provide thorough analysis of competitive spectrum sharing scenarios. The problem of how to share common portions of the spectrum has been widely addressed in the technical literature, especially in the context of heterogeneous and cognitive networks. Similarly to previous models, also in this case the quality of service perceived by a system (e.g., user, network) strictly depends on the behavior of the other entities. Furthermore, one of the most important aspects of cognitive terminals resides in their rationality. This makes game theory convenient to provide formal tools to model the interactions and competitions among users, to derive equilibrium criteria and to study the optimality and the stability of the solution [19]. In this context, another relevant aspect that can be further considered in the definition of game models is the temporal evolution of the system [3, 20, 21].

Game theory plays a fundamental role all throughout this work. In particular, since we model the interaction/competition among different entities (i.e., players) always assuming selfish behavior in the maximization of their satisfaction, we resort to non–cooperative game theoretic tools [8] to analyze the dynamics among users and operators. In this scenario, each entity (e.g., user, network) maximizes her own payoff, regardless of the status of the other entities. The most famous solution concept for a non–cooperative game is the *Nash Equilibrium (NE)*, that is a strategy profile such that each player cannot reduce its experienced cost by deviating unilaterally from the chosen strategy. A pure-strategy NE is an equilibrium for which each player deterministically chooses an action (with probability 1). Moreover, the equilibrium concept adopted for multi–stage games is the *Subgame Perfect Equilibrium (SPE)*, which is defined as a strategy profile which is a NE for every subgame [8]. The study of the existence of pure strategy equilibria is very important. The basic assumption behind the employment of game tools for congestion problems, such as the one we are studying, is that end users repeatedly play their best response until a stable state is achieved. When instead no pure strategy exists, the end users continue to play their best response without achieving any stable state. In this case, we introduce the concept of (pure strategy) ϵ–NE (and (pure strategy) ϵ–SPE). An ϵ–NE is a strategy profile that approximately satisfies the condition of NE. Namely, given a real non–negative parameter ϵ, a strategy profile is said to be an ϵ–NE if it is not possible for any player to gain more than ϵ by unilaterally

deviating from her strategy. Note that every (pure strategy) NE is a (pure strategy) ϵ–NE in which $\epsilon = 0$. The concept of ϵ–SPE is defined similarly, allowing some player in some decision point of the game tree to play a strategy that is worse no more than ϵ with respect to the best response action. Finally, since non–cooperative games are inherently distributed, the "quality" of the solution might be far from the one achievable with a centralized optimization process. Therefore, the quality of the equilibria is characterized in terms of their associated Price–of–Stability (PoS), see [22] and Price–of–Anarchy (PoA), see [23], defined, respectively, as the ratio between the "social" cost (sum of all the costs) of the best equilibrium (PoS) or the worst equilibrium (PoA), and the one obtained at the optimal solution, i.e., the one minimizing the social cost without equilibrium constraints. Further details on game theory concepts can be found in [8].

We propose several game models related to the problem of *resource sharing*, in terms of both available networks and available spectrum bands. In particular, the structure of the thesis is such that each chapter focuses on a different game model, with a specific scenario for which this model can be applied. The main distinction (from a game theoretical perspective) that can be done is based on the utility/cost functions adopted by the users. In the first part of the thesis, users play using cost functions that are mainly based on the perceived congestion, i.e., number of other users choosing the same resource. Namely, the problem of wireless access/mesh network selection is casted as a *congestion game* [12] where each user is selfish, rational, and selects the access network that maximizes the perceived quality of service. From one side, this assumption provides simple game models, that can be easily analyzed from a game theoretic point of view. This model is also suitable when we consider the association process in wireless networks. However, when we deal with the spectrum sharing problem (instead of available networks, we consider available portions of the spectrum), the congestion–based function might not reflect properly the quality perceived by the users. Therefore, for this scenario, we also consider utility functions that are based on the real throughput achievable by the users. The details of the thesis are discussed in the following, and summarized in Figure 1.1.

First, we present the **Network Selection Game (NSG)** (Chapter 2), that formally is a single-choice congestion game with player specific cost functions. The game models the problem of network selection, where multiple users compete in order to select the "best" available access point. We compare different user cost functions in terms of quality of the equilibria (with respect to the optimum) and actual throughput perceived

by the users. These games are such that a NE always exists in pure strategy. We then introduce the **Wireless Mesh Network Association Game (WMNAG)** (Chapter 3), where we consider the problem of association in wireless mesh networks. New cost functions are introduced in order to capture the end-to-end quality perceived by the users. In particular, for these multi–choice congestion games with player–specific cost functions the Nash equilibrium in pure strategy might not exist. Furthermore, we also study realistic scenarios through simulations. Then, we extend the previous models in order to bring the networks into the competition (Chapter 4). Namely, we propose a two–stage game where both networks and users take decisions aiming at maximizing their own revenue. Also in this case the pure–strategy SPE might not exist, and we study the (pure strategy) ϵ–SPE.

Then, we consider a different scenario, where users sharing the same spectrum might choose among different spectrum opportunities. Also in this case, we first consider congestion–based models, where the quality perceived by each user depends on the number of other users selecting the same spectrum band. In particular, since the availability of spectrum opportunities is in general time-varying, we introduce a **Spectrum Selection Game (SSG)** (Chapter 5) that accounts for the time-varying availability of the spectrum.

Finally, we introduce the **Spectrum Sharing Game with Interference Model**, where users take decisions on how to exploit the available spectrum aiming at maximizing a utility function that is based on the Shannon capacity. Interference between users is modeled considering the geographical distribution of the users. A complete framework for the 2–player model is provided (Chapter 6) and preliminary results on the N–player case are discussed (Chapter 7). Furthermore, since characterization of the equilibria strictly depends on the distances between interfering users, we use stochastic geometry to provide probability distributions on users strategies and predict the performance of large networks.

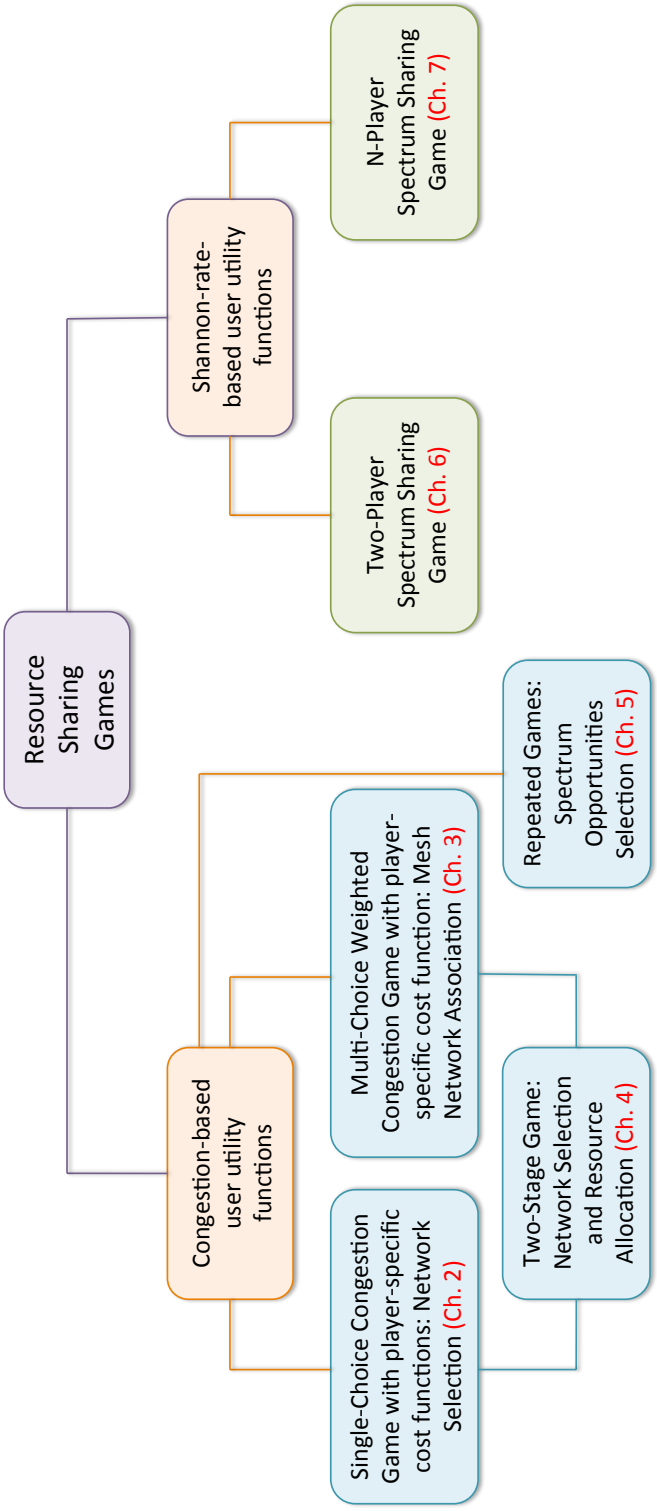

Figure 1.1: Structure of the thesis.

Chapter 2: Network Selection in Wireless Access Networks

Wireless access networks are often characterized by the interaction of different end users, different communication technologies, and different network operators. The first part of this thesis analyzes the dynamics among these "actors" by focusing on the processes of *wireless network selection* (Chapter 2–3), where end users may choose among multiple available access networks to get connectivity, and *resource allocation* (Chapter 4), where network operators may set their radio resources to provide connectivity.

The basic problem of *network selection* refers to the dynamic and automatic choice of the "best" wireless access network to connect to. In classical cellular systems, the network selection is mainly guided by physical layer parameters, and the mobile terminal often associates to the "best received" base station, i.e., the closest (in terms of electromagnetic transmission) to the end user equipment. Such selection policy is obviously not suited for other wireless access scenarios eventually featuring heterogeneous wireless access technologies. For instance, a WiFi user may favor connecting to a less loaded Access Point (AP) at larger distance, rather than to a very close, highly loaded one. The specific parameters to drive the selection strategy itself are highly dependent on the specific wireless access technology, thus novel parameters must be accounted in the selection procedure [24].

Even if the proposed model is rather general and not dependent on the specific quality measure, we introduce three approximate but consistent measures for the perceived quality of the access process which model realistic technological scenarios. More precisely, one function depends only on the users' perceived interference level, whereas the other two functions also account for the actual achievable rate upon accessing the network. We prove that the three games always admit pure Nash equilibria, further providing practical solution algorithm to derive such equilibria which leverages the mathematical programming formulation of the network selection problem. The quality of the equilibria is then characterized in terms of their associated Price–of–Stability (PoS), see [22] and Price–of–Anarchy (PoA), see [23]. The actual throughput and fairness degree of the equilibrium situations are also assessed through system level simulation by resorting to the NS2 network simulator [25].

This chapter is organized as follows: Sec. 2.1 sets the background by reviewing previously published literature in the field of network selection. Sec. 2.2 defines the network selection game model, whilst Sec. 2.3 provides the mathematical programming formulation to compute and characterize the quality of the Nash Equilibrium (NE). The numerical results on the evaluation of the NE are reported in Sec. 2.4. Concluding remarks are reported in Sec. 2.5.

2.1 Related Work

Work related to the problem of network selection mainly deals with two major aspects: the definition of novel metrics aimed at measuring the perceived quality of accessing users and steering the selection decisions, and the design of communication protocols customized to the multi–network scenarios. References [26], [27] and [28] fall in the former research track, and examine quality functions based on different parameters, such as transfer completion time, download throughput, traffic load and received signal strength, in order to propose an intelligent strategy for network selection in multi–access network scenario. A mathematical approach, based on the combination of Grey Relational Analysis (GRA) and Analytic Hierarchy Processing (AHP) is adopted in [29] and in [30]. The authors tackle the problem of network selection developing quality functions to determine the user's utility related to different selection choices. A similar mathematical technique is used in [31]. The authors formulate the network selection problem as a Multi–Attribute Decision Making (MADM) problem that deals with the evaluation of different networks, taking into account many attributes, such as access technology, supported services, and cost.

Research of the latter track usually focuses on specific network scenarios or technologies. Bernaschi *et al.* [32] propose a vertical handover protocol to handle the user mobility between WLAN and cellular systems. The problem of load balancing in 802.11 WLAN is studied in [33] and in [34]. The former proposes an intelligent association control to obtain the fairest solution, in terms of max–min fairness, whereas the latter proposes a mechanism to drive mobile users towards the most appropriate point of access to the network, taking into account both user preferences and network context.

Referring to IEEE 802.11–based networks, Lee and Miller address in [35] the problem of selecting among several 802.11–based APs, by proposing an effective solution to distribute roaming information to the users, which can be used to discriminate in the access phase. References [36] and [37] propose decentralized

approaches to choose among multiple APs aiming at achieving an efficient and fair share of wireless–access resources. In [38], the authors describe a methodology for evaluating the potential bandwidth between a client and an AP based on delays experienced by beacon frames. The potential bandwidth is used as the metric adopted by users in the association phase.

WiFi association is addressed through game theoretic tools in [39], [40] and [41]. All the three works consider non–cooperative game models with the users trying to selfishly minimize a cost function which depends on the current congestion of the WiFi access points. In [40] and [41], the cost function depends only on the current congestion level of the access points, whereas Chen [39] extends to cost functions that include also the association fee that each user has to pay to get access to a specific access point. Besides analytical modeling of the network selection game, reference [40] also introduces a practical association protocol for Wireless LANs; namely, the authors propose to let APs broadcast information on the current congestion level such that the accessing users can dynamically play their best reply strategies which are proven to converge to an equilibrium. A common feature of the aforementioned works is that they all consider the case of atomic players (and atomic games, consequently), with each single player contributing to the costs/utilities of the others in non–negligible manner.

On the other hand, non–atomic games are considered in [42], [43] and [44]. Namely, Shakkottai *et al.* [42] consider the case of link–layer multi-homing where a single device can split its traffic across multiple access points she is associated to. Different from the present work, the game model used in their work comes from the family of population games, which are non–atomic, that is, the contribution to the cost of each user is assumed to be negligible. A similar population game model is analyzed in [43] in case the actual throughput perceived by the accessing user depends on transmission/scheduling policies of the network operator. Non–atomic games are also used in [44] to model the problem of selecting the best network. Again, the solution concept adopted for the game is the Wardrop Equilibrium and the proposed cost function depends on the delay experienced by user packets.

Differently from previous work, we provide a comprehensive framework that models the problem of network selection, investigating different strategies (cost functions) which may fit different access technologies. We address the problem by resorting to congestion games, which provide a powerful tool to represent

situations where resources are shared among/congested by multiple players. Finally, we provide extensive simulations in order to compare the different strategies.

2.2 The Network Selection Game

2.2.1 The Reference Scenario

We consider a reference scenario composed of m APs[1] and n users, where each AP is tuned on a specific radio resource and each user can choose the AP to connect to. We use the following notation: we denote an AP by a and the set of APs by A; we denote a radio resource available to AP by f and the set of radio resources by F; we denote a user by u and the set of users by U. We assume that the available radio resources f at each AP a are frequency channels. Each AP a is characterized by a frequency f on which it transmits and by a *coverage area*, i.e., the area covered by the transmission range of the access point. Frequency reuse is allowed among different access points. The network topology defines the APs' number, positions, frequencies, and coverage areas.

2.2.2 The Game Theoretic Model

We model this scenario as a non–cooperative game in which users are players and their action is the selection of an AP (and frequency) among the available ones. The availability of an action for a user is determined by the network topology and the user's position. More precisely, each user can select one AP among all the ones whose coverage area includes the user's position. In the model, the coverage areas are arbitrary, while in the experimental setting discussed in Section 2.4 we will adopt a specific propagation model. We denote by $A_u \subseteq A$ the set of APs available to user u, and by $A_u^f \subseteq A$ the set of APs transmitting on frequency f and available to user u. Moreover, we define F_u as the set of frequencies that user u can choose. We report an example of network in Figure 2.1, where $m = 2$, $n = 10$. Black circles denote users, lines between users and access points denote associations, and dashed lines delimit coverage areas.

Two users selecting different APs tuned on the same frequency do interfere if they are in the range of both APs. Each user u is assigned a cost function $c_u(f, z_u^f)$ that depends on the *congestion level* z_u^f perceived by user u on frequency f (three different expressions of $c_u(f, z_u^f)$ will be proposed in the next section). We

[1]Hereafter, we will use the terms 'access points', 'access networks' and 'networks' interchangeably. In practice, access points can be IEEE 802.11 hot spots, 3G/4G base stations.

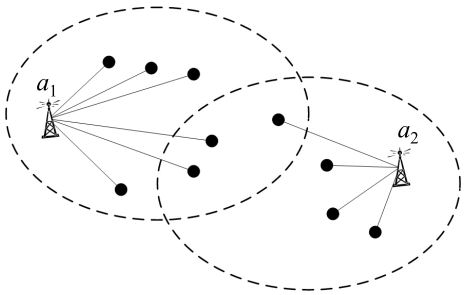

Figure 2.1: A network with two access points.

denote by $X_u^f \subseteq U$ the set of users that use frequency f and interfere with user u. In general, each user u can congest frequency f with a specific *weight* ω_u^f. For instance, the congestion weight of a user can be a function of the distance between the user and the AP or of the user's traffic. The congestion level z_u^f perceived by user u on frequency f is defined as $z_u^f = \sum_{u \in X_u^f} \omega_u^f$. Reasonably, we assume that the cost increases as the congestion level increases, thus $c_u(f, z_u^f)$ is strictly monotonically increasing in z_u^f.

The model drastically simplifies when all the users congest the APs (and consequently the frequencies) with the same weight $\omega_u^f = 1$. We denote by x_u^f the cardinality of X_u^f, formally, $x_u^f = |X_u^f|$, i.e., the number of users that connect to frequency f and interfere with user u. When all the users congest the APs with the same weight, we have $z_u^f = x_u^f$ (the corresponding game is *non–weighted*). Finally, given an action profile, denoted by S, let n_a be the number of users that connect to AP a.

The **Network Selection Game (NSG)** can be formally defined as:

$$\text{NSG} = \langle U, \{F_u\}_{u \in U}, \{c_u(f, z_u^f)\}_{u \in U, f \in F} \rangle.$$

The game we are considering is a congestion game [12] that is: *asymmetric* (different users can have different available actions), *single–choice* (each user can select only one AP), and with *player–specific* cost functions (each user can have a different cost function). Furthermore, it is worth noting that different users of the same frequency may perceive different congestions.

It can be further shown that the game defined above can be reduced to a *crowding game* [45], i.e., a symmetric single–choice congestion game with player–specific cost functions that are monotonically increasing

in the level of congestion. The formal proof is presented in [46] for a similar game model. This equivalence leads to a prominent property when the game is non–weighted: it is proved to always admit a pure strategy NE [45]. The literature on congestion games shows that best–response dynamics surely converge to pure strategy NEs, in case NEs do exist [12]. This allows us to study safely only situations where the users' actions are in equilibrium. Therefore, independently of the specific definition of $c_u(f, z_u^f)$, we can focus on algorithms to find pure NEs. When instead the game is weighted, the existence of pure NEs depends on the definition of $c_u(f, z_u^f)$. We discuss details in the section where we study the weighted congestion game.

2.2.3 Cost Functions

In this section, we define three different cost functions, which approximate the actual access cost under different wireless access technologies.

Cost Function 1: Interference–Based

In general wireless access networks, the quality of service obtained by each user strictly depends on the perceived actual throughput. Since the nominal bandwidth is shared among all connected users, the quality/cost perceived by an accessing user depends on the number of competing users sharing the very same resource. It is thus reasonable to introduce a cost function which depends directly on the cardinality of the interfering users. This may well represent the case of access networks characterized by "soft capacity" like the uplink of CDMA–based systems under open loop power control, where the perceived quality of a transmission depends almost exclusively on the interferers number and each transmission/user congests the shared resource evenly [47]. In this case, for all $u \in U$, $f \in F$, we have:

$$\omega_u^f = 1, \qquad z_u^f = x_u^f, \qquad c_u(f, z_u^f) = x_u^f$$

The game is non–weighted. In particular, when frequency reuse is not allowed, the game admits an exact potential function. In this case all the users perceive the same congestion from f and the potential function is the one provided by Rosenthal in [12], formally, $\Psi(S) = \sum_{a=1}^{m} \sum_{k=1}^{n_a} k$, where S is the users' strategy profile. (We recall that in a potential game every action profile that minimizes the potential function is a NE.)

Cost Function 2: Weighted Interference–Rate

Wireless technologies used in access networks may feature rate–adaptation mechanisms that dynamically adapt the nominal rate to the received signal strength. Therefore, it is worth considering a cost function that accounts both for the number of interferers and for the nominal rate. We denote by R_u^a the rate perceived by user u connecting to a. We denote by T_u^a the inverse of the rate R_u^a perceived by user u to connect to a, i.e., $T_u^a = \frac{1}{R_u^a}$. Moreover, since the cost function is defined with respect to the chosen frequency, we define (with a slight abuse of notation):

$$T_u^f = \min_{a \in A_u^f} T_u^a$$

where A_u^f is the set of APs available to user u using frequency f.

The accessing users may then congest the shared resource in different ways. As an example, in IEEE 802.11 access networks the highest interference is caused by users with the lowest rate due to the well known performance "anomaly" [48]. Thus, it is reasonable to assume that each user congests the resources with a specific weight that depends on the inverse of the rate the user perceives. Formally, defining ω_u^f as the inverse of the rate we have:

$$\omega_u^f = T_u^f, \qquad z_u^f = \sum_{u' \in X_u^f} T_{u'}^f, \qquad c_u(f, z_u^f) = T_u^f \cdot z_u^f$$

Although the game is weighted, the results discussed in [49] show that when the cost functions are separable, i.e., when the cost is defined as the product of a player–specific parameter and the congestion level, the game always admits a pure NE. The game with this cost function does not admit any potential function.

Cost Function 3: Interference–Rate

We observe here that the practical implementation of Cost Function 2 requires the knowledge for a user of the rate values adopted by all the other users in the network, which may be not feasible or too expensive to achieve. We propose here an approximate cost function combining the interference and rate which requires more limited information to be distributed throughout the users. In case the nominal rate and the number of competing users is available, we may define a cost function to capture the portion of bandwidth achievable to

each user, as the current nominal rate divided by the number of interferers.

Since in the cost functions we consider the inverse of the rate, we obtain the product between the number of interferers and the reverse of the rate perceived by users. Formally, for all $u \in U, f \in F$, we have:

$$\omega_u^f = 1, \qquad z_u^f = x_u^f, \qquad c_u(f, z_u^f) = T_u^f \cdot x_u^f$$

The game with this cost function does not admit any potential function.

2.3 Finding Nash Equilibria

The literature on congestion games generally resorts to the minimization of potential functions to calculate Nash equilibria. However, our games do not always admit any potential function. Thus, we propose a solution approach based on a mathematical programming formulation of the network selection problem, that can be used in realistic scenarios for all the cost functions.

To this end, we introduce the following parameters, defined as $\forall\ u \in U, f \in F, a \in A$:

$$b_{ua} = \begin{cases} 1 & \text{if user } u \text{ can select access point } a \\ 0 & \text{otherwise} \end{cases}$$

$$d_{uf} = \begin{cases} 1 & \text{if user } u \text{ can select frequency } f \\ 0 & \text{otherwise} \end{cases}$$

$$t_{af} = \begin{cases} 1 & \text{if } a \text{ transmits on frequency } f \\ 0 & \text{otherwise} \end{cases}$$

$$i_{uvf} = \begin{cases} 1 & \text{if users } u \text{ and } v \text{ interfere on frequency } f \\ 0 & \text{otherwise} \end{cases}$$

Given a generic topology, b_{ua} is equal to 1 if user u is within the coverage area of a. The value of each

b_{ua} (and also the reverse of the nominal rates T_u^as) are computed once the propagation model is chosen. Furthermore, d_{uf} is equal to 1 if user u is covered by at least one AP that is using frequency f. Then, F_u is the set of frequencies that user u can choose, i.e., such that $d_{uf} = 1$.

We define the assignment of a user to a frequency by introducing a binary decision variable, $\forall\, u \in U, f \in F$:

$$y_{uf} = \begin{cases} 1 & \text{if user } u \text{ chooses frequency } f \\ 0 & \text{otherwise} \end{cases}$$

and similarly we define a binary decision variable for the association of each user to an AP, $\forall\, u \in U, a \in A$:

$$s_{ua} = \begin{cases} 1 & \text{if user } u \text{ chooses AP } a \\ 0 & \text{otherwise} \end{cases}$$

Note that variable x_u^f introduced in Section 2.2 is:

$$x_u^f = \sum_{v \in U} y_{vf} i_{uvf}.$$

Recalling that ω_u^f is the congestion weight of user u to frequency f, the congestion level z_u^f of frequency f is:

$$z_u^f = \sum_{v \in U} \omega_v^f y_{vf} i_{uvf}.$$

With the social cost as the objective function, i.e.,

$$\sum_{u \in U} \sum_{f \in F} y_{uf} c_u \left(f, z_u^f\right) \tag{2.1}$$

the socially–optimal network selection is a solution of the following mathematical programming problem:

$$\min \sum_{u \in U} \sum_{f \in F} y_{uf} c_u \left(f, z_u^f\right) \tag{2.2}$$

s.t.

$$\sum_{a \in A_u} s_{ua} = 1 \qquad \forall\, u \in U \tag{2.3}$$

$$\sum_{f \in F_u} y_{uf} = 1 \qquad \forall\, u \in U \tag{2.4}$$

$$s_{ua} t_{af} \leq y_{uf} \qquad \forall\, u \in U, f \in F, a \in A \tag{2.5}$$

where constraints (2.3) and (2.4) ensure that each user chooses only one frequency and one AP among available ones, while (2.5) guarantees that the frequency chosen by user u is the frequency used by AP a if and only if s_{ua} is equal to one.

A (pure strategy) NE can be found by solving the following feasibility problem:

$$\text{constraints (2.3), (2.4), (2.5)}$$

$$d_{uk} y_{uf} c_u\left(f, z_u^f\right) \leq c_u\left(k, z_u^k + \omega_u^k\right) \qquad \begin{array}{l} \forall u \in U, f, \\ k \neq f \in F \end{array} \tag{2.6}$$

where constraints (2.6) force each user u to select the frequency which minimizes u's cost function, that is, they ensure that, if a user unilaterally changes her action, then she cannot reduce her cost (i.e., definition of NE).

The selection of a specific NE can be easily addressed by introducing an objective function. For instance, the worst NE (needed for calculating PoA) can be obtained by maximizing (2.1), whereas the best NE (needed for calculating PoS) can be obtained by using (2.2). For all the cost functions a mixed–integer linear formulation has been provided. This model has been used to characterize the optimal allocation and the best/worst equilibrium of the games.

2.4 Experimental Evaluation

We report an experimental evaluation of the access strategies associated to the three cost functions previously proposed. At first, we introduce the experimental setting used in our simulations, then we compare different scenarios in terms of both equilibrium inefficiency (i.e., PoA and PoS) and the average perceived throughput by the users. Hereafter, we will denote by 1, 2, and 3 the cost functions 1, 2 and 3 presented in Sec. 2.2.3. Furthermore, we consider also the case in which users select the nearest AP, i.e., $c_u(f, z_u^f) = T_u^f$, regardless of the number of interferers. We will denote this cost function by "nearest–AP". Note that this is not a game anymore, then it is considered only in the throughput evaluation as a performance benchmark.

2.4.1 Experimental Setting

We consider a multi–access network deployed on a square area with edge L and composed by n users and m APs with a coverage range of r meters.

We have implemented a generator able to create synthetic instances representing the simulated network scenarios. The generating tool randomly draws the position of the m APs and the n users, so that each user is covered by at least one AP. Moreover, all throughout this section we assume that each AP uses a different frequency, which is the "best" situation for the users since inter–AP interference is null. We will relax this assumption in the following section.

For the sake of experimentation, we refer to the standard 802.11g and we adopt the free space propagation model in [50], that define the Signal–to–Noise Ratio (SNR) as:

$$\text{SNR} = 10 \log \frac{P_r}{N}, \quad P_r = P_t \cdot G_t \cdot G_r \left(\frac{\Lambda}{4\pi d} \right)^2$$

where $P_t = 0.01$ W, $G_t = G_r = 1$, Λ is the wavelength and can be derived by frequency that is set to 2.437 GHz and noise is $N = 3 \cdot 10^{-11}$ W.

The SNR threshold to have correct reception is set to 5.05 dB which corresponds to a circular coverage area of radius $r = 100$ meters. According to the distance d between the user and the AP, when this is shorter than the radius, the software assigns the larger actual rate that the user can obtain from that AP (rate adaptation scheme). Table 2.1 reports, for each distance and SNR, the actual rate and the corresponding value

Table 2.1: Achievable rates in a 802.11g scenario.

Distance [*meters*]	SNR [*dB*]	Rate [*Mbit/s*]	T
≤ 10	≥ 25.05	54	1.8
≤ 20	≥ 19.03	48	2
≤ 30	≥ 15.51	36	2.7
≤ 45	≥ 11.99	24	4
≤ 60	≥ 9.49	18	5.5
≤ 75	≥ 7.55	12	8.3
≤ 90	≥ 5.97	9	11.1
≤ 100	≥ 5.05	6	16.6

of T used in our simulations.

The parameter T used in the model is a normalization of the inverse of rate R, so that the number of interferers and the inverse of rate are comparable. In this case we assume that $T = 10^8/R$. This normalization could not be effective if the number of users or APs increases. In general, we have found that an effective normalization should depend on n and m so that the worst case of rate (that corresponds to the maximum value of T) is comparable with the average number of users per AP. For this reason we propose the following normalization:

$$T_{max} = \frac{n}{m}\beta$$

where T_{max} is the maximum value of T and β should be chosen in the interval $[1, 4]$ (in our simulations $\beta = 3.32$).

2.4.2 Evaluating Equilibrium Inefficiency

To compare the different cost functions, we find the optimal solution and best and worst equilibria formalizing the mathematical models presented in Section 2.3 with AMPL [51] and solving them with CPLEX [52]. All the results reported in this section are averaged on 100 randomly generated instances where APs are fixed, varying the users' position.

We initially discuss the cases for which the PoA assumes the largest values. This happens for a "corridor" topology with $m = 3$ APs and $r = 100$ meters. The "corridor" topology, illustrated in Figure 2.2 (c) denotes a scenario where the access points are deployed on a straight line. Figure 2.3 reports the PoA using cost function 1. These results show that the maximum value of PoA is $1.\overline{6}$ and it can be reached only with 3 users, moreover PoA is different from 1 only when the number of users is a multiple of the number of APs. In fact,

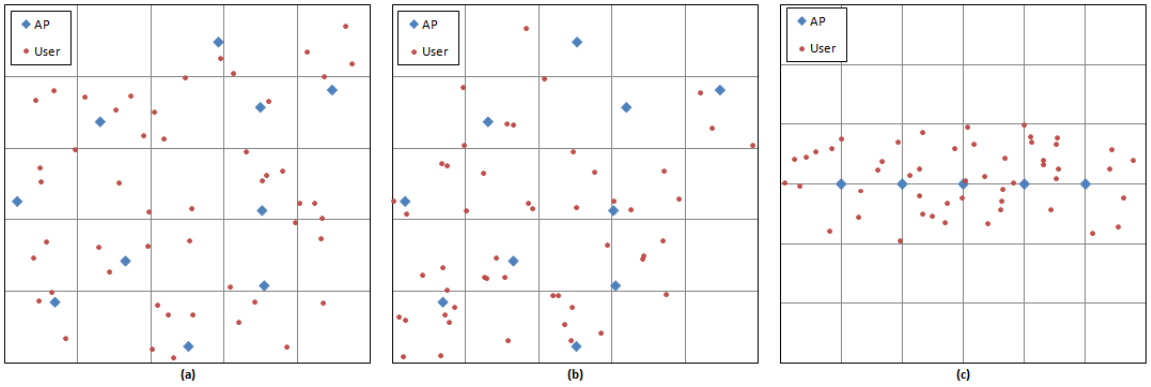

Figure 2.2: Examples of the different topologies: uniform (a), non–uniform (b) and corridor (c).

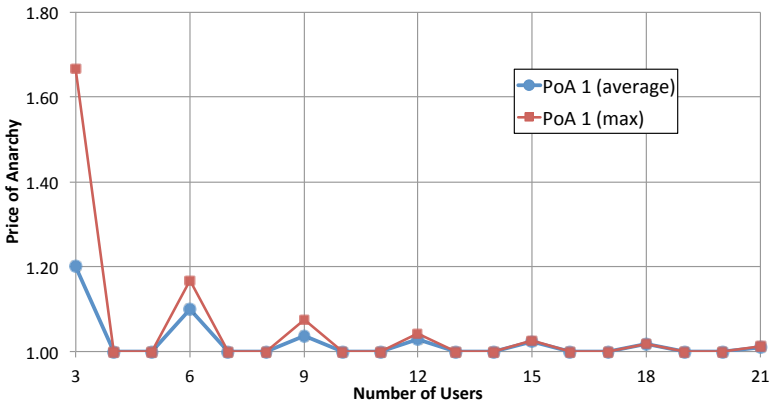

Figure 2.3: PoA using cost function 1 (interference–based).

it can be proved that when the number of users is a multiple of the number of APs, there exist two equilibria and only one is optimal, then the PoA is greater than 1. In contrast, when the number of users is not a multiple of the number of APs, only one equilibrium exists and this corresponds to the optimal solution (see [53] for the analytical proof).

Differently from PoA, the PoS is always equal to one with cost function 1, and therefore the best equilibrium always corresponds to the optimal solution. The dependency of PoA on n for cost functions 2 and 3 is similar to the one of cost function 1. The unique significant differences concern the maximum values of PoA at $n = 3$: 1.43 for cost function 2, and 1.35 for cost function 3 (for $n > 6$ PoA < 1.1 for all the cost functions). Differently from what happens in the case with cost function 1, PoS with cost functions 2 and 3 can be larger than 1 and then the optimal solution may not be an equilibrium.

Table 2.2: PoS and PoA in different topologies.

	Uniform (a)		Non–uniform (b)		Corridor (c)	
Function	PoS	PoA	PoS	PoA	PoS	PoA
1	1.00000	1.00733	1.00000	1.00615	1.00000	1.01156
2	1.00000	1.00563	1.00020	1.00490	1.00019	1.00078
3	1.00497	1.01079	1.00493	1.00696	1.00805	1.01108

Now, we analyze three different realistic scenarios. In case (a), we consider a topology with $L = 500$ meters, $r = 100$ meters, $m = 10$ APs and $n = 50$ users. Both users and APs are randomly deployed with a uniform distribution. In case (b), we consider the same topology with users deployed using a non–uniform distribution. To obtain the non–uniform distribution we assume that the square arena is divided into sub–areas, e.g., four quadrants, and in each sub–area users are deployed uniformly using different densities. Finally, topology (c) is a "corridor" with $L = 600$, $m = 5$ APs and $n = 50$ uniform users. Examples of these topologies are given in Figure 2.2.

Table 2.2 reports PoS and PoA for the three different topologies, varying the used cost function. The main result coming from this analysis is that both PoS and PoA are very close to one, regardless of the specific adopted cost function. In other words, the quality of the equilibria is very close to the optimal solution of the network selection problem. This means that in realistic settings, there is no significant difference, in terms of social cost, between the optimal solution (achievable with a centralized coordination among the users) and any equilibrium of the game (achievable by users through best response dynamics).

2.4.3 Evaluating Actual Throughput and Fairness

In this section we provide a practical comparison of different selection strategies, evaluating the actual throughput perceived by users and the degree of fairness achievable with the proposed cost functions. For this analysis, we have fed into NS2 [25] the solutions obtained by optimization models, representing the association of users to APs at the equilibrium. We have used NS2 version 2.33, supporting rate adaptation. The interference distance has been set to 100 meters (as APs radius) and we have changed the SNR table used for the rate adaptation, so that the associations between rate and distance shown in Table 2.1 are verified. Moreover, in our settings each AP works on a different frequency channel. Finally, users transmit using UDP connections at the same rate in the range [500 Kbit/s – 6 Mbit/s].

To measure the degree of fairness, we consider the Jain's fairness index [54], formally:

$$J = \frac{(\sum_{u \in U} \theta_u)^2}{n \cdot \sum_{u \in U} \theta_u^2}$$

where θ_u represents the throughput of user u.

Anticipating the main outcomes of the simulation analysis, thoroughly described hereafter, we can say that: (i) cost function 3 provides the best trade–off between actual throughput and fairness for all the tested scenarios; (ii) cost function 2 provides performances very close to the ones of cost function 3, except for the fairness in strongly asymmetric settings; (iii) nearest–AP selection leads to low actual throughput in strongly asymmetric settings and low fairness in the other tested scenarios; (iv) cost function 1 generally leads to both actual throughput and fairness lower than the ones obtained under cost function 3.

Moving to the detailed simulation analysis, we initially focus on realistic strongly asymmetric settings. We consider a scenario with $m = 2$ APs and $n = 20$ users. All users are in the range of both APs but they are very closed to one AP. We report in Figure 2.4 the average throughput per user in the Best Equilibrium (BE), using different cost functions and increasing the UDP load. Cost function 1 and nearest–AP lead to a low throughput compared to the other cost functions: -10% and -45%, respectively. Cost functions 2 and 3 are almost equivalent in terms of throughput. We report in Figure 2.5 the Jain's fairness index. Cost functions 3 and nearest–AP provide the best fairness index, whereas cost function 2 leads to -23% and cost function 1 to -9%.

Hereafter, we consider the three different topologies (a), (b) and (c) with $n = 50$ users presented previously in Section 2.4.2. Figure 2.6 reports the average throughput per user in the uniform scenario (a). In general, we have observed by simulations that BE and Worst Equilibrium (WE) are very close in terms of actual throughput. This is obvious if we consider that, increasing the number of users, PoS and PoA come closer. We report an example of this in Figure 2.7 and from now on, we will consider only the BE.

Figure 2.8 reports the Jain's fairness index. We can observe that cost function 1 guarantees fairness, but a lower throughput with respect to the best (-8%). Nearest–AP selection ensures a high average throughput, especially increasing the UDP load, but it has the lowest degree of fairness (-8%). In this case, we can recognize a good trade–off in cost functions 2 and 3, that in general ensure a good throughput and, at the

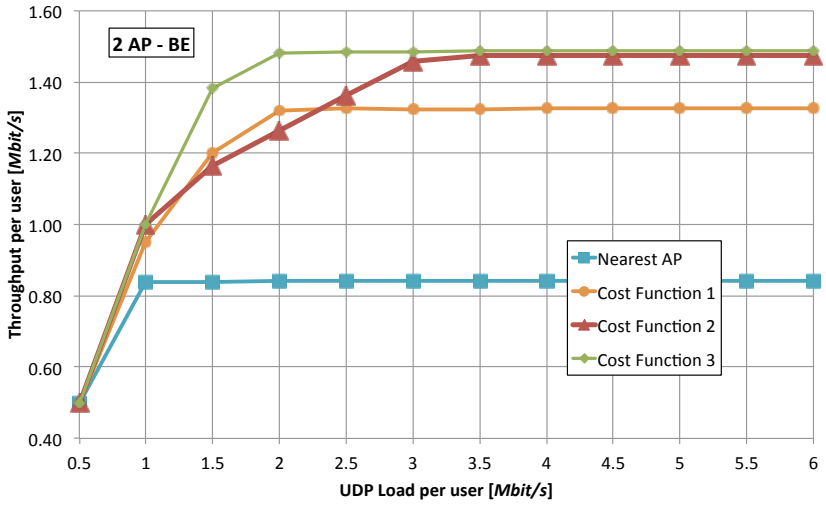

Figure 2.4: Average throughput (BE) per user in 2–AP strongly asymmetric settings, increasing the UDP load.

same time, guarantee fairness to the solution.

Under non–uniform topologies (b), users can be distinguished depending on density of the zone they lay in. High, medium, and low density zones/users are defined. Figure 2.9, 2.10 and 2.11 report the average throughput per user, each figure for a different density, whereas Figure 2.12 reports the Jain's fairness index (calculated over all the users). Also in this case, we can identify in cost functions 2 and 3 a high level of fairness and a good trade–off also in terms of throughput, whereas the nearest–AP selection has always a low fairness degree (-6% from the best).

Finally, we consider the "corridor" topology (c) and we report in Figure 2.13 and 2.14 the throughput and the fairness index respectively. In this case, cost functions 2 and 3 provide the best trade–off between actual throughput and fairness. Cost function 1 leads to a low throughput (-20%) and to a low fairness (-5%).

2.4.4 Discussion on the Implementation Overhead

Finally, we compare the cost functions in terms of applicability of the corresponding selection strategy. In particular, we focus on the amount of information needed by each user for the selection of the access network. Cost function 1 requires only the information on the number of users associated to each AP, while cost function 3 requires in addition the user's nominal rate. The information of the current nominal rate can be

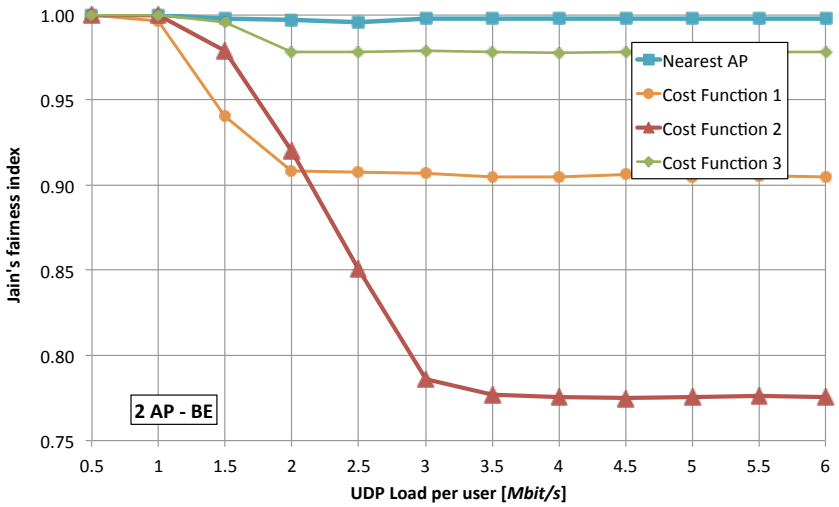

Figure 2.5: Jain's fairness index (BE) in 2–AP strongly asymmetric settings, increasing the UDP load.

easily available locally. Indeed, referring to IEEE 802.11 access networks, the drivers of commercial cards do provide hooks to monitor the current rate adopted for transmissions. The information on the current number of interferes should be provided by the AP itself through beaconing messages[2], or locally estimated by the accessing users.

On the other hand, the calculation of cost function 2 requires each user to know also the current nominal rate adopted by all the other users associated to the same AP which would require a higher signaling overhead to be actually implemented.

2.5 Concluding Remarks

In this chapter, we have analyzed the dynamics that arise among multiple end users that try to connect to the "best" available access networks. Due to the selfish nature of the users, we resorted to non–cooperative game theory to model the competition in accessing shared wireless networks. We analyzed three game models which differ in the access cost function each end user tends to minimize and reasonably represent three realistic cases of wireless access technologies. To solve the games, we proposed a mathematical programming formulation for the network selection problem which is able to return the best and worst equilibria for a thorough evaluation of the equilibria quality in terms of PoS and PoA. The experimental results (validated by

[2] As an example, always in the field of IEEE 802.11 networks the IEEE 802.11k standard could be used to support the exchange of additional information.

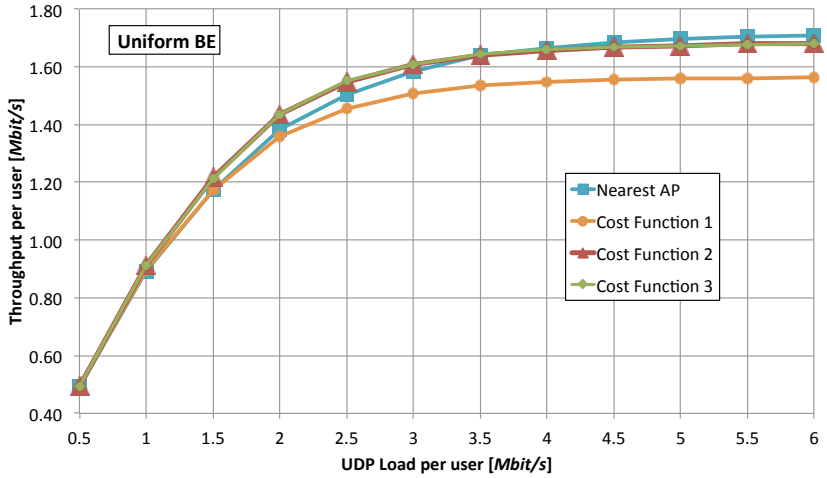

Figure 2.6: Average throughput (BE) per user in uniform topologies.

system level simulation) showed that, when end users selfishly act by minimizing the perceived access cost, the achieved equilibria are pretty close to the social optimal solution. Therefore, in the reference scenario, best response dynamics appear to be an effective technique to find close–to–optimal solutions in a distributed way.

Publications: [55], [53], [56]

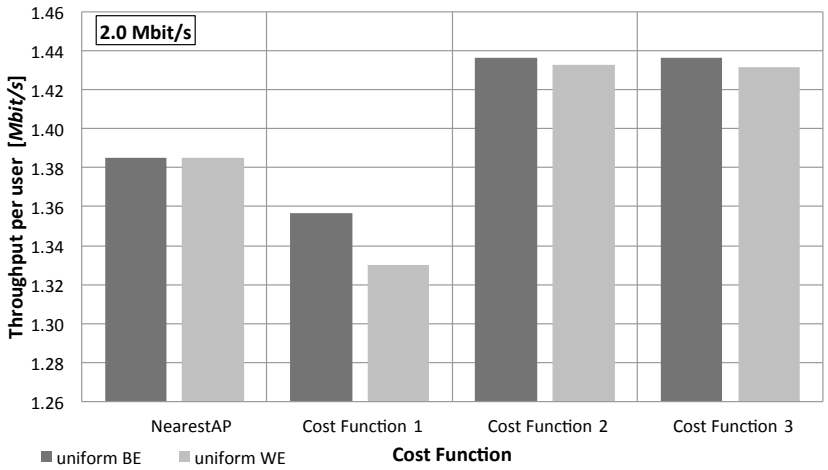

Figure 2.7: Average throughput per user in BE and WE uniform topologies with 2 Mbit/s UDP load.

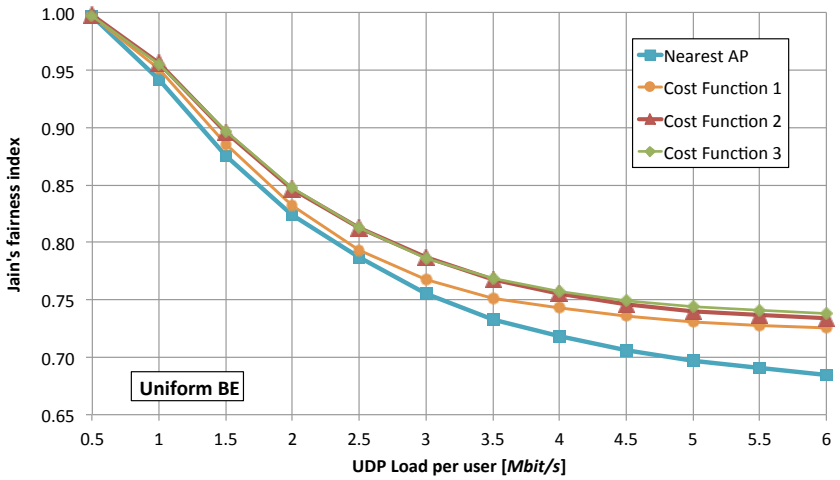

Figure 2.8: Jain's fairness index (BE) in uniform topologies, increasing the UDP load.

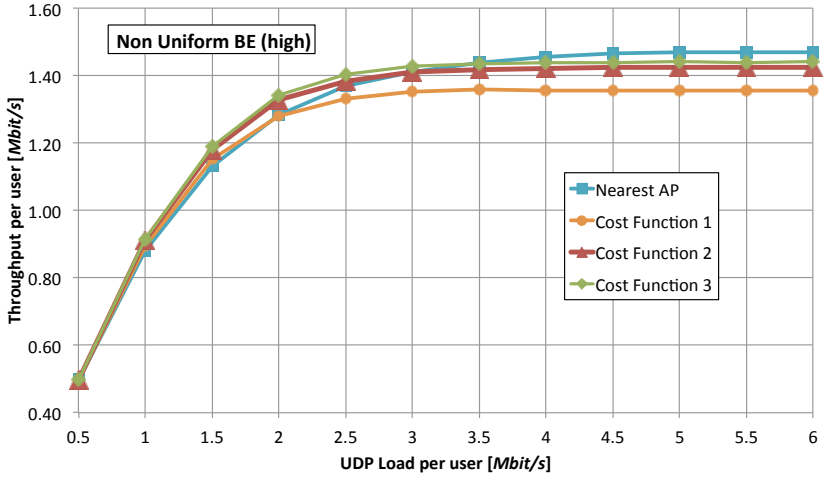

Figure 2.9: Average throughput (BE) per user (located in high density zones) non–uniform topologies.

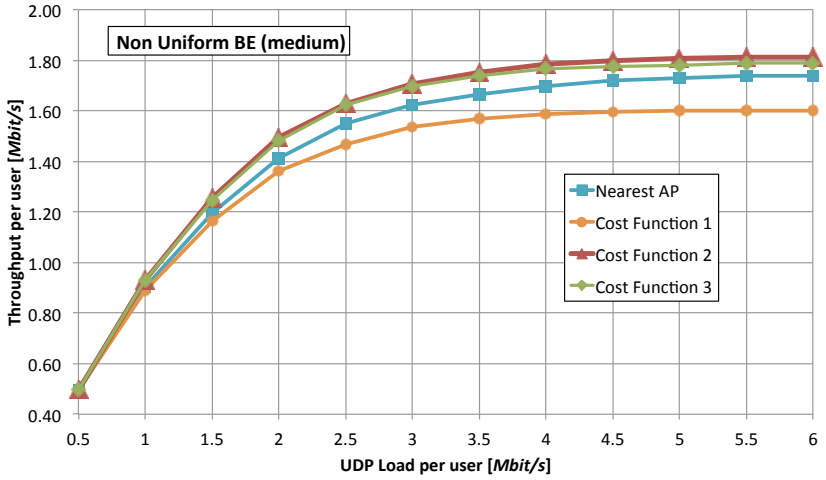

Figure 2.10: Average throughput (BE) per user (located in medium density zones) non–uniform topologies.

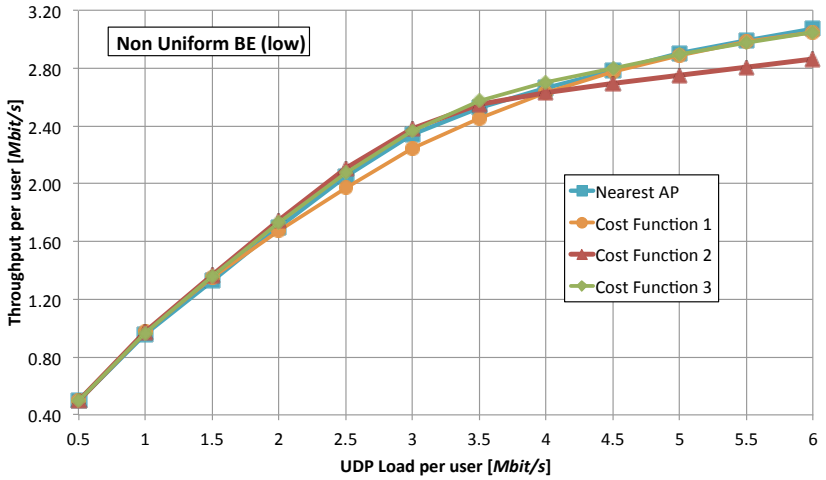

Figure 2.11: Average throughput (BE) per user (located in low density zones) in non–uniform topologies.

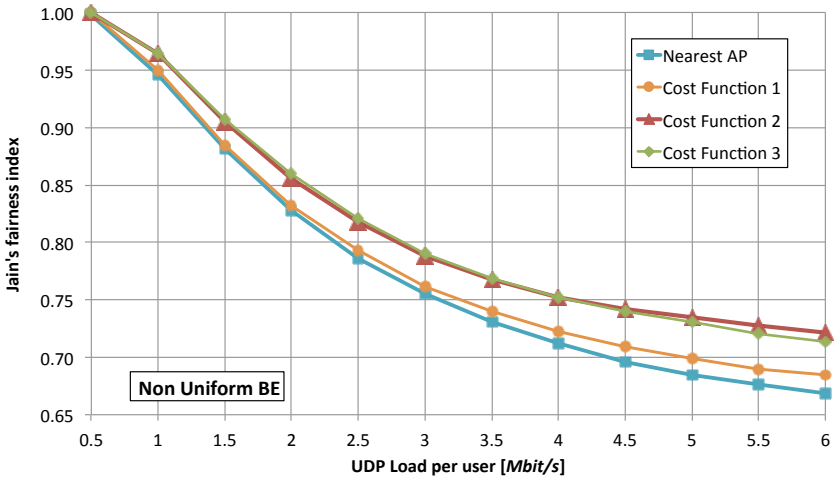

Figure 2.12: Jain's fairness index (BE) in non–uniform topologies, increasing the UDP load.

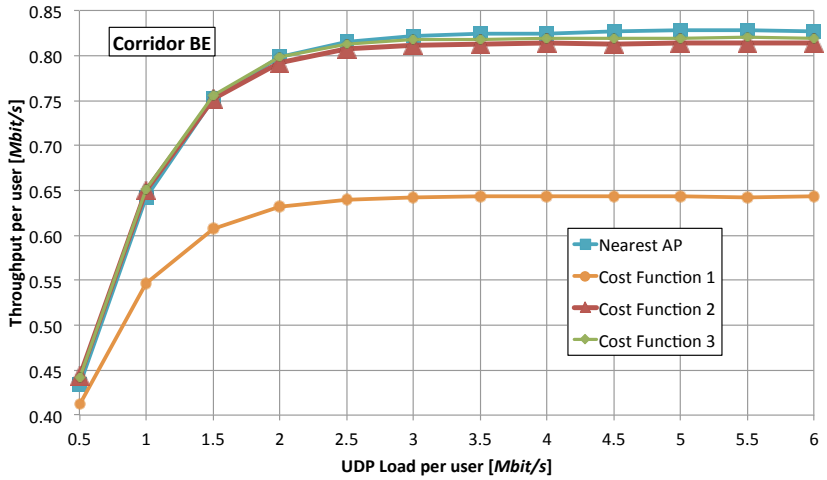

Figure 2.13: Average throughput (BE) per user in corridor topologies, increasing the UDP load.

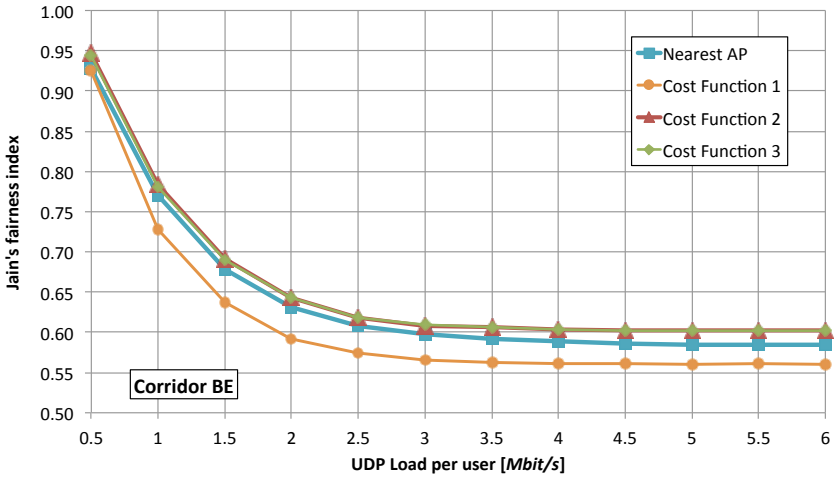

Figure 2.14: Jain's fairness index (BE) in corridor topologies, increasing the UDP load.

Chapter 3: Access Point Association in Wireless Mesh Networks

In the previous chapter, we have considered the association to wireless access networks as a process driven by the quality of the wireless link between the accessing mobile station and the wireless access point, which takes into account both the received signal strength to/from the wireless access point and the number of users sharing a specific resource. However, in case connectivity is provided through a Wireless Mesh Network (WMN), the quality perceived by the user depends also on "global" network–wide parameters. These parameters include the length of the multi–hop wireless path to reach up to the Internet gateway, and the interference level perceived by the traffic flow along such path.

WMNs have been widely recognized as a cost effective solution for providing wireless connectivity/access to mobile users. Such success is mainly due to the high flexibility of the mesh networking paradigm which has many advantages in terms of self–configuration capabilities and reduced installation costs. Several WMNs deployments and initiatives have flourished worldwide with different goals and application targets [1, 57]. WMNs are composed of a mix of fixed and mobile nodes interconnected through multi–hop wireless links, and they often feature a hierarchical architecture. At the top of the hierarchy, Mesh Gateways (MGs) are equipped with wireless/wired connectivity cards and act as gateways toward the wired backbone. The Mesh Routers (MRs) have twofold functionalities: they act as classical Access Points (APs) towards the end users (access segment), and they have the capability to set up a wireless backbone by connecting to other mesh routers through point to point wireless links to transport the access traffic to/from the MGs. The users, or user STAtions (STAs), can consequently get access to the network services through multi–hop paths towards one or more MGs.

In this chapter, the association problem is formalized as a non–cooperative game where accessing stations selfishly play to minimize their own perceived association cost which shall account for the characteristics of the entire path to reach the WMN gateway. To capture the end–to–end quality perceived by each STA, we introduce two simple but consistent metrics that capture the contention perceived by the user's flow along a given path of the WMN backbone (from the access MR to the MG). The first metric relates the perceived

contention to the number of wireless devices interfering the given path; the second metric leverages the airtime parameter introduced in the IEEE 802.11s standard. After formalizing the game, we discuss how the quality of the Nash equilibria can be characterized in terms of PoS and PoA; we further experimentally study realistic sample network scenarios showing simulation results on the quality of the equilibria.

The chapter is organized as follows: Sec. 3.1 overviews the related work in the field and comments further on the novel contributions of the present work. In Sec. 3.2, we formalize the association game for WMNs, whose properties are highlighted in Sec. 3.2.4. A mathematical programming formulation to find the Nash Equilibria of the association game is proposed in Sec. 3.3. In Sec. 3.4, we discuss experimental results on the quality of the equilibria under realistic network scenarios. Sec. 3.5 concludes the chapter.

3.1 Related Work

Most of the currently deployed WLANs operate according to the IEEE 802.11 standard [58], which defines access point association procedures based on the Received Signal Strength Indicator (RSSI), only. Without going into the details of the association protocols, the STAs associate to the access point with the highest RSSI. It is commonly known that RSSI is not the proper metric to be used in the association phase [59]. Indeed, the relation between RSSI and actual throughout perceived by the STA is not often easily predictable, and high RSSI values do not necessary mean high access throughput. The main shortcoming of RSSI–based association comes from the fact that RSSI does not directly account for the contention/congestion at the specific access point, which can often lead to poor resource utilization. To this extent, much work has been carried out to improve the metrics used in the association phase in WLANs [60] by leveraging measures/estimates on access interference [61], on the actual access point bandwidth [38, 62], on user fairness, and network–wide load balancing [33, 63].

All the aforementioned references focus on the case of hot–spot–like access patterns, and consequently the metrics for association capture the "local" quality of the wireless access segment. On the other hand, the issue of designing effective association schemes in WMNs is fundamentally different, since the metric driving the association must account also for "global" quality parameters of the overall network. Within this field, the most common approach in designing association algorithms/protocols leverages the network *airtime* metric to assess the quality of multi–hop paths [64]. The airtime of a wireless link in the wireless backbone

measures the transfer time of a test frame including the time overhead introduced by the access protocol and the link quality in terms of frame error rate.

Athanasiou *et al.* propose in [65] and later in [59] an association scheme which couples the quality and the current load of the access links with a modified version of the airtime metric accounting for both the uplink and downlink segments. The authors further propose a practical cross–layer protocol to implement the association procedures. Along the same lines, Wang *et al.* propose in [66] a dynamic association protocol which couples the plain airtime metric for the backbone links, formalized later in Eq. (3.2), with an estimate of the access airtime at the mesh access points. On the other hand, the work in [67] focuses on the definition of metrics to assess the quality of the access segment. Namely, two metrics are proposed accounting respectively for the expected transmission time and the average load of the mesh access points. A modified version of the airtime is considered also in [68], whereas Ashraf *et al.* propose an association metric which includes also the average load (queue length) of the gateways [69].

All the aforementioned approaches for WMNs share the common goal to design practical association protocols. In contrast, in this work we are interested in studying the dynamics and equilibria of the association process in wireless mesh networks by leveraging tools and concepts of game theory.

Game theory is widely used to investigate the competition, cooperation, and interaction of multiple agents. The notable work in [70] also resorts to congestion games to analyze the association process in WLAN, but the used metric is the access airtime, defined in Eq. (3.2). The main novel contribution of the current work is in the fact that we also account for network–wide metrics in the game definition. To our best knowledge, this is one of the first attempts to formalize the problem of association in wireless mesh networks through a game.

3.2 The WMN Association Game

3.2.1 The Reference Scenario

We consider a generic wireless mesh network composed of N network devices, including mesh access points, mesh routers and gateways. Unless differently specified, in the following, we will use access points, routers and gateways to refer to mesh access points, mesh routers and mesh gateways, respectively. In particular, A is the set of the access points and G is the set of gateways. The network provides multi–hop access to

a set of STAs U. All the traffic is assumed to flow to/from the gateway, whereas cross–traffic among STAs is neglected at this stage[1]. Each access point is connected through multi–hop paths to at least one gateway. The set P includes all the available routing paths in the network. The STAs can be potentially "covered" by multiple access points, and can consequently "decide" to get connectivity to/from one specific access point, which, in turn, will reach the gateway through a specific multi–hop path. Upon association to a specific access point, the quality perceived by the STA depends on the quality of the multi–hop path to/from the gateway. The set $P_i \subseteq P$ denotes all the routing paths available for STA i.

3.2.2 The Game Theoretic Model

We model the Wireless Mesh association problem as a non–cooperative game in which STAs are rational players aiming at minimizing their costs, their strategy space is composed by all the available routing paths[2] and their payoffs are the association costs which account for the contention along the multi–hop path to the gateway. In particular, the quality of wireless multi–hop paths is a long–debated issue and depends on multiple parameters affecting/involving different layers of the communication protocols: the wireless propagation conditions, the specific wireless technologies, the path–wise interference of concurrent/contending flows. We are not interested in defining here a complete and refined end–to–end metric, but rather we are focusing on the study of the dynamics of association in WMNs. To this extent, we leverage a simplified but consistent cost function c_{ij} for the STA i over the routing path j, defined as:

$$c_{ij} = L_j + I_j^i, \tag{3.1}$$

L_j being the *path length* (number of hops in the path), and I_j^i the *path contention cost*, that is, the contention level experienced by the flow generated by STA i along path j. In other words, the cost term I_j^i of STA i depends on the choices of the other STAs in the mesh network. Two different approaches to model this parameter are presented later on in this section.

[1] Nevertheless the proposed approach can be extended to the case of cross–traffic.

[2] As mentioned before, each STA actually chooses one access point and not a path. However, we assume a one–to–one correspondence between access points and paths and here we consider paths since they are related to the cost function.

The **Wireless Mesh Network Association Game (WMNAG)** can be formally defined as:

$$\text{WMNAG} = \langle U, \{P_i\}_{i \in U}, \{c_{ij}\}_{i \in U, j \in P_i} \rangle.$$

We assume here that STAs playing the WMNAG have knowledge of the quality of the entire path behind an access point; namely, the path length to reach the internet gateway (L_j), and the average interference perceived along that path (I_i^j) is known by each STA. Such information could be easily broadcasted by the very same access points through periodic beaconing. As an example, the beacons used in WiFi hot spots can be enhanced to include additional information on the quality of the entire path to the Internet gateway.

The WMNAG is a multi–choice weighted congestion game with player–specific cost functions. Each STA, selecting a path, may interfere multiple wireless links (*multi–choice*), and the congestion of each STA to each link depends on the cardinality of the interference set (*weighted*). Furthermore, the cost function is *player–specific* since the cost of a STA depends only on a subset of the interfered links.

In [45], the author proves that a weighted congestion game in which players have equal payoff functions always admits at least one pure strategy equilibrium. In [71], the authors prove that congestion games in which each player is affected only by the congestion of a subset of resources always admit pure strategy equilibria. In this case, the game is assumed to be non–weighted. In [72], the authors show that both weighted congestion games and games with player–specific delay functions possess pure Nash equilibria in the case of single choice games, i.e., when the players can choose only one resource. To the best of our knowledge, no result deals with weighted games when utility functions are player–specific. Before proving that in fact the game may not admit pure–strategy Nash equilibria, we formally introduce two different cost functions.

3.2.3 Cost Functions

In this sections, we introduce two approaches to model the parameter I_i^j, which yield two different cost functions in the WMNAG.

Cardinality–Based Cost Function

The contention level experienced by a given user flow along a wireless multi–hop path is ideally proportional to the number of wireless devices which interfere with that path [73]. To this extent, a first, simple metric

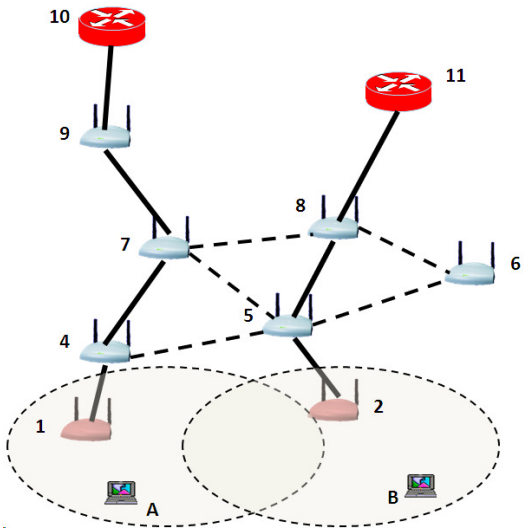

Figure 3.1: Sample topology of a Wireless Mesh Network.

to capture the *path contention cost* can be based on the well–known concept of *interfering set*. For every network device in N, the *interfering set* includes all the other devices which interfere with the given one and are currently used to deliver STAs traffic. The *path contention cost* I_j^i can be calculated as the sum of the cardinalities of all the interference sets of all the nodes on path j. In Figure 3.1, dotted lines represent interference relations, whereas bold lines represent traffic flows; STA A is associated to access point 1 and reaches gateway 10 through the path 1-4-7-9-10; STA B is associated to access point 2 and reaches gateway through path 2-5-8-11. Focusing on STA B, the interference set of device 5 is composed of nodes 4 and 7, whereas the interference set of node 8 is composed of node 7, only. Note that node 6 is not accounted in the interference set of device 5 since it is not servicing any traffic. The overall interference cost for path 2-5-8-11 caused by traffic of STA A over path 1-4-7-9-10 will then be equal to 3.

The same concept of *interference set* can be applied also to those cases where paths are not disjoint by properly defining *a virtual interference graph* to be used for calculating the interference cost. Figure 3.2a reports the case of two flows (to/from two STAs A and B) partially sharing the same path to the gateway, whereas Figure 3.2b reports the virtual graph used to calculate the interference cost of the two flows.

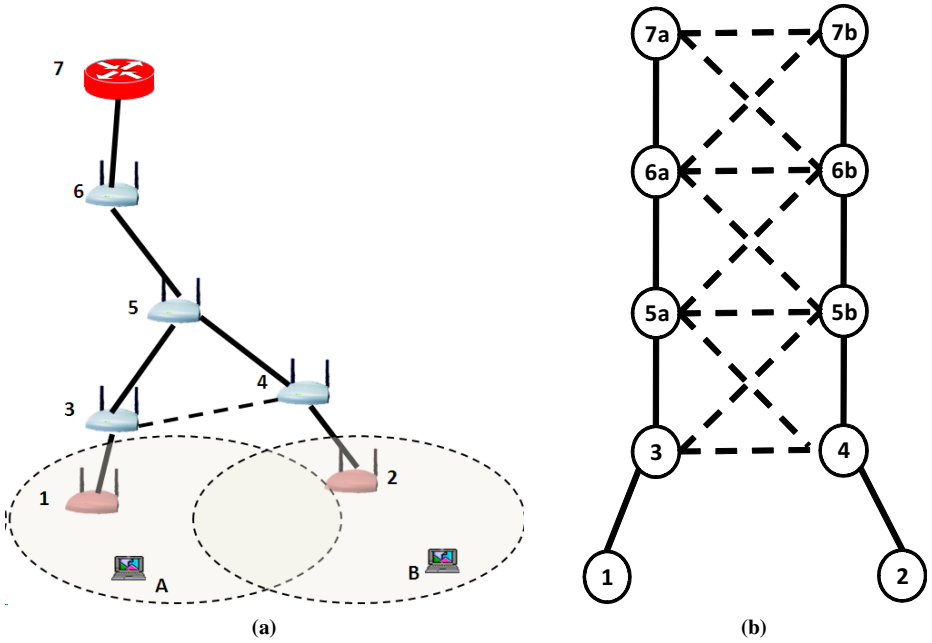

Figure 3.2: (a) Topology of a mesh network with non–disjoint paths. (b) Virtual graph to calculate the path contention cost in the case of non–disjoint paths.

Airtime–Based Cost Function

A limitation of the previous metric is in the fact that different links (e.g., in terms of modulation, distance, transmitted power) induce the same interference on a given link. To overcome this simplification, we extend here the cost metric by leveraging the airtime parameter proposed by the IEEE 802.11s standard as a consistent link quality measure. The airtime of the generic wireless link (i, j) in the wireless backbone is defined as:

$$T_{ij} = \left(O_{ca} + O_p + \frac{B_t}{r(i,j)} \right) \frac{1}{1 - e_{pt}(i,j)}, \tag{3.2}$$

being $r(i, j)$ the nominal data rate of link (i, j), $e_{pt}(i, j)$ the frame error rate, B_t the reference frame size, O_{ca} and O_p the overhead related to the channel access and the protocol, respectively. Intuitively, the airtime captures the channel occupation time for a test transmission over a wireless link. Ideally, wireless links with longer airtime values take longer time to deliver information, and thus produce interference onto the other links for longer time.

To this extent, in the calculation of the interference contribution of the path contention metric it is reason-

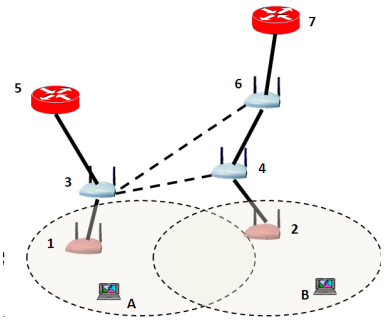

Figure 3.3: Sample topology of a Wireless Mesh Network.

able to give a higher cost to links with higher airtime value. Therefore, the *path contention cost* perceived by STA i along path j, i.e., I_j^i, can be calculated as the sum of the airtime values of all the wireless links in the interference sets of all the nodes on path j.

As an example, Figure 3.3 reports a network configuration where two STAs select different but interfering paths to get connectivity to mesh gateways[3]. Namely, STA A uses path $1-3-5$ (path 1), whereas STA B goes through path $2-4-6-7$ (path 2). Let T_{ij} be the airtime value for the wireless link between device i and device j. The overall interference contribution perceived by STA A is given by the sum of the airtime values of all the nodes in the interference set of node 3, i.e., node 4 and node 6. Then, it can be expressed by:

$$I_1^a = T_{46} + T_{67}$$

Similarly, the interference perceived by STA B is given by the sum of the airtime values for the interference set of nodes 4 and node 6. Since node 4 and node 6 have the same interfering node, i.e., node 3, the interference cost for STA B is:

$$I_2^b = T_{35} + T_{35}$$

3.2.4 Non–Existence of Pure Strategies Association Equilibria

Hereafter, we show that the proposed WMNAG with general interference relations among wireless devices may not admit any Nash equilibrium in pure strategies. We prove it by providing a simple counterexample. Let us consider the network topology reported in Figure 3.4 composed of 3 access points, 6 mesh routers and

[3]Interference relations among wireless devices are indicated with dashed lines.

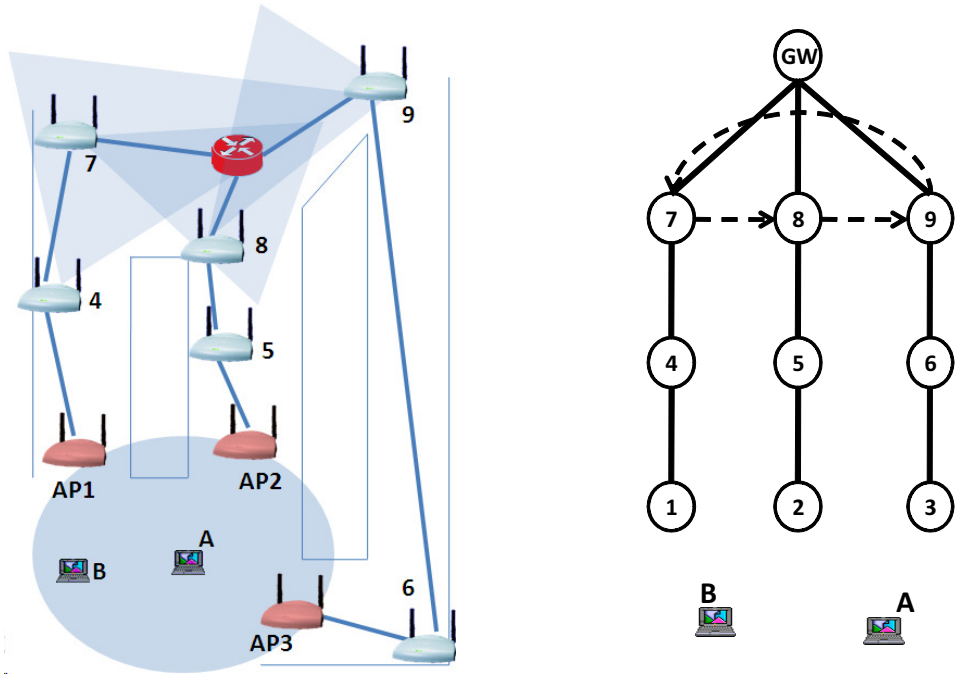

Figure 3.4: Sample of network topology which does not admit any pure strategy Nash equilibrium (left) and corresponding interference graph (right).

1 gateway. The network provides connectivity to two STAs A and B which can choose to associate to each one of the three access points. The two STAs play using the cardinality–based cost function. Let j be the path provided by AP j. The three paths in the network are interference free except for the three mesh routers 7, 8 and 9, which reach the gateway through directional antennas with cone of interference depicted in Figure 3.4. The equivalent topology for the calculation of the access cost is also reported in Figure 3.4. Note that the directional interference relations are represented through arrows. If STA A associates to AP 1 (i.e., path 1) and STA B associates to AP 2 (i.e., path 2), the respective association costs are:

$$c_{A1} = L_1 + I_1^A = 3 + 1 = 4$$

$$c_{B2} = L_2 + I_2^B = 3 + 2 = 5$$

STA B has incentive to move to AP 3 getting a lower association cost:

$$c_{B3} = L_3 + I_3^B = 3 + 1 = 4$$

Associating to AP 3, STA B starts generating interference towards path 1 (from MR9 to MR7). Then A perceive a new association cost:

$$c_{A1} = L_1 + I_A = 3 + 2 = 5$$

Consequently, STA A has incentive to move to AP 2 triggering a new move of STA B. The two STAs keep changing their played strategy never reaching a steady state regardless of the initial strategy profile. It is easy to extend the very same example to the airtime–based cost function by properly setting the airtime of the wireless links.

The peculiarity of the presented game scenario is the asymmetry in the interference relations among wireless links. Even if NE may not exist in the WMNAG (as shown), it is worth to point out here that in our experimental evaluations we have found a NE for all the association games with symmetric interference patterns.

3.3 Finding Nash Equilibria

The WMNAG presented in the previous section may admit in general multiple equilibria that differentiate in terms of costs experienced by the STAs. As done before, we characterize the quality of different equilibria in terms of their social cost, defined as the cumulative costs of all the STAs. Furthermore, we analyze the difference between equilibria and the optimal association evaluating PoS and PoA. To find optimal equilibria (minimizing/maximizing the social cost) and the optimal association (minimizing the social cost without equilibrium constraints) we provide a set of mixed integer linear mathematical programming formulations for the cardinality–based and airtime–based cost functions. Mathematical formulations for the WMNAG are discussed in Appendix A.

3.4 Experimental Evaluation

In this section, we provide simulation results to assess the quality of the equilibria in realistic sample network topologies under the cardinality–based and the airtime–based cost functions. Two types of performance evaluation are carried out: first, we characterize the association game by numerically computing the PoS and PoA under different network topologies, then we compare the outcome of the association game under differ-

ent association policies. The main findings out of this analysis for both cost functions can be summarized as follows:

1. the equilibria of the association game are similar in quality to the optimal solution, i.e., PoS and PoA are pretty close to 1 in all the tested scenarios;

2. association strategies that account for end–to–end contention in the WMN backbone lead to lower interfered association paths compared with "interference–agnostic" strategies.

3.4.1 Performance Evaluation Setting

To evaluate the outcome of the association games, we have developed a network topology generator for WMNs which deploys parametric topologies with different number of STAs N, number of access points, number of routers and number of gateways. The software randomly deploys all the network devices and STAs in a square area of side L and calculates the shortest paths between all the access points and the gateways using the hop count as well as the airtime metric. Every device has a circular coverage/interference region with radius r, and can feature up to 4 network interface cards which can be tuned to different orthogonal channels. STAs are randomly scattered throughout the square network arena with the constraint to be covered by at least two access points (and paths), and the end–to–end connectivity from each access point to at least one gateway is enforced by the tool.

When considering the airtime–based cost function, upon the deployment of the WMN devices, the tool properly assigns airtime values to all the links in the wireless topology. The airtime calculation utility works under the following assumptions:

- wireless devices are equipped with omnidirectional antennas;
- transmissions are performed at the maximum allowed power in each reference band (EIRP=100mW);
- transmissions are affected by additive white Gaussian noise (AWGN).

Moreover, the following SNR/distance relations have been used at 2.4 and 5 GHz, respectively.

$$SNR_{2.4GHz} = 81 - 36\log(d) \tag{3.3}$$

$$SNR_{5GHz} = 75 - 36\log(d) \tag{3.4}$$

From the two equations above, the bit error rate has been obtained according to the IEEE standards. Namely, the IEEE 802.11a at 54Mbps (OFDM with 64–QAM) has been adopted for the backbone transmission and the IEEE 802.11g at 12Mbps (OFDM with QPSK) for the access network. Tables 3.1 and 3.2 report the relations between SNR, BER, distance and airtime values used in setting up the game environment[4].

Table 3.1: Airtime values for IEEE 802.11g at 12Mbps (QPSK).

SNR [dB]	d[m]	BER	Airtime [ms]
[0,1]	[167,178]	5.63 10^{-2}	1.4664
[1,2]	[156,167]	3.75 10^{-2}	1.4383
[2,3]	[147,156]	2.28 10^{-2}	1.4166
[3,4]	[138,147]	1.25 10^{-2}	1.4018
[4,5]	[129,138]	5.95 10^{-3}	1.3926
[5,6]	[121,129]	2.38 10^{-3}	1.3876
[6,7]	[114,121]	7.72 10^{-4}	1.3854
[7,8]	[107,114]	1.91 10^{-4}	1.3846
[8,9]	[100,107]	3.63 10^{-5}	1.3844
[9,10]	[94,100]	3.87 10^{-6}	1.3843

Table 3.2: Airtime value for IEEE 802.11a at 54Mbps (64 QAM).

SNR [dB]	d[m]	BER	Airtime [ms]
[0,1]	[113,121]	1.78 10^{-1}	0.4103
[1,2]	[106,113]	1.57 10^{-1}	0.4001
[2,3]	[100,106]	1.37 10^{-1}	0.3909
[3,4]	[94,100]	1.18 10^{-1}	0.3826
[4,5]	[88,94]	1.01 10^{-1}	0.3751
[5,6]	[82,88]	8.38 10^{-2}	0.3681
[6,7]	[77,82]	6.76 10^{-2}	0.3617
[7,8]	[73,77]	5.23 10^{-2}	0.3559
[8,9]	[68,73]	3.84 10^{-2}	0.3508
[9,10]	[64,68]	2.65 10^{-2}	0.3465

The game instances generated by the topology tool are fed into the optimization models presented in Appendix A. In particular, the models have been implemented in AMPL [51] and solved with CPLEX [74]. Hereafter, all the reported results have been obtained averaging over 20 instances of the same type of the game (i.e., users and network devices positions), unless differently specified.

[4]Note that the proposed solution technique is independent on the specific rule/procedure to assign airtime values to wireless links.

Table 3.3: PoS and PoA for network topologies with 10 mesh routers and 3 gateways under different number of APs and STAs.

		N=15	**N=25**	**N=35**	**N=45**	**N=55**	**N=65**
6 APs	*PoS*	1.003	1.003	1.012	1.01	1.018	1.003
	PoA	1.036	1.023	1.022	1.026	1.022	1.007
7 APs	*PoS*	1.001	1.005	1.011	1.012	1.008	1.006
	PoA	1.018	1.019	1.013	1.028	1.027	1.012
8 APs	*PoS*	1.006	1.018	1.006	1.002	1.003	1.011
	PoA	1.009	1.036	1.028	1.010	1.014	1.016

Table 3.4: PoS and PoA for network topologies with 4 access points, 9 mesh routers and 4 gateways under different number of association strategies per STA.

	2 Strategies		**3 Strategies**	
N	*PoS*	*PoA*	*PoS*	*PoA*
15	1.044	1.080	1.039	1.109
25	1.032	1.060	1.041	1.089
35	1.037	1.058	1.136	1.162

3.4.2 Equilibria under Cardinality–Based Cost Function

Table 3.3 refers to a small–size WMN deployment featuring a variable number of access points (6,7 and 8), 10 mesh routers, 3 gateways, $L = 1000$ meters, $r = 20$ meters and a variable number of STAs (N). The main result coming from the table is that the equilibria of the association game are almost of the same quality and very much close to the optimal association, i.e., PoS and PoA are similar and very close to 1. Said in other words, if the STAs play the association game selfishly, according to the defined cost function, the "distributed" equilibrium is similar in quality to the "centralized" optimal solution. We note here that the network deployments of Table 3.3 may feature a low number of strategies for the end STAs, that is, the average number of access points covering each STA is around 2.5 for most of the cases. To this extent, it is worth studying whether similar results on the quality of Nash Equilibria hold true for larger strategy spaces.

Table 3.4 reports the PoS and PoA for network topologies constrained to have at least 2 and 3 association alternatives per STA. The quality of the equilibria is still close to the optimum, even if a slight increase in the PoS and PoA can be appreciated as the number of STAs and the number of strategies per STAs increase.

Figures 3.5, 3.6, and 3.7 compare the quality of the contention–aware association game against two other association policies, under the very same setting of Table 3.3. Namely, $ShortestPath$ refers to the case where the STA chooses the access point closest to the gateway, whereas the $Closest$ association policy

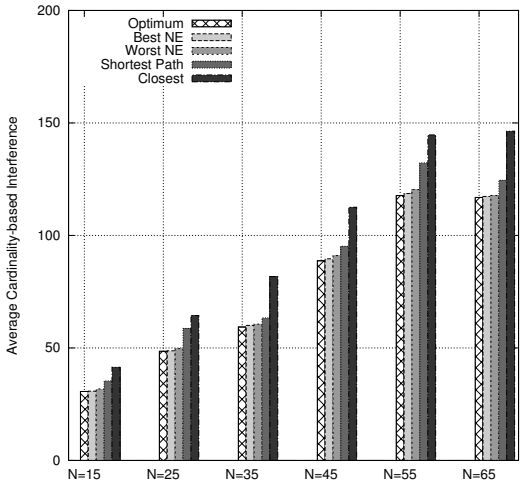

Figure 3.5: Average perceived interference under different association policies for WMNs with 6 access points, 10 mesh routers and 3 gateways.

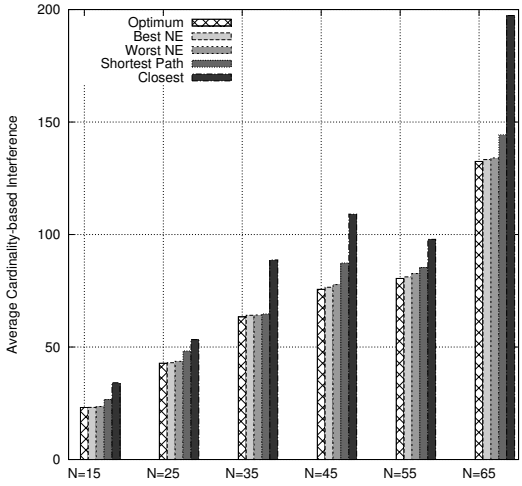

Figure 3.6: Average perceived interference under different association policies for WMNs with 7 access points, 10 mesh routers and 3 gateways.

favors the access point closest to the STA. The figures report the average interference perceived by the STAs. As expected, the equilibria of the contention–aware association game provide an association cost close to the optimum, whereas "interference–agnostic" association strategies always lead to higher association costs.

3.4.3 Equilibria under Airtime–Based Cost Function

Similar results have been obtained for games featuring the airtime–based cost function. Table 3.5 reports the PoS and PoA for WMNs of different sizes. As in the case of cardinality–based cost function, the NE of the

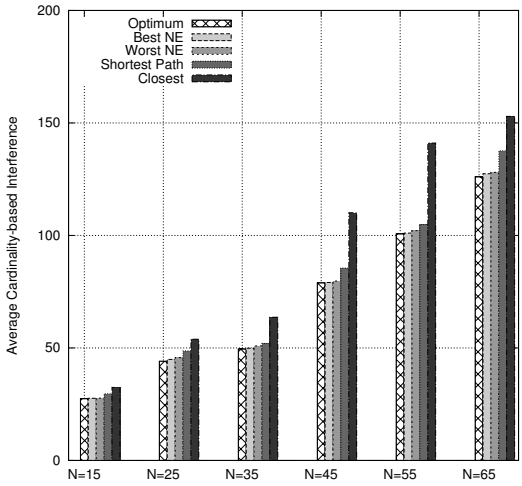

Figure 3.7: Average perceived interference under different association policies for WMNs with 8 access points, 10 mesh routers and 3 gateways.

Table 3.5: PoS and PoA for network topologies with variable number of access points, 10 mesh routers and 3 gateways under different number of STAs.

		N=15	**N=25**	**N=35**	**N=45**	**N=55**	**N=65**
6 APs	*PoS*	1.002	1.003	1.006	1.005	1.001	1.003
	PoA	1.005	1.005	1.004	1.007	1.002	1.004
7 APs	*PoS*	1.003	1.002	1.002	1.004	1.005	1.002
	PoA	1.005	1.003	1.004	1.005	1.007	1.003
8 APs	*PoS*	1.004	1.005	1.006	1.001	1.001	1.003
	PoA	1.009	1.007	1.008	1.002	1.002	1.004

WMNAG are pretty close to the optimum, that is, also considering the more general cost function based on the airtime, the competitive dynamic among the STAs leads to solutions which are very close to the "social" optimum.

Figures 3.8, 3.9, and 3.10 compare the average association cost (average airtime) for different association strategies. As clear from the figures, the NE of the WMNAG are characterized by association costs which are extremely close to the social optimum. On the other hand, the other association policies perform poorly leading to an increase in the association cost (and consequently in the perceived airtime) which can go up to 40%. Notably, the association cost increases with the number of STAs in the network.

Finally, it is worth analyzing the case where multiple orthogonal channels can be used in the wireless backbone. A behavior similar to the one with a single channel has been observed in the multichannel case with respect to the PoS and PoA. On the other hand, the availability of multiple channels allows one to

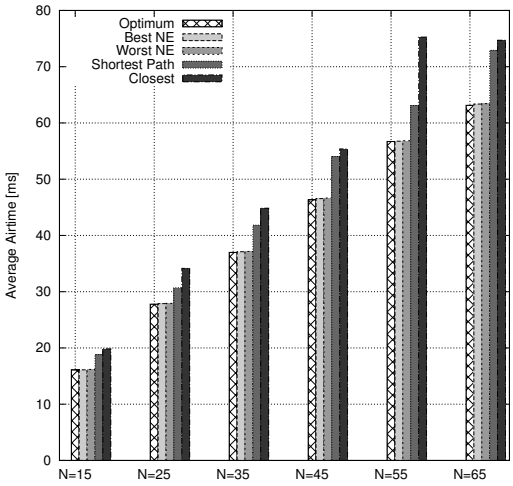

Figure 3.8: Average perceived airtime under different association policies for WMNs with 6 access points, 10 mesh routers and 3 gateways.

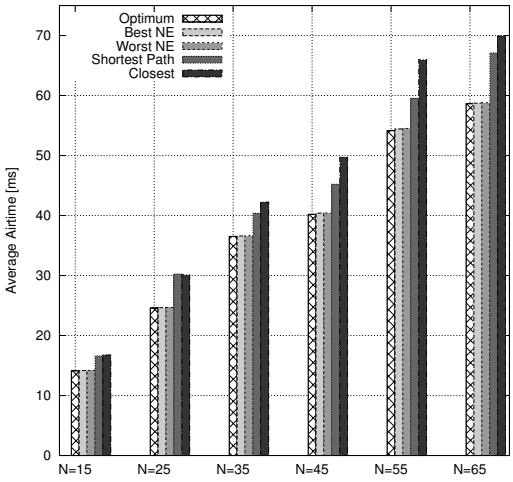

Figure 3.9: Average perceived airtime under different association policies for WMNs with 7 access points, 10 mesh routers and 3 gateways.

reduce the interference among multi–hop paths in the wireless backbone. Figures 3.11, 3.12, and 3.13 report the average association cost (airtime) perceived by the end STAs under different association policies. As expected, the average perceived cumulative airtime in the case of multiple channels (four channels in the wireless backbone) is lower than in the single channel case. Moreover, interference–agnostic association strategies lead to higher association costs with respect to airtime–based association metrics.

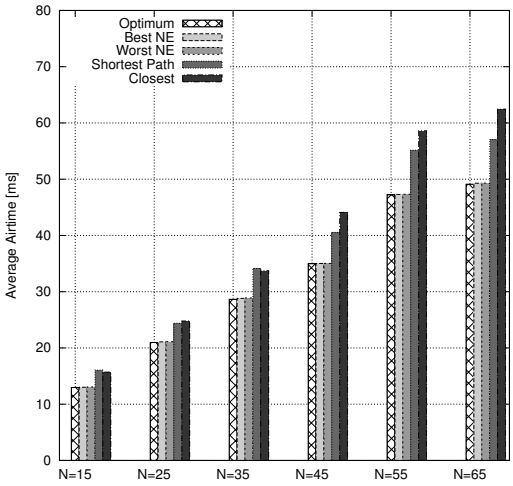

Figure 3.10: Average perceived airtime under different association policies for WMNs with 8 access points, 10 mesh routers and 3 gateways.

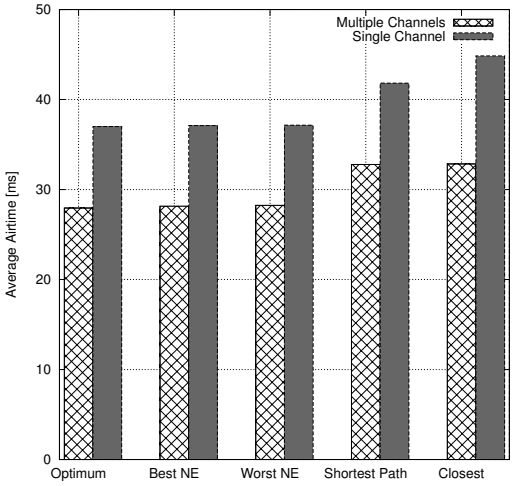

Figure 3.11: Average perceived airtime under different association policies for WMNs with 6 access points, 35 STAs, 3 gateways and 10 mesh routers.

3.4.4 The Technology for All Test Case

In order to analyze a realistic scenario, we consider the network topology of the Technology For All (TFA) initiative [1]. The network topology is reported in Figure 3.14.

Such topology features 17 access points and mesh routers, and 4 gateways[5]. 50 and 75 STAs have been drawn randomly in the network area (circles in FigureFigureFigure 3.14) and the presented results

[5]The real TFA topology features 1 gateway directly connected through dedicated point–to–point links to three more "remote gateways". For the sake of the association dynamics, we have considered the additional "remote gateways" as gateways.

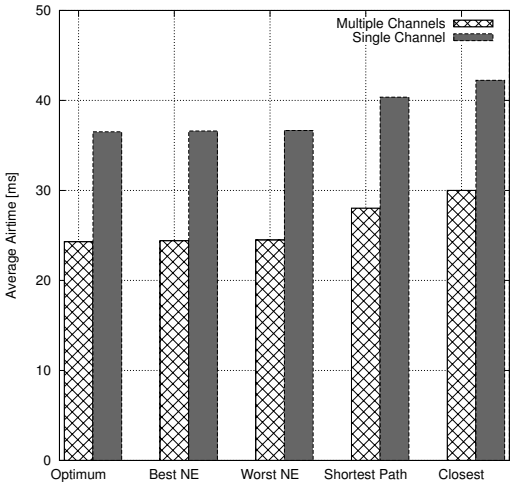

Figure 3.12: Average perceived airtime under different association policies for WMNs with 7 access points, 35 STAs, 3 gateways and 10 mesh routers.

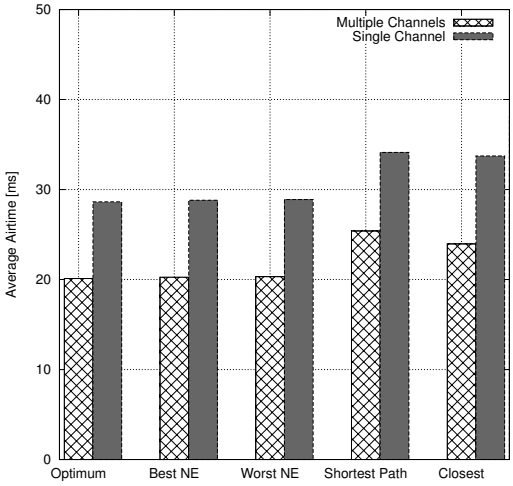

Figure 3.13: Average perceived airtime under different association policies for WMNs with 8 access points, 35 STAs, 3 gateways and 10 mesh routers.

are averaged over 20 STAs deployments. Each STA has, on average, 2.5 access point to associate to.

Figure 3.15 provides the simulation results. The graphs confirm the existing gap in terms of association cost among the different association strategies. As expected, interference–agnostic association strategies can increase the association cost up to 60% ($N = 75$ and $Closest$ association policy).

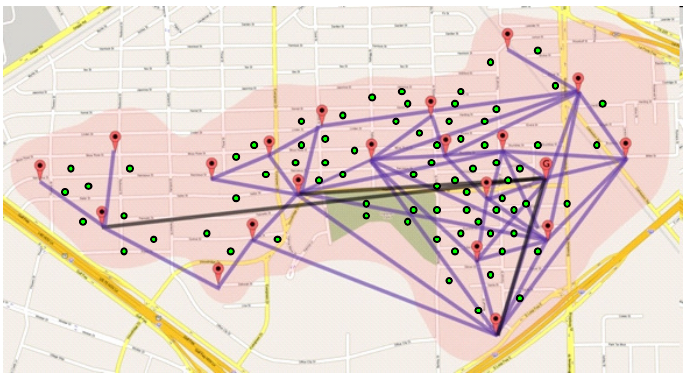

Figure 3.14: Reference TFA Network Scenario [1].

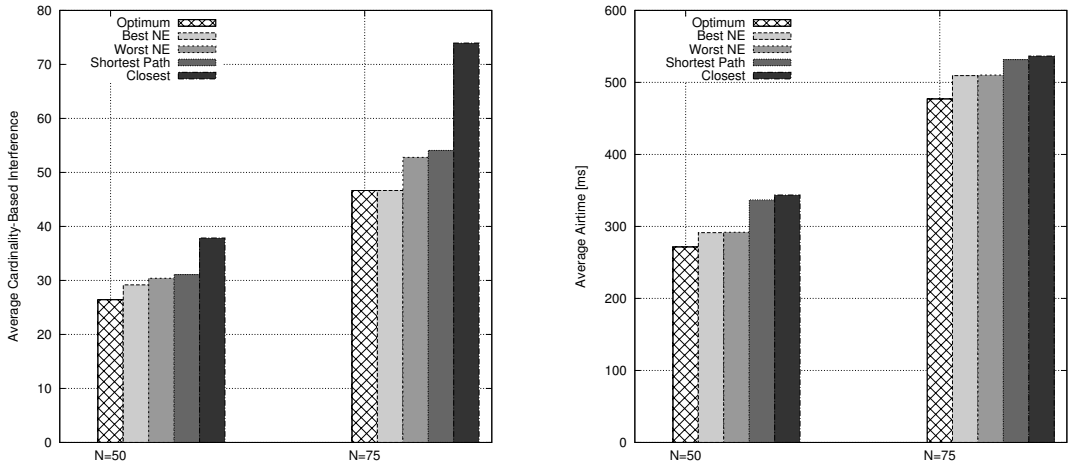

Figure 3.15: Average association cost under different association policies for both the cardinality–based (left) and the airtime–based (right) cost function.

3.5 Concluding Remarks

In this chapter, we have analyzed the dynamics of network association in Wireless Mesh Networks by resorting to game theoretic tools. Namely, we have formalized the association problem as a non–cooperative game in which STAs selfishly play to minimize a perceived association cost accounting for the path length and the path interference to reach the gateway. We have further proposed two metrics to measure the path interference based on the number of interfering devices along the path and on the airtime parameters. A quantitative framework has been proposed to determine and characterize the Nash equilibria of the aforementioned game under the two interference metrics. The simulation results derived for sample network topologies suggest that the game features equilibria which are pretty close to the optimal (centralized) association pattern.

Publications: [75], [76]

Chapter 4: Joint Access Selection and Resource Allocation

In previous chapters, we have discussed how the proliferation of wireless access technologies, and the evolution of the end–user terminals are leading fast towards a ubiquitous, pervasive and rich connectivity offer, such that the end users will be always connected/covered by multiple access networks/technologies. This scenario creates new opportunities and poses novel challenges not only on the end user side (*network selection* problem), as highlighted so far, but also on the network side. In fact, network operators have to tackle a *resource allocation* problem which requires the proper setting/planning of the available radio resources (e.g., frequencies, time–slots, spreading codes, etc.) throughout their deployed access network infrastructures. The resource allocation driving criteria may include the maximization of the overall revenues for the operator, the maximization of the provided geographical coverage, and/or the maximization of the network spectral efficiency, under tight/loose constraints on the quality perceived by the accessing users.

In this chapter, we study how the competition among different network operators influences the game of the users both in the NSG and in the WMNAG. In the first case, we assume that networks (i.e., access points) can choose among different frequencies in order to maximize the number of connected users. In the second game, we consider that operators compete among themselves to capture the largest number of accessing STAs by properly setting the multi–hop paths in their managed WMN backbones. In both cases, we formalize the resource allocation as a *multi–leader/multi–follower two–stage game* where in the first stage the network operators (i.e., the leaders) play by choosing their resource allocation strategies, while in the second stage the users/STAs (i.e., the followers) play the network selection/association game described in the two previous chapters.

We first consider the NSG (Sec. 4.2). We formally prove that when the quality measure adopted by the users only depends on the interference level, the two–stage game always admits a pure strategy subgame perfect Nash equilibrium, whereas under the other two quality measures it may not exist. In these latter cases, we leverage the concept of ϵ–subgame perfect equilibrium to find suboptimal equilibrium situations. We provide a mathematical programming model to solve the two–stage game. Finally we assess the quality

of the SPEs through experimental evaluation. Then we consider the WMNAG (Sec. 4.3). We formalize the two–stage game. We show that any subgame perfect equilibrium for this game is Pareto optimal. Finally, we develop a solution method based on the enumeration of all the operators strategies, to characterize the equilibria of this game.

This chapter is organized as follows: Sec. 4.1 discusses previous work related to the resource allocation problem. In Sec. 4.2, we present the two–stage game for the NSG presented in Chapter 2. In Sec. 4.3, we discuss the two–stage game for the WMNAG presented in Chapter 3. Concluding remarks are reported in Sec. 4.4.

4.1 Related Work

Game theory has been widely used to address resource allocation problems. Niyato and Hossain propose in [18] a game–theoretic approach for studying bandwidth allocation in heterogeneous wireless networks. Different from our work, the focus is on resource allocation only, and the problem is cast as a bankruptcy (cooperative) game where different networks form a coalition to provide bandwidth to the end users. The concepts of *core* and *Shapely value* are used to determine the quality of the bandwidth allocation. A cooperative game is used in [77] to model the allocation of bandwidth within the several access technologies further managing the distribution of excess bandwidth among operators.

Non–cooperative games are used in the field of resource allocation in [78], [18], [9] and [79]. In [78] the focus is on the problem of bandwidth allocation in 802.16–like networks, whereas, reference [18] introduces a non–cooperative game to model the interactions of different access networks (WLAN, cellular systems and WMAN). In this work, the authors derive both long–term and short–term criteria to allocate bandwidth within different technologies to incoming users. A similar non–cooperative scenario in the field of resource allocation is addressed in [79] which addresses the competition of WLANs sharing unlicensed frequency bands. A stage-based noncooperative game is proposed to analyze competition scenarios between two wireless networks.

The aforementioned manuscripts either assume cooperation among network operators, or only focus on the resource allocation problem. Different than the reference literature, we extend the network selection model to include operators in the competitive dynamics.

4.2 Network Selection Resource Allocation Game

Consider the reference scenario introduced in Sec. 2.2.1. In general, an operator may own and run several network devices (APs) to cover different–sized areas. Hereafter, we start off by considering a simplified case where a network operator only owns a single AP[1], which may well represent those cases where the area to be covered is limited (conference rooms, hotel lounges, etc.) and multiple APs (belonging to multiple operators) may be concurrently deployed to provide connectivity. This slightly simplified but consistent scenario allows us to get insightful results on the dynamics of the competition among operators. To this end, we introduce a two–stage game model capturing also the competition among the operators. We further provide the mathematical model to solve the game, and finally discuss some numerical results, considering the different cost functions from the user side.

The game we consider has two groups of players: users and operators. We assume that the two groups of players do not "play" simultaneously and decisions times are decoupled. Therefore, we are dealing with a (multi–leader/multi–follower) two–stage game. First, operators (i.e., the leaders) compete selecting the most convenient frequency. Then, users (i.e., the followers) react to the APs' actions, selecting the best frequency/AP. The user game, once that frequencies have been fixed, is the same described in Sec. 2.2. Each user tries to minimize a given cost function, $c_u(f, x_u^f)$, selecting the "best" frequency. In contrast, APs try to maximize the number of connected users by operating at the most convenient frequency.

As mentioned before, the equilibrium concept adopted for multi–stage games is the *subgame perfect equilibrium* (SPE), which can be qualitatively defined as the strategy profile (for leader(s) and follower(s)) which is a NE of every subgame of the original game [8]

In Sec. 2.2, we show that a pure strategy equilibrium for the user game always exists, regardless of the specific cost function. In contrast, the existence of a pure strategy SPE for the two–stage game is guaranteed only when users adopt cost function 1. In particular, the following propositions hold true.

Proposition 4.2.1. *The two–stage game in which users play with cost function* 1 *always admits a pure strategy SPE.*

Proof. Call n the number of users and m the number of operators. First, assume that all the operators have

[1] In this section we will refer to network 'operator' and 'AP' indifferently.

m available frequencies. We can prove that there is always an SPE in which all the operators use a different frequency. Assume that all the operators choose different frequencies and call f the frequency of operator a. If it changes its frequency, then there is always at least an assignment of users to operators that is a NE of the second stage of the game such that a does not gain more rather than by using f. To show that, call f' the new frequency of a. When there is no operator using frequency f' whose coverage area overlaps with the coverage area of a, the cost of all the users in the coverage area of a is the same when a uses f and f', and therefore no additional user connects a when it uses f'. When there is at least an operator, say a', using frequency f', then all the users selecting f' are indifferent between connecting a or a' and therefore there is an assignment of users to operators such that a, when using f', gains exactly as when it uses f.

When operators have less than m available frequencies, the proof is by mathematical induction. The basis of the induction is the setting with two operators. It is easy to see that, for every combination of frequencies available to the operators, a pure strategy SPE exists. The inductive step is to show that, given a setting that admits a pure strategy SPE and adding a new operator, the new setting admits at least a pure strategy SPE. □

Proposition 4.2.2. *The two–stage game in which users play with cost function* 2 *may not admit any pure strategy SPE.*

Proof. The proof is by a counterexample. Consider a scenario with two operators a and a' that can choose either the same frequency or different ones. A user u_1 is covered only by a and thus it will be connected to a. Another user u_2 is in the overlapping coverage region between a and a', and thus it can decide between a and a'. The rate parameters for u_1 and u_2 are such that: $T^a_{u_2} < T^{a'}_{u_2} < 2T^a_{u_2}$ and $T^a_{u_1} = 3T^a_{u_2}$. If the two operators decide to use the same frequency, user u_2 chooses a, since $c_{u_2}(a) = T^a_{u_2}(T^a_{u_1} + T^a_{u_2}) < c_{u_2}(a') = T^{a'}_{u_2}(T^a_{u_1} + T^{a'}_{u_2})$. In this case, a and a' have two and zero users, respectively. If the two operators decide to use different frequency, user u_2 chooses a', since $c_{u_2}(a) = T^a_{u_2}(T^a_{u_1} + T^a_{u_2}) = (2T^a_{u_2})^2 > c_{u_2}(a') = (T^{a'}_{u_2})^2$. The operators have one user each. It is clear that networks keep changing their frequencies since a wants to use the same frequency of a', but a' replies switching to a different one. Therefore, the game does not admit any pure strategy SPE. □

Proposition 4.2.3. *The two–stage game in which users play with cost function* 3 *may not admit any pure strategy SPE.*

The proof is omitted, being similar to the proof of Proposition 4.2.2. Therefore, for the two–stage game, with cost functions 2 and 3, the equilibrium is not guaranteed to always exist.

However, we have shown in Sec. 2.4, that from the user side, these two functions lead to better performance, in terms of both throughput and fairness. In order to characterize stable states for the two–stage game even when users adopt functions 2 and 3, we introduce the concept of (pure strategy) ϵ–NE and (pure strategy) ϵ–SPE. In our two–stage game model, given that the equilibrium non–existence problem is due to the first stage game, we allow operators to play in the first stage game an ϵ–NE, while we force users to play in the second stage games a pure strategy NE.

4.2.1 Mathematical Programming Model

We extend the mathematical programming formulation presented in Sec. 2.3 to solve the two–stage game. The computation of an SPE requires the computation of the NEs of all the possible subgames. We denote by γ a single subgame and by Γ the set of all the subgames. With a slight abuse of notation, we denote by $\gamma(s_{a_1}, \ldots, s_{a_m})$ the specific subgame induced by operators' action profile $(s_{a_1}, \ldots, s_{a_m})$. Note that in each subgame γ the frequency assignment is fixed, then the problem is the same as described in Sec. 2.2. For the case of two operators, i.e., $A = \{a_1, a_2\}$ and two frequencies, i.e., $F = \{f_1, f_2\}$, it is possible to identify four different subgames. Namely, at the stage of the operators, we can have the following cases: a_1 and a_2 choose the same frequency, either f_1 or f_2, or the two operators choose different frequencies (a_1 selects f_1 and a_2 selects f_2 or the opposite).

We can state the extended mathematical programming formulation. Parameter b_{ua} remains unchanged,

instead the other parameters depend also on subgame γ as:

$$d_{uf}^{\gamma} = \begin{cases} 1 & \text{if } u \text{ can select } f \text{ in } \gamma \\ 0 & \text{otherwise} \end{cases}$$

$$t_{af}^{\gamma} = \begin{cases} 1 & \text{if } a \text{ transmits on } f \text{ in } \gamma \\ 0 & \text{otherwise} \end{cases}$$

$$i_{uu'f}^{\gamma} = \begin{cases} 1 & \text{if } u \text{ and } u' \text{ interfere on } f \text{ in } \gamma \\ 0 & \text{otherwise} \end{cases}$$

Indeed, these parameters have the same meaning of the corresponding parameters previously introduced, with the exception that in this case they are valid only for a specific subgame γ. With the same approach, we extend the variables on the basis of γ as:

$$y_{uf}^{\gamma} = \begin{cases} 1 & \text{if } u \text{ chooses } f \text{ in } \gamma \\ 0 & \text{otherwise} \end{cases}$$

$$s_{ua}^{\gamma} = \begin{cases} 1 & \text{if } u \text{ chooses } a \text{ in } \gamma \\ 0 & \text{otherwise} \end{cases}$$

For each user u, we define the congestion level:

$$(z_u^f)^{\gamma} = \sum_{v \in U} \omega_v^f y_{vf}^{\gamma} i_{uvf}^{\gamma}$$

that is the congestion level perceived by u when selects f in γ. Similarly, we define the number of users associated to each AP, corresponding in this case to the variable that each AP a wants to maximize:

$$n_a^{\gamma} = \sum_{u \in U} s_{ua}^{\gamma}$$

Furthermore, we introduce a binary variable for every subgame γ that assumes a value of one only when γ is on the SPE path as:

$$h^{\gamma} = \begin{cases} 1 & \text{if } \gamma \text{ is on the equilibrium path} \\ 0 & \text{otherwise} \end{cases}$$

We now describe the constraints of the model. A subset of the constraints are the same of the users' game described in Sec. 2.2–2.3. In particular, the following feasibility constraints guarantee that each user selects only one network and one frequency per subgame γ.

$$\sum_{a \in A_u} s_{ua}^{\gamma} = 1 \qquad \forall\, u \in U, \gamma \in \Gamma$$

$$\sum_{f \in F_u} y_{uf}^{\gamma} = 1 \qquad \forall\, u \in U, \gamma \in \Gamma$$

$$s_{ua}^{\gamma} t_{af}^{\gamma} \leq y_{uf}^{\gamma} \qquad \forall\, u \in U, f \in F, a \in A, \gamma \in \Gamma$$

And similarly, we define the NE constraints for the users, for each subgame γ:

$$d_{uk}^{\gamma} y_{uf}^{\gamma} c_u \left(f, (z_u^f)^{\gamma}\right) \leq c_u \left(k, (z_u^k)^{\gamma}\right) \qquad \begin{array}{r} \forall u \in U, f, \\ k \neq f \in F, \gamma \in \Gamma \end{array}$$

We need now to define the equilibrium constraints of the operators on the basis of the users' actions in all the subgames. Since, as shown in the previous section, a two–stage game may not admit any SPE in pure strategies, we need to search for the best ϵ–NE (i.e., with the minimum value of ϵ) for the first–stage game, obtaining thus an ϵ–SPE for the whole game. Given a value of ϵ, the ϵ–Nash constraints for the operators are:

$$n_a^{\gamma} + \epsilon \geq n_a^{\gamma'} h^{\gamma} \qquad \begin{array}{r} \forall\, a \in A, \gamma(s_a, s_{-a}) \in \Gamma, \\ \gamma'(s'_a, s_{-a}) \in \Gamma \end{array} \tag{4.1}$$

that is, at the (approximate) equilibrium (identified by $h^{\gamma} = 1$) operator a cannot gain more than ϵ by

(unilaterally) changing its action. We need to force that there is one (approximate) equilibrium:

$$\sum_{\gamma \in \Gamma} h^{\gamma} = 1$$

Finally, we want to select the best approximate equilibrium by minimizing the value of ϵ under the constraint that it is non–negative:

$$\begin{aligned} \min \quad & \epsilon \\ \text{s.t.} \quad & \epsilon \geq 0 \end{aligned}$$

Although the above formulation has non–linear constraints, it can be cast as a mixed–integer linear formulation.

4.2.2 Experimental Evaluation

We evaluate hereafter the two–stage game. In particular, we first address the existence of SPEs and the quality of the approximate SPEs, then we quantify the impact of the competition among networks onto the users' perceived access costs.

Existence of SPEs and Approximation Degree

We focus on the existence of (pure strategy) SPEs with cost functions 2 and 3 and on the characterization of the best ϵ–Nash approximation degree we can obtain. Cost function 1 is not considered in this analysis, since Proposition 4.2.1 assures the existence of SPEs. To derive SPEs and approximated SPEs, the linear model discussed in Sec. 4.2.1 is formalized in AMPL and solved through CPLEX. To get a tractable but insightful scenario, we have exhaustively analyzed cases with two operators and two available frequencies with variable number of users (from 2 to 100). All the results are averaged on 100 randomly generated instances.

First, we evaluate the fraction of games not admitting any SPE. Results for cost functions 2 and 3 are reported in Figure 4.1. The non–existence fraction may be significative ($> 40\%$ with 100 users) under both cost functions, and generally increases with the number of users. Cost function 3 grants better results than cost function 2. As clear from the proof of Proposition 4.2.2, the non–existence is due to the relative positions of

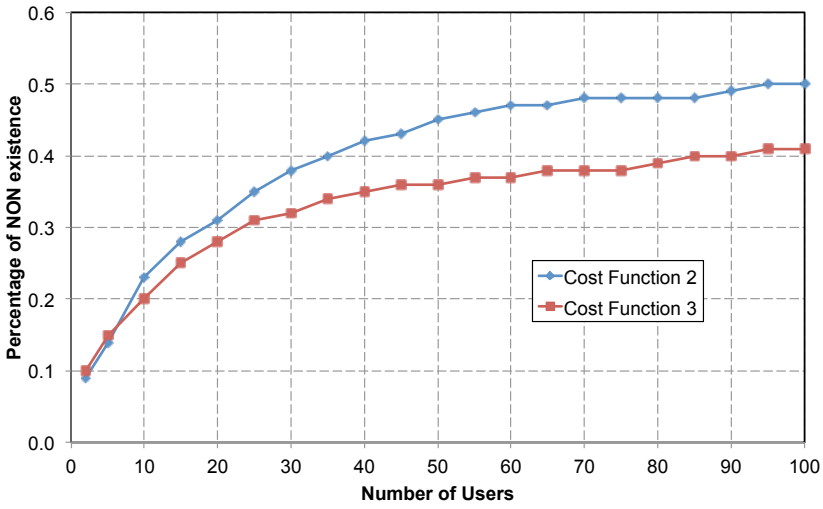

Figure 4.1: Percentage of non–existence of any SPE (in pure strategies).

APs and users. We conjecture that cost function 2 presents a space of relative positions (for which equilibrium does not exist) wider than cost function 3.

Second, it is worth studying the approximation degree of ϵ–SPE equilibria. To this end, we are interested in the ϵ–SPEs with minimum ϵ. For both cost functions, we evaluate the average minimum ϵ (Figure 4.2) and the average minimum ϵ, normalized on the maximum number of users achievable by each network (Figure 4.3). The former measures the number of users each network looses, whereas the latter measures the number of users each network looses with respect to all the potential users. In both figures, the very same parameters are reported only for those cases with ϵ strictly larger than zero (i.e., those cases where the games admitting equilibrium in pure strategy exists are not considered). The two cost functions provide very similar results. We observe that, increasing the number of users, ϵ increases. This reflects the fact that each network loses a larger number of users at the ϵ–SPE as the number of users increases. However, the normalized ϵ tends to zero asymptotically, which means that the loss due to equilibria approximation becomes negligible as the users population increases.

Quality of the ϵ–SPEs for the Users

We evaluate the efficiency of (approximate) equilibria in terms of users' social costs to understand how the competition between operators affects PoS. In our analysis, we do not consider the operators' utility, since

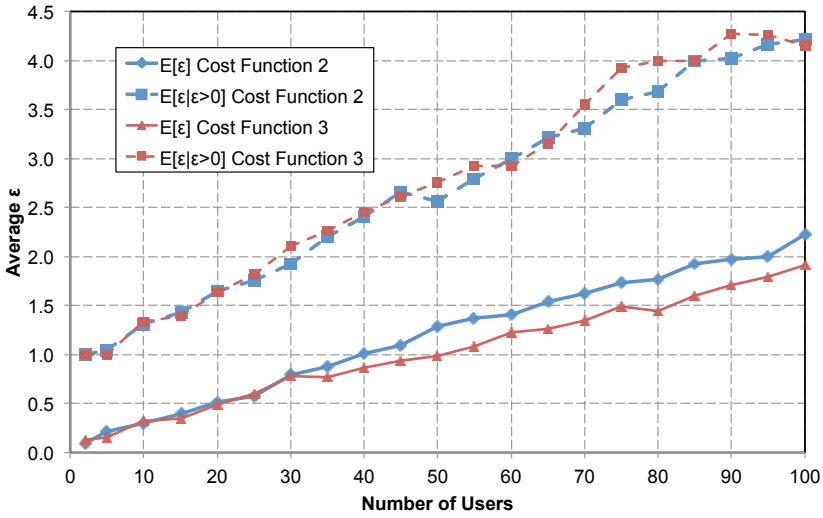

Figure 4.2: Average minimum value of ϵ.

every equilibrium is Pareto efficient for the operators (we have indeed that the operators utilities sum up to the total number of users).

As done before, we consider a scenario with two networks and two available frequencies and an increasing number of users. Furthermore, we do not consider cost function 1 since, under this scenario, there always exists an SPE in which operators use different frequencies (that corresponds to the situation in which PoS is minimum). Under the same settings as in the previous section, we find the optimal (approximate) equilibrium for the users among those that minimize ϵ. In addition, we find the equilibria of the users' game when operators are forced to play different frequencies (corresponding to the case in which the users' cost is minimum) and the same frequency (corresponding to the case in which the users' cost is maximum), respectively.

Figure 4.4 and Figure 4.5 report the average number of interferers and the average T (inverse of the rate) per users, respectively; Figure 4.6 shows the average cost per user calculated according to cost functions 2 and 3 for the equilibria of games played according to cost function 2 and 3. Two different scales are used for the values of the two different cost functions. The results have been scaled such that the lines corresponding to the situations in which operators use the same frequency with cost functions 2 and 3 overlap and the same when operators use different frequencies.

The main result is that the competition among operators affects the cost of the users. In fact, even if the

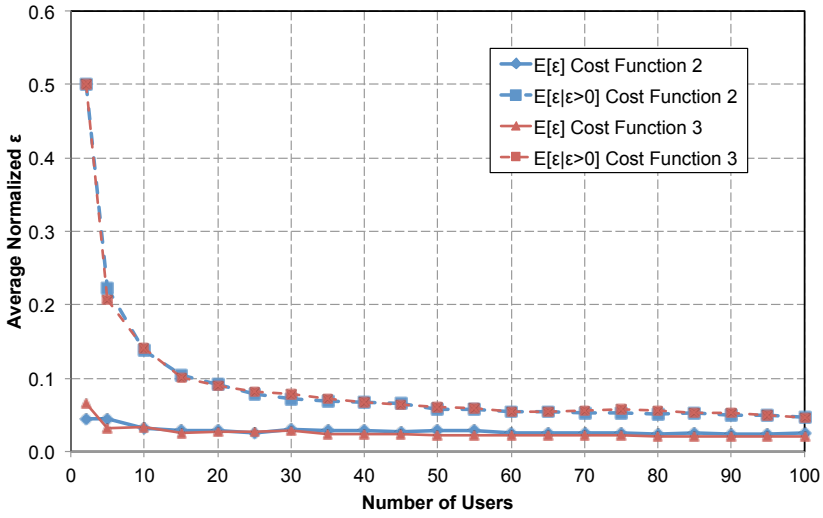

Figure 4.3: Average normalized minimum value of ϵ.

rate is close to the case where different frequencies are used, the number of interferers increases. This leads to an increase in the users-perceived cost of 16% for cost function 3 and 10% for cost function 2. This result is confirmed by the evaluation of the actual throughput (by Ns2 based simulations) that shows a behavior similar to the curves in Figure 4.6 (and, due to this, omitted here).

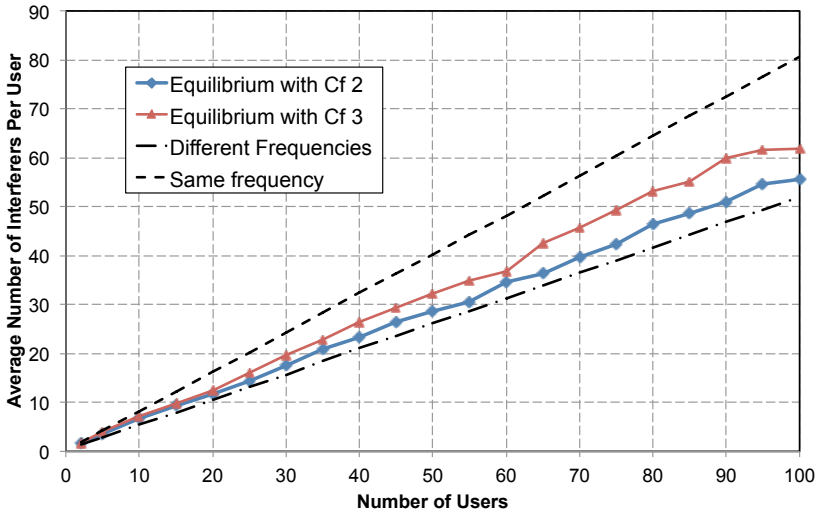

Figure 4.4: Average number of interferers per user.

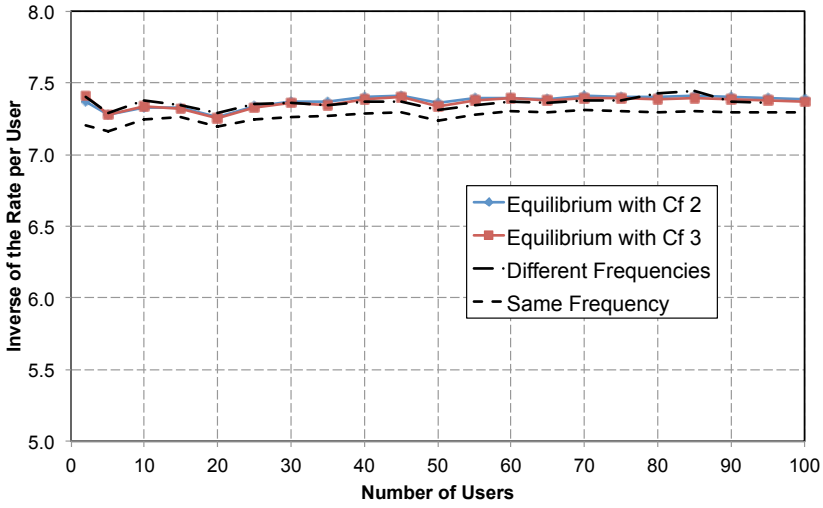

Figure 4.5: Average inverse of rate per user.

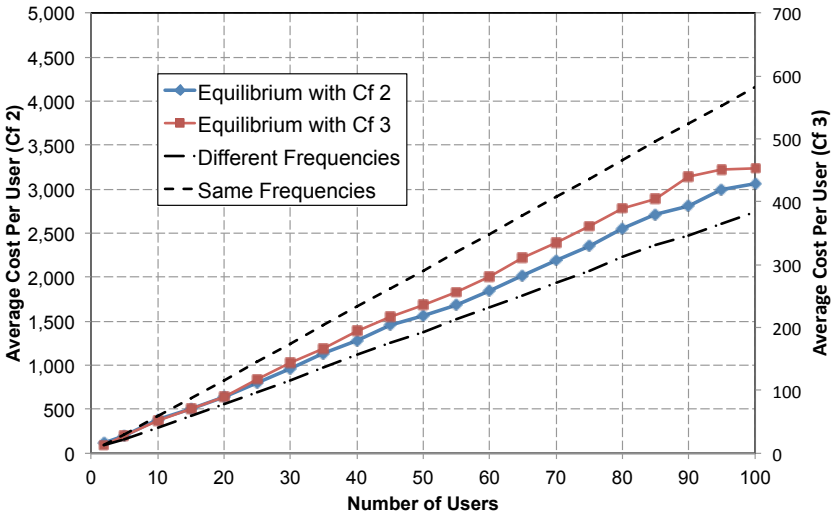

Figure 4.6: Average cost per user.

4.3 WMN Association Resource Allocation Game

In this section, we consider the reference scenario presented in Sec. 3.2.1. In that case, the focus was on the association given static WMN topologies. Namely, routing paths were fixed between the access points and the gateways; thus, the STAs, by choosing the access point to associate, inherently choose also the routing path towards the gateways. However, in practical settings, the specific route from each access point to a gateway is usually determined by the routing protocol/policy implemented in the wireless backbone by the network operator. As an example, the network operator may choose the gateway to act as a traffic sink, or may eventually favor specific multi–hop paths [2].

To this extent, it is reasonable to assume that multiple paths are available from each access point towards a gateway, or, similarly, that the network operator may choose a specific gateway among multiple opportunities to route the traffic collected by a given access point. Such decision may have the purpose to balance the load among the gateways of the WMN, or, in a competitive scenario with multiple WMN operators in the same arena, to "capture" the larger number of customers (STAs) by offering paths with higher quality.

Hereafter, we focus on the latter competitive scenario, and drop the assumption of a fixed routing pattern in the wireless mesh network. Each WMN operator owns a set of access points, mesh routers, and a given number of gateways in the wireless backbone. Multiple operators compete with the target to maximize their own revenues (number of customers) by properly setting the "best" path from the operated AP to one of the available gateways.

As done in Section 3.2 for the association problem, we can model the WMN operators competition as a game. Let O be the set of operators. For each operator $j \in O$, let S_j be the *strategy set*, that is the set of multi–hop paths which can be offered by operator j. The *strategy space* S is the set of all the possible combinations of strategies played by the WMN operators, i.e., $S = S_1 \times S_2 \times \cdots \times S_n$. An element $S \in S$, S=$(S_1, S_2, \ldots, S_n)$ with $S_j \in S_j$, is a *strategy profile*. We can formally define the **Bi–Level Association Game (BiAG)** as:

$$\text{BiAG} = \langle O, S, \{p_j(S, WMNAG)\}_{j \in O} \rangle. \tag{4.2}$$

It is further reasonable to decouple the decision time of end STAs and network operator, by assuming that

[2] e.g., to implement load balancing techniques at the gateways and/or at the wireless mesh routers.

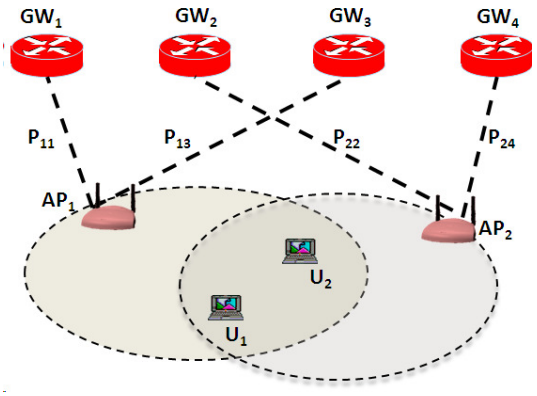

Figure 4.7: Sample WMN scenario with two operators (access points) each one with two available paths.

WMN operators play their strategies first, whereas end STAs play the association game right after, being the WMN operators' actions fully observable by the end STAs [3]. The BiAG belongs to the class of multi–stage games: namely, it is a multi–leader, multi–follower game where leaders are the network operators choosing their routing pattern, whereas followers are the STAs, playing the underlying association game.

The payoffs for the STAs are the ones defined in Section 3.2, whereas the payoffs for the generic WMN operator j associated to the strategy profile S, $p_j(S, WMNAG)$, can be defined as the number of STAs which decide to associate to the network of operator j under the operators' strategy profile S. Consequently, the payoffs of the game among the network operators depend on the underlying WMNAG, i.e., the association game played by the STAs.

Figure 4.7 depicts a scenario with two operators owning one access point each providing connectivity to STAs U_1 and U_2. Two multi–hop paths (dashed line) to a couple of gateways are available from each access point (operator). Operator 1's strategy set is composed of paths P_{11} towards gateway 1 and P_{13} towards gateway 3. Similarly, the strategy set of operator 2 is composed of paths P_{22} and P_{24}. The paths composing the strategy sets of the operators may be generally composed of multiple wireless network devices which can interfere one another.

Therefore, referring to the example reported in Figure 4.7, the two operators have to choose first which path to activate from their operated access points, and then the two STAs have to play the association game

[3]The assumption is reasonable given the different dynamics involved in the two processes of network configuration and STA association. Usually, network configuration has longer dynamics than user association.

defined in Section 3.2.

As done before, we are interested in characterizing the SPEs for the two–stage game. It can be easily shown that:

Theorem 4.3.1. *Any subgame perfect equilibrium for BiAG is Pareto optimal for the network operators.*

Proof. The proof comes from the observation that for every strategy profile of the operators the payoffs of the operators sums up to the total number of STAs. Consequently, given a NE point for the BiAG, it cannot exist another strategy profile where the payoff of some operators improves without decreasing the payoff of any other operator. By contradiction, if such strategy profile existed, some operators would get a higher number of assigned STAs and the others would get the same number of STAs. This leads to a greater sum of payoffs, that corresponds to a greater number of STAs, which contradicts the starting assumption. □ □

To find and characterize the equilibria of the BiAG for small size instances, we develop a solution method based on the enumeration of all the operators strategies. Namely, for each point of the strategy space S, we find the WMNAG equilibria using the technique proposed in Section 3.3. Algorithm (1) formalizes the solution procedure in a pseudo–code. Each iteration of the **for** cycle in Algorithm (1) requires the solution

Algorithm 1 Solve BiAG

```
1: for S ∈ S do
2:     Solve WMNAG(S)
3: end for
4: Search for Operators Equilibria
```

of the WMNAG which leads to association relations among STAs and access points. The quality of such assignment is then evaluated with respect to the operators utility, thus determining the NE of the overall BiAG.

From the operators point of view, a strategy profile is a Nash equilibrium if there is no player (i.e., operator) which has incentive in modifying its strategy unilaterally. Therefore, a strategy profile $S = (S_j, \mathbf{S_{-j}})$ is a Nash equilibrium for the operators if and only if:

$$p_j((S_j, \mathbf{S_{-j}}), WMNAG) \geq p_j((S_j^*, \mathbf{S_{-j}}), WMNAG)$$

$$\forall \quad S_j^* \in S_j, \qquad \forall \quad j \in O,$$

where S_j is the strategy played by operator j, and $\mathbf{S_{-j}}$ indicates the set of strategies played by all the other operators but j.

From the considerations above, the procedure to determine the Nash Equilibria of the BiAG can be formalized in the following Algorithm (2). We have applied the solution method to sample network scenarios

Algorithm 2 Search for Operators Equilibria

```
1:  S_eq = {∅}
2:  for S = (S_j, S_-j) ∈ S do
3:     flag = 1
4:     for j ∈ O do
5:        for S_j^* ∈ S_j do
6:           if !(p_j((S_j, S_-j), WMNAG) ≥ p_j((S_j^*, S_-j), WMNAG)) then
7:              flag = 0
8:           end if
9:        end for
10:    end for
11:    if flag = 1 then
12:       S_eq += S
13:    end if
14: end for
15: Return S_eq
```

featuring 2 and 3 operators owning one access point each, and being able to activate 2 and 3 paths towards gateways. The number of mesh routers in all the topologies has been fixed to 5 for each operator, whereas the number of STAs has been varied from 15 to 45. All the STAs can access all the access points in the scenario.

Table 4.1 reports the cost ratio among the equilibrium and the local optimum. The local optimum represents the solution in which, fixed the strategies of the access points, the cost perceived by the users is optimized. The ratio is very close to one. This is consistent with the fact that PoS and PoA for the single stage game (WMNAG) are very close to one.

Table 4.2 reports the cost ratio among the equilibrium and the global optimum where all the choices (routing patterns and association) are globally optimized to reduce the STAs perceived cost. This measure reflects the cost increase perceived by the STAs due to the double competition among operators and among STAs themselves. Similarly to the WMNAG, the quality of the subgame perfect equilibria is close to the global optimum. However, the network configuration with 3 operators (access points) and 3 paths for each

operator features a slightly higher cost increase for the STA which can go up to 30%.

Table 4.1: Characteristics of the BiAG Nash equilibria. Cost ratio at the equilibrium versus the local optimum.

	N=15	**N=25**	**N=35**	**N=45**
2x2	1.005	1.000	1.004	1.006
2x3	1.013	1.006	1.007	1.001
3x2	1.025	1.001	1.014	1.004
3x3	1.004	1.003	1.002	1.005

Table 4.2: Characteristics of the BiAG Nash equilibria. Cost ratio at the equilibrium versus the global optimum.

	N=15	**N=25**	**N=35**	**N=45**
2x2	1.005	1.010	1.006	1.006
2x3	1.163	1.014	1.008	1.001
3x2	1.161	1.009	1.109	1.028
3x3	1.018	1.093	1.110	1.303

4.4 Concluding Remarks

In this chapter, we have discussed how the NSG and the WMNAG can be extended in order to include also the operators in the competition process. In both cases, we proposed a two–stage game model where operators play first by competitively choosing their strategies (i.e., frequencies or routing patterns) to capture the highest number of end users, which, in turn, play the network selection/association games in the second stage of the game.

In the network selection resource allocation game, each operator dynamically plans its radio resources. Formal results on the existence of subgame perfect equilibria have been derived for all the game instances. Even if the proposed two–stage game may not always admit any pure strategy equilibrium, it is possible to enforce approximated equilibria with a quality loss reasonably small ($< 3\%$). Thus, the proposed game model can be suitably adopted to represent and drive the dynamics of practical network scenarios. Finally, we have shown that competition among operators increases the inefficiency of the equilibria for the users in two out of three cost functions.

In the WMN association game, the network operators are allowed to set and modify the routing patterns in the WMN backbone to capture the highest number of associating users. Numerical evaluations have shown that the Nash subgame perfect equilibria of the multi–leader, multi–follower game are very close to the global

optimal solution.

Publications: [55], [56], [76]

Chapter 5: Spectrum Sharing Games in a Time–Varying Scenario

Differently from previous chapters, hereafter we consider the spectrum sharing problem, where users compete for different portion of the spectrum. In particular, this scenario perfectly fits in the Cognitive Radio Networking (CRN) paradigm [80], where cognitive devices [81] are allowed to opportunistically access vast portions of the spectrum in order to enhance spectrum utilization. To reach such ambitious goal, cognitive terminals must be geared with enhanced *spectrum management* capabilities (i.e., spectrum sensing, spectrum decision, spectrum sharing, spectrum mobility).

In particular, we consider a CRN scenario where greedy and selfish secondary users opportunistically exploit the spectrum portions vacated by primary users. To this extent, we propose a non–cooperative game theoretic framework to study the inherent competition among secondary users in the cognitive spectrum selection process. Namely, the proposed framework accounts for: *(i)* the time–varying radio environment in terms of availability and quality of the spectrum portions (*spectrum decision*); *(ii)* the interference among secondary users (*spectrum sharing*); *(iii)* the cost associated to spectrum handover (*spectrum mobility*).

We take here a constructive approach by analyzing, at first, a static game in which *spectrum mobility* is neglected, and secondary users evaluate different spectrum opportunities, considering both the quality–of–service and the corresponding congestion level. This model is a straightforward extension of the game models presented in Chapter 2. Different quality measures for the spectrum opportunities are considered and evaluated in the game framework, including the spectrum bandwidth, and the spectrum opportunity holding time. The cost of spectrum mobility is also accounted in the analytical framework. Numerical results are reported to assess the quality of the game equilibria.

Then, we move to a dynamic game formulation which accounts for the temporal evolution of the system, the corresponding time–varying primary users activity, and the costs associated to spectrum mobility.

The chapter is organized as follows: in Sec. 5.1, we briefly overview previous works on the issue of spectrum management, highlighting the novelty of our contribution. In Sec. 5.2 we present the static (one–shot) game, whereas in Sec. 5.3 we formalize the repeated game. Concluding remarks are reported in Sec. 5.4.

5.1 Related Work

The problem of spectrum management has been widely investigated in the last few years, especially focusing on the different functionalities of the cognitive cycle. The main issues of spectrum sensing are highlighted in [82], whereas an optimal framework is proposed in [83] with the aim of addressing both the interference avoidance and the spectrum efficiency problem. In [84], the concept of *time–spectrum block* is introduced to model the spectrum allocation problem in cognitive networks, and a distributed protocol is presented to enable users to share the spectrum holes. The problem of spectrum management is addressed also in [85], where a central spectrum policy server coordinates spectrum demands, whereas distributed approaches are adopted in [86] and in [87]. A comprehensive survey is provided in [88].

As pointed out in [88], the issue of spectrum decision, which is of paramount importance to determine the success of CRNs, is still scarcely addressed in the literature, with the notably exception of [89] and [90]. In [89], spectrum matching algorithms are presented to support QoS for cognitive radio users. The spectrum decision is based on statistical characteristics of spectrum bands. In [90], the authors propose and compare three schemes for frequency channel selection that are based on the load and interference perceived in each channel by users. In our work, we follow a similar approach, but, in addition, we analyze the interaction among users and the temporal evolution of the system.

Most of the aforementioned work addresses the problem of spectrum management proposing protocols and algorithms aimed at handling specific functionalities of cognitive nodes. Differently, we provide here a comprehensive theoretical framework to analyze the spectrum management problem. Since we thoroughly resort to game theory, it is worth commenting on other game theoretic approaches applied to cognitive radio networks. Solutions resorting to game theory for modeling the interactions among cognitive users in sharing the same spectrum portions may be generally distinguished with respect to the inspiration of the game models they resort to; namely, in cooperative and non–cooperative game models.

Cooperative game models assume the cooperation among users, who decide to coordinate each other in order to maximize the global utility of the system. In [91], the authors analyze a multi–hop wireless scenario where nodes need to agree on a fair allocation of spectrum. In [92], the authors focus on the spectrum access problem, and propose a resource allocation algorithm to maximize spectrum efficiency. Both these works

leverage the concept of Nash Bargaining Solution to guarantee fairness and optimality. Nevertheless, in several network scenarios, the cooperation among users postulates the existence of a common control channel to be used to distribute cooperation signalling traffic. On the other side, works based on non–cooperative game models drop the cooperation assumption and study competitive scenarios where players are selfish entities. As an example, the authors of [19] cast the spectrum sharing as a non cooperative game, and derive general guidelines to implement local (and greedy) algorithms to drive the sharing decision of the users. Similarly, in this chapter we target non–cooperative scenarios where the secondary cognitive users act selfishly to maximize local utility functions. Different from the aforementioned piece of work, we include in the game formulation also aspects of spectrum decision and spectrum mobility, besides spectrum sharing ones.

A relevant aspect that can be further considered in the definition of secondary users strategies is the temporal evolution of the system. This can be modeled using extensive–form games. In [3], the authors propose non–cooperative repeated game in which users leverage the outcome of previous game stages to improve their own revenues. Another interesting solution is presented in [17], where the authors model the problem of spectrum sharing as an oligopoly market competition and use a Cournot game to obtain the spectrum allocation for secondary users. Since users are supposed to have partial knowledge on other users' strategies, an extensive–form game is proposed, in which players adapt their strategies by observing the evolution of the game. Different from these valuable approaches, we consider the variability of the underlying primary users, which forces time varying access strategies (Spectrum OPportunities, SOPs) for the secondary users (players), and we characterize the temporal evolution of the spectrum management process by secondary users.

5.2 Spectrum Selection Game

5.2.1 The reference scenario

We consider a scenario composed of primary and secondary users sharing a given portion of the spectrum, which is subdivided into orthogonal channels (sub–bands), throughout the chapter referred to as Spectrum OPportunities (SOP) (see Figure 5.1). Each primary user is licensed to transmit arbitrarily on a specific sub–band (SOP). Time is divided into epochs which can be defined as the time period where the activity of

primary users does not change[1,2]. Secondary users can opportunistically access to SOP which are vacant in a given epoch, with the firm constraint to handover whenever the SOP gets occupied by a licensed primary user.

For the sake of presentation, the interference relations among users can be modeled through interference ranges, i.e., when two users are closer than these ranges, they interfere. If a primary user is transmitting on a given SOP, any secondary user which is closer than the primary interference range (R_p) must remain silent on that SOP. In a similar way, two secondary users do interfere when transmitting on the same SOP if they are closer than the secondary interference range (R_s).

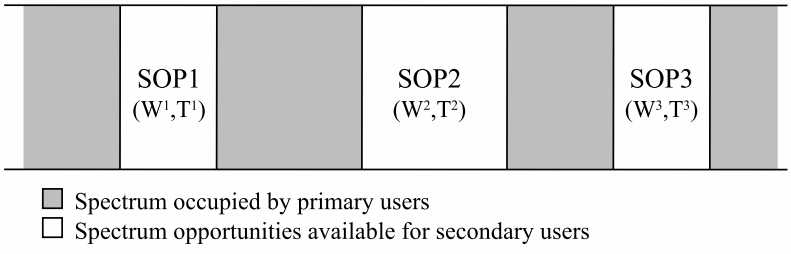

Figure 5.1: Example of spectrum opportunities characterized by different parameters (e.g., bandwidth W and holding time T).

We denote by B the set of SOPs, by N the set of secondary users, and by B_i ($i \in N$) the subset of spectrum opportunities available for secondary user i, i.e., SOP with no primary users or with an active primary user that is out of primary interference range. In a time–varying scenario, due to the primary activity, the set B_i can change at each epoch. The activity of each primary user is modeled as a binary traffic source driven by the evolution of a two–state Markov chain, with parameters p_j, probability for primary user j to become active given that it was not active at the previous epoch, and q_j, probability to deactivate given that it was active in the previous epoch. Finally, we denote by N_i the subset of secondary users that interfere with i.

5.2.2 The game theoretic model

In our game model, the secondary users are the players and their strategy space is composed of the available SOPs. As done in previous models, we assume each user to be rational, choosing the SOP that maximizes the perceived quality–of–service (QoS), which depends on the features of each SOP, in terms of SOP bandwidth

[1] Conversely, the primary users' activities can change from epoch to epoch.

[2] Note that we are not concerned here with the timescale of epochs, which depends on the time variability of the primary users' activity.

and SOP congestion, i.e., number of other users sharing the same SOP. Furthermore, we associate to each possible strategy (available SOP) a cost function $c_i(k, x_i^k)$ that is specific for user i, for the chosen spectrum opportunity k and, in general, depends on the aforementioned factors (i.e., spectrum opportunity characteristics). Moreover, $c_i(k, x_i^k)$ is monotonically increasing in x_i^k, that is the congestion level of resource k perceived by user i (number of users selecting SOP k and belonging to N_i).

The **Spectrum Selection Game (SSG)** can be formally defined as:

$$SSG = \langle N, \{B_i\}_{i \in N}, \{c_i(k, x_i^k)\}_{i \in N, k \in B_i} \rangle.$$

It can be shown that SSG belongs to the class of *congestion games* [12]. Specifically, it can be reduced to a *crowding game* [45], i.e., a *single–choice* (each player selects only one resource) congestion game with *player–specific* cost functions (each player can have a different cost function, with the constraint to be increasing in the level of congestion). Moreover, the game is *non–weighted*, since users congest the resources with the same weight and with linear cost functions. We report the proof in Appendix B. From this equivalence it directly comes that also our game does admit at least one pure–strategy Nash equilibrium [45] for any cost function $c_i(k, x_i^k)$ that is increasing in the level of the congestion. Therefore, we can safely limit us to search for pure strategy equilibria.

5.2.3 Cost Functions

As done before, we compare different cost functions. The functions that we are considering for the SSG are very similar to the ones introduced for the NSG. First, we consider the case where the number of users sharing the same SOP is known. In this case, users may select a SOP on the basis of a cost function that depends on the number of interferers. Formally, we have the following interference–based cost function:

$$c_i(k, x_i^k) = x_i^k \tag{5.1}$$

Furthermore, other pieces of information may be available at the secondary users; as an example, SUs may get to know the nominal bandwidth associated to the given SOPs, as well as the average SOP availability

time. This information can be obtained by the secondary users through direct observations of the channel, and/or implementing some type of predicting/learning techniques. In this work, we are not concerned on how the information can be obtained, but, on the other end, we aim at evaluating the impact of this further knowledge on the secondary users spectrum management policies.

Since we are dealing with cost functions, we consider parameters that are in inverse proportion to SOP quality parameters, the bandwidth and the holding time (the larger the bandwidth and the holding time, the lower the cost function). In general, these parameters are *user–specific*, i.e., they are different for each user. For this reason, we introduce the parameter W_i^k, that is in inverse proportion to the bandwidth that user i can obtain from SOP k, and T_i^k, that is in inverse proportion to the average holding time of SOP k for user i.

We consider two different cost functions that include the number of interferers, the bandwidth and the expected holding time. The first cost function is just a linear combination of the three factors (interference, bandwidth and holding time):

$$c_i(k, x_i^k) = \lambda_i x_i^k W_i^k + (1 - \lambda_i) T_i^k \tag{5.2}$$

The first term represents the inverse of the portion of bandwidth perceived by each user, that is the total available bandwidth divided among x_i^k users (we recall that W_i^k is proportional to the inverse of the bandwidth). The second term is simply the expected holding time. The weights λ_i represent the preference of user i to the bandwidth with respect to the holding time.

The second cost function we consider is the product of the three defined parameters:

$$c_i(k, x_i^k) = x_i^k W_i^k T_i^k \tag{5.3}$$

The reason for which we consider (and compare) both these two functions is that, a priori, we cannot say which one is better from the users' perspective. In fact, we can observe that cost function (5.3) represents the total amount of bandwidth that can be used by each user, defined as: $[\text{Bandwidth} \cdot \text{Time}/\text{Interfering Users}]$, whereas cost function (5.2) does not reflect this property. On the other side, cost function (5.2) allows users to give a preference between bandwidth and holding time, whereas the other does not.

5.2.4 Experimental Evaluation

The experimental setting used in our simulations is a network deployed on a square area with edge L, composed by m primary users and m corresponding bands, n secondary users and circular interference radii $R_p = R_s = r$. We have implemented an instance generator that randomly draws the position of users and generates primary traffic on the basis of activity parameter p_j.

For the sake of simplicity, we assume that spectrum characteristics are the same for all users, i.e., W_i^k and T_i^k do not depend on i, and secondary users have the same preference, i.e., the same weight λ.

Inspired by the simulation scenario used in [83], we classify available spectrum bands in six classes, resulting from the combination of *low/medium/high activity* and *low/high opportunity*. The level activity depends on p (the larger p, the higher activity) whereas high/low opportunity represent the spectrum bands with $p < q$ and $p > q$, respectively. Table 5.1 reports the parameters associated to each one of the $m = 18$ considered bands.

Clearly, the achievable throughput that a user can obtain using a specific SOP depends not only on the bandwidth, but also on other parameters related to the specific radio technology, such as the modulation scheme and the coding rate . In this scenario, we do not consider these transmission details, and we only make the reasonable assumption that the actual throughput is somehow proportional to the available bandwidth. Finally we remark that the average holding time can be calculated as the inverse of p. Given the average bandwidth and holding time, we derive parameters W^k and T^k as specified in Table 5.1.

As mentioned before, to study the quality of equilibria we evaluate the PoS and the PoA. To find the best/worst equilibrium and the optimal solution of our game we resort to a mathematical programming model, whose formulation is provided in Appendix C. We have formalized the problem with AMPL [51] and solved it with CPLEX commercial solver [52]. All the results reported are averaged on 100 randomly generated instances, varying the position of users, and varying the primary activity according to parameters reported in Table 5.1.

Table 5.2 shows the results obtained on a uniform topology with $n = 20$ secondary users, in case $L = 500$ and $r = 100$ meters. We report the average parameters ($\overline{x}_i^k$, $\overline{T}^k$, $\overline{W}^k$) obtained by users at the best Nash equilibrium solution, using the three proposed cost functions and varying λ for the function (5.2). Moreover,

we evaluate also the actual bandwidth [KHz] and the holding time [sec] perceived by users. Finally, to compare the best/worst equilibria with the optimal solution, we report the value of PoS and PoA.

We can observe that using cost function (5.1) only the number of interferers is minimized, whereas W^k and T^k are in general greater than one. On the other side, using cost function (5.2), we can give different weights to bandwidth and holding time, varying the value of λ. Finally, cost function (5.3) provides a good tradeoff among all the considered factors.

We can further observe that PoS and PoA are both very close to one. This means that there is no difference, in terms of social cost, between the optimal solution, that could be reached with a coordination among users, and the equilibria that users reach playing selfishly.

In Figure 5.2 we report the probability for a generic secondary user to occupy one of the eighteen SOPs numbered as in Table 5.2. First, we can observe that using cost function (5.1) users spread almost evenly among different SOPs, since they are considered equal in terms of bandwidth and holding time. In contrast, using cost function (5.2) with $\lambda = 1$, users choose based on SOP's bandwidth and interference level only, thus high bandwidth SOPs are favored. Finally, using cost function (5.2) with $\lambda = 0.5$ and cost function (5.3), users take a tradeoff choice still favoring SOPs with high bandwidth and high holding time. In general, we can also observe that SOPs with lower activity are preferred by secondary users.

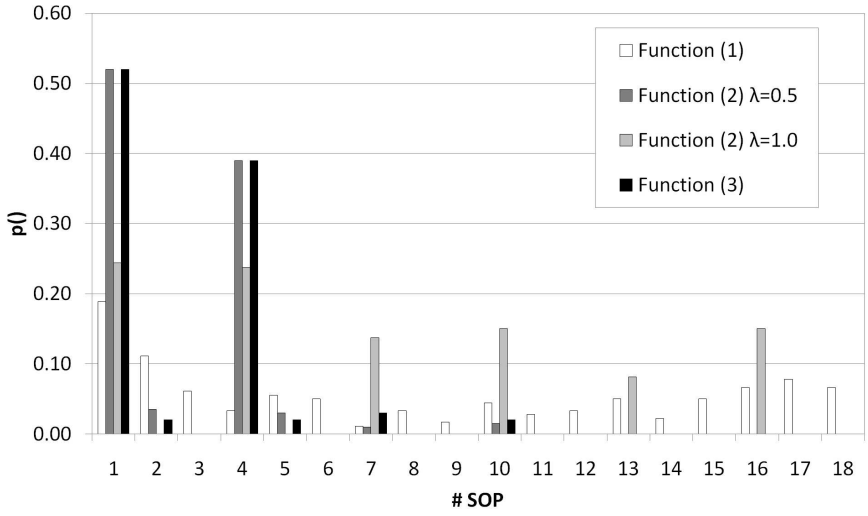

Figure 5.2: Probability for a generic secondary user to occupy one SOP when varying the cost function.

Table 5.1: Spectrum Opportunities Features

Spectrum Class	Low Activity						Medium Activity						High Activity					
	Low Opportunity			High Opportunity			Low Opportunity			High Opportunity			Low Opportunity			High Opportunity		
Spectrum band k	1	2	3	4	5	6	7	8	9	10	11	12	13	14	15	16	17	18
p	0.2	0.2	0.2	0.2	0.2	0.2	0.5	0.5	0.5	0.5	0.5	0.5	0.8	0.8	0.8	0.8	0.8	0.8
q	0.1	0.1	0.1	0.5	0.5	0.5	0.3	0.3	0.3	0.8	0.8	0.8	0.3	0.3	0.3	0.9	0.9	0.9
Bandwidth [KHz]	250	100	70	250	100	70	250	100	70	250	100	70	250	100	70	250	100	70
W^k	1	2.5	3.5	1	2.5	3.5	1	2.5	3.5	1	2.5	3.5	1	2.5	3.5	1	2.5	3.5
Holding Time [sec]	5	5	5	5	5	5	2	2	2	2	2	2	1.25	1.25	1.25	1.25	1.25	1.25
T^k	1	1	1	1	1	1	2.5	2.5	2.5	2.5	2.5	2.5	4	4	4	4	4	4

Table 5.2: Results obtained on a uniform topology with $n = 20$ secondary users, $L = 500$ and $r = 100$ meters

Cost Function	(5.1)	(5.2)											(5.3)
		$\lambda = 0$	0.1	0.2	0.3	0.4	0.5	0.6	0.7	0.8	0.9	1.0	
$\overline{x}_i^k$	1.000	3.250	1.220	1.220	1.220	1.220	1.220	1.030	1.030	1.000	1.000	1.000	1.220
$\overline{W}^k$	2.186	1.008	1.135	1.135	1.135	1.135	1.098	1.000	1.000	1.000	1.000	1.000	1.060
Bandwidth [*KHz*]	150.83	249.25	236.50	236.50	236.50	236.50	240.25	250.00	250.00	250.00	250.00	250.00	244.00
$\overline{T}^k$	2.250	1.000	1.000	1.000	1.000	1.000	1.038	1.278	1.278	1.323	1.323	2.125	1.075
Holding Time [*sec*]	3.250	5.000	5.000	5.000	5.000	5.000	4.925	4.445	4.445	4.389	4.389	3.270	4.850
PoS	1.000	1.000	1.004	1.008	1.012	1.015	1.025	1.004	1.006	1.000	1.000	1.000	1.043
PoA	1.000	1.000	1.030	1.059	1.086	1.111	1.116	1.206	1.091	1.042	1.022	1.000	1.092

5.3 Dynamic Spectrum Management as a Multi–Stage Game

In this section, we consider a time–varying scenario, as the one shown in Figure 5.3. In this case, secondary users are required not only to classify different SOPs and choose the best available one, but also to move to a new SOP whenever a primary user kicks in, or switching is still more convenient (*spectrum mobility*). In Sec. 5.3.1 we define the repeated game, proposing a new cost function that users can adopt playing the game. Then, in Sec. 5.3.2, we evaluate the performance of the proposed model.

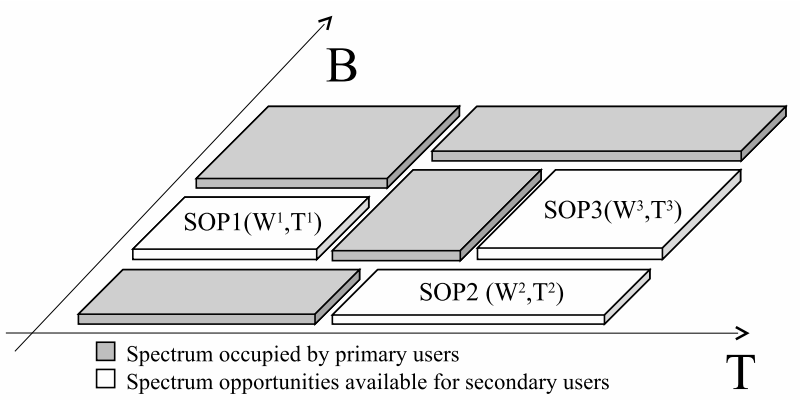

Figure 5.3: Example of spectrum opportunities in a time–varying scenario.

5.3.1 Game Model

To capture the temporal evolution of the system, we repeat the previous game, i.e., the *static game*, multiple times. We assume that time is divided into epochs, and at each epoch primary users can stochastically activate or deactivate as described in Sec. 5.2. In this way, the subset of SOPs available for each user can change. Playing the new stage of the game, we introduce a switching cost K_{mk}, that a user has to pay if it decides to change the spectrum opportunity from m to k. This cost can represent the switching delay experienced by a user switching over a wide frequency range. We assume $K_{mk} = 0$ whenever $m = k$, i.e., when user does not switch to a new SOP.

Therefore, the cost function each user tries to minimize is the following:

$$\widetilde{c}_i(k, x_i^k) = c_i(k, x_i^k) + K_{mk} \tag{5.4}$$

where m is the SOP used by the user i in the previous epoch and $c_i(k, x_i^k)$ may be anyone of the cost function previously defined. A multi–stage game is essentially an extensive–form game and therefore the appropriate solution concept is *subgame perfect equilibrium*, i.e., a strategy that is of equilibrium in each possible subgame. In our case, a subgame is representative of every possible state (e.g., characterized by primary users' activation and secondary users' undertaken actions) wherein the game can be. Due to the impressive number of possible subgames and the unavailability of information over the future states to users, the computation of a subgame perfect equilibrium is not practical in our case. Each user computes its optimal strategy on–line stage by stage on the basis of the past stages but ignoring the possible future evolution of the game.

5.3.2 Experimental Evaluation

We report here an experimental evaluation of the multi–stage game using a setting similar to the one used in Sec. 5.2.4. In this analysis, the instance generator randomly draws the position of users and generates primary traffic on the basis of activity parameters p_j and q_j over a time composed by E epochs.

We report here on the case in which users adopt the cost function (5.4), with $c_i(k, x_i^k)$ replaced by the function (5.3). Moreover, the switching cost is assumed to be fixed, namely $K_{mk} = K$, $\forall m, k \neq m \in B$, whereas $K_{mk} = 0$, $\forall m, k = m \in B$. We consider a simulation scenario composed by $n = 20$ secondary users, $m = 9$ primary users, using a subset of $m = 9$ spectrum opportunities defined in Table 5.1, and $E = 10$ epochs.

Figure 5.4 reports the comparison between the two cases where the best Nash equilibrium and the best solution (with respect to the social cost) are derived. Namely, the average cost function (5.3), the SOP quality (proportional to the inverse of (5.3) and defined as [Bandwidth $\cdot$ Time/Interfering Users]), and the average switching probability are plotted versus the switching cost in Figure 5.4.a, 5.4.b, and 5.4.c, respectively. Increasing the switching cost K, the average per–user cost $c_i(k, x_i^k)$ (i.e., without K) increases, whereas the average switching probability decreases. This means that the users tends to reduce the number of handovers, but "loosing" in terms of interference, bandwidth and holding time of the chosen SOP. Notably, the switching probability tends to zero as K keeps increasing. Finally, we observe that as the switching cost increases, the average SOP quality perceived by the secondary users decreases. In other words, secondary users tend to

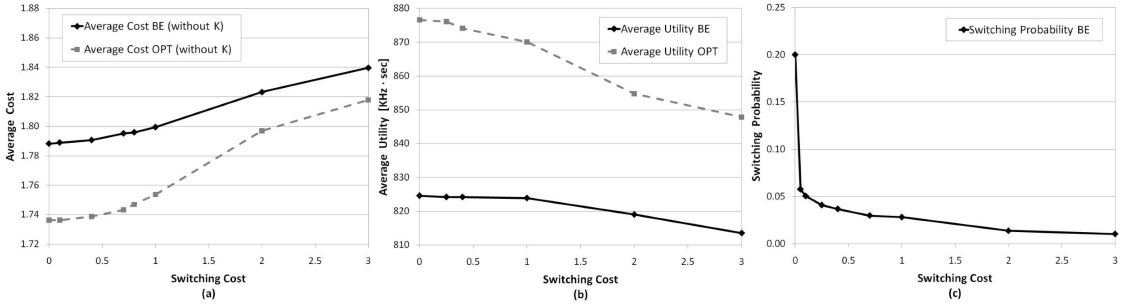

Figure 5.4: Average cost (a), Average SOP quality (b) and average switching probability (c) perceived by users at the best Nash equilibrium (BE) and at the optimal solution (OPT).

remain on the chosen SOP even if better ones become available, due to the high switching cost.

5.4 Concluding Remarks

In this chapter, we propose a framework to evaluate *spectrum management* functionalities in Cognitive Radio Networks. Since one of the most important aspects of cognitive terminals resides in their rationality, we resort to a game theoretical approach to model the spectrum access process among secondary users who can opportunistically select the "best" available channel without interfering primary users. The proposed framework can be adopted by secondary users in order to characterize different spectrum opportunities, share available bands with other users and evaluate the possibility to move in a new channel whenever it is necessary or convenient. Moreover, we consider a time varying scenario, where the cost of spectrum handover is introduced in the game. Numerical results show that, increasing the switching cost, the switching probability decreases. This means that secondary users tend to remain in their chosen SOP even if better ones become available.

Publications: [46]

Chapter 6: Two–Player Spectrum Sharing Game with Interference Model

In all the game models presented so far, the utility/cost function adopted by the users depends on other players strategies only in terms of congestion. In fact, in order to deal with tractable expressions of the perceived quality, we have always assumed that the throughput perceived by the user could be approximated by the ratio between the nominal throughput and the congestion, i.e., the number of users that are choosing the very same resource. However, this approximation could not reflect the "real" satisfaction perceived by the users. Therefore, we now introduce a new spectrum sharing game model, that differs from previous ones especially in the definition of the users' utility function. Namely, we adopt a specific interference model between users based on the distances between interfering nodes. Furthermore, we represent the quality perceived by each user using an expression for the achievable throughput that is based on the Shannon capacity.

Since we are dealing now with a more complicated game model, we first provide a complete framework for the 2–player case, i.e., two pairs of communicating users that share two bands of spectrum (Chapter 6). Then, we extend the analysis considering the more general case of N pairs of transmit–receive pairs in an *ad hoc* network (Chapter 7).

In particular, we consider a Gaussian interference game (GIG) [3], where two transmitter and receiver pairs (each pair being a player) spread power across two bands of spectrum, with each player subject to a sum power constraint. Each player's payoff function is the sum of the Shannon rate achieved on each band, where the Shannon rate is calculated assuming random Gaussian codebooks and where interference is treated as noise. Each pair of users makes selfish decisions regarding which portion of the spectrum to use. This corresponds to deciding how to split the total power budget for transmission among the two sub–channels. We model the problem as a non–cooperative game in which selfish users aim at maximizing the achieved throughput.

We consider first a symmetric scenario where the received normalized interference powers (X) are equal and the received normalized signal powers (D) are equal, so that the problem has only these two parameters. By this parameter reduction we are able to explicitly characterize allocations that are socially optimal as well

as all Nash equilibria, and thereby explicitly compute the Price–of–Stability (PoS) and Price–of–Anarchy (PoA) in terms of (X, D). We then consider an asymmetric scenario where the interference powers are unequal ($X_i \neq X_j$), and we characterize the socially optimal allocations and the Nash equilibria. Moreover, we study the stability of the Nash equilibria. Finally, we analyze the game using stochastic geometry. Analytical and numerical results show how this tool might be integrated in the analysis of the 2–player game.

The chapter is organized as follows: Sec. 6.1 reviews previous work, Sec. 6.2 presents the game model. Sec. 6.3 and Sec. 6.4 discuss the optimal solution and the equilibria of the game, respectively. Sec. 6.5 studies the problem using stochastic geometry. Sec. 6.6 concludes the chapter.

6.1 Related Work

This section overviews previous work related to the spectrum sharing problem with interference model. Sec. 6.1.1 discusses the optimal power allocation problem for both the single–user and the multi–user case. Sec. 6.1.2 reviews previous work on spectrum sharing games.

6.1.1 Optimal Power Allocation

Hereafter, we discuss the main literature about the non–convex problem of optimal power and spectrum management. We first describe the general model adopted by the considered reference, then we present the optimal sum rate allocation.

Model

We consider a scenario composed by N pairs of users (each one is a transmitter–receiver pair) that want to communicate sharing the same portion of spectrum. The Gaussian interference channel is model by:

$$r_i = h_{ii} s_i + \sum_{j \neq i} s_j h_{ji} + z_i$$

where s_i is the signal transmitted by transmitter i and r_i is the signal received by receiver i including both interference and additive Gaussian noise z_i. The direct and cross channel gains are represented by h_{ii} and h_{ij}, respectively.

Without loss of generality, hereafter we assume that the channel is over a unit bandwidth frequency

band $[0, 1]$. We assume that each user uses a random Gaussian codebook, and only decodes the signal from its own transmitter, treating interference from others as noise. Therefore, each user i has the following achievable rate:

$$R_i = \int_0^1 \log\left(1 + \frac{p_i(f)|h_{ii}(f)|^2}{\sigma_i(f) + \sum_{j\neq i} p_j(f)|h_{ji}(f)|^2}\right) df$$

where $h_{ii}(f)$ and $h_{ji}(f)$ denote the frequency selective channel gains, $\sigma_i(f)$ is the noise Power Spectral Density (PSD) and $p_i(f)$ is the PSD of user i. Reasonably, $h_{ji}(f)$, $\sigma_i(f)$ and $p_i(f)$ are assumed to be *piecewise bounded continuous functions* over the band $f \in [0, 1]$.

Finally, in order to handle with a simpler rate function, we consider the following normalization:

$$R_i = \int_0^1 \log\left(1 + \frac{p_i(f)}{n_i(f) + \sum_{j\neq i} p_j(f)\alpha_{ji}(f)}\right) df \tag{6.1}$$

where $\alpha_{ji}(f) \triangleq \frac{|h_{ji}(f)|^2}{|h_{ii}(f)|^2}$ and $n_i(f) \triangleq \frac{\sigma_i(f)}{|h_{ii}(f)|^2}$. Note that the assumption that all the selective functions are piecewise bounded continuous functions is important because it allows one to approximate them by piecewise constant functions, by subdividing the frequency band in a sufficiently large number of small pieces, and assuming these functions to be flat in each piece. Formally, this approximation is proved in [2] (see *Lemma 1*).

Optimal single–user power allocation: the waterfilling problem

Before going into the details of the optimal power allocation for a multi–user scenario, we recall the optimal solution for the single–user case. This problem is known as waterfilling problem [93]. As mentioned before, assume that we can divide the channel into a set of non–interfering sub–channels. In each sub–channel we assume the channel to be flat. The extension to a general frequency selective channel is straightforward [93].

The user has to decide how to split the total available power P among K sub–channels. Let P_k be the power allocated to the kth sub–channel (of bandwidth B_k). The optimal power allocation is the one that maximizes the sum of the rates achieved in each band subject to the power constraint $\sum_k P_k = P$. Note that the expression of the rate is the same given in Eq. (6.1), assuming that $\alpha_{ji} = 0 \; \forall \; i \neq j$. Furthermore, the integral is replaced by a sum over the K channels.

In this case, the optimization problem can be solved by Lagrangian methods. The optimal power alloca-

tion is:

$$P_k^* = \left(\frac{1}{\lambda} - n_k\right)^+$$

where we define $x^+ := \max(0, x)$ and n_k has the same meaning as in Eq. (6.1), i.e., it is the ratio between the noise power and the direct channel gain (inverse of the SNR). The Lagrangian multiplier λ is chosen such that the power constraint is satisfied.

The idea of the waterfilling is clearly explained in Figure 6.1. In each sub–band, the power is proportional to the perceived SNR (inverse of n_k). In particular, whenever two bands experience the same SNR, the power is the same. In contrast, when the noise in one band is too large, the user decide not to use that sub–channel, i.e., the power is zero.

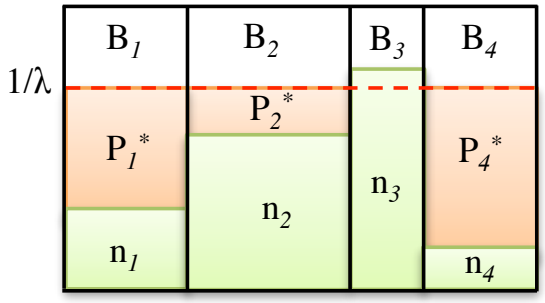

Figure 6.1: Waterfilling power allocation.

The waterfilling problem is a special case of the spectrum sharing problem that we are considering in this chapter. In fact, it considers only one user. This allows us to provide an explicit optimal allocation. Unfortunately, the problem is more complicated when we consider multiple users.

Optimal multi–user power allocation

We now provide an overview of the main results found in the literature that deal with the optimal solution for the multi–user case. As done also before, we assume that the optimal solution is the one that maximizes the sum of the rates of all the users. In general, this function is not the only one that could be maximized. A complete comparison of different objective functions for this problem is provided in [94].

All the following results are further based on the fact that there are essentially two co–existence strategies for users to reside in a common band: *frequency sharing* (FS) and *frequency division multiplexing* (FMD).

Formally, a frequency sharing (FS) scheme of N users is any power allocation in the form:

$$p_i(f) = p_i \qquad \forall\, f \in [0,1],\ \forall\, i = 1 \dots N$$

In contrast, a FDM scheme of N users is any power allocation in the form:

$$\begin{cases} p_i(f)p_j(f) = 0 \qquad \forall\, i \neq j \\ \sum_{i=1\dots N} p_i(f) = p \end{cases} \qquad \forall\, f \in [0,1]$$

The first result, proved in [2], establishes a sufficient condition for FDM to be optimal.

Theorem 6.1.1. *Consider a N–user frequency selective interference channel. If $\alpha_{ji}(f) \geq \frac{1}{2}$, $\forall\ j \neq i$, $\forall\ f \in [0,1]$, there always exists an FDM power allocation scheme, in which all users' rate are higher or unchanged (w.r.t. the FS power allocation scheme).*

Note that, even if the theorem only considers FDM vs. FS, it can be considered a sufficient condition for FDM being the optimal strategy (over all the possible strategies). This can be explained considering the flat approximation mentioned before. In fact, we can always approximate the PSD of a user as FDM or FS, eventually subdividing the band in a large number of small bands. A similar result has been derived also in [5]. A further extension is the following:

Theorem 6.1.2. *Consider a N–user frequency selective interference channel. For any two users i and j (among all the N users) and for any frequency band $[f_1, f_2]$, if $\alpha_{ji} \geq \frac{1}{2}$ and $\alpha_{ij} \geq \frac{1}{2}$, $\forall\ f \in [f_1, f_2]$, then FDM of user i and j leads to a higher payoff (w.r.t. the FS power allocation scheme) for all the N users.*

Note that since this condition guarantees that FDM benefits *all* the N users, under this condition, all the *Pareto optimal points* of the rate region can be achieved. In [3], the authors derive a similar condition:

Theorem 6.1.3. *Consider a N–user frequency selective interference channel. If $\alpha_{ji}\alpha_{ij} > 1$, then in any Pareto efficient power allocation $p_i(f)$ and $p_j(f)$ are orthogonal.*

In Figure 6.2, we compare the different thresholds provided in [2] and [3].

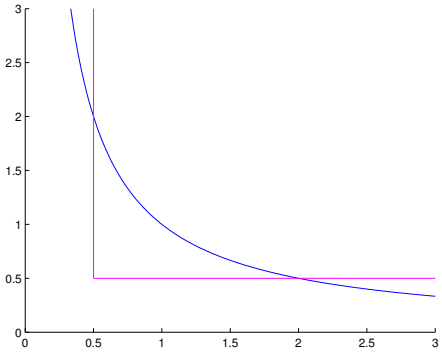

Figure 6.2: Comparison between threshold provided in [2] and [3].

In the following, we report the main results concerning the optimal solution of the maximum sum rate problem. We start with the simplest case: 2–user symmetric flat case. This represents the case in which 2 users share the same band, and such that $\alpha_{ji}(f) = \alpha_{ji}(f) = \alpha$ and $n_1(f) = n_2(f) = n = 1, \forall\ f \in [0, 1]$. This case is analyzed in [2].

Formally, the optimization problem is the following:

$$r^o(p) \triangleq \max_{p(f)} \int_0^1 \log\left(1 + \frac{p_1(f)}{1 + \alpha p_2(f)}\right) + \log\left(1 + \frac{p_2(f)}{1 + \alpha p_1(f)}\right)$$

$$\text{s. t.} \int_0^1 p_i(f)df \leq \frac{p}{2}, \quad i = 1, 2$$

$$p_1(f) \geq 0, p_2(f) \geq 0, \quad \forall\ f \in [0, 1]$$

Theorem 6.1.4. *The optimal solution for the* 2*–user symmetric flat case is the following:*

$$r^o(p) = r^*(p)$$

In particular:

$$r^*(p) \triangleq conv_p(r(p))$$

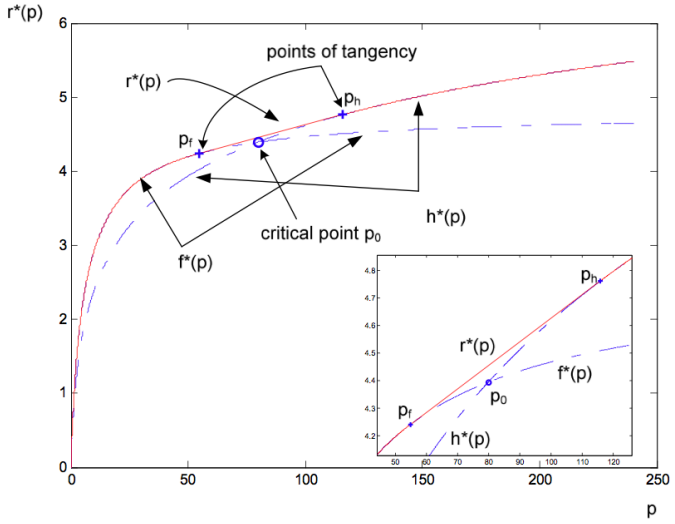

Figure 6.3: Optimal solution for the 2–user symmetric flat case [2] .

where $conv_p$ indicates the convex envelope and

$$r(p) \triangleq \max\{f^*(p), h^*(p)\} = \begin{cases} f^*(p) & \text{if } p \in [0, p_0] \\ h^*(p) & \text{if } p \in [p_0, \infty] \end{cases}$$

$$p_0 = 2\left(\frac{1}{2\alpha^2} - \frac{1}{\alpha}\right)$$

Finally, $f^*(p)$ ($h^*(p)$) is the optimal solution, when the optimization problem is solved with the constraint that only FS (FDM) scheme is available. The optimal solution is reported in Figure 6.3. In other words, when $0 < p \leq p_f$, the optimal scheme is FS. When $p \geq p_h$, the optimal scheme is FDM. When $p_f < p < p_h$ the optimal solution is achieved with a mixed scheme, as the one reported in Figure 6.4.

The optimal solution for the 2–user asymmetric flat case is analyzed in details in [4]. In contrast with the symmetric case, now there are five different regions at the optimal solution. Namely, the optimal solution changes with the total available power (or similarly the channel gains). When the power constraint is large, it is optimal to divide the total bandwidth into two orthogonal bands (FDM). When we have a small power constraint, FS is optimal. In the middle there are are three scenarios. The optimal solution has three bands, one shared and one used exclusively by each user. Otherwise, there are two bands: one shared and one used exclusively only by the user with the larger power constraint. These regions are reported in Fig 6.5.

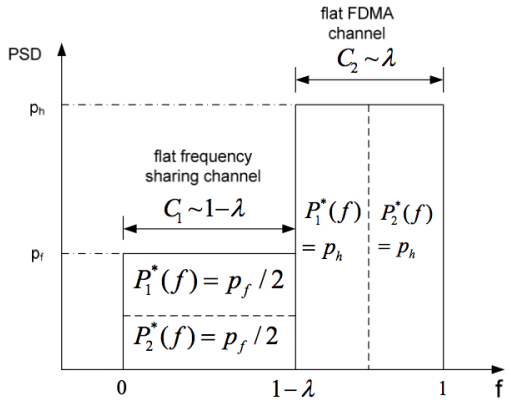

Figure 6.4: Mixed scheme to achieve the optimal solution when $p_f < p < p_h$ [2].

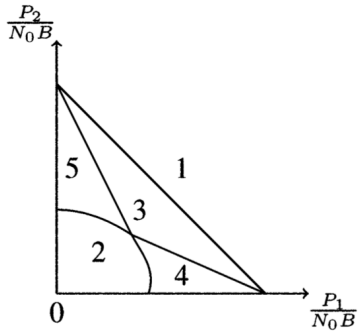

Figure 6.5: Optimal solution for the 2–user asymmetric flat case [4].

We now briefly discuss the extension of the 2–user symmetric flat case to the N–user case. Details are reported in [5]. In this case, the solution is a natural extension to the optimal solution presented in Figure 6.6.

We now conclude presenting the very general model (N–user asymmetric frequency selective), deeply analyzed in [2], in which the authors further assume that the objective function is an arbitrary weighted sum rate.

$$\max_{p(f)} \int_0^1 \sum_{i=1}^{N} \omega_i \log\left(1 + \frac{p_i(f)}{n_i(f) + \sum_{j \neq i} \alpha_{ji}(f) p_j(f)}\right)$$

$$\text{s. t.} \int_0^1 p_i(f) df \leq p, \;\; \forall\, i = 1 \ldots N$$

$$p_i(f) \geq 0, \;\; \forall\, f \in [0,1], \; \forall\, i = 1 \ldots N$$

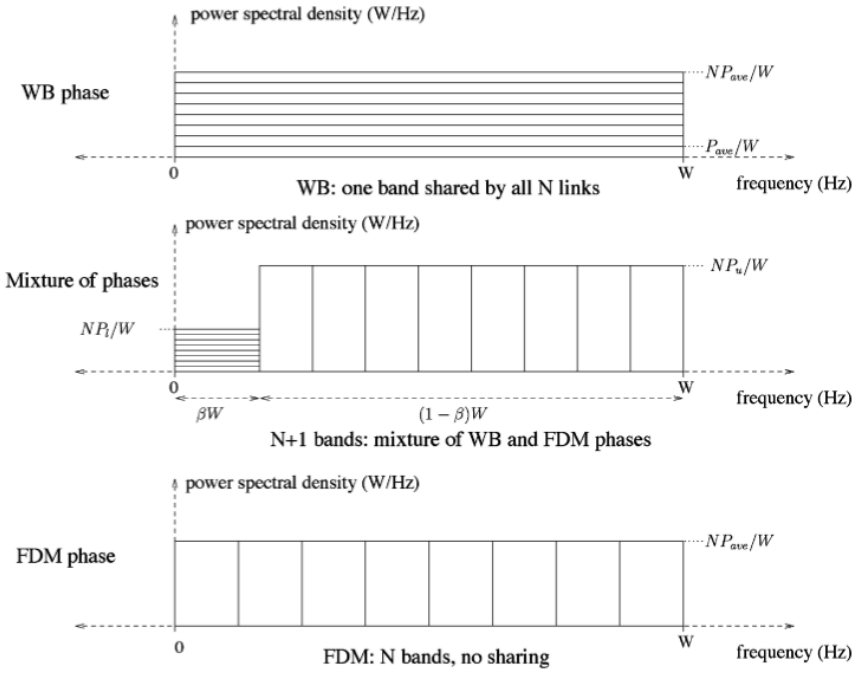

Figure 6.6: Optimal solution for the N–user symmetric flat case [5].

The main results are reported in the following. The first theorem concerns the number of bands required to achieve the optimal solution. A first version of this theorem appears in [3]. Then it has been refined in [4], and also proved in [2].

Theorem 6.1.5. *In the N–user asymmetric flat case the optimal spectrum and power allocation consists of at maximum $N+1$ bands, with power flat in each band.*

Theorem 6.1.6. *In the N–user asymmetric frequency selective case, the optimal solution is the following:*

$$R^o = R^*$$

where

$$R^* \triangleq \max \int_0^1 R^*(\mathbf{p}(f), f)df$$

$$\text{s.t.} \int_0^1 \mathbf{p}(f)df \leq \mathbf{p},\ \mathbf{p}(f) \geq 0,\ \forall\ f \in [0,1]$$

and

$$R^* \triangleq conv_p R(\mathbf{p}(f), f)$$

In other words, the optimal solution of the non–convex optimization problem equals that of its convex relaxation. This has a big role in the assessment of the complexity of solving the general problem. In fact, the continuous frequency non–convex problem has been proved to be NP–hard (the proof of this complexity characterization relies on a reduction from the equipartition problem) [94] and to have zero duality gap [94], [2].

Finally, we point out the main distinction that can be done in this context:

1. $\mathbf{p}(\mathbf{f})$ is a piecewise bounded continuous function;

2. $\mathbf{p}(\mathbf{f})$ must be flat in every sub–channel.

Note that the first case is the one considered in this section. However, we believe that this model is unrealistic for reasonable transceivers, since it assumes that we can (eventually) divide the whole band in many small pieces (necessary assumption to prove the theorems). Recall the approximation lemma mentioned at the beginning of this section. Therefore, we consider the second case, called *discrete* frequency model, in which the spectrum is divided into a fixed number of channels with fixed bandwidth. With this constraint, we cannot derive the optimal solution using the results found in previous work. Namely, this problem has been proved to be strongly NP–hard (in this case the proof is based on a reduction in polynomial time from the strongly NP–complete independent set problem) [94] and not only it does not have zero duality gap, but it is also hard to approximate.

6.1.2 Spectrum Sharing Games

The spectrum sharing game has been widely addressed in the literature. In [3], the authors study the spectrum sharing game for multiple players capable of spreading their power budget across a shared portion of spectrum. The authors investigate and analyze the equilibria of the game, focusing on the issues of fairness and efficiency. They also propose punishment strategies that allow competing entities to reach a fair and efficient operating point. The game between users is analyzed also in [95]. The authors consider the power control problem with SINR as objective function, in both the selfish and the cooperative scenario. They characterize the equilibria and identify the conditions where the Pareto and the Nash equilibrium coincide.

The spectrum sharing problem has also been analyzed from the network's point of view. In [96], the authors analyze the spectrum competition between two contending networks. They characterize the Nash equilibria of the game and discuss the different behavior varying the pathloss exponent. In [97], a similar model is proposed to analyze the spectrum sharing problem between two network operators sharing two carriers. Based on the water–filling algorithm proposed in [98], the authors prove the existence of the Nash equilibria of the game, and characterize the different behavior varying the channel gains between the two contending communicating pairs. In [99], two system pairs sharing two frequency bands are considered. In particular, the model comprises an interference channel in parallel with an interference relay channel. For two different relaying strategies, the existence and the uniqueness of the equilibrium are analyzed. A similar scenario is discussed also in [100], where the authors consider a network with both shared and protected bands, and power allocation is similarly based on the water–filling solution. A formal proof that the game is supermodular is derived as well as conditions for the existence and uniqueness of the Nash equilbria.

The spectrum sharing problem has been discussed also in the context of Cognitive Radio Networks [101]. In [102] and [103], the authors consider the problem of spectrum sharing among secondary users. In contrast with other work, the power control is analyzed with a constraint on the total interference perceived by the primary system. Namely, the interference is measured using the interference temperature. This is a parameter that measures the power and bandwidth occupied by the secondary interference. In both the papers, the authors identify the Nash equilibria and analyze their properties. Also in [104], the authors analyze the spectrum sharing problem with multi–channels, considering the co–channel interference among secondary users and the interference temperature regulation imposed by primary systems. Existence and properties of the Nash equilibria are investigated. In [105], the authors model the spectrum competition among networks that have to decide both the channel and the power allocation. The Nash equilibria of the non–cooperative game are characterized and a cooperative technique is proposed in order to improve the opportunistic solution. In [106], the channel competition is played among selfish users, instead of networks. The authors characterize the equilibria and discuss the efficiency with respect to the optimal channel allocation. In [46], a spectrum selection game is proposed. Competitive users take decisions on which channels to use, not only depending on the number of other users that are sharing the same channel, but also taking into account the different

parameters that characterize the available spectrum opportunity. Furthermore, a multi–stage game is proposed for the dynamic spectrum management.

6.2 System Model

In this section, we describe the system model for the 2–player case that is analyzed in this chapter. The spectrum band is assumed to be divided into two orthogonal channels with equal bandwidth B. Players are indexed as $1, 2$ and we let $i \in \{1, 2\}$ indicate a player and $j \neq i$ as the other player. The distance between the generic receiver i and the contending transmitter j is denoted by x_i, whereas d_i is the distance between transmitter i and receiver i. To simplify the problem and reduce the number of model parameters we assume throughout this chapter that $d_1 = d_2 = d$. Each pair has to decide how to split its total transmission power P between the two available bands, taking into account the behavior of the contending pair. Moreover, given a

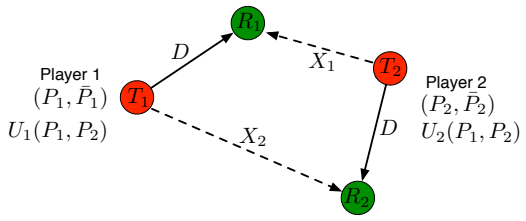

Figure 6.7: Two transmitter and receiver pairs (players) split their power over two orthogonal bands.

certain power budget P available for each one of the two pairs, the strategy space of the generic transmitter i is $P_i \in [0, 1]$. Namely, P_i is the fraction of P that pair i uses in the left band and $\bar{P}_i = 1 - P_i$ is the fraction of power in the right band. The utility (payoff) function of player i is defined as the sum of achievable Shannon rates over the two bands when the interference from player j is treated as noise. We assume a channel model with pure pathloss attenuation so that the received power from a unit power transmission over a distance r is $r^{-\alpha}$, for $\alpha > 2$ the pathloss exponent. Assuming a noise power of $\tilde{\eta}$ on each band, the player i utility function for transmission powers $(\tilde{P}_i, \tilde{P}_j) \in [0, P]^2$ is

$$\tilde{U}_i = B \log_2 \left(1 + \frac{\tilde{P}_i d^{-\alpha}}{\tilde{\eta} + \tilde{P}_j x_i^{-\alpha}} \right) + B \log_2 \left(1 + \frac{\bar{\tilde{P}}_i d^{-\alpha}}{\tilde{\eta} + \bar{\tilde{P}}_j x_i^{-\alpha}} \right) \tag{6.2}$$

in units of bits per second. To summarize, under the above model assumptions, the spectrum sharing problem can be modeled as a non–cooperative game, where the players are the two transmitter and receiver pairs, the actions are the possible power splits over the two bands, and the payoffs are the sum of the achievable Shannon rates over the two bands.

We remove nuissance parameters B, P, η, α from the model as follows. First note the payoff is linear in B and hence we define the normalized utility $U_i = \tilde{U}_i/B$ with units of spectral efficiency (bits per second per Hertz); this removes B. Multiply the numerator and denominator in the SINR in each band by $1/P$ and define the normalized transmission power as $P_i = \tilde{P}_i/P \in [0, 1]$, and the normalized noise power as $\eta = \tilde{\eta}/P$; this removes P. Define the received Signal–to–Noise ratio (SNR) under maximum transmission power on a band as $D = d^{-\alpha}/\eta$, and the received Interference–to–Noise ratio (INR) under maximum transmission power on a band as $X_i = x_i^{-\alpha}/\eta$; this removes η, α. The utility function becomes:

$$U_i = \log_2\left(1 + \frac{P_i D}{1 + P_j X_i}\right) + \log_2\left(1 + \frac{\bar{P}_i D}{1 + \bar{P}_j X_i}\right). \tag{6.3}$$

Each one of the two players is assumed to be selfish. This means that each transmitter allocates power between the two bands trying to maximize the player's achieved throughput (i.e., without taking into account the global optimum). The stable operating points for the two players are the Nash equilibria, i.e., pairs $(P_1, P_2) \in [0, 1]^2$ from which neither player has incentive to unilaterally deviate.

As done for the previous games, we assess the inefficiency of the Nash equilibria from the system point of view. Therefore, we compare the Nash equilibria with the "globally" optimal solution, i.e., the one that could be achieved with a centralized control. Similarly to the previous analysis, we consider the sum of the utilities of all the players, $U_T = U_1 + U_2$. In particular, the social/global optimal sum utility is:

$$U_T^* = \max_{(P_1,P_2)\in[0,1]^2} U_T(P_1, P_2). \tag{6.4}$$

Finally, we can note that, due to the geometry of the problem, some pairs of x_1 and x_2 (distances) are not

allowed. For example, it is easy to see that if we fix x_1, then x_2 has to be such that:

$$\max\{0, x_1 - 2d\} \leq x_2 \leq x_1 + 2d \tag{6.5}$$

Given α and η, it is straightforward to write the same expression in terms of X_1 and X_2.

6.3 The Optimal Solution

In this section, we discuss the optimal solution of the previous problem, for the two–player case, both when we assume symmetric interference ($X_i = X_j$) and for the more general asymmetric case ($X_i \neq X_j$). As highlighted before, the optimization problem that we are considering here is different from the waterfilling problem in the fact that we are considering 2 pairs of users. Moreover, it is also different from the multi–user model discussed in Sec. 6.1.1, since we are assuming a discrete frequency model.

The difficulty of the optimization problem lies in the fact that we are considering a fixed division of the spectrum (2 orthogonal channels with equal bandwidths B). All the optimization problems discussed in the previous section explicitly derive the optimal solution both for the 2–user and for the N–user case, assuming that an arbitrary division of the spectrum in many sub–bands is allowed. This assumption strongly influences the way in which the optimal solution of the problem can be derived. Removing this flexibility invalidates some of the results found in previous work. Hereafter, we provide the exact optimal solution for the symmetric case ($X_i = X_j$) and we numerically derive the optimal solution for the asymmetric case ($X_i \neq X_j$).

6.3.1 Symmetric Optimal Solution

In the symmetric scenario, the utility function that we want to maximize is the following:

$$U_T(P_i, P_j) = \log\left(1 + \frac{P_i D}{1 + P_j X}\right) + \log\left(1 + \frac{(1-P_i)D}{1 + (1-P_j)X}\right) + \log\left(1 + \frac{P_j D}{1 + P_i X}\right) + \log\left(1 + \frac{(1-P_j)D}{1 + (1-P_i)X}\right)$$

The globally optimal allocations are the maximizers of U_T:

$$\text{Opt} = \underset{(P_1,P_2)\in[0,1]^2}{\arg\max}\ U_T(P_1,P_2) \tag{6.6}$$

The optimal solution is reported in the following theorem.

Theorem 6.3.1. *The set of optimal power allocations for the* 2*–player symmetric game is:*

$$\text{Opt}\begin{cases} \{(0.5,0.5)\} & \text{if } X<\tilde{D} \\ \{(P_i,P_j): P_i+P_j=1\} & \text{if } X=\tilde{D} \\ \{(0,1),(1,0)\} & \text{if } X>\tilde{D} \end{cases} \tag{6.7}$$

where $\tilde{D}=\sqrt{1+D}-1$. *Moreover, the function* U_T *is concave for* $X>\tilde{D}$, *and has a saddle point at* $P=(0.5,0.5)$ *for* $X<\tilde{D}$.

Proof. The proof is in Appendix D. □

Note that the function U_T that we are maximizing is a continuous twice differentiable function defined over the set $\mathcal{C}=[0,1]^2$. It is concave for $X<\tilde{D}$ and has a saddle at $(0.5,0.5)$ for $X>\tilde{D}$. In particular, the optimal allocation is for both players to spread their power equally over the two bands when the interference is small relative to the signal ($X<\tilde{D}$), while the optimal allocation is to perform frequency division and put all power in (complementary) bands when the interference is large relative to the signal ($X>\tilde{D}$). Figure 6.8 illustrates the function U_T for $X>\tilde{D}$ (left) and $X<\tilde{D}$ (right).

In fact, it is worth noting that these two regimes coincide with the FS and FDM schemes discussed in Sec. 6.1.1. However, completely different approaches have been used to obtain the two solutions.

6.3.2 Asymmetric Optimal Solution

Now, we assume $X_i\neq X_j$. Therefore, we consider the following utility function:

$$\begin{aligned} U_T(P_i,P_j) = &\log\left(1+\frac{P_iD}{1+P_jX_i}\right)+\log\left(1+\frac{(1-P_i)D}{1+(1-P_j)X_i}\right) \\ &+\log\left(1+\frac{P_jD}{1+P_iX_j}\right)+\log\left(1+\frac{(1-P_j)D}{1+(1-P_i)X_j}\right) \end{aligned} \tag{6.8}$$

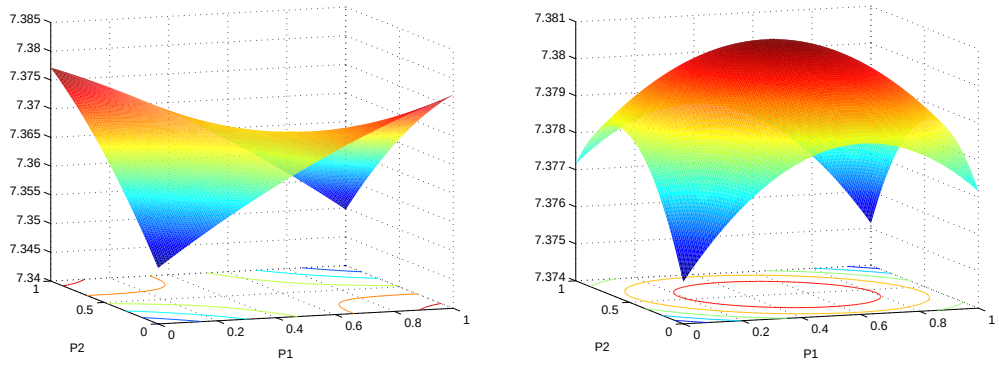

Figure 6.8: The sum utility function $U_T(P_1, P_2)$ has a saddle at $(0.5, 0.5)$ (left) for $X > \tilde{D}$ but is concave for $X < \tilde{D}$ (right).

In [107], we have reported the following claim:

Claim 6.3.1. *The optimal solution for the asymmetric game is given by:*

$$\text{Opt} = \begin{cases} \{(0,1),(1,0)\} & \text{if } X_i + X_j + X_i X_j > D \\ \{(P_i, P_j) : P_i + P_j = 1\} & \text{if } X_i + X_j + X_i X_j = D \\ \{(0.5, 0.5)\} & \text{if } X_i + X_j + X_i X_j < D \end{cases} \tag{6.9}$$

Moreover, the function U_T is concave for $X_i + X_j + X_i X_j < D$, and has a saddle point at $P = (0.5, 0.5)$ for $X_i + X_j + X_i X_j > D$.

Figure 6.9 reports the two different regions for the claimed optimal solution. In the following, we first show that the claim is wrong, but then we prove with numerical evaluation that indeed it is very close to the actual solution. Finally, we conclude with some ideas on how the exact analytical solution might be.

Idea at the basis of the claim

The claim reported in [107] is mainly based on the following two considerations. First, since we are dealing with a continuous function, we study the KKT conditions associated with the optimization problem. Therefore, we first consider the following partial derivative:

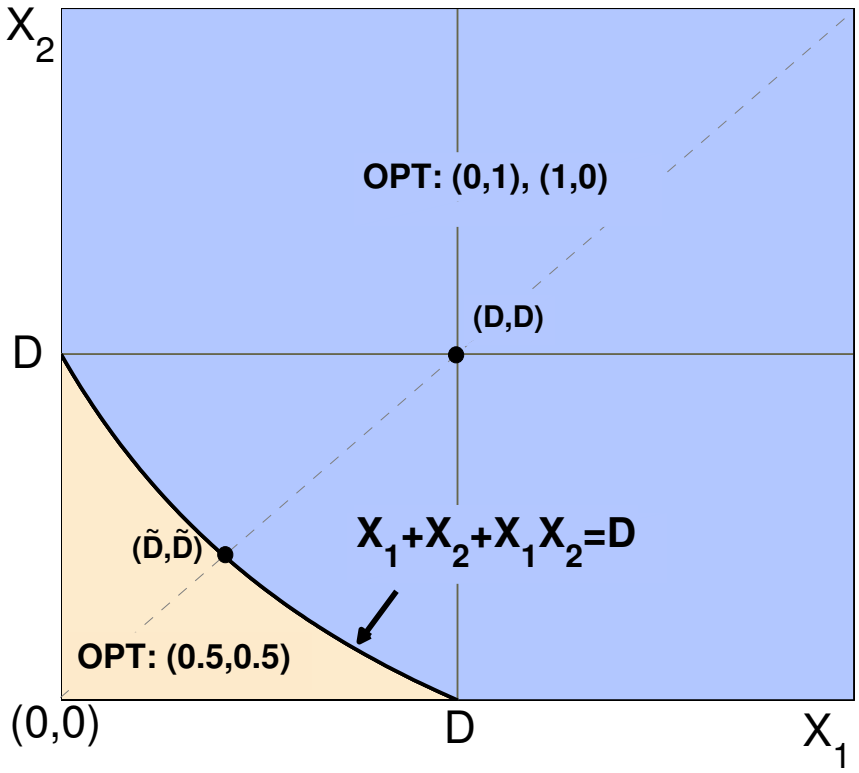

Figure 6.9: Optimal solution for the asymmetric case $X_1 \neq X_2$.

$$\frac{\partial U_T}{\partial P_i} = \Bigg[\frac{(1-2P_j)X_i + (1-2P_i)D}{(1+P_jX_i+P_iD)(1+(1-P_j)X_i+(1-P_i)D)} + \\ + \frac{-X_jP_j}{(1+P_iX_j)(1+P_iX_j+P_jD)} + \frac{X_j(1-P_j)}{(1+(1-P_i)X_j)(1+(1-P_i)X_j+(1-P_j)D)}\Bigg]$$

Remember that we want to maximize U_T, that corresponds to minimize $-U_T$. Therefore, the Lagrangian is defined as follows:

$$\mathscr{L} = -U_T(\mathbf{P}, \lambda, \mu) - \sum_{i=1,2} \lambda_i P_i + \sum_{i=1,2} \mu_i \left(P_i - 1\right)$$

that comes from the constraints $-P_i \leq 0$ and $P_i \leq 1$. A necessary condition for a point to be a local minimum is that there exist Lagrange multipliers such that:

$$\frac{\partial \mathscr{L}}{\partial P_i} = 0 \qquad \forall\, i = 1, 2$$

with λ_i and μ_i both equal to zero when the point is not on the boundaries of the feasible regions. In fact, in this case, all the constraints are inactive.

Therefore, if we want to provide sufficient condition for the point $(P_i, P_j) = (0, 1)$ to be a local optimum, we proceed as follows. Since $P_i = 0$, then $\lambda_i \geq 0$ and $\mu_i = 0$, and since $P_j = 1$, then $\lambda_j = 0$ and $\mu_j \geq 0$. The partial derivatives evaluated at the point $(0, 1)$ are:

$$\frac{\partial U_T}{\partial P_i}(0,1) = \frac{(D - X_i - X_j - X_i X_j)}{(1 + X_i)(1 + D)}$$

$$\frac{\partial U_T}{\partial P_j}(0,1) = \frac{-(D - X_i - X_j - X_i X_j)}{(1 + X_j)(1 + D)}$$

The KKT conditions are:

$$-\frac{\partial U_T}{\partial P_i}(0,1) - \lambda_i + \mu_i = \frac{-(D - X_i - X_j - X_i X_j)}{(1 + X_i)(1 + D)} - \lambda_i = 0$$

$$-\frac{\partial U_T}{\partial P_j}(0,1) - \lambda_j + \mu_j = \frac{(D - X_i - X_j - X_i X_j)}{(1 + X_j)(1 + D)} + \mu_j = 0$$

that becomes:

$$\frac{-(D - X_i - X_j - X_i X_j)}{(1 + X_i)(1 + D)} = \lambda_i \geq 0$$

$$\frac{-(D - X_i - X_j - X_i X_j)}{(1 + X_j)(1 + D)} = \mu_j \geq 0$$

This means that the condition that has to be satisfied is the following:

$$-(D - X_i - X_j - X_i X_j) > 0 \Longleftrightarrow X_i + X_j + X_i X_j > D$$

This is a necessary condition for $(0, 1)$ and $(1, 0)$ to be a local optimum. The second consideration, that leads to the very same threshold, is simply based on the comparison between the value of the utility function U_T in $(0, 1)$ and the value in $(0.5, 0.5)$. This comparison has been motivated by extensive numerical simulations that show how the function U_T switches only between two different regimes: a concave function

with maximum in $(0.5, 0.5)$ and a function with a saddle in $(0.5, 0.5)$. In fact, it is easy to prove that:

$$U_T(P_i = 1, P_j = 0) > U_T(P_i = 0.5, P_j = 0.5) \iff X_i + X_j + X_i X_j > D$$

Counterexample

We now show, with a counterexample, that claim 6.3.1 is wrong. Consider the case in which $X_i + X_j + X_i X_j = D$, then all the solutions should be all the points (P_i, P_j) for which $P_i + P_j = 1$.

We assume $X_i = 1$, $X_j = 2$ and $D = X_i + X_j + X_i X_j = 5$. For (P_i, P_j) with $P_i + P_j = 1$, it holds that:

$$e^{U_T(P_i, P_j)} \equiv (1 + X_i)^2 (1 + X_j)^2 = 4 \cdot 9 = 36.$$

Let $P_i = 6/25$, $P_j = 3/4$ then $P_i + P_j = 99/100$ and

$$e^{U_T(6/25, 3/4)} = \frac{1174941989}{32634000} \approx 36.00361552 \ldots > e^{U_T(1/2, 1/2)}.$$

Therefore, when $X_i \neq X_j$, the claim is not true. It is worth saying that the same approach adopted for finding the optimal solution in the symmetric case does not lead to any good result when we assume $X_i \neq X_j$, therefore we proceed with a numerical evaluation of the optimal solution.

Numerical Evaluation

In this section, we show that even if we have proved that claim 6.3.1 is wrong, in fact it is very close to the actual solution of the problem, especially when reasonable values of X_i and X_j are taken into account.

As mentioned before, extensive simulations show that the claimed solution is very close to the actual solution. Therefore, we have solved numerically the optimization problem for many pairs of (X_i, X_j). Figure 6.10 and 6.11 report the obtained solutions (when $D = 1$). In the square $[0, 1]^2$ we have considered $10,000$ points (step 0.01), and for each one we provide the obtained solution. All points but three report a solution that is the same of the one that we have claimed. Different optimal solutions are obtained on the line $X_i + X_j + X_i X_j = D$ or very close to it. Referring to Figure 6.10 and 6.11, we can assume that the solution

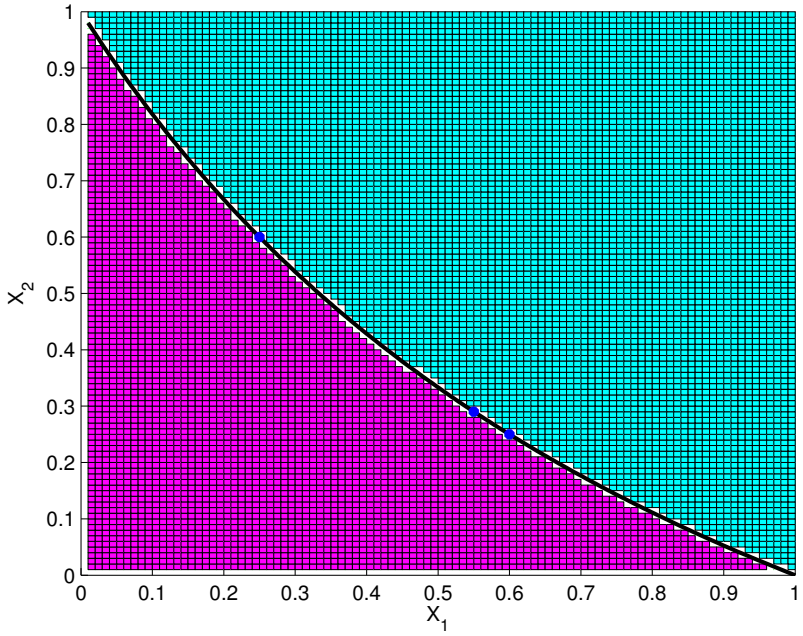

Figure 6.10: Numerical optimal solution ($D = 1$).

might not be the claimed one in the white region in which the curve $X_i + X_j + X_iX_j = D$ lies. However, even in these cases, the actual solution is very close to the claimed one and the difference between the utility function evaluated at the optimal point and at the claimed solution is of the order of 10^{-6}. Furthermore, to analyze in details what happens on the threshold line, we consider 100 points on this line. Figure 6.12 reports the difference between the utility function at the optimal solution and at the claimed solution, when X_i goes from 0 to 1 and X_j is such that $X_i + X_j + X_iX_j = D$. Note that when $X_i = X_j$, i.e., the symmetric case, the difference is zero, as expected. This happens for $X_i = X_j = \sqrt{2} - 1 = 0.41$. Furthermore, as mentioned, the difference in terms of utility functions is very small and negligible.

Finally, it is worth mentioning that there is a difference between the claimed solution and the one provided by simulations also for $X_i >> X_j$. Namely, when the two Xs are very asymmetric, the solution is not the one claimed in 6.3.1, even if it is very close.

Thresholds for the Exact Solution

We conclude this section discussing some ideas on how the analytical optimal solution might look like. From the numerical solutions, we have observed that most of the points return a solution that coincides with

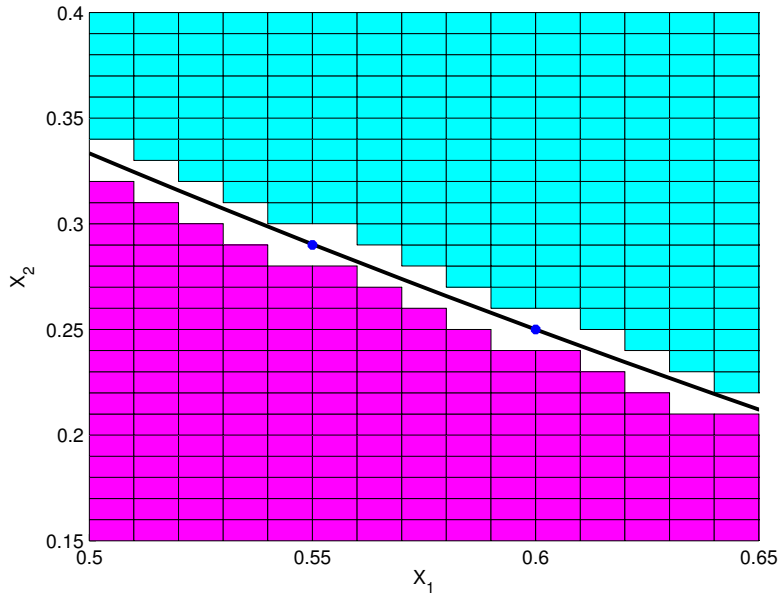

Figure 6.11: Zoom on the numerical optimal solution ($D = 1$).

the one claimed in 6.3.1. The behavior of the optimal solution is not clear in the area close to the line $X_i + X_j + X_iX_j = D$. Therefore, we might assume that there exist two functions $s(X_i, X_j) \geq 0$ and $r(X_i, X_j) \geq 0$, such that whenever $X_i + X_j + X_iX_j - r(X_i, X_j) \leq D \leq X_i + X_j + X_iX_j + s(X_i, X_j)$ we do not know the optimal solution. In contrast, when $D > X_i + X_j + X_iX_j + s(X_i, X_j)$ the optimal solution is $\{(0, 1), (1, 0)\}$ and when $D < X_i + X_j + X_iX_j - r(X_i, X_j)$ the optimal solution is the point $(0.5, 0.5)$. Moreover, when $X_i \neq X_j$, it holds that $s(X_i, X_j) \neq 0$, $r(X_i, X_j) \neq 0$ and the solution is the point (P_i^*, P_j^*) with zero derivative and $0 < P_i^* < 1, 0 < P_j^* < 1, P_i^* \neq 0.5, P_j^* \neq 0.5$.

In order to provide the optimal solution, we should first provide these two functions. However, also this calculation does not seem to be straightforward. However, from numerical evaluation, we expect the region of the unknown optimal solution to be very small (recalling Figure 6.10 and 6.11 this region is the white area). For this reason, hereafter we will assume Claim 6.3.1 to be the optimal solution for the asymmetric problem.

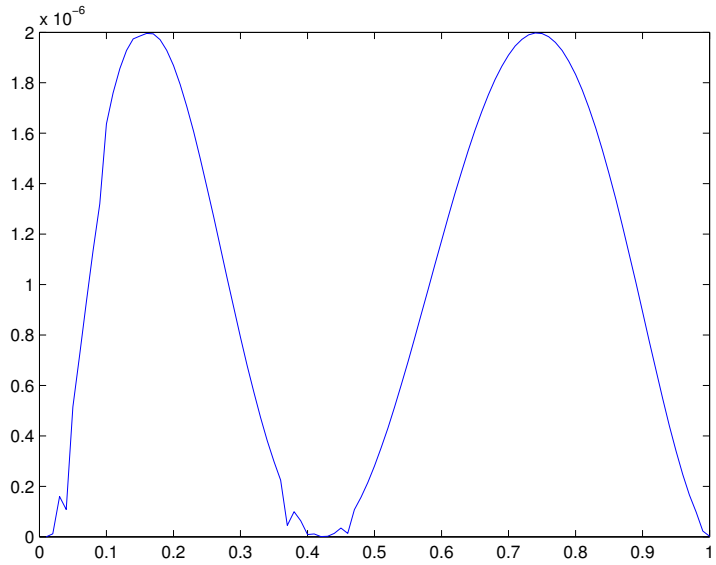

Figure 6.12: Difference between the utility function at the optimal solution and at the claimed solution, when X_i goes from 0 to 1 and X_j is such that $X_i + X_j + X_i X_j = D$.

6.4 The 2–Player Game

This section analzes the quality of the equilibria in the 2–player game. In the first part we consider the symmetric case, i.e., when $X_i = X_j = X$, while in the second part we extend the analysis to the more general asymmetric case with $X_i \neq X_j$.

6.4.1 The symmetric case

For this subsection we assume $X_i = X_j = X$. Generally speaking, the Nash equilibria of a game can be found using the best response functions. The Best Response (BR) is the strategy (or strategies) which produces the most favorable outcome for a player, taking other players' strategies as given. Therefore, the Nash equilibrium is the point at which each player in a game has selected the best response (or one of the best responses) to the other players' strategies. Note that this approach can be properly used when users deal with functions that are continuous in their strategies. This explains why we adopt this method here, but we do not do the same with the congestion–based utility functions.

To evaluate the best response function of the generic player i, we consider the partial derivative with respect to P_i, of the utility function (i.e., Eq. (6.3), with $X_i = X$):

$$\frac{\partial U_i}{\partial P_i} = \frac{[(1-2P_j)X + (1-2P_i)D]D\log_2 e}{(1+P_jX+P_iD)(1+(1-P_j)X+(1-P_i)D)} \tag{6.10}$$

Therefore, the best response of player i is, by definition, the maximum of the utility function, over all possible strategies of player j. In other words, the best response function is given by the points in which the partial derivative is equal to zero. The above function is equal to zero when the numerator is null, that is:

$$P_i = \frac{1}{2} + \frac{X}{D}\left(\frac{1}{2} - P_j\right). \tag{6.11}$$

It is easy to see that these points are maxima of the function (and not minima).

Since the domain of the function is [0,1], i.e., $(P_i, P_j) \in [0,1]^2$, the best response function cannot be outside this range. Therefore, we consider the following cases:

$$P_i = \frac{1}{2} + \frac{X}{D}\left(\frac{1}{2} - P_j\right) < 0 \Longleftrightarrow P_j > \frac{1}{2}\left(1 + \frac{D}{X}\right) \tag{6.12}$$

$$P_i = \frac{1}{2} + \frac{X}{D}\left(\frac{1}{2} - P_j\right) > 1 \Longleftrightarrow P_j < \frac{1}{2}\left(1 - \frac{D}{X}\right) \tag{6.13}$$

This implies that whenever P_i is less than 0 (or greater than 1) the best response is fixed to 0 (or 1).

Finally, the best response for player i, $P_i^*(P_j)$, is the following function:

$$P_i^*(P_j) = \begin{cases} 1 & \text{if } X > D \text{ and } 0 \leq P_j < \frac{1}{2}\left(1 - \frac{D}{X}\right) \\ 0 & \text{if } X > D \text{ and } \frac{1}{2}\left(1 + \frac{D}{X}\right) < P_j \leq 1 \\ \frac{1}{2} + \frac{X}{D}\left(\frac{1}{2} - P_j\right) & \text{otherwise} \end{cases} \tag{6.14}$$

These best response functions are illustrated in Figure 6.13. Their intersection give the Nash equilibria, as stated in the following theorem.

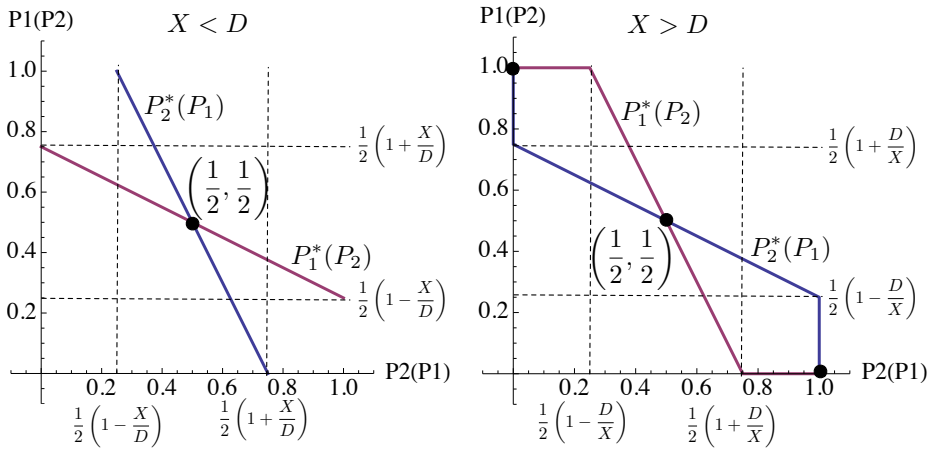

Figure 6.13: The intersection of the best response functions $P_1^*(P_2), P_2^*(P_1)$ give the Nash equilibria. The set of equilibria depends upon $X \lessgtr D$.

Theorem 6.4.1. *The* 2*–player symmetric game admits the following Nash equilibria:*

$$\text{NE} = \begin{cases} \{(0.5, 0.5)\} & \text{if } X < D \\ \{(P_i, P_j) : P_i + P_j = 1\} & \text{if } X = D \\ \{(0,1), (0.5, 0.5), (1,0)\} & \text{if } X > D \end{cases} \tag{6.15}$$

Proof. A pure strategy Nash equilibrium is a point at which each player has selected the best response to the other players' strategies. In this game, the point in which the two best responses cross is the solution of the following system:

$$\begin{cases} (1-2P_j)X + (1-2P_i)D = 0 \\ (1-2P_i)X + (1-2P_j)D = 0 \end{cases} \tag{6.16}$$

that is $P_i = P_j = 0.5$. This is the unique equilibrium when $X < D$. However, when $X > D$ the best responses cross in two other points, i.e., $(0,1)$ and $(1,0)$. When $X = D$ the two best responses coincide with the line $P_i + P_j = 1$, i.e., there is an infinite number of equilibria. □

We assess the quality of the Nash equilibria via PoS and PoA.

Theorem 6.4.2. *The Price–of–Stability (PoS) for the symmetric game is:*

$$\mathrm{PoS} = \begin{cases} 1 & \text{if } X \leq \tilde{D} \text{ or } X > D \\ \frac{\log_2(1+D)}{2\log_2\left(1+\frac{0.5D}{1+0.5X}\right)} & \text{if } \tilde{D} < X \leq D \end{cases} \tag{6.17}$$

and it has a maximum that is unbounded in D, i.e., $\lim_{D\to\infty} \max_{X\geq 0} \mathrm{PoS}(X, D) = \infty$.

Proof. First, it is easy to see that $\tilde{D} \leq D$. Therefore there are two cases. When $X \leq \tilde{D}$ or $X > D$ the best equilibrium coincides with the global optimum, i.e., $\mathrm{PoS} = 1$. Otherwise, $\mathrm{PoS} > 1$. Namely, it is possible to see that the $\lim_{X\to\tilde{D}^+} \mathrm{PoS} = 1$. Since:

$$\frac{\log_2(1+D)}{2\log_2\left(1+\frac{0.5D}{1+0.5\tilde{D}}\right)} = 1 \tag{6.18}$$

it follows that the PoS is continuous at $X = \tilde{D}$. In contrast, the function is discontinuous at $X = D$. This point is also the maximum of the PoS, since the function is monotonically increasing in the interval $(\tilde{D}, D)$. The upper bound of the PoS (as $X \to D^-$) is:

$$\lim_{X\to D^-} \mathrm{PoS} = \frac{\log_2(1+D)}{2\log_2\left(\frac{2(1+D)}{2+D}\right)} \tag{6.19}$$

and it is easy to see that:

$$\lim_{D\to 0} \lim_{X\to D^-} \mathrm{PoS} = 1, \lim_{D\to\infty} \lim_{X\to D^+} \mathrm{PoS} = \infty \tag{6.20}$$

Therefore, the PoS is unbounded when $D \to \infty$. □

Theorem 6.4.3. *The Price–of–Anarchy (PoA) for the symmetric game is:*

$$\mathrm{PoA} = \begin{cases} 1 & \text{if } X \leq \tilde{D} \\ \frac{\log_2(1+D)}{2\log_2\left(1+\frac{0.5D}{1+0.5X}\right)} & \text{if } X > \tilde{D} \end{cases} \tag{6.21}$$

and it is unbounded, i.e., $\lim_{X\to\infty} \mathrm{PoA} = \infty$.

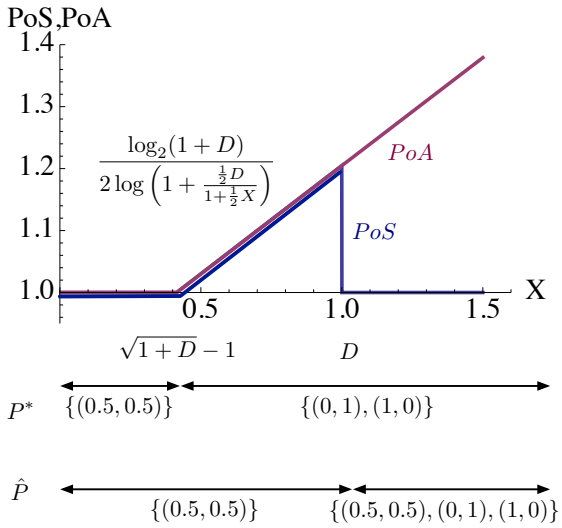

Figure 6.14: PoS and PoA for the 2–player symmetric case for $D = 1$.

Proof. It is easy to see that

$$\lim_{X\to\infty} \frac{\log_2(1+D)}{2\log_2\left(1+\frac{0.5D}{1+0.5X}\right)} = \infty \tag{6.22}$$

Therefore, the $\lim_{X\to\infty} \text{PoA} = \infty$. □

Figure 6.14 shows PoS and the PoA as a function of X for $D = 1$ (for which $\tilde{D} = \sqrt{2} - 1 \approx 0.414$). Both curves are plotted to highlight the interval in which they coincide. Note that the PoS is in general bounded, and goes to infinity only when D goes to infinity. In contrast the PoA goes to infinity whenever X goes to infinity, i.e., for every D. The conclusion is that in general the PoS is very close to one, i.e., the best equilibrium is very close to the optimum, but at the same time, when X is large, e.g., in dense networks, the worst equilibrium could be "infinitely" worse than the optimal solution. A similar result is also given in [3], where the authors show that the inefficiency resulting from choosing to spread power equally among available bands can be arbitrarily large.

6.4.2 The asymmetric case

In this section, we consider the case in which $X_i \neq X_j$. In order to characterize the Nash equilibria of the game, we consider the partial derivative of the utility function, i.e., Eq. (6.3), for player i:

The best response of each player is similar to the previous case, since the function of player i depends

$$\frac{\partial U_i}{\partial P_i} = \frac{[(1-2P_j)X_i + (1-2P_i)D]D\log_2 e}{(1+P_jX_i+P_iD)(1+(1-P_j)X_i+(1-P_i)D)} \tag{6.23}$$

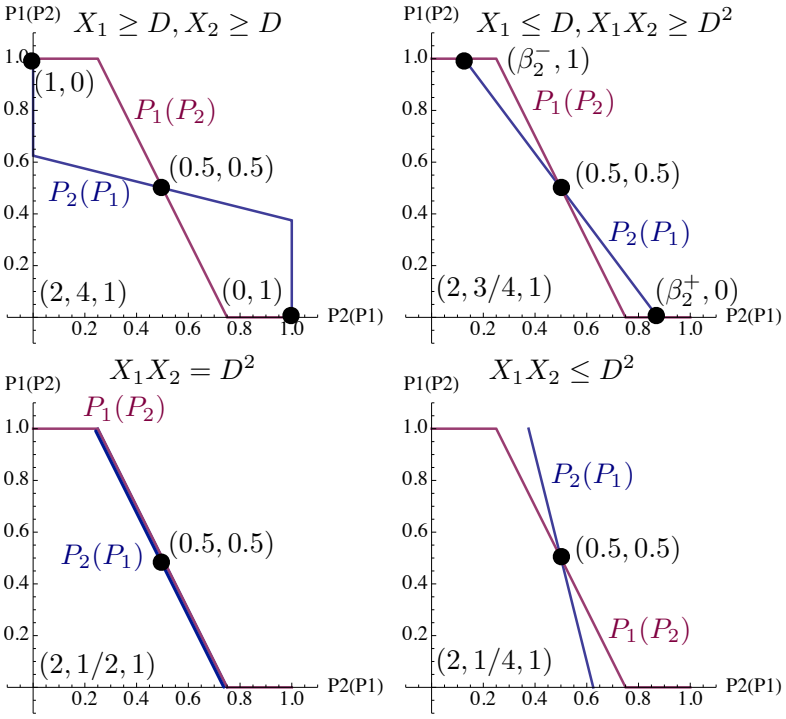

Figure 6.15: Best response functions for the 2–player asymmetric game.

only on X_i. Namely, the best response for player i, i.e., $P_i^*(P_j)$, is the following function:

$$P_i^*(P_j) = \begin{cases} 1 & \text{if } X_i > D \text{ and } 0 \leq P_j < \frac{1}{2}\left(1 - \left(\frac{D}{X_i}\right)\right) \\ 0 & \text{if } X_i > D \text{ and } \frac{1}{2}\left(1 + \left(\frac{D}{X_i}\right)\right) < P_j \leq 1 \\ \frac{1}{2} + \frac{X_i}{D}\left(\frac{1}{2} - P_j\right) & \text{otherwise} \end{cases} \tag{6.24}$$

The Nash equilibria are the intersections of the two best response functions $P_1^*(P_2)$, $P_2^*(P_1)$, illustrated in Figure 6.15. The following theorem gives the Nash equilibria of the asymmetric game.

Theorem 6.4.4. *The 2–player asymmetric game has Nash equilibria given by:*

$$\text{NE} = \begin{cases} \{(0.5, 0.5)\} & \text{if } X_i X_j < D^2 \\ \{(P_i, P_j) : P_i = 0.5 + \frac{D}{X_i}(0.5 - P_j)\} & \text{if } X_i X_j = D^2 \\ \left\{(0.5, 0.5), \left(0.5\left(1 + \frac{X_i}{D}\right), 0\right), \left(0.5\left(1 - \frac{X_i}{D}\right), 1\right)\right\} & \text{if } X_i \leq D, X_i X_j > D^2 \\ \{(0.5, 0.5), (0, 1), (1, 0)\} & \text{if } X_i > D, X_j > D \end{cases} \tag{6.25}$$

Proof. As in the previous case, the pure strategy Nash equilibrium is the point at which each player has selected the best response to the other players' strategies. The two best responses always cross at $(0.5, 0.5)$. This is the unique equilibrium when $X_i X_j < D^2$. However, when $X_i X_j > D^2$, the best responses cross in other two points. Namely, when both X_i and X_j are greater than D, these two points are $(0, 1)$ and $(1, 0)$. In contrast, when $X_i \leq D$ (and, consequently, $X_j > D$), these points are $P_i = 0.5\left(1 \pm \frac{X_i}{D}\right)$, with $P_j = 0$ and $P_j = 1$, respectively. When $X_i X_j = D^2$ the two best responses coincide and there is an infinite number of equilibria. □

To assess the quality of the Nash equilibria, we consider the optimal solution characterized in Sec. 6.3.2. The behavior of the Nash equilibria and the optimal solution (varying X_i and X_j) is highlighted in Figure 6.16, where $\beta_i^{\pm} = 0.5\left(1 \pm \frac{X_i}{D}\right)$. Note that there exist four regions. When $X_i X_j > D^2$, the game admits three equilibria and the optimum is in $(0, 1)$ and $(1, 0)$. In particular, when both X_i and X_j are greater than D, the PoS is one, since the best equilibrium and the optimum coincide. In contrast, when X_i (or X_j) is less than D, the best equilibrium is worse than the optimum, then the PoS is greater than one. The PoA is in both cases greater than one. We do not report the expressions, that can be easily derived as done for the symmetric case. When $X_i X_j < D^2$ and $X_i X_j + X_i + X_j > D$, the game admits a unique equilibrium, that does not coincide with the optimum, then PoS and PoA coincide and are greater than one. In contrast, when $X_i X_j + X_i + X_j < D$, the optimal solution and the unique equilibrium coincide. Similar conditions on the uniqueness of the equilibrium are discussed also in [98] and [100]. Finally, along the curve $X_i X_j = D^2$ the two best responses coincide and there exists an infinite number of equilibria. Note that the corresponding regions of the symmetric case, i.e., $[0, \tilde{D}]$, $[\tilde{D}, D]$, $[D, \infty)$, can be identified along the line $X_1 = X_2$.

For the sake of completeness, we also highlight the available region (due to the geometry of the problem) defined by Eq. (6.5). In particular, assuming $\eta = 10^{-3}$, we report the curves for $\alpha = 2$ and $\alpha = 4$. Namely,

the unfeasible region (between the magenta curves and the axes in Figure 6.16) is very small, and decreases when α increases.

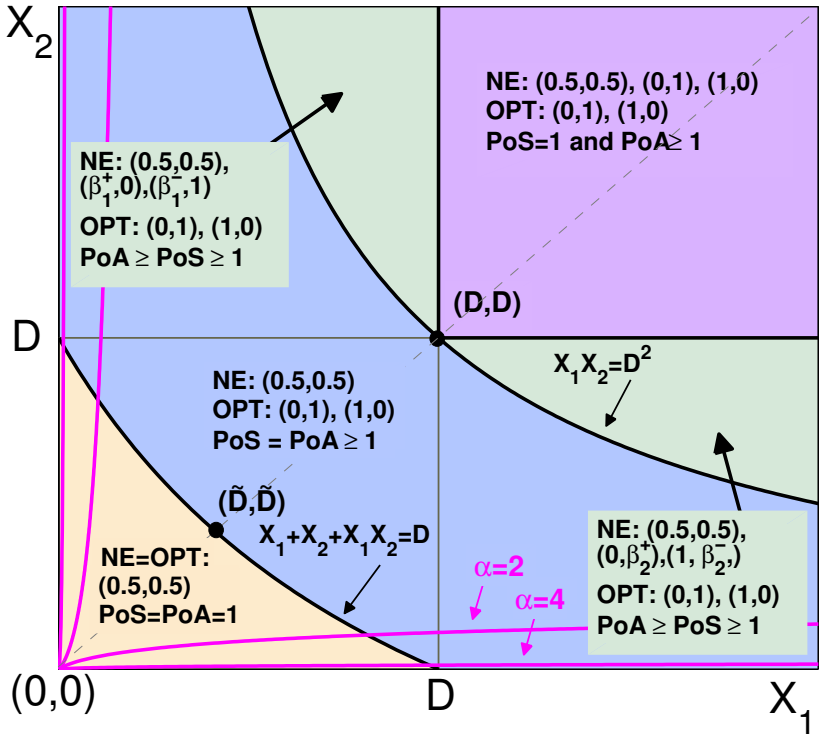

Figure 6.16: Nash equilibria and optimal allocations as a function of X_1, X_2.

6.4.3 Stability of the Nash equilibria

In this section, we study the stability of the equilibria for the 2–player game. We consider only the asymmetric case, since the symmetric one can be easily derived. First, recall that the best response for player i, $P_i^*(P_j)$, is the following function:

$$P_i^*(P_j) = \left[\frac{1}{2} + \frac{X_i}{D}\left(\frac{1}{2} - P_j\right)\right]_0^1 \tag{6.26}$$

where we define $[x]_0^1 := \max(0, \min(1, x))$.

We now prove the following theorem:

Theorem 6.4.5. *The Nash equilibria of the* 2*–player asymmetric game can be classified as follows:*

$$\begin{array}{ll} \textit{when } X_iX_j < D^2 & \{(0.5, 0.5)\} \textit{ is the unique equilibrium and is stable} \\ \textit{when } X_iX_j = D^2 & \textit{infinite number } \{(P_i,P_j) : P_i = 0.5 + \frac{D}{X_i}(0.5 - P_j)\} \\ & \textit{of unstable equilibria} \\ \textit{when } X_iX_j > D^2 & 3 \textit{ equilibria and } \{(0.5, 0.5)\} \textit{ is the only unstable} \end{array} \tag{6.27}$$

Proof. To prove the theorem, let us assume that the players are at the equilibrium in $(0.5, 0.5)$ and one of the two decides to deviate of a small ϵ. Let us observe the sequence of the best responses:

$$P_j = \frac{1}{2} + \epsilon \qquad \Rightarrow \qquad P_i(P_j) = \frac{1}{2} + \frac{X_i}{D}\left(\frac{1}{2} - \frac{1}{2} - \epsilon\right) = \frac{1}{2} - \frac{X_i}{D}\epsilon$$

$$P_i = \frac{1}{2} - \frac{X_i}{D}\epsilon \qquad \Rightarrow \qquad P_j(P_i) = \frac{1}{2} + \frac{X_j}{D}\left(\frac{1}{2} - \frac{1}{2} + \frac{X_i}{D}\epsilon\right) = \frac{1}{2} + \frac{X_iX_j}{D^2}\epsilon$$

After N cycles, we obtain:

$$P_i = \frac{1}{2} - \frac{X_i}{D}\left(\frac{X_iX_j}{D^2}\right)^N \epsilon \qquad P_j = \frac{1}{2} + \left(\frac{X_iX_j}{D^2}\right)^N \epsilon$$

Therefore, if $X_iX_j < D^2$ the two best responses converge ($N \to \infty$) to $(0.5, 0.5)$, proving the first part of the theorem (see Figure 6.17a). Furthermore, it is clear that when $X_iX_j > D^2$ the equilibrium in (0.5) is not stable (see Figure 6.17b).

We now prove that the other two equilibria (that exist when $X_iX_j > D^2$) are stable. First, consider the case in which $X_i > D$ and $X_j > D$. Assume that the users have reached the equilibrium in $(0, 1)$. Note that player 1 has a best response equal to 0 for every $P_j \in [\frac{1}{2} + \frac{1}{2}\frac{D}{X_i}, 1]$. This means that if player 2 deviates of an $\epsilon < \frac{1}{2}\frac{D}{X_i}, 1$, the best response of player 1 does not change, and therefore also player 2 will be incentivized to return to the equilibrium $(0, 1)$, since her best response is equal to 1 for every $P_i \in [0, \frac{1}{2} - \frac{1}{2}\frac{D}{X_j}]$. When $X_iX_j > D^2$ but one of the two Xs is less than D, we observe that first the two user move to a point different from the equilibrium, but at the next step they will come back again at the same stable point (see Figure 6.17c).

Finally, we analyze the case in which $X_i X_j = D^2$. In this case, all the equilibria (infinite number) are unstable. In fact, every ϵ changing in the played strategies lead the two player to reach a new different equilibrium (see Figure 6.17d). □

We conclude the section summarizing the domain of attraction for the region $[0,1]^2$. This means that we want to characterize the equilibrium to which a generic starting strategy profile converges due to the best response dynamics. Figure 6.18 shows the domains of attraction for four different starting points that lie in different quadrants of the region (thinking at $(0.5, 0.5)$ as the center). We can note that for two out of the four quadrants, the equilibrium to which the two players converge depends on which player moves first. Therefore, when $X_i X_j > D^2$, we have two different cases, reported in Figure 6.19a and 6.19b. In contrast, when $X_i X_j < D^2$, any strategy profile converges to the unique equilibrium, Figure 6.19c.

6.5 Stochastic Characterization of the 2–player game

In previous sections, we have completely characterized the 2–player game. In particular, we have observed that the equilibrium strategy chosen by a user and the quality of this equilibrium with respect to the optimum strictly depend on the distances between each receiver and the interfering transmitter (note that X_i and X_j directly depend on the distances between interfering nodes).

In general, the interfering distances between competing users depend on how the users are distributed in the considered region. For this reason, we decide to characterize the 2–player game resorting to stochastic geometry. In particular, we want to provide a stochastic characterization of the equilibrium strategies, i.e., in terms of joint probability density function of the distances between each interferer/receiver pair. The goal of this analysis is to provide a tool that can be properly used for performance evaluation and network design. In the simple scenario with 2 pairs of users, this means providing probability distribution on the different regions highlighted in Figure 6.16 (e.g., probability of uniqueness of the equilibrium). In the next chapter we will discuss how the stochastic characterization might be extended to the N–player game. This allows us to predict the performance of large networks.

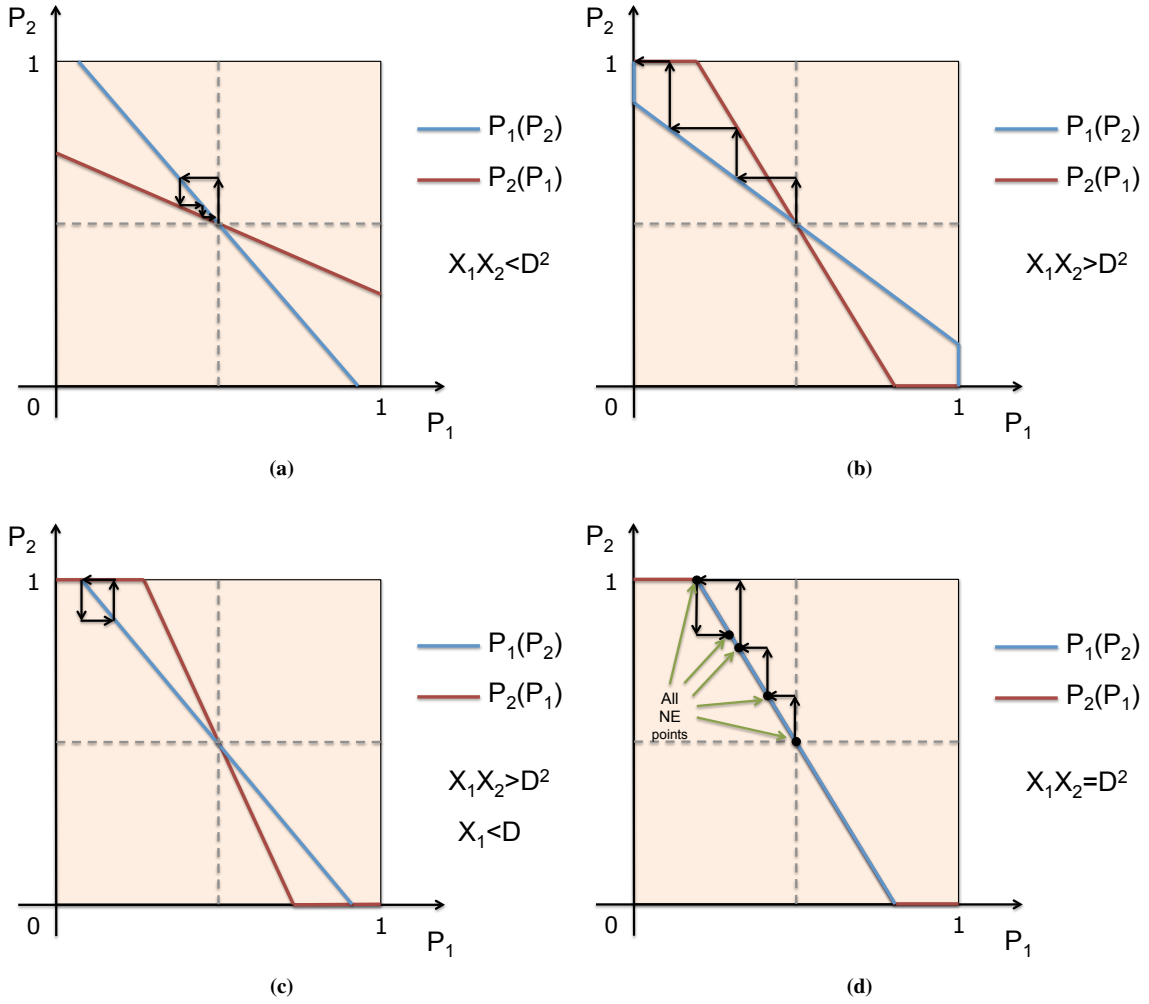

Figure 6.17: Best response dynamics when (a) $X_iX_j < D^2$, (b) $X_iX_j > D^2$, (c) $X_iX_j > D^2$ and (d) when $X_iX_j = D^2$.

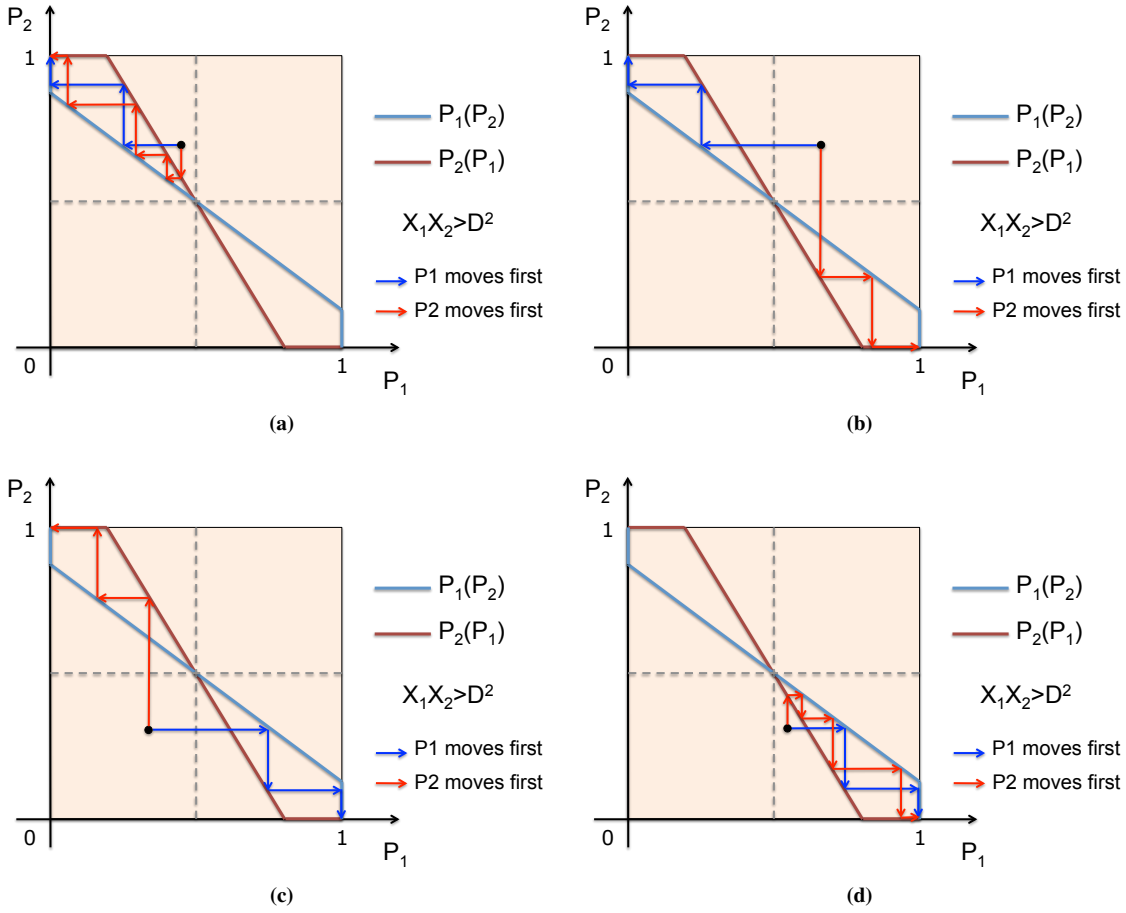

Figure 6.18: Best response dynamics from different starting points.

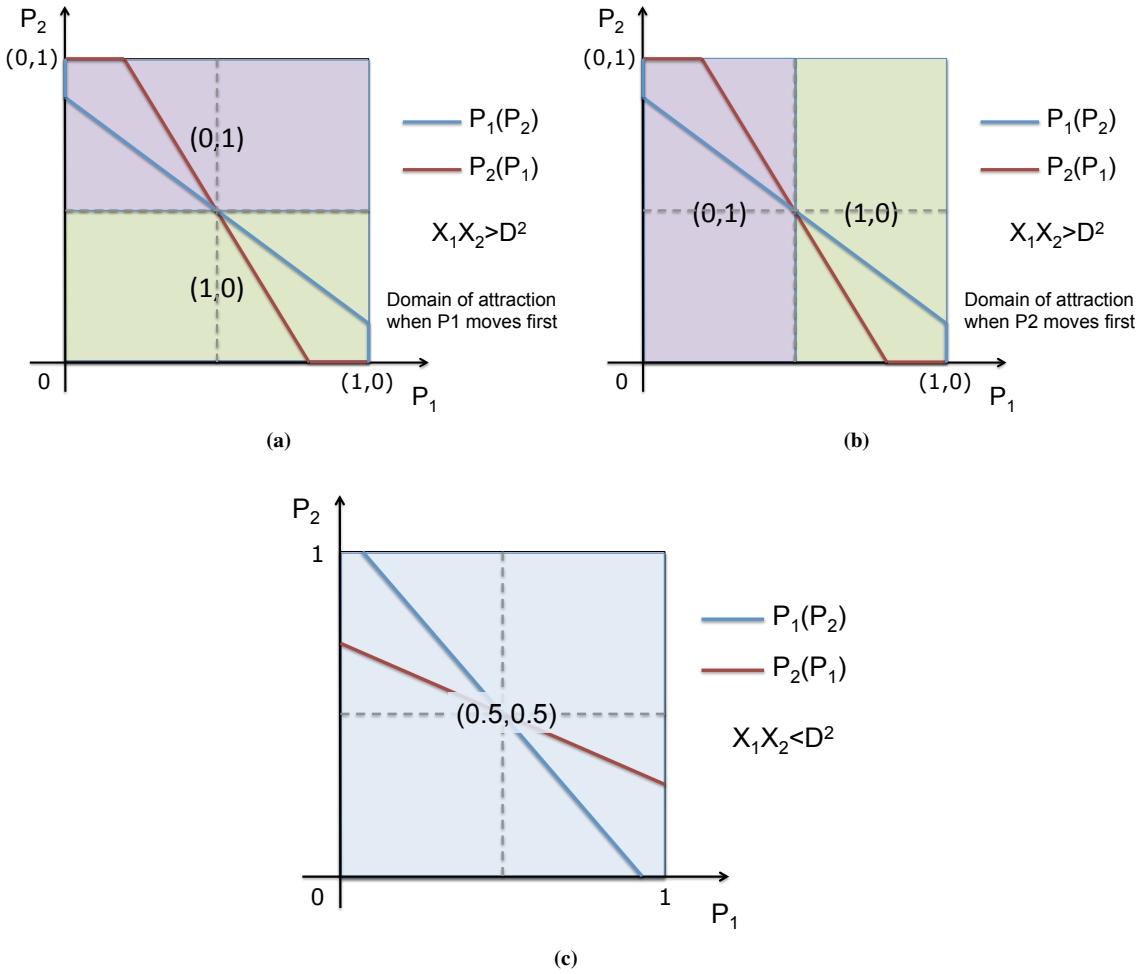

Figure 6.19: Domain of attraction when (a) $X_i X_j > D^2$ and P1 moves first, (b) $X_i X_j > D^2$ and P2 moves first and (c) when $X_i X_j < D^2$.

6.5.1 Joint pdf of the mutual interfering distances

In this section, we derive the joint probability density function $f_{x_1,x_2}(x_1, x_2)$, i.e., joint distribution of the two interfering distances x_1 and x_2. For the sake of simplicity, we will use the pure distances between users, instead of the SNR and the INR used so far. Furthermore, for readability of the section, we will use indexes 1 and 2 to indicate the two pairs of users. The topology we are considering is reported in Figure 6.20.

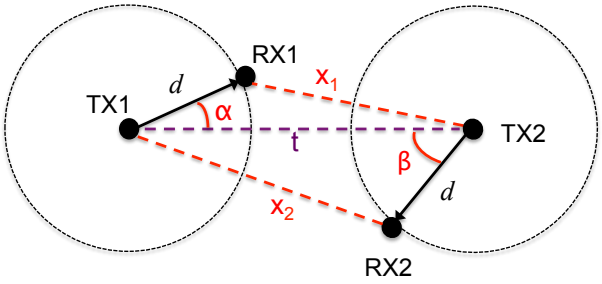

Figure 6.20: 2–player topology.

The aim of this analysis is to characterize the joint distribution of the two random variables x_1 and x_2. It is easy to verify that they are not independent. However, once that we fixed t, the distance between the two transmitters, x_1 and x_2 are conditionally independent. Furthermore, due to the geometry of the problem (the sum of any two sides of a triangle must be greater than the third side), the following inequalities must hold:

$$|d - t| \leq x_1 \leq d + t$$

$$|d - t| \leq x_2 \leq d + t$$

$$\max\{|d - x_1|, |d - x_2|\} \leq t \leq \min\{d + x_1, d + x_2\}$$

Figure 6.21 clearly shows why distances x_1 and x_2 have to be between $|d - t|$ and $d + t$.

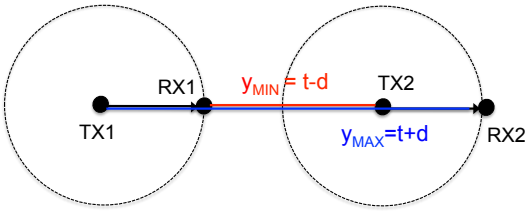

Figure 6.21: Example that shows the min and max values of x_1 and x_2.

In order to derive $f_{\mathsf{x}_1,\mathsf{x}_2}(x_1, x_2)$, it is easier to consider the corresponding joint Cumulative Density Function (cdf):

$$F_{\mathsf{x}_1,\mathsf{x}_2}(x_1, x_2) = \int_0^\infty F_{\mathsf{x}_1,\mathsf{x}_2|\mathsf{t}}(x_1, x_2|t) f_{\mathsf{t}}(t) dt \tag{6.28}$$

To simplify the analysis, we first characterize the conditional joint cdf, $F_{\mathsf{x}_1,\mathsf{x}_2|\mathsf{t}}(x_1, x_2|t)$, that, recalling that the two random variables are conditionally independent, can be written as:

$$F_{\mathsf{x}_1,\mathsf{x}_2|\mathsf{t}}(x_1, x_2|t) = \mathbb{P}(\mathsf{x}_1 \leq x_1, \mathsf{x}_2 \leq x_2|t) = \mathbb{P}(\mathsf{x}_1 \leq x_1|t)\mathbb{P}(\mathsf{x}_2 \leq x_2|t) \tag{6.29}$$

Therefore, we consider the following probability:

$$\mathbb{P}(\mathsf{x}_1 \leq x_1|t)$$

By the geometry of the problem (law of cosines) we can write x_1^2 as:

$$x_1^2 = d^2 + t^2 - 2dt\cos\alpha$$

Therefore, we can write the following:

$$\mathbb{P}(\mathsf{x}_1 \leq x_1|t) = \mathbb{P}(\sqrt{d^2 + t^2 - 2dt\cos\alpha} \leq x_1|t) = \mathbb{P}(d^2 + t^2 - 2dt\cos\alpha \leq x_1^2|t) =$$

$$= \mathbb{P}\left(\cos\alpha \geq \frac{(d^2 + t^2) - x_1^2}{2dt}\middle| t\right) \tag{6.30}$$

We know that, since α and β are uniformly distributed angles, their cosine is a random variable, w, that has the following distribution.

Proposition 6.5.1. *The random variable* w*, cosine of a uniformly distributed angle, has the following*

Probability Density Function (pdf):

$$f_{\mathsf{w}}(w) = \frac{1}{\pi\sqrt{1-w^2}} \qquad -1 \leq w \leq 1 \tag{6.31}$$

and the following Cumulative Density Function (cdf):

$$F_{\mathsf{w}}(w) = \frac{1}{2} + \frac{\sin^{-1} w}{\pi} \qquad -1 \leq w \leq 1 \tag{6.32}$$

It is worth noting also that the sine of a uniformly distributed angle has the same pdf and that the sum (mod π) of two uniformly distributed random variables in $[0, \pi]$ has the same distribution of the two variables [108].

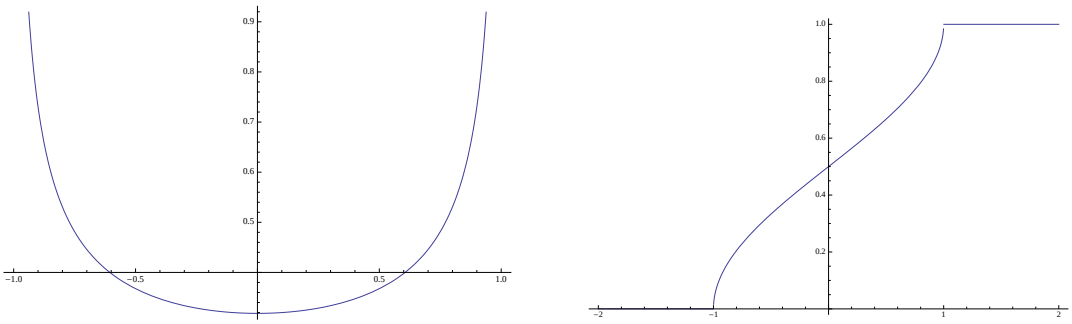

Figure 6.22: Probability (left) and cumulative (right) density function of $\cos\alpha$.

In Figure 6.22, we report the plot of the pdf and cdf. We can note that even if the angle is uniformly distributed, the cosine is not uniform. The reason why this happens is well explained by Figure 6.23, that shows how the same range of cosine values (segments on the x–axis) are given by different ranges of angles.

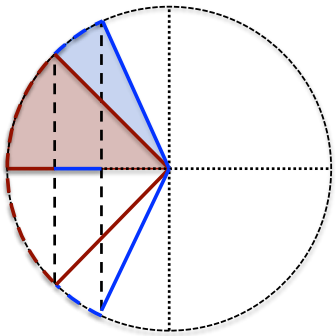

Figure 6.23: Relationship between the distribution of an angle and its cosine.

Using the previous result, we can now state the following theorem.

Theorem 6.5.2. *The conditional joint cdf of* x_1 *and* x_2 *is the following:*

$$F_{\mathsf{x}_1,\mathsf{x}_2|\mathsf{t}}(x_1,x_2|t) =$$
$$= \begin{cases} 0 & x_1 < |d-t| \quad \textit{OR} \quad x_2 < |d-t| \\ \left[1 - F_{\mathsf{w}}\left(\frac{(d^2+t^2)-x_1^2}{2dt}\right)\right]\left[1 - F_{\mathsf{w}}\left(\frac{(d^2+t^2)-x_2^2}{2dt}\right)\right] & |d-t| \le x_1 \le d+t \quad \textit{AND} \quad |d-t| \le x_2 \le d+t \\ \left[1 - F_{\mathsf{w}}\left(\frac{(d^2+t^2)-x_1^2}{2dt}\right)\right] & |d-t| \le x_1 \le d+t \quad \textit{AND} \quad x_2 > d+t \\ \left[1 - F_{\mathsf{w}}\left(\frac{(d^2+t^2)-x_2^2}{2dt}\right)\right] & x_1 > d+t \quad \textit{AND} \quad |d-t| \le x_2 \le d+t \\ 1 & x_1 > d+t \quad \textit{AND} \quad x_2 > d+t \end{cases} \tag{6.33}$$

where $F_{\mathsf{w}}(w)$ *is given in Prop. 6.5.1.*

Proof. Recalling Eq. (6.30) and Prop. 6.5.1, we can write the following:

$$\mathbb{P}\left(\cos\alpha \ge \frac{(d^2+t^2)-x_1^2}{2dt}\middle| t\right) = 1 - F_{\mathsf{w}}\left(\frac{(d^2+t^2)-x_1^2}{2dt}\middle| t\right) \tag{6.34}$$

Then, consider the argument of the cdf $F_{\mathsf{w}}(w)$ (that has to be between -1 and 1):

$$\frac{d^2+t^2-x_1^2}{2dt} < -1 \qquad \Longrightarrow \qquad x_1 > d+t$$

$$\frac{d^2+t^2-x_1^2}{2dt} > 1 \qquad \Longrightarrow \qquad x_1 < |d-t|$$

This means that

$$\mathbb{P}\left(\cos\alpha \ge \frac{(d^2+t^2)-x_1^2}{2dt}\middle| t\right) = \begin{cases} 0 & x_1 < |d-t| \\ 1 - F_{\mathsf{w}}\left(\frac{(d^2+t^2)-x_1^2}{2dt}\right) & |d-t| \le x_1 \le d+t \\ 1 & x_1 > d+t \end{cases} \tag{6.35}$$

Finally, from Eq. (6.29), we can write:

$$F_{\mathsf{x}_1,\mathsf{x}_2|\mathsf{t}}(x_1,x_2|t) = \mathbb{P}\left(\cos\alpha \ge \frac{(d^2+t^2)-x_1^2}{2dt}\middle| t\right)\mathbb{P}\left(\cos\beta \ge \frac{(d^2+t^2)-x_2^2}{2dt}\middle| t\right) =$$

$$= \left[1 - F_{\mathsf{w}}\left(\frac{(d^2+t^2)-x_1^2}{2dt}\right)\right]\left[1 - F_{\mathsf{w}}\left(\frac{(d^2+t^2)-x_2^2}{2dt}\right)\right] =$$

$$= \begin{cases} 0 & x_1 < |d-t| \quad \text{OR} \quad x_2 < |d-t| \\ \left[1 - F_{\mathsf{w}}\left(\frac{(d^2+t^2)-x_1^2}{2dt}\right)\right]\left[1 - F_{\mathsf{w}}\left(\frac{(d^2+t^2)-x_2^2}{2dt}\right)\right] & |d-t| \le x_1 \le d+t \quad \text{AND} \quad |d-t| \le x_2 \le d+t \\ \left[1 - F_{\mathsf{w}}\left(\frac{(d^2+t^2)-x_1^2}{2dt}\right)\right] & |d-t| \le x_1 \le d+t \quad \text{AND} \quad x_2 > d+t \\ \left[1 - F_{\mathsf{w}}\left(\frac{(d^2+t^2)-x_2^2}{2dt}\right)\right] & x_1 > d+t \quad \text{AND} \quad |d-t| \le x_2 \le d+t \\ 1 & x_1 > d+t \quad \text{AND} \quad x_2 > d+t \end{cases}$$

□

The plot of the function is in Figure 6.24.

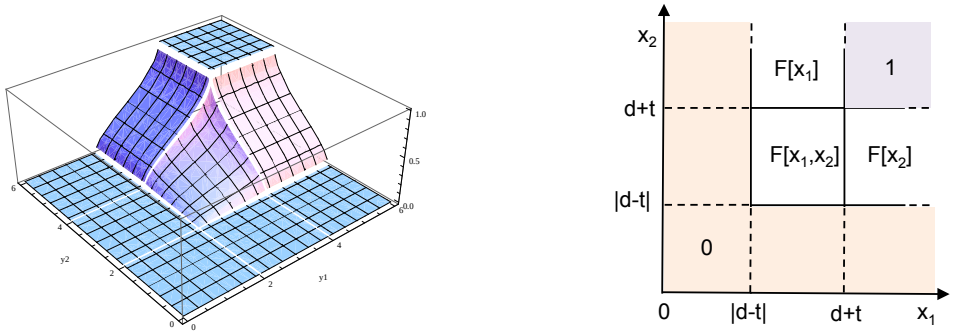

Figure 6.24: Conditional joint cdf of x_1 and x_2 when $d = 1$ and $t = 3$.

From the previous result, it is straightforward to derive the joint pdf.

Theorem 6.5.3. *The conditional joint pdf of* x_1 *and* x_2 *is the following:*

$$f_{\mathsf{x}_1,\mathsf{x}_2|\mathsf{t}}(x_1, x_2|t) =$$

$$= \begin{cases} \dfrac{x_1 x_2}{\pi^2 d^2 t^2 \sqrt{\left[1-\left(\frac{d^2+t^2-x_1^2}{2dt}\right)^2\right]\left[1-\left(\frac{d^2+t^2-x_2^2}{2dt}\right)^2\right]}} & |d-t| \le x_1 \le d+t \; \textit{AND} \; |d-t| \le x_2 \le d+t \\ 0 & \textit{otherwise} \end{cases} \tag{6.36}$$

Proof. In order to derive the conditional joint pdf, we consider the double partial derivative with respect to x_1 and x_2:

$$f_{\mathsf{x}_1,\mathsf{x}_2|\mathsf{t}}(x_1, x_2|t) = \frac{\partial^2 F_{\mathsf{x}_1,\mathsf{x}_2|\mathsf{t}}(x_1, x_2|t)}{\partial x_1 \partial x_2}$$

First, note that:

$$\frac{\partial}{\partial x_1}\left[1 - F_{\mathsf{w}}\left(\frac{(d^2+t^2)-x_1^2}{2dt}\right)\right] = \frac{-x_1}{\pi dt\sqrt{1-\left(\frac{d^2+t^2-x_1^2}{2dt}\right)^2}}$$

plotted in Figure 6.25. The single derivative is always negative, but it is worth noting that when we do the product of the two partial derivatives we finally obtain a positive function, as the pdf has to be.

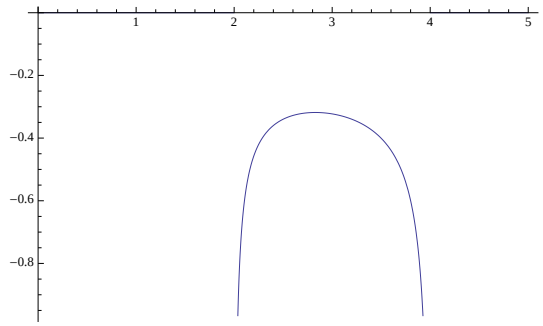

Figure 6.25: Partial derivative of the cumulative density function.

Then, we obtain:

$$f_{\mathsf{x}_1,\mathsf{x}_2|\mathsf{t}}(x_1,x_2|t) = \frac{\partial^2 F_{\mathsf{x}_1,\mathsf{x}_2|\mathsf{t}}(x_1,x_2|t)}{\partial x_1 \partial x_2}$$

$$= \begin{cases} \dfrac{x_1 x_2}{\pi^2 d^2 t^2 \sqrt{\left[1-\left(\frac{d^2+t^2-x_1^2}{2dt}\right)^2\right]\left[1-\left(\frac{d^2+t^2-x_2^2}{2dt}\right)^2\right]}} & |d-t| \le x_1 \le d+t \text{ AND } |d-t| \le x_2 \le d+t \\ 0 & \text{otherwise} \end{cases}$$

□

Figure 6.26 shows the conditional joint distribution function and the comparison between the theoretical expression and simulation results (the two coincide as expected).

Note that when we do the derivative with respect to x_1 and x_2, we obtain a function different from zero only in the region $\{(x_1,x_2) : |d-t| \le x_1 \le d+t, |d-t| \le x_2 \le d+t\}$. This is in fact consistent with the topology constraints mentioned at the beginning of this section.

We now consider the unconditional distribution functions:

$$f_{\mathsf{x}_1,\mathsf{x}_2}(x_1,x_2) = \int_0^\infty f_{\mathsf{x}_1,\mathsf{x}_2|\mathsf{t}}(x_1,x_2|t) f_{\mathsf{t}}(t) dt$$

$$F_{\mathsf{x}_1,\mathsf{x}_2}(x_1,x_2) = \int_0^\infty F_{\mathsf{x}_1,\mathsf{x}_2|\mathsf{t}}(x_1,x_2|t) f_{\mathsf{t}}(t) dt$$

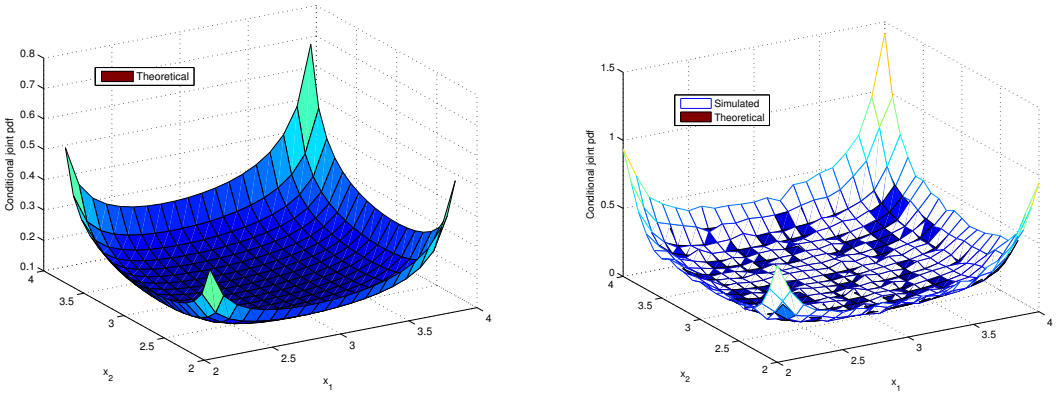

Figure 6.26: Conditional joint pdf of x_1 and x_2 when $d = 1$ and $t = 3$.

In order to provide an explicit expression, we need to introduce the pdf of t, i.e., $f_{\mathsf{t}}(t)$. We consider, for the 2–player case, the following cdf:

$$F_{\mathsf{t}}(t) = \left(\frac{t}{L}\right)^2$$

that comes from the fact that we assume to have a transmitter in the center of a circle arena of radius L, and the other transmitter uniformly distributed in the arena. Recall that t represents the distance between the two transmitters. Figure 6.27 reports example of the considered topology that also shows that, given L, the maximum distance between one transmitter and the other receiver (i.e., x_i) is $L + d$.

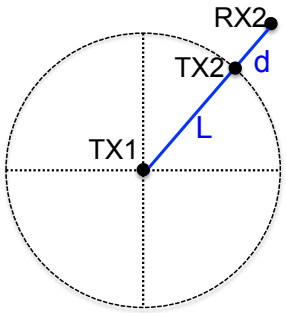

Figure 6.27: Topology considered for the analysis of the 2–player joint distribution.

Then, the pdf is:

$$f_{\mathsf{t}}(t) = \frac{2t}{L^2} \qquad 0 \leq t \leq L$$

We can now state the following theorem.

Theorem 6.5.4. *Assuming that the distance t between the two transmitters has the following pdf:*

$$f_{\mathsf{t}}(t) = \frac{2t}{L^2} \qquad 0 \le t \le L$$

the joint pdf of x_1 and x_2 is the following:

$$f_{\mathsf{x}_1,\mathsf{x}_2}(x_1,x_2) = \\ = \frac{2x_1x_2}{\pi^2 d^2 L^2} \int_{\max\{|d-x_1|,|d-x_2|\}}^{\min\{d+x_1,d+x_2\}} \frac{1}{t\sqrt{\left[1-\left(\frac{d^2+t^2-x_1^2}{2dt}\right)^2\right]\left[1-\left(\frac{d^2+t^2-x_2^2}{2dt}\right)^2\right]}} dt \quad (6.37)$$

where the support of this function is $\{(x_1,x_2) : 0 \le x_1 \le L+d, 0 \le x_2 \le L+d, x_1-2d \le x_2 \le x_1+2d\}$.

Proof. The proof comes directly substituting $f_{\mathsf{t}}(t)$ and $f_{\mathsf{x}_1,\mathsf{x}_2|\mathsf{t}}(x_1,x_2|t)$ in:

$$f_{\mathsf{x}_1,\mathsf{x}_2}(x_1,x_2) = \int_0^\infty f_{\mathsf{x}_1,\mathsf{x}_2|\mathsf{t}}(x_1,x_2|t) f_{\mathsf{t}}(t) dt$$

where $f_{\mathsf{x}_1,\mathsf{x}_2|\mathsf{t}}(x_1,x_2|t)$ is given by Thm. 6.5.3. Then, we obtain:

$$f_{\mathsf{x}_1,\mathsf{x}_2}(x_1,x_2) = \frac{2x_1x_2}{\pi^2 d^2 L^2} \int \frac{1}{t\sqrt{\left[1-\left(\frac{d^2+t^2-x_1^2}{2dt}\right)^2\right]\left[1-\left(\frac{d^2+t^2-x_2^2}{2dt}\right)^2\right]}} dt \quad (6.38)$$

We have already shown that both the two terms in square brackets are positive if and only if:

$$|d-x_1| \le t \le d+x_1 \qquad |d-x_2| \le t \le d+x_2$$

The case in which both are negative is not allowed by the geometry of the problem. Therefore, given x_1 and x_2, t can have values only in the following range:

$$\max\{|d-x_1|,|d-x_2|\} \le t \le d+\min\{x_1,x_2\}$$

Then we can write the joint probability distribution:

$$f_{\mathsf{x}_1,\mathsf{x}_2}(x_1,x_2)=\frac{2x_1x_2}{\pi^2d^2L^2}\int_{\max\{|d-x_1|,|d-x_2|\}}^{\min\{d+x_1,d+x_2\}}\frac{1}{t\sqrt{\left[1-\left(\frac{d^2+t^2-x_1^2}{2dt}\right)^2\right]\left[1-\left(\frac{d^2+t^2-x_2^2}{2dt}\right)^2\right]}}dt$$

where the support is $\{(x_1,x_2):0\leq x_1\leq L+d, 0\leq x_2\leq L+d, x_1-2d\leq x_2\leq x_1+2d\}$. □

Note that even when all the parameter (λ,x_1,x_2,d,L) are equal to 1, we obtain the following integral:

$$f_{\mathsf{x}_1,\mathsf{x}_2}(x_1,x_2)=\frac{2}{\pi^2}\int_0^2\frac{1}{t\left(1-\frac{t^2}{4}\right)}dt$$

that cannot be found explicitly.

Finally, we provide some numerical evaluations of the joint probability distribution function. First we report the plots obtained numerically evaluating the integral. Results are reported in Figure 6.28.

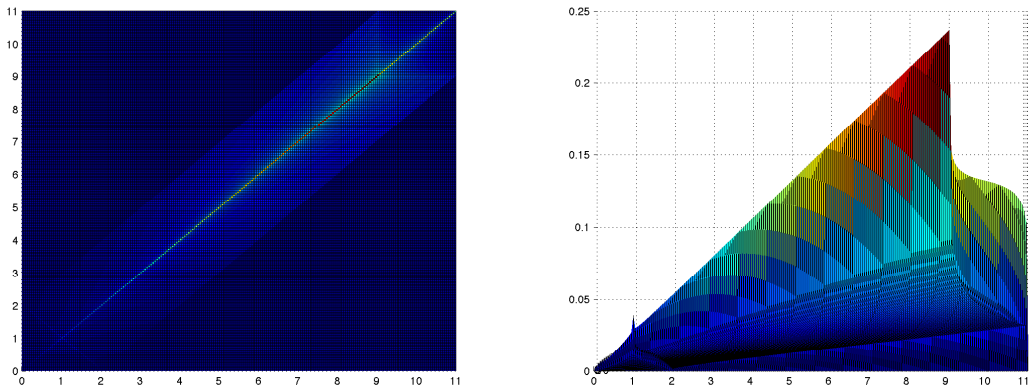

Figure 6.28: Joint distribution of x_1 and x_2 numerically evaluating the integral. Parameters used for the simulations: $L=10$, $d=1$.

By simulations, we have obtained the plots reported in Figure 6.29. Note that since $L=10$ and $d=1$, the values of x_1 and x_2 are in the range $[0,11]$.

As expected, the plot obtained with the numerical evaluation of the integral and by simulation of the topology have the same shape. However, it is worth noting that, due to normalization (integral of the joint distribution over the domain has to be equal to 1), the two plots have different heights at the peak.

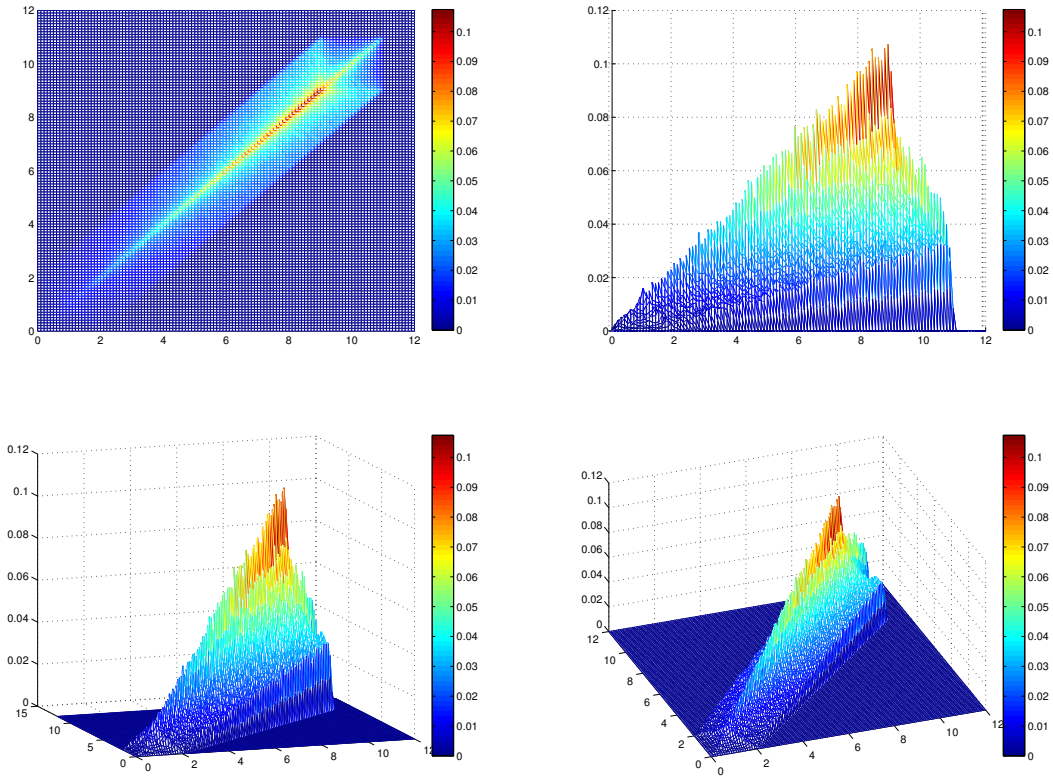

Figure 6.29: Joint distribution of x_1 and x_2 obtained by simulations. Parameters used for the simulations: $L = 10$, $d = 1$.

6.5.2 Applications to game theory

We now apply the results obtained in the previous section in order to characterize, in terms of probabilities, the 2–player game. For instance, assume that we have two pairs of users randomly deployed in a circle arena of radius L. What is the probability that, given L, the 2–player game admits a unique equilibrium? From the previous analysis, we know that the equilibrium is unique when $X_1 X_2 < D^2$. The region is highlighted in Figure 6.30. Since we are dealing with pure distances, we derive the following corollary.

Corollary 6.5.5. *The condition for the uniqueness of the equilibrium does not depend on α and η and in terms of pure distances can be written as:*

$$x_1 x_2 > d^2 \tag{6.39}$$

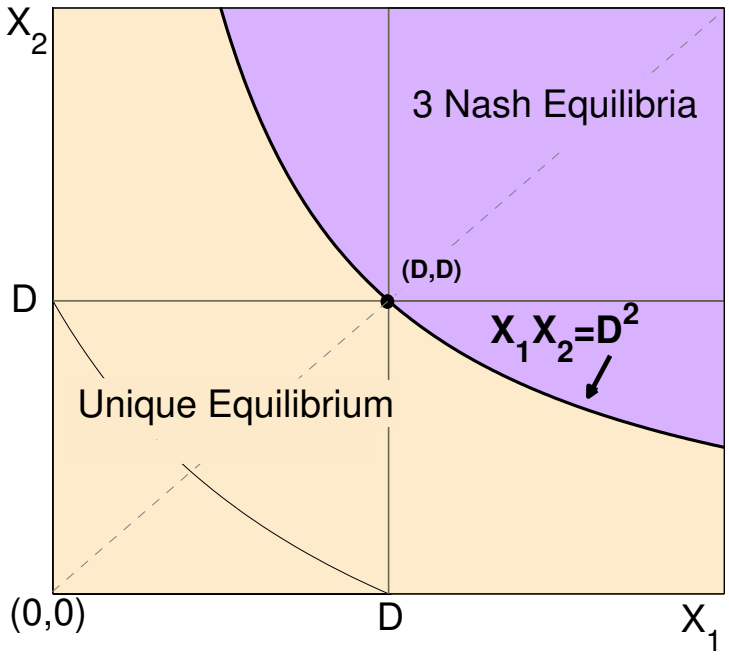

Figure 6.30: Different regions for the Nash equilibria.

Moreover, we also characterize the probability that the optimum and the unique equilibrium coincide. We already know that this happens when $X_iX_j + X_i + X_j < D$. Therefore, we derive the following corollary.

Corollary 6.5.6. *The condition for the unique equilibrium to coincide with the optimal solution depends on α and η and in terms of pure distances can be written as:*

$$x_1^{-\alpha}x_2^{-\alpha} + \eta x_1^{-\alpha} + \eta x_2^{-\alpha} - \eta d^{-\alpha} > 0 \tag{6.40}$$

In order to derive the aforementioned probabilities, we need to consider the joint distribution of x_1 and x_2, $f_{\mathsf{x}_1,\mathsf{x}_2}(x_1, x_2)$, given in Thm. 6.5.4. Clearly, for different values of L, we obtain a different probability for the equilibrium to be unique. Note that we are deploying two pairs of users uniformly at random on a circle arena of radius L. Since we cannot provide explicitly the joint pdf given in Eq. (6.37), we cannot even provide explicit expressions for the probabilities we are interested in. Therefore, we provide hereafter a numerical evaluation. Namely, we numerical evaluate the integral of the joint pdf $f_{\mathsf{x}_1,\mathsf{x}_2}(x_1, x_2)$, given in

Thm. 6.5.4, over the different regions that in Figure 6.16 characterize the equilibria. In particular, we first derive the probability that the equilibrium is unique (orange region in Figure 6.30), that is given by (recall Cor. 6.5.5):

$$\mathbb{P}(\text{unique}) = \int_{(x_1,x_2):x_1x_2>d^2} f_{\mathsf{x}_1,\mathsf{x}_2}(x_1,x_2)dx_1dx_2$$

When the equilibrium is not unique, we consider two cases. The case in which the three equilibria are $(0.5, 0.5)$, $(0, 1)$ and $(1, 0)$ (pink region in Figure 6.16):

$$\mathbb{P}(\text{(0,1)–(1,0) equilibria}) = \int_{(x_1,x_2):x_1<d\wedge x_2<d} f_{\mathsf{x}_1,\mathsf{x}_2}(x_1,x_2)dx_1dx_2$$

and the case in which the equilibria depend on the parameter β as highlighted in the green region of Figure 6.16:

$$\mathbb{P}(\text{mixed equilibria}) = \int_{(x_1,x_2):x_1x_2<d^2\wedge(x_1>d\vee x_2>d)} f_{\mathsf{x}_1,\mathsf{x}_2}(x_1,x_2)dx_1dx_2$$

For completeness, we also provide the probability that there is an infinite number of equilibria. Note that this probability should be zero:

$$\mathbb{P}(\text{Infinite number of NE}) = \int_{(x_1,x_2):x_1x_2=d^2} f_{\mathsf{x}_1,\mathsf{x}_2}(x_1,x_2)dx_1dx_2$$

Finally, we evaluate the probability that the unique equilibrium and the optimal solution coincide (orange region in Figure 6.16), that from Cor. 6.5.6 is:

$$\mathbb{P}(\text{coincide with the optimum}) = \int_{(x_1,x_2):x_1^{-\alpha}x_2^{-\alpha}+\eta x_1^{-\alpha}+\eta x_2^{-\alpha}-\eta d^{-\alpha}>0} f_{\mathsf{x}_1,\mathsf{x}_2}(x_1,x_2)dx_1dx_2$$

Numerical results for all these probabilities are reported in Figure 6.31. We consider four different values of d and L varies from 0.1 to 50. We assume $\eta = 10^{-3}$ and $\alpha = 4$. Clearly, the probability of having a unique equilibrium, that corresponds to the case in which players decide to use the whole spectrum, increases with L. This is reasonable since increasing L, also the average distance between the interfering pairs increases (x_1 and x_2), so for a fixed d, the probability of $x_1x_2 > d^2$ increases. This corresponds to the case in which users

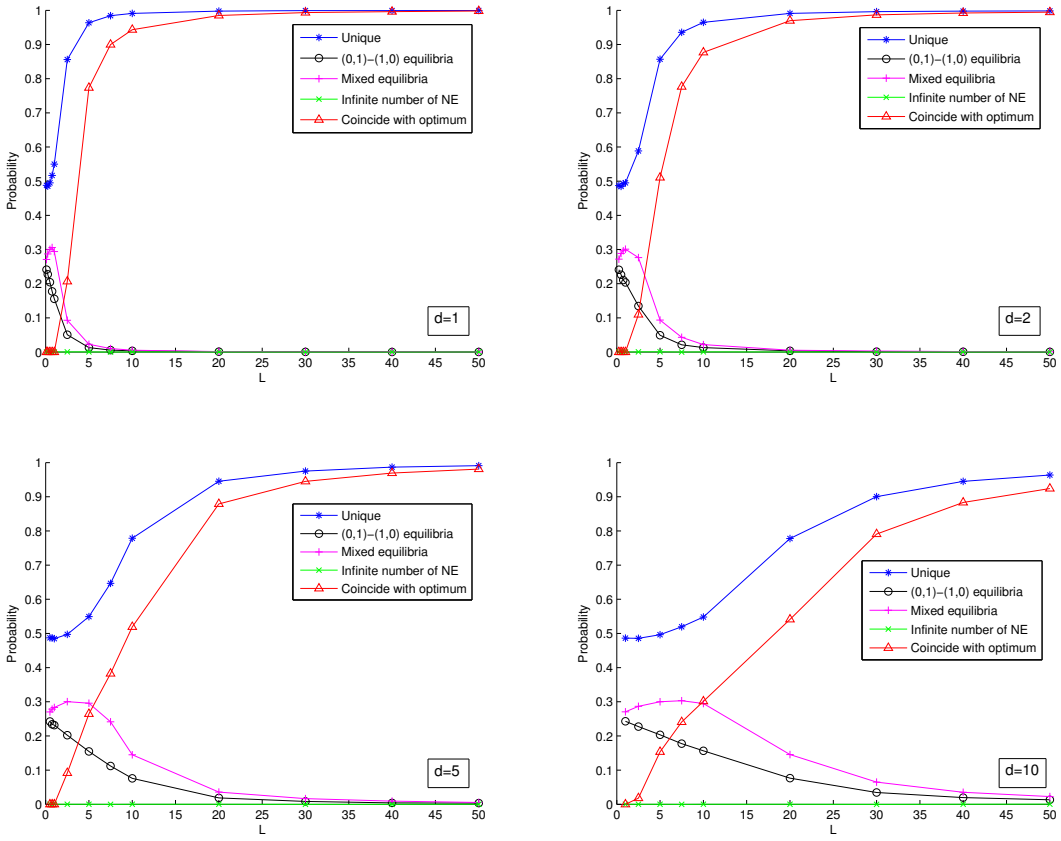

Figure 6.31: Probability of having different Nash equilibria for the 2–player game, increasing L, for different values of d, assuming $\eta = 10^{-3}$ and $\alpha = 4$..

want to use the whole same spectrum since the interfere is small enough. In particular, we can see that when $L < d$ that probability is around 50% and then starts increasing, approaching 1 when $L \simeq 5d$. Note that the probability of having an infinite number of Nash equilibria is very close to zero, as expected. Sometimes it can be slightly different from zero for numerical issues in the evaluation of the integral.

Furthermore, the probability that optimum and unique equilibrium coincide has a similar behavior of the probability of uniqueness, but it is lower. This is clear, since when the equilibrium and the optimum coincide, the equilibrium is unique, but the opposite is not always true.

Finally, we discuss some trivial limits on the probabilities considered before. First, we can see that, for a fixed d, increasing L, also the probability of having a unique equilibrium increases, since the two players are far apart and decide to use the whole portion of the available spectrum. When $L = 0$, the two transmitters coincide, then $x_1 = x_2 = d$, that corresponds to the case in which there exists an infinite number of Nash

equilibria. In contrast, when $L = \epsilon$ for any small $\epsilon > 0$, we can have three different cases. Namely, each x can be a little bit greater than d or a little bit smaller (remember that $x^2 = d^2 + \epsilon^2 - 2d\epsilon\cos\alpha$). We can see this in Figure 6.32. In fact, when receiver 1 is on the left arch AB, then x is greater than d, in contrast when is on the right arch, is smaller, and when the two transmitter are close (ϵ is small) the two arches (left and right) are more or less of the same length, meaning that we can be with probability 0.5 on the left or on the right arch (in fact the angle is uniformly chosen at random). Therefore, the probability of unique equilibrium is equal to 0.5 (given by the probability that both the xs are greater than d , i.e., 0.25, plus the probability that only one x is greater and the other is smaller, but still above the line $x_1x_2 = d^2$, and this happens with probability 0.25). In contrast, the probability of having three equilibria is 0.5. In particular, this is half split between having $\{(0,1),(1,0),(0.5,0.5)\}$ (both xs are less than d and this happens with probability 0.25) and $(0.5,0.5)$ with the mix equilibria (when only one x is greater than d, below the line $x_1x_2 = d^2$). This explains why pink and black curves (Figure 6.31) approach 0.25 when L gets small enough.

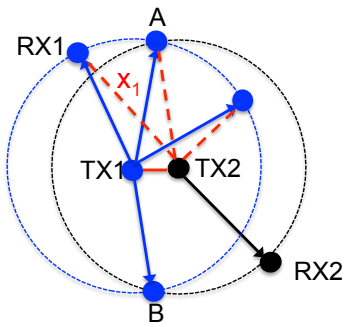

Figure 6.32: Scenario that explains the limit for L that approaches zero.

In contrast, when we fix L, increasing d corresponds to decreasing the probability of uniqueness of the equilibrium. This corresponds to the case in which the area, in which the two pairs of users are deployed, is fixed. Therefore, increasing the distance between communicating pairs, the interference increases as well, and transmitters might decide to use different bands of the spectrum. Finally, note that when L goes to zero the optimum never coincides with the equilibrium in $(0.5,0.5)$. In fact, the optimal solution always corresponds to split and use different portions of the spectrum. The reason why, when $L = \epsilon$, with ϵ small, this probability approaches zero is clear also from Figure 6.30. In fact, when $L = \epsilon$, the two xs are both close to d (see Figure 6.32), therefore they never satisfy the condition given by Eq. (6.40).

6.6 Conclusion

This chapter focuses on spectrum sharing games, where the interference between players is modeled on the basis of the geographical position of the nodes. Furthermore, the utility function adopted by the users is based on the Shannon capacity. First, we deeply analyze the optimal solution of the problem. We show why it is not straightforward to derive it. We analytically provide the optimal solution for the symmetric case. We numerically study the asymmetric optimal solution. The analytical characterization of this result is part of future work.

Then, we analytically characterize the Nash equilibria of the 2–player game. We assess their quality with respect to the optimum using the PoS and the PoA and we also study their stability.

Finally, resorting to stochastic geometry, we provide a stochastic characterization of the 2–player game. We derive the joint probability distribution on the distances between interfering pairs of users. Using this result, we numerically evaluate the probability distribution over the possible strategies for the 2–player game. Future work will attempt to derive simple analytical approximations for the equilibria distribution as a function of the system parameters (L, d).

Publications: [107]

Chapter 7: Spectrum Sharing Game with Interference Model and N players

In the previous chapter, we have analyzed the 2–player spectrum sharing game with interference. In this chapter we consider the N–player game. The analysis in this case becomes very complicated and a full characterization, such as the one provided for the 2–player case, is hard to obtain. We first give some preliminary results about the analytical characterization of the equilibria. Then, we use our observations on the sum–rate optimal allocations in the 2–player asymmetric game to motivate a distributed player power allocation update heuristic that improves the sum rate utility above that achieved by the full–spread equilibrium. Our simulation results demonstrate that for networks with low spatial density a fixed full–spread equilibrium is socially optimal, but the gap between the full–spread equilibrium and the social optimum increases in the spatial density.

The aim of the second part of this chapter is to provide a partial and approximate characterization of the equilibria of the N–player game using stochastic geometry. A first assumption that can be made is based on the fact that the sum interference is often well–approximated by its largest value. The resulting game model is simplified by the fact that the best response function of each user in each band depends only on his nearest neighbor. In this context, it is worth noting that whenever two pairs of users are coupled (the nearest transmitter for receiver RX_i is TX_j, and the nearest transmitter for receiver RX_j is TX_i), the sub–game becomes a 2–player game. The probability for which this happens represents the first fundamental quantity that we derive in the second part of this chapter. We refer to it as *coupling probability*. In general, the coupling probability depends on the density of the users and, consequently, on the average distance between a receiver and its closest interfering transmitter. The complexity of the model mainly comes from the fact that we are dealing with random variables that are usually dependent on one another. We provide an analytical upper bound expression for the coupling probability and we compare this with simulation results. Furthermore, we provide the exact value of the coupling probability when the density of the users goes to zero.

Finally, using the results described above, we provide a characterization of the equilibria distributions for the N–player game. The final goal is to show how the equilibria distribution can be approximated using

the coupling probability together with the assumption that we can approximate the perceived interference considering the nearest neighbor only.

This chapter is organized as follows: Sec. 7.1 presents the game model. In Sec. 7.2, we discuss some preliminary results obtained using a game simulator. Sec. 7.3 introduces stochastic geometry as a promising approach for the characterization of the N–player game and Sec. 7.4 concludes the chapter.

7.1 The N–player game model

The game model for the general N–player case is a natural extension of the game model presented in Sec. 6.2. We consider N pairs of users competing for the same spectrum that is divided into two orthogonal sub–channels. The utility function of the generic player i is the following:

$$U_i = \log_2\left(1+\frac{P_i D}{1+\sum_{j\neq i} P_j X_{ij}}\right)+\log_2\left(1+\frac{\bar{P}_i D}{1+\sum_{j\neq i} \bar{P}_j X_{ij}}\right) \tag{7.1}$$

where $X_{ij} = x_{ij}^{-\alpha}/\eta$ is the interference to noise ratio from transmitter j to receiver i when full power is used on a band, and x_{ij} is the distance between transmitter j and receiver i. We present the following theorem that guarantees that the N–player game always admits a pure–strategy Nash equilibrium. Note that the same result is highlighted also in [3], however the authors do not report the formal proof, that is then reported in the following.

Theorem 7.1.1. *The strategy profile $P_i = 0.5, \forall\, i \in N$ is always a Nash equilibrium of the N–player game, and we refer to it as full–spread equilibrium.*

Proof. The best response function $P_i^*(\mathbf{P}_{-i})$ of player i is obtained by solving

$$\frac{\partial U_i(\mathbf{P})}{\partial P_i} = 0$$

for every P_i, where $\partial U_i(\mathbf{P})/\partial P_i$ is given by:

$$\frac{\partial U_i}{\partial P_i} = \frac{\left[\sum_{j\neq i}(1-2P_j)X_{ij} + (1-2P_i)D\right] D\log_2 e}{(1+\sum_{j\neq i} P_j X_{ij} + P_i D)(1+\sum_{j\neq i}(1-P_j)X_{ij} + (1-P_i)D)} \tag{7.2}$$

Therefore, for every i:

$$\sum_{j \neq i}(1-2P_j)X_{ij} + (1-2P_i)D = 0. \tag{7.3}$$

Projecting P_i^* onto $[0,1]$ gives:

$$P_i^*(\mathbf{P}_{-i}) = \left[\frac{1}{2} + \sum_{j \neq i}\frac{X_{ij}}{D}\left(\frac{1}{2} - P_j\right)\right]_0^1 \tag{7.4}$$

Therefore, we have a system with N equalities and in N variables. It is straightforward to see that $P_i = 0.5$, $\forall i \in N$ is always a solution of the previous system. This proves the theorem. □

However, this solution is not guaranteed to be the only equilibrium of the game. This result is clearly explained also considering the 2–player case. When $X_1 X_2 = D^2$ the system (7.3) is composed by two linearly dependent equalities and there is an infinite number of Nash equilibria. Therefore, (7.4) is always a solution but it is not guaranteed to be the only one. A sufficient condition for this solution to be the unique equilibrium (provided also in [3]) is: $\sum_{j \neq i} X_{ij} < D \quad \forall\, i \in N$. However, the condition is pretty far from the actual threshold already for the 2–user case, as shown in Figure 7.1. Furthermore, the characterization of the best response for the N–player game is discussed also in [97, 100].

7.1.1 Optimal solution and full–spread equilibrium

In this section, we compare, through simulations, the optimal solution with the full–spread Nash equilibrium, in which every player plays the strategy $P_i = 0.5$. Furthermore, in order to improve the Nash equilibria of the N–player game, we propose a heuristic algorithm that starts from the Nash equilibrium in which all users play the strategy $P_i = 0.5$ and aims at improving the efficiency of the allocation. Namely, from the results of the 2–player game, we have found that whenever two pairs of users are such that X_{ij} and X_{ji} satisfy:

$$X_{ij} + X_{ji} + X_{ij}X_{ji} > D \tag{7.5}$$

they should use different halves of the spectrum, instead of the whole band. Therefore, we can motivate the users to implement local moves towards the optimum, reducing the interference perceived from their neighbors. The goal of the heuristic is to approximate the global optimal solution only with local changes.

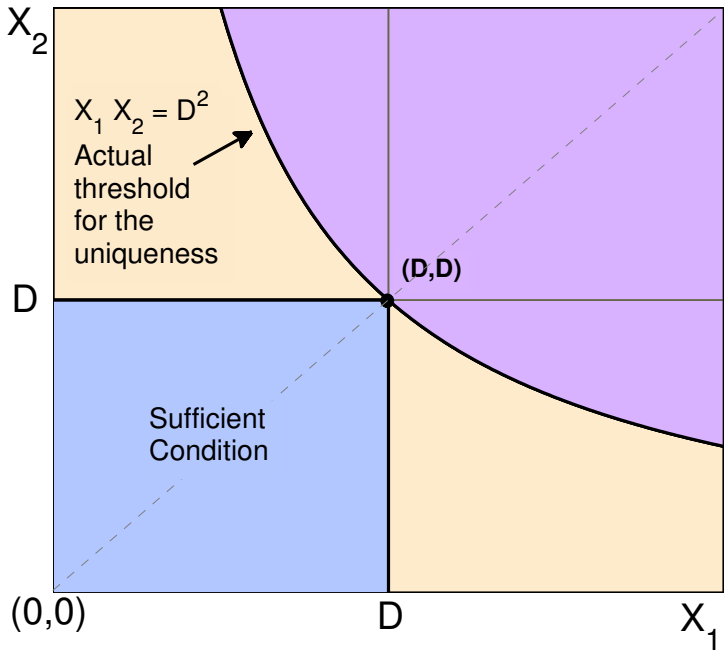

Figure 7.1: Comparison between sufficient condition and actual threshold for the uniqueness of the Nash equilibrium in the 2–player game.

The heuristic is illustrated in Algorithm 3.

Algorithm 3 Heuristic algorithm

1: Initialize $P_i = 0.5 \quad \forall\, i = 1 \dots N$
2: **while** $\exists (i,j) | X_{ij} + X_{ji} + X_{ij}X_{ji} > D$ and $P_i = P_j = 0.5$ **do**
3: Set $(P_i, P_j) = \begin{cases} (0,1), & \text{w.p. } 0.5 \\ (1,0), & \text{w.p. } 0.5 \end{cases}$
4: **end while**

We have implemented an instance generator able to create instances representing the network scenario. The generator takes as input the following parameters: the number of pairs N, the distance d between each transmitter and receiver and the edge L of the square arena where the N pairs are randomly deployed. Once all the pairs are deployed over the arena, the INRs X_{ij} between each transmitter j and each receiver i are evaluated by the generator. The optimal solution has been obtained writing the optimization problem, i.e., (6.6)), in AMPL [51] and solving it with the non–linear solver MINOS [109]. Numerical results are discussed in the following. Namely, we consider an arena with $L = 200$ and $d = 25$. The parameters for the evaluation

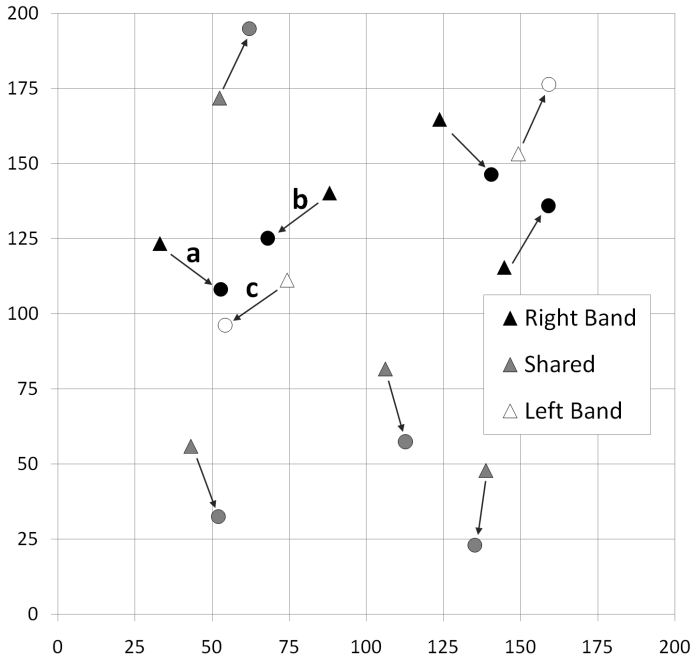

Figure 7.2: Sample of the considered topology when $N = 10$.

of the total utility are $\eta = 10^{-3}$, $\alpha = 4$ and $B = 1$. An example of the considered topology is reported in Figure 7.2. Hereafter, all the reported results are averaged values on 30 randomly generated instances.

In Figure 7.3, we report the total utility achieved by the users as a function of increasing N. When the number of users is small (say $2, \ldots, 10$) the optimum and the Nash equilibrium are very close. This is consistent with the theoretical results obtained for the 2–player game. In fact, when the number of pairs is small, they are far enough apart (i.e., the average X_{ij} is small enough) and the optimal solution coincides with the equilibrium, i.e., each player splits power equally over the two bands. As the spatial density of the network increases, the average interference increases, and the equal split equilibrium achieves an increasingly poor sum utility relative to the optimal utility. The heuristic is able to improve the sum utility above that achieved by the equal split equilibrium, but there is still a significant gap between the heuristic sum utility and the optimal. In Figure 7.4, we report the ratio between the utility function at the optimal solution and at the full–spread equilibrium. Formally, we cannot call this PoA, because we did not prove that the equilibrium of Theorem 7.1.1 is the worst equilibrium. However, extensive simulations show that this is always the worst equilibrium that we can find.

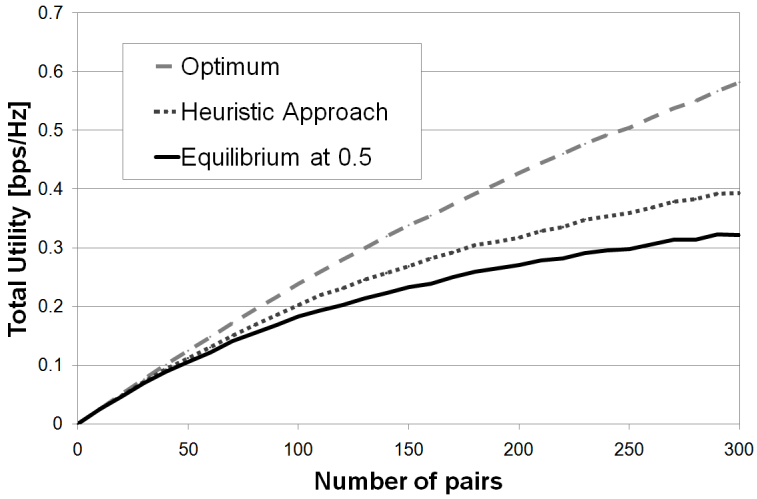

Figure 7.3: Total utility (optimal, full–spread equilibrium, heuristic) for the N–player game as a function of N.

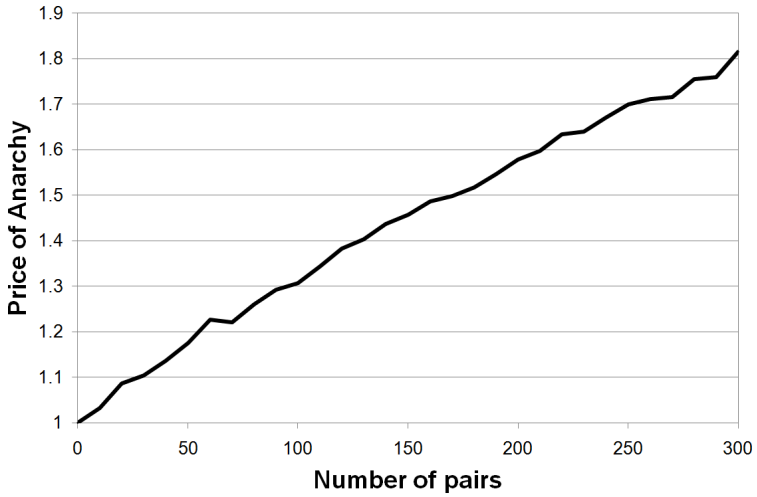

Figure 7.4: PoA of the full–spread equilibrium.

7.2 Preliminary results using a game simulator

The previous section highlights that the analytical analysis of the N–player game might be very complicated. Therefore, we first provide some numerical results that show the equilibria distribution increasing the density of the users λ. Namely, we have implemented a game simulator that we use to characterize a large number of Nash equilibria and study their quality. A pseudo–code is reported in Algorithm 4. The simulator starts from a random allocation of the power vector. Then, given the strategies played by all the other players ($\mathbf{P}_{-i}$), it evaluates the best response for player i, provided explicitly by Eq. (7.4). For each player, it compares the best response with the actual power. If there exists at least one player that is not playing her best response, the allocation is not an equilibrium. One player among those who are not playing their best response is randomly chosen and forced to deviate towards the best response power. The **while** cycle is then repeated until no player wants to unilaterally deviate from the chosen strategy, i..e, the equilibrium has been reached. The same algorithm can be run multiple times if one wants to find many (potentially different) equilibria of the game.

Algorithm 4 Game Simulator

1: Initialize $P_i = \text{rand}(1) \quad \forall\, i = 1 \dots N$
2: **while** There exists at least a player k that has updated its P_k in the last step **do**
3: Evaluate best response BR_i for each player i
4: Look for a player k such that $BR_k \neq P_k$
5: **if** such player exists **then**
6: $P_k \leftarrow BR_k$
7: **end if**
8: **end while**

We consider a square arena in which we deploy pairs of users uniformly at random, such that the density of the user is λ, defined as $N/|A|$, where N is the number of points and A is the arena. Hereafter, all the reported results are averaged values on 100 randomly generated instances. We characterize the equilibria, evaluating the probability of selecting a specific action. In particular, from the 2–player game, we have observed that there are some regions in which players play 0 and 1 (note that these strategies are symmetric) or 0.5. Therefore, we evaluate the probability of a user of choosing the strategy 0.5, or strategies 0 or 1 (that we put together due to their symmetry), or one among all the other strategies, that we will indicate with *"oth"*. Since we are dealing with continuos variables, once that we have reached the equilibrium, we use the

discretization reported in Figure 7.5. Moreover, note that we are assuming that the best response function of

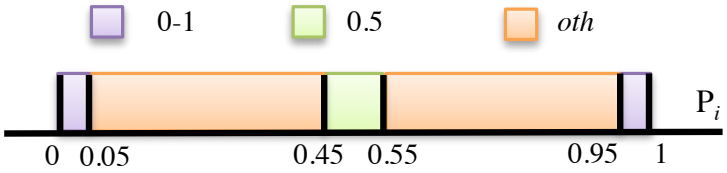

Figure 7.5: Discretization used in the simulations.

each player depends on the overall interference perceived by the users.

We report some experimental results obtained with the game simulator. We assume $\eta = 10^{-3}$, $\alpha = 4$, and different values of d. Figure 7.6 and 7.7 (left) report the probability of selecting a specific strategy increasing the density of the users. For both cases, we observe that all users select 0 or 1 when the density is high (users are close to each other). In contrast, they tend to use the whole spectrum (full–spread equilibrium) when they are far enough (small density).

For both cases, we have also evaluated the average distance to the closest interfering transmitter, conditioned to the chosen strategy. Figure 7.6 and 7.7 (right) show the average distance to the closer interfering node for different strategies. We can observe that the average distance for players who select strategies 0 or 1 and "*oth*" is constant. In contrast, when the distance to the nearest interferer is sufficiently large (low density), users decide to play 0.5.

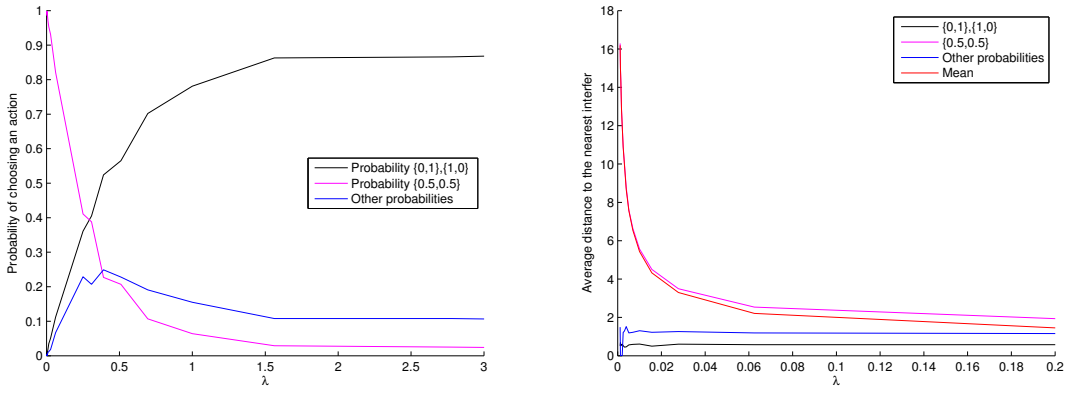

Figure 7.6: Results obtained for $d = 1$.

The numerical results confirm that the probability of selecting a specific strategy is related to the geographical distribution of the users. In fact, the average distance to the nearest interferer for players that play

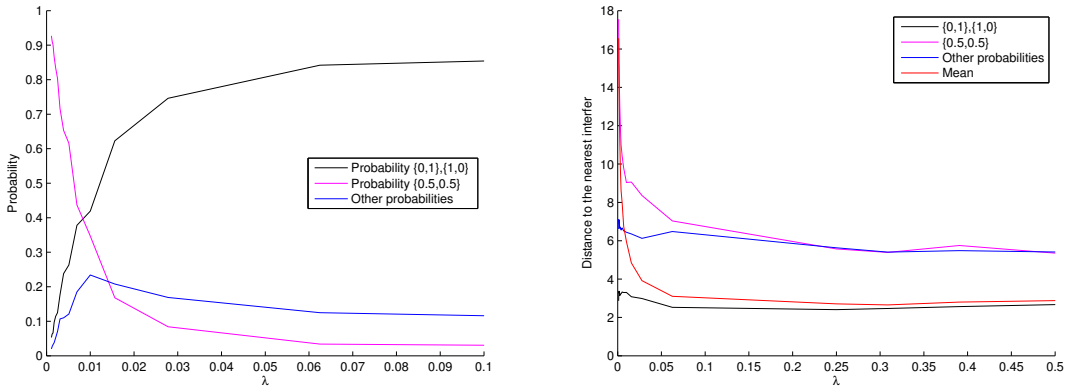

Figure 7.7: Results obtained for $D = 1$.

$(0,1)-(1,0)$ or "*oth*" strategy is constant and does not change with the density. Namely, Figure 7.6 and 7.7 (right) confirms that is the distance to the nearest neighbor to dictate the strategy chosen by the users and this supports the idea that the game can be approximated considering the nearest neighbor only.

Therefore, we now compare the equilibria distribution when players play according to the best response given by the sum interference and when they play according to the best response that accounts for the maximum interferer only. Formally, we introduce the *sum-game* and the *max-game*.

Definition 7.2.1 (Sum-game)**.** *The sum-game is the game in which the player play using the following best response function:*

$$P_i^*(\mathbf{P}_{-i}) = \left[\frac{1}{2} + \sum_{j \neq i} \frac{X_{ij}}{D}\left(\frac{1}{2} - P_j\right)\right]_0^1 \tag{7.6}$$

Definition 7.2.2 (Max-game)**.** *The max-game is the game in which the player play using the following best response function:*

$$P_i^*(P_j) = \left[\frac{1}{2} + \frac{X_{ij}}{D}\left(\frac{1}{2} - P_j\right)\right]_0^1 \quad \textit{where} \quad j : X_{ij} = \max_k X_{ik} \tag{7.7}$$

As proved in Sec. 7.1, the sum–game always admits at least one pure strategy Nash equilibrium, i.e., the full–spread equilibrium. We now prove that this is always a Nash equilibrium (in pure strategies) also for the max–game.

Theorem 7.2.3. *The strategy profile $P_i = 0.5, \forall\, i \in N$ is always a Nash equilibrium for the max– game.*

Proof. The proof comes directly from the best response analysis. In fact, assume that all players are playing the strategy $P_j = 0.5 \; \forall j \in N$. This is an equilibrium since no player wants to unilaterally deviate. In fact, for every player i, whose nearest neighbor is player j, with $P_j = 0.5$, the best response is:

$$P_i^* \left(\frac{1}{2}\right) = \left[\frac{1}{2} + \frac{X_{ij}}{D}\left(\frac{1}{2} - \frac{1}{2}\right)\right]_0^1 = \frac{1}{2}$$

that proves the theorem. □

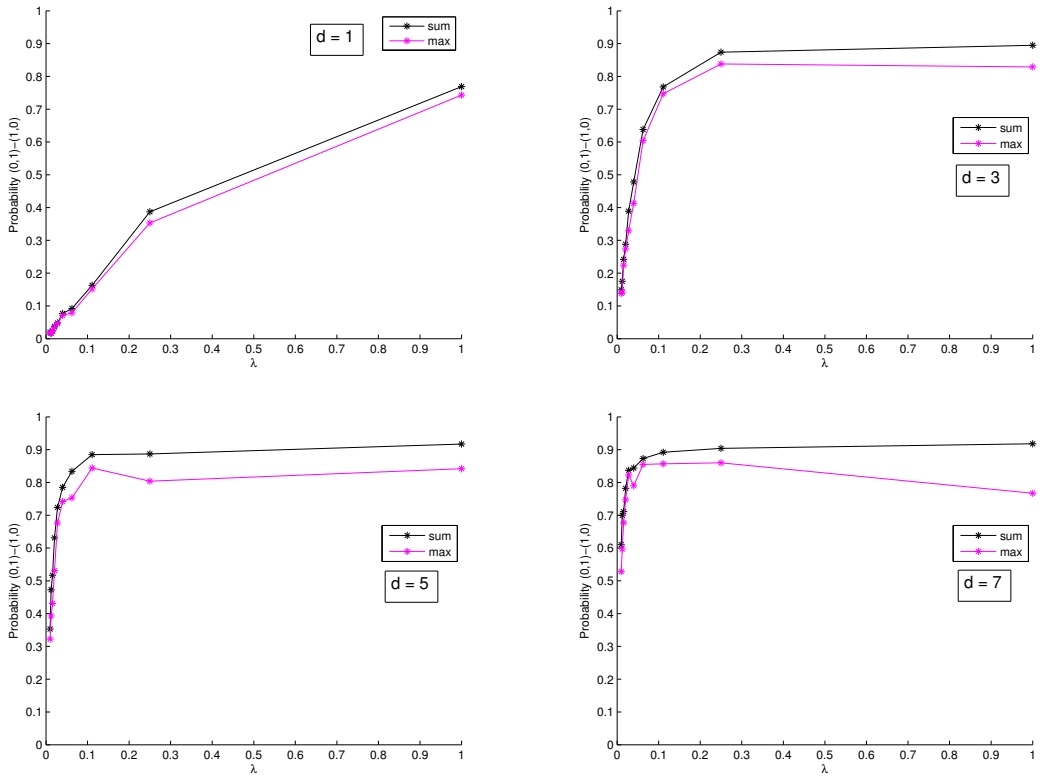

Figure 7.8: Probability of selecting strategies $(0, 1)$ or $(1, 0)$, for different values of d and increasing λ.

In the following we report some numerical results that compare the simulated equilibria distributions when players play the sum–game and the max–game. Figures 7.8 and 7.9 compare the probabilities of selecting $(0, 1) - (1, 0)$ and $(0.5, 0.5)$ for different values of d, assuming $N = 25$ players, i.e., couples of nodes, and increasing the density λ of the users. For completeness, Figure 7.10 reports the probabilities of selecting "other" strategies. As expected, the curves are pretty close, especially for the low–density regime.

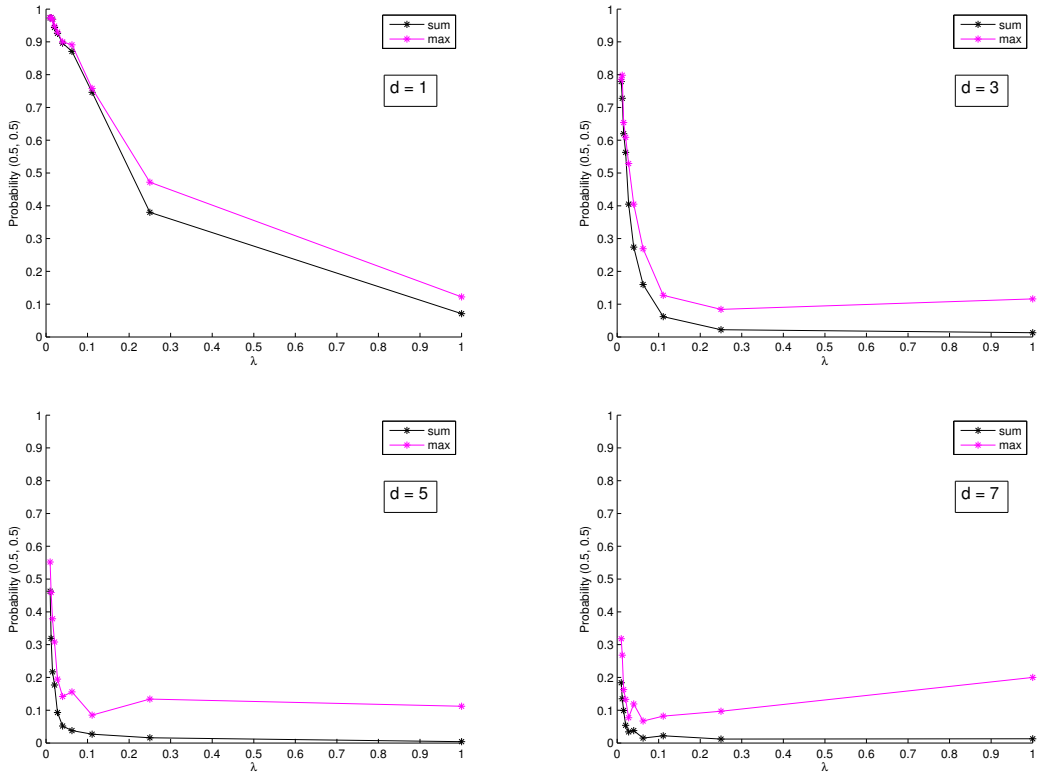

Figure 7.9: Probability of selecting strategy $(0.5, 0.5)$, for different values of d and increasing λ.

7.3 Stochastic characterization of the N–player game

In this section, we introduce stochastic geometry as a promising approach for the characterization of the N–player game. From one side this approach allow us to deal with a more tractable game model, but at the same time we will be able to predict the performance of the game in large networks only on the basis of the users distribution. To the best of our knowledge, this is one of the first works that provides a stochastic characterization for the spectrum sharing game.

7.3.1 Reference model

Hereafter, we assume that users are arbitrary placed over a given arena. We know that the equilibria of the game depend on the distances between interfering nodes. However, in such a scenario, the distances x_{ij} between each pair of nodes are random variables that depend on the specific user's distribution. Therefore, also the equilibria are random variables, whose distributions can be properly derived using stochastic geometry.

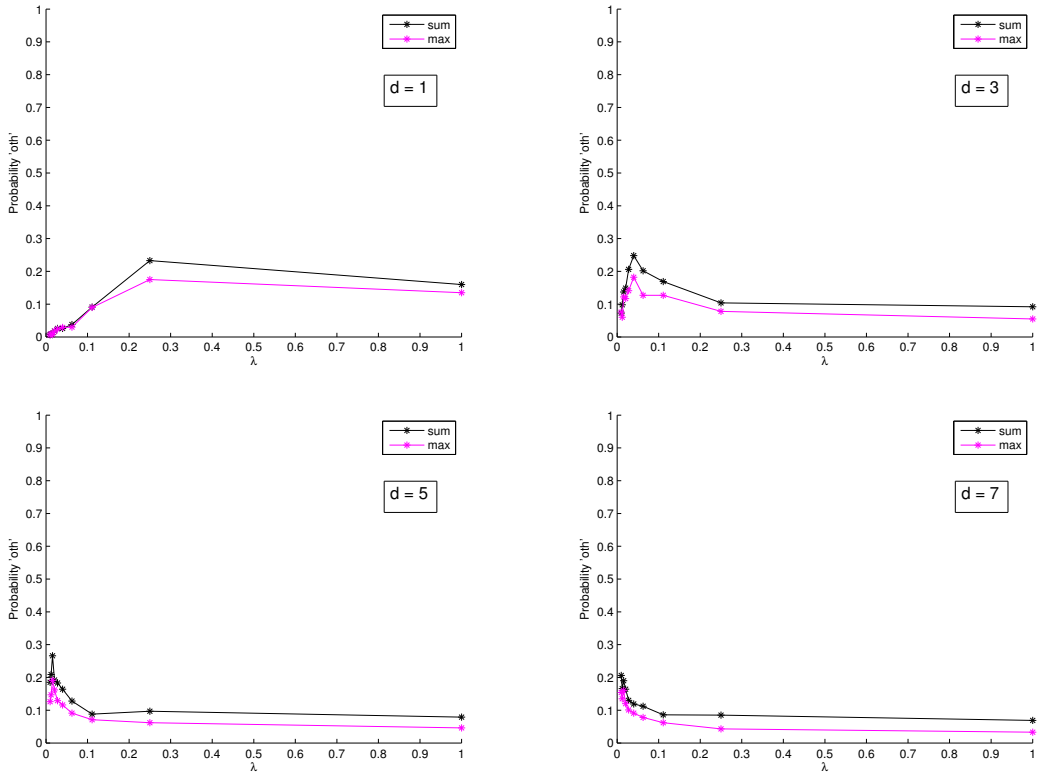

Figure 7.10: Probability of selecting "other" strategies, for different values of d and increasing λ.

This approach provides general results on the spectrum sharing game and can be applied for any arbitrary distribution of the nodes. However, as common in network models, we assume that nodes form a *homogeneous Poisson point process* (PPP) with density λ.

Definition 7.3.1 (Homogeneous Poisson point process (PPP))**.** *A PPP with intensity $\lambda > 0$ in m–dimensions is a random countable collection of points $\Pi_{m,\lambda} \subset \mathbb{R}^m$ such that:*

- *For two disjoint subsets $A, B \subset \mathbb{R}^m$ the number of points from Π in these sets are independent random variables.*
- *The number of points in any compact set $A \subset \mathbb{R}^m$, where $\Pi \cap A = \Pi(A)$, is a Poisson random variable with parameter $\lambda|A|$, for $|A|$ the volume of A. Therefore:*

$$\mathbb{P}(\Pi(A) = k) = \frac{1}{k!} e^{-\lambda|A|} (\lambda|A|)^k, k \in \mathbb{Z}^+. \tag{7.8}$$

Moreover, since the interfering relationships among users are strictly related to the distances between them, we recall the following fundamental proposition on the *void probability*. Namely, given a compact set A, we call void probability the probability that there are no points in A. Formally:

Proposition 7.3.2 (Void Probability)**.** *Given a PPP with intensity λ and a compact set A, the probability that there are no points in A is:*

$$\mathbb{P}(\Pi(A) = 0) = e^{-\lambda|A|} \tag{7.9}$$

Given this model, we have already highlighted the fact that the equilibria distribution depends on the distances among users, that are random variables that can be described using the aforementioned Poisson model. However, in the propagation model that we are assuming, the interference decreases polynomially with the pathloss factor (α). As mentioned before, a reasonable assumption that we can make is that the sum of the interference contributions perceived by each user is well–approximated by the maximum of these terms [110]. In other words, we approximate the interference considering the nearest interfering transmitter only.

This assumption allow us to simplify the model, reducing the N–player game to small sub–games. We can do this using the directed–influence–graph–based approach.

Definition 7.3.3 (Directed influence graph)**.** *The* directed influence graph *associated to an N–player game is a directed graph in which each vertex corresponds to a pair of nodes, and a directed edge from i to j represents the fact that TX_i is the nearest interferer for RX_j.*

By definition of directed influence graph, it is worth noting that the following property holds:

Remark 7.3.4. *In every directed influence graph, each vertex has in–degree equal to* 1*. In contrast, the out–degree might be* 0*,* 1*, or greater than* 1*.*

In Figure 7.11a, we show an example of a 6–player game, i.e., there are 6 pairs of transmitter and receiver that interfere each other. Assuming that the choice of each player is mostly influenced by the nearest neighbor, we can simplify the game considering only the interactions highlighted in Figure 7.11b, where each receiver

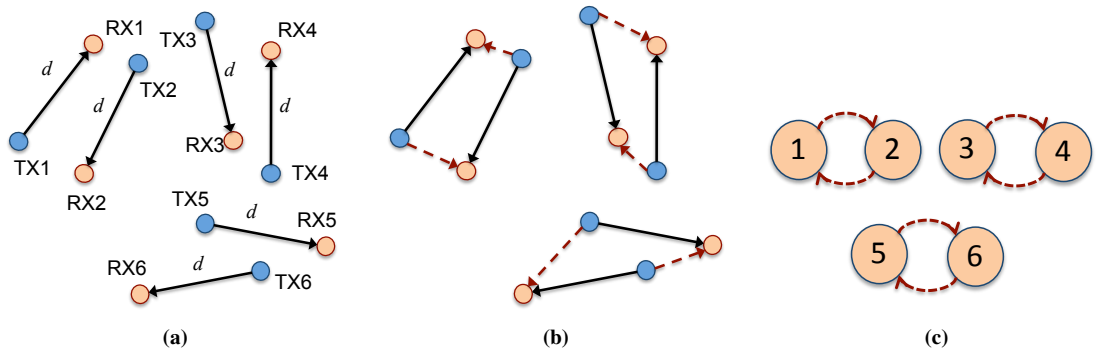

Figure 7.11: Example of a 6–player game (a), the interference relationships (b) and the associated directed influence graph (c).

is associated to his closest interfering transmitter. In this case, all pairs of nodes are coupled. The associated directed influence graph is reported in Figure 7.11c. We can observe that, in this case, we obtain couples of players that mutually interfere each other. Formally, we provide the following definition.

Definition 7.3.5 (Couple)**.** *We say that two pairs of users (TX_i, RX_i) and (TX_j, RX_j) form a* couple*, or simply are* coupled*, if the nearest interfering transmitter for receiver RX_j is TX_i, given that the nearest interfering transmitter for receiver RX_i is TX_j. Two couple pairs form a* 2*-clique in the directed influence graph.*

In general, we might not have that all users are coupled. Therefore we introduce also the following definitions.

Definition 7.3.6 (Cycle)**.** *We say that three or more pairs of users form a* cycle*, when the nodes of the associated directed influence graph have all in–degree and out–degree equal to* 1*.*

Definition 7.3.7 (Chain)**.** *We say that one or more pairs of users form a* chain*, when the nodes of the associated directed influence graph have in–degree and out–degree equal to* 1*, except for the leaves of the chain that have out–degree equal to zero.*

Examples of a couple, a cycle and a chain are reported in Figure 7.12.

Finally, note that every network can be represented as a directed influence graph that is composed by one or more isolated sub–graphs. In particular, every isolated sub–graph has the following property.

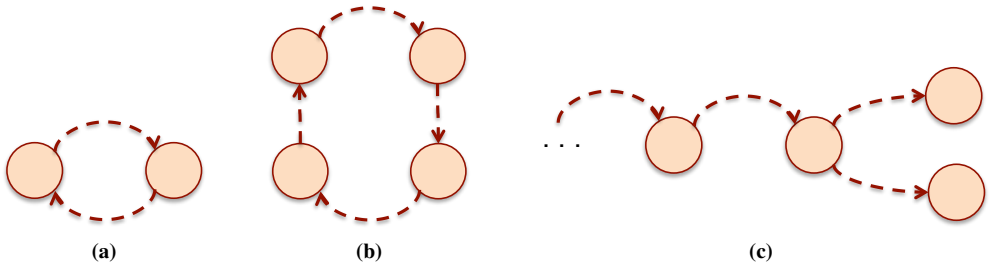

Figure 7.12: Example of a couple (a), a cycle (b), and a chain (c).

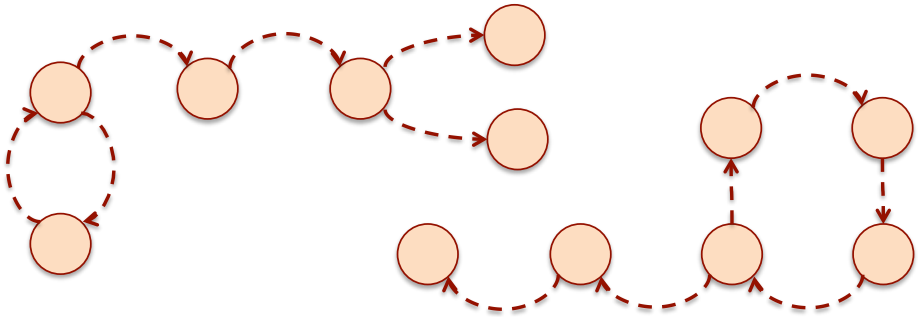

Figure 7.13: Examples of isolated sub–graphs.

Proposition 7.3.8. *Every isolated sub–graph is necessarily composed by one and only one* couple *or* cycle *and might have one or more* chains *connected to it.*

Proof. The rationale of this property is the following. In any isolated graph, two cycles or two couples or one cycle and one couple would be connected by a chain. The chain connecting two couples/cycles must have at least one node with in-degree equal to 2. This contradicts Remark 7.3.4. Furthermore, it is easy to see that a chain cannot be isolated by itself. This comes again from Remark 7.3.4, i.e., each node has in–degree equal to 1. □

Examples of isolated graphs are reported in Figure 7.13.

Finally, it is easy to see that the analysis of the game using the directed influence graph can be done in two steps:

1. Analysis of the isolated sub–games in all the couples and cycles of the graph;

2. Analysis of the best-response reactions of the nodes in the chains, whose moves are influenced only by

the couple/cycle connected to it.

Note that whenever we have coupled pairs of users, we can study the sub–games between them using the results obtained for the 2–player game. Therefore, we are interested in deriving the probability of being coupled, that is defined in the following.

Definition 7.3.9 (Coupling probability)**.** *The* coupling probability $P_c(\lambda)$ *is the probability that two pairs of nodes are coupled and it depends on the density* λ*.*

We also define the conditional coupling probability.

Definition 7.3.10 (Conditional coupling probability)**.** *The* conditional coupling probability $P_{c|\mathrm{x}_i}(\lambda, x_1)$ *is the probability that two pairs of nodes are coupled, given that the distance between RX*$_i$ *and TX*$_j$ *is* x_i*. It depends on* λ *and* x_1*.*

The main goal of this analysis is to provide an analytical characterization of the equilibria distribution using the aforementioned techniques. Numerical evaluations show that there exists a regime (the low density regime) in which nodes are either coupled or belong to a chain that is connected to a couple. Figure 7.14 shows the probability distribution over different types of nodes increasing λ. The following analysis aim at deriving the coupling probability. In particular, for the low density regime we will derive the exact value of coupled nodes. This represents the fraction of nodes that play 2–player subgames and for which we are able to fully characterize the equilibria distribution. For the other nodes, we use the directed–influence–graph approach in order to predict the performance of the game.

7.3.2 Coupling probability

In this section, we characterize the coupling probability, i.e., the probability that two pairs of users are coupled. Consider the topology reported in Figure 7.15. Let t be the distance between the two transmitters and y the distance between the two receivers. Assume that TX_2 is the nearest interferer for RX_1. Note that this means that there is no other transmitter in the circle area of radius x_1 and center in RX_1. What is the probability that TX_1 is the nearest interferer for RX_2? This means that there is no transmitter in the circle of radius x_2 and center in RX_2. Refer now to Figure 7.18. Given that there is no transmitter in the circle with center in RX_1 and radius x_1, the coupling probability is proportional to the area of the non–overlapping

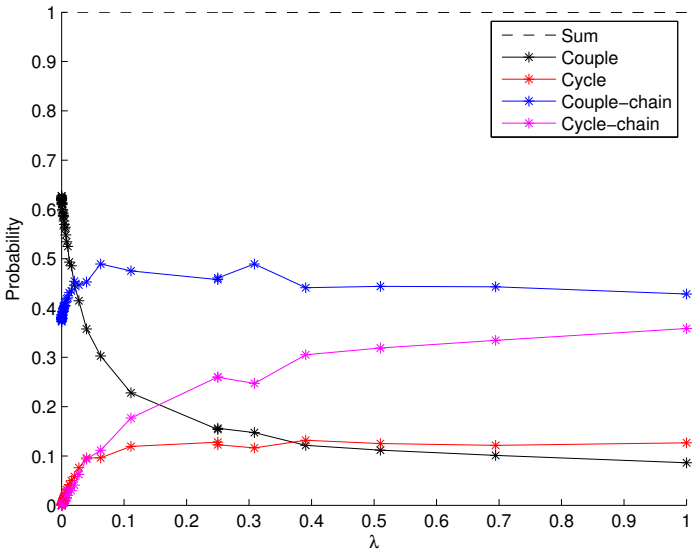

Figure 7.14: Probability distribution over different types of node in the directed influence graph increasing λ.

green lune. In fact, the probability that TX_1 is the nearest transmitter for RX_2 corresponds to the probability that there is no transmitter in the circle with center in TX_2 and radius x_2, knowing, by assumption, that there is no transmitter in the overlapping lens. We now recall some results that are useful to characterize the area of the lune, i.e., the concave-convex area bounded by the two circular arcs belonging to the circles of radius x_1/x_2 and center in $\mathrm{RX}_1/\mathrm{RX}_2$.

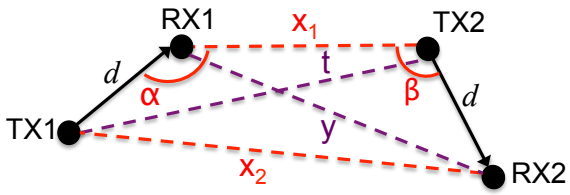

Figure 7.15: Scenario considered for the evaluation of the coupling probability.

Proposition 7.3.11. *For circles of radius a and b, with $b > a$, whose centers are separated by a distance c,*

refer to Figure 7.16, the area of the lune $\Gamma_L(a,b,c)$ *is given by:*

$$\Gamma(a,b,c) = \frac{1}{2}\sqrt{(a+b+c)(b+c-a)(a-b+c)(a+b-c)} + \\ + a^2 \sec^{-1}\left(\frac{2ac}{b^2-a^2-c^2}\right) - b^2 \sec^{-1}\left(\frac{2bc}{b^2-a^2+c^2}\right) \quad (7.10)$$

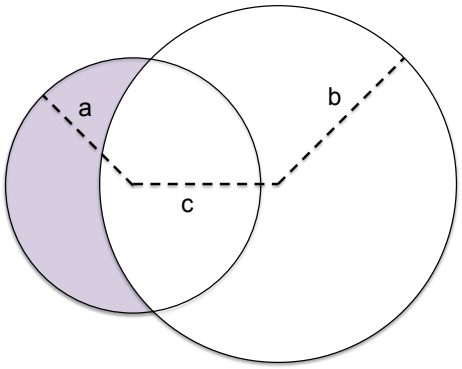

Figure 7.16: The colored ares is the lune given by two circles of radius a and b, with $b > a$, whose centers are separated by c.

We now report, without proving, the following claim.

Claim 7.3.1. *The area of the lune* $\Gamma(a,b,c)$ *is monotonic increasing in* a*, and monotonic decreasing in* b*.*

Note that in Figure 7.18, we are interested in evaluating the area of the lune given by the circle of radius x_2 minus the circle of radius x_1.

Proposition 7.3.12. *The area of the lune obtained as the difference between the circle of radius* x_2 *and the*

circle of radius x_1 is given by (refer to Figure 7.17):

$$\Delta(x_1,x_2,y)=\begin{cases}\pi x_2^2 & \textit{if } y\geq x_1+x_2 \quad \textit{Figure 7.17a}\\ \pi(x_2^2-x_1^2) & \textit{if } x_2\geq x_1+y \quad \textit{Figure 7.17b}\\ 0 & \textit{if } x_1\geq x_2+y \quad \textit{Figure 7.17c}\\ \Gamma(x_2,x_1,y) & \textit{if } x_2\leq x_1, y<x_1+x_2, x_2<x_1+y, x_1<x_2+y \quad \textit{Figure 7.17d}\\ \pi x_2^2-(\pi x_1^2-\Gamma(x_1,x_2,y)) & \textit{otherwise} \quad \textit{Figure 7.17e}\end{cases} \tag{7.11}$$

where the function $\Gamma(a,b,c)$ is defined in Prop. 7.3.11.

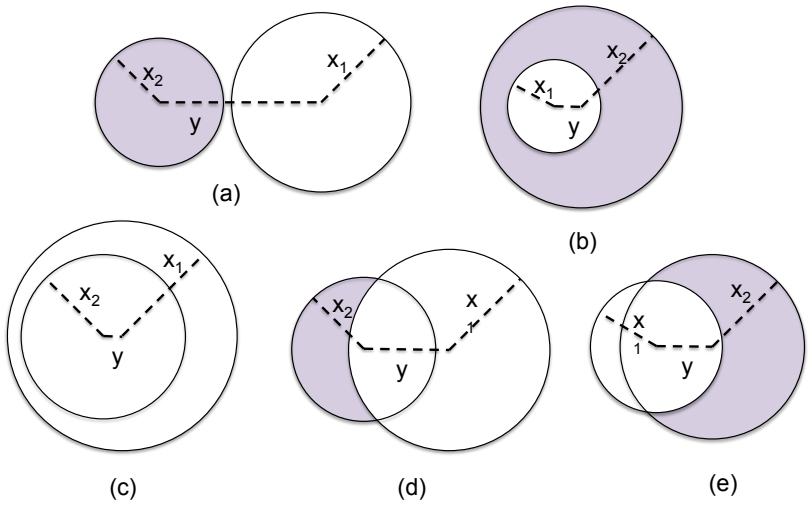

Figure 7.17: Different cases for the calculation of the area of the lune.

Lemma 7.3.13. *Given the claim 7.3.1, it follows that the area of the lune, $\Delta(x_1,x_2,y)$, is monotonic increasing in x_2.*

The area of the lune depends on the two radii (x_1 and x_2) and the distance between the two centers (y). All these quantities are random variables, whose distributions depend on how the pairs of users are deployed. Furthermore, all these quantities are related one to each other by the geometry of the problem. Therefore, if we want to characterize the area of the lune, we need to derive the joint distribution $f_{\mathsf{x}_1,\mathsf{x}_2,\mathsf{y}}(x_1,x_2,y)$.

The complexity of this analysis comes from the fact that we cannot decouple the random variables, being dependent on one each other. Therefore, we simplify the calculation conditioning on x_1, that gives the

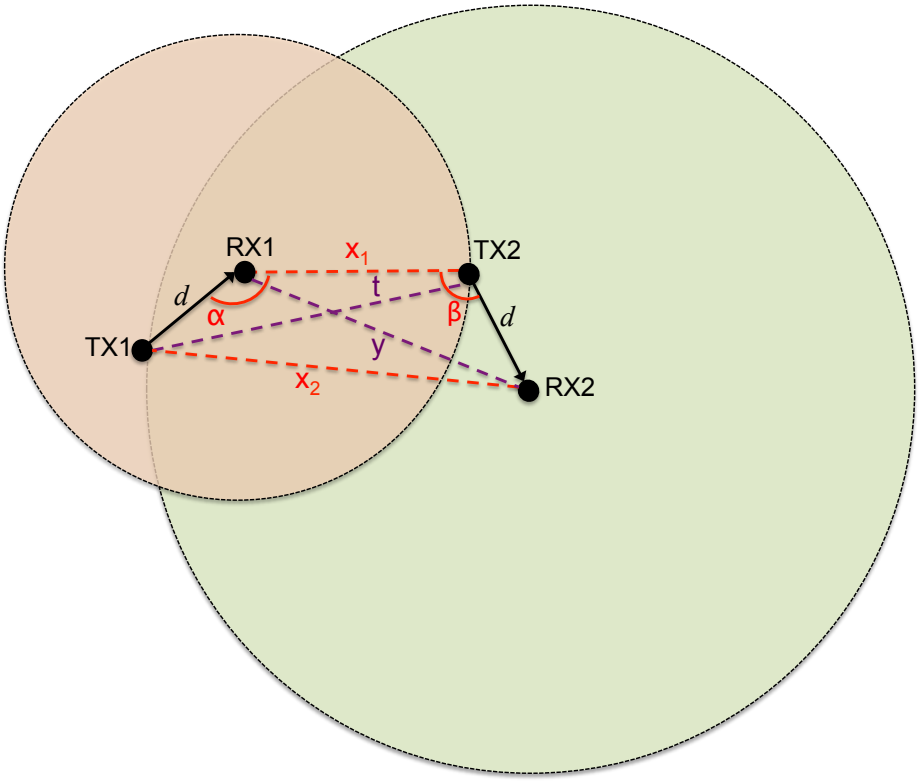

Figure 7.18: The coupling probability is proportional to the area of the non–overlapping green lune.

following:

$$f_{\mathsf{x}_1,\mathsf{x}_2,\mathsf{y}}(x_1,x_2,y)=\int_0^{\infty}\int_{|x_1-d|}^{x_1+d} f_{\mathsf{x}_2|\mathsf{x}_1,\mathsf{y}}(x_2|x_1,y)f_{\mathsf{y}|\mathsf{x}_1}(y|x_1)f_{\mathsf{x}_1}(x_1)dydx_1$$

First, recall that x_1 is a random variable that represents the distance between RX_1 and its nearest interferer. The distribution of the nearest interferer is given in [111] and is the following:

$$f_{\mathsf{x}_1}(x_1)=2\lambda\pi x_1 e^{-\lambda\pi x_1^2} \qquad x_1\geq 0 \tag{7.12}$$

where λ is the intensity of the Poisson point process that characterizes the distribution of the nodes.

We now derive the conditional distribution of y, $f_{\mathsf{y}|\mathsf{x}_1}(y|x_1)$. Unless specified otherwise, in the following we are assuming that x_1 is given. Note that this assumption is fundamental. In fact, given x_1, the considered topology is determined only by the two angles α and β, that we assume to be uniformly distributed between $[0,2\pi]$. The distribution of the cosine of a uniformly distributed angle has already been introduced

in Prop. 6.5.1.

In the following lemma, we prove the first result for the derivation of the conditional distribution of y.

Lemma 7.3.14. *Given x_1 and d,* t *and* y *are independent and have the same distribution.*

Proof. First, we can observe that, given x_1, t and y only depend on α and β, respectively. This is clear observing Figure 7.19. The two triangles $TX_1\widehat{RX_1}TX_2$ and $RX_1\widehat{TX_2}RX_2$ are built in the same way: x_1 is fixed, d is fixed, the angle between these two edges is uniformly distributed. These three elements completely define each one of the two triangles. Therefore, not only t and y are independent, but they also have the same distribution. □

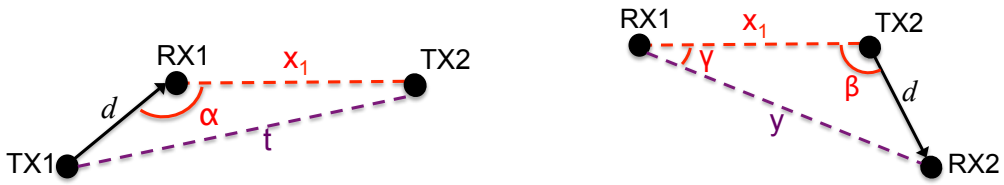

Figure 7.19: Triangles derived from the considered topology.

In order to derive the distributions of t and y, we can note that, using the law of cosines, the following relationships between the edges and the angles hold:

$$t^2 = d^2 + x_1^2 - 2dx_1 \cos\alpha \tag{7.13}$$

$$y^2 = d^2 + x_1^2 - 2dx_1 \cos\beta \tag{7.14}$$

$$\cos\gamma = \frac{x_1^2 + y^2 - d^2}{2x_1 y} \tag{7.15}$$

Define the auxiliary random variable $\mathsf{z} = \mathsf{y}^2$, whose conditional distribution is reported in the following lemma.

Lemma 7.3.15. *The conditional probability density function (pdf) of* z *is:*

$$f_{\mathsf{z}|\mathsf{x}_1}(z|x_1) = \frac{1}{\pi\sqrt{k_1^2 - (z-k_2)^2}} \qquad (x_1-d)^2 \leq z \leq (x_1+d)^2 \tag{7.16}$$

and the associated conditional cumulative density function (cdf) is:

$$F_{\mathsf{z}|\mathsf{x}_1}(z|x_1) = \frac{1}{2} + \frac{\sin^{-1}\frac{z-k_2}{k_1}}{\pi} \qquad (x_1-d)^2 \leq z \leq (x_1+d)^2 \tag{7.17}$$

where:

$$k_1 \triangleq \frac{(x_1+d)^2 - (x_1-d)^2}{2} \qquad \textit{and} \qquad k_2 \triangleq \frac{(x_1+d)^2 + (x_1-d)^2}{2}.$$

Proof. We can observe that y^2 depends on some constant values, i.e., d and x_1, and on $\cos\beta$. Therefore, z follows the same distribution of $\cos\beta$. However, the support is $[(x_1-d)^2, (x_1+d)^2]$. Note that there is a precise meaning for the parameters k_1 and k_2. In fact, k_1 can be seen as a normalization factor, whereas k_2 represents the shift factor w.r.t. the pdf of the cosine, that is centered in 0 and has support between $[-1, 1]$. □

We now derive the distribution of y.

Lemma 7.3.16. *The conditional pdf of* y *is:*

$$f_{\mathsf{y}|\mathsf{x}_1}(y|x_1) = \frac{2y}{\pi\sqrt{k_1^2 - (y^2-k_2)^2}} \qquad |x_1-d| \leq y \leq (x_1+d) \tag{7.18}$$

and the associated conditional cdf is:

$$F_{\mathsf{y}|\mathsf{x}_1}(y|x_1) = \frac{1}{2} + \frac{\sin^{-1}\frac{y^2-k_2}{k_1}}{\pi} \qquad |x_1-d| \leq y \leq (x_1+d) \tag{7.19}$$

where k_1 and k_2 are defined in Lemma 7.3.15. Furthermore, it follows from Lemma 7.3.14 that t *has the same distribution.*

Proof. Note that:

$$F_{\mathsf{y}|\mathsf{x}_1}(y|x_1) = \mathbb{P}(\mathsf{y} < y|x_1) = \mathbb{P}(\mathsf{y}^2 < y^2|x_1) = \mathbb{P}(\mathsf{z} < y^2|x_1) = F_{\mathsf{z}|\mathsf{x}_1}(y^2|x_1)$$

Therefore,

$$F_{\mathsf{y}|\mathsf{x}_1}(y|x_1) = F_{\mathsf{z}|\mathsf{x}_1}(y^2|x_1) = \frac{1}{2} + \frac{\sin^{-1}\frac{y^2-k_2}{k_1}}{\pi} \qquad |x_1 - d| \leq y \leq (x_1 + d)$$

and, by derivation, we can write the conditional pdf. □

In the following, we report some numerical results. For all the distributions that we derive, we compare the analytical expressions with simulation results. Figures 7.20-7.21-7.22 report the conditional pdf and cdf of y and y^2, when $x_1 = 5$ and $d = 1$, $d = 3$ and $d = 7$, respectively.

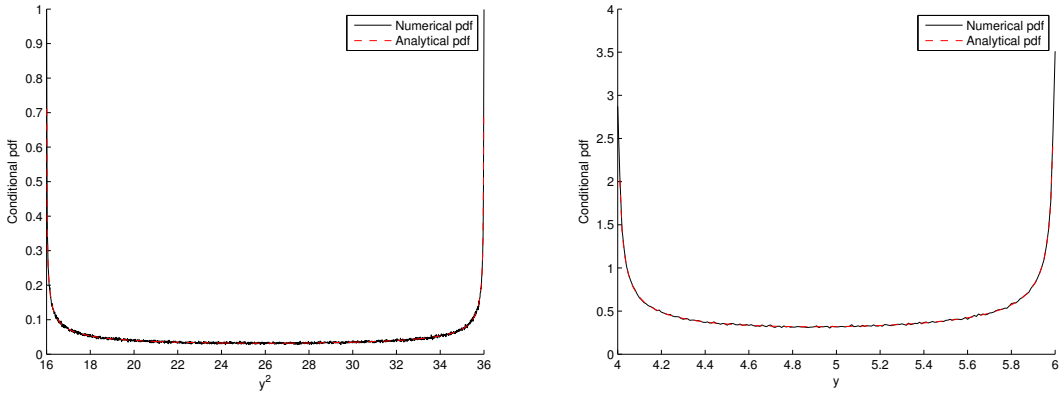

Figure 7.20: Conditional pdf of y^2 (left) and y (right) when $x_1 = 5$ and $d = 1$.

The next step is to characterize the conditional distribution of x_2. Therefore, consider the topology reported in Figure 7.23. We can write x_2^2 as:

$$x_2^2 = d^2 + y^2 - 2dy\cos(\alpha - \gamma) \tag{7.20}$$

that, substituting y from Eq. (7.14), becomes:

$$x_2^2 = 2d^2 + x_1^2 - 2dx_1\cos\beta - 2d\sqrt{d^2 + x_1^2 - 2dx_1\cos\beta}\cos(\alpha - \gamma)$$

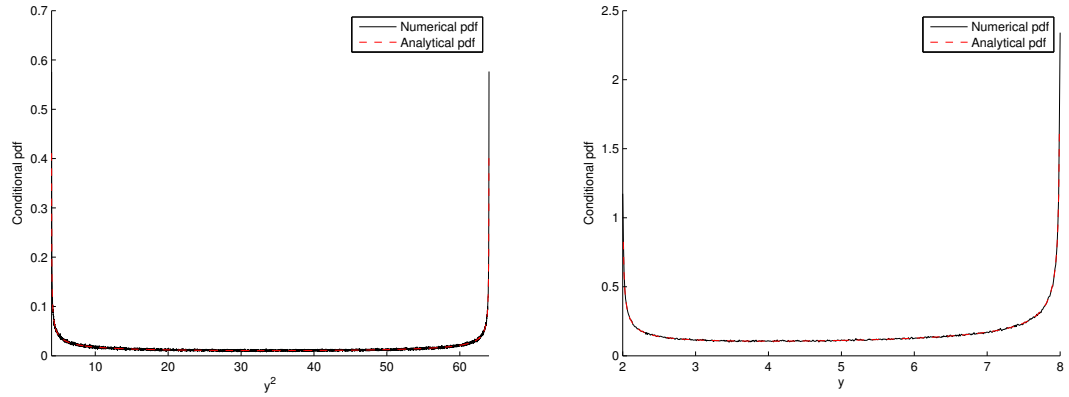

Figure 7.21: Conditional pdf of y^2 (left) and y (right) when $x_1 = 5$ and $d = 3$.

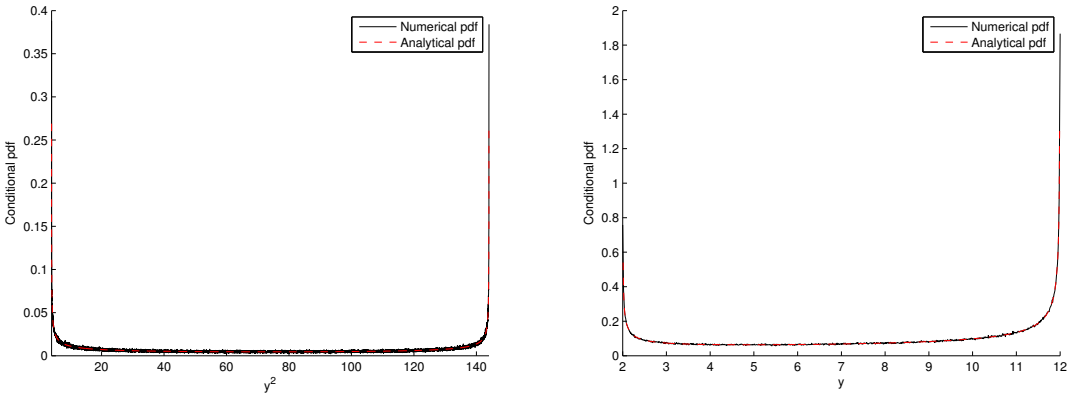

Figure 7.22: Conditional pdf of y^2 (left) and y (right) $x_1 = 5$ and $d = 7$.

Furthermore, recall that:

$$\cos(\alpha - \gamma) = \cos\alpha\cos\gamma + \sin\alpha\sin\gamma$$

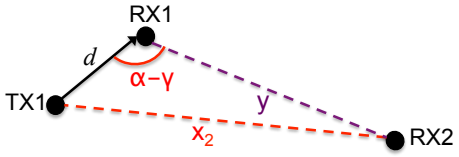

Figure 7.23: Triangle used to characterize x_2.

From this expression of x_2^2, it is clear that the conditional distribution of x_2 is a rather complicated function of t, y, α, β and γ. Therefore, we try to simplify the analysis, recalling *Ptolemy's theorem*:

Theorem 7.3.17. *If a quadrilateral, given with its four vertices A, B, C, and D in order, is inscribable in a*

circle (see Figure 7.24), then the product of the measures of its diagonals is equal to the sum of the products of the measures of the pairs of opposite sides:

$$|\overline{AC}| \cdot |\overline{BD}| = |\overline{AB}| \cdot |\overline{CD}| + |\overline{BC}| \cdot |\overline{AD}|$$

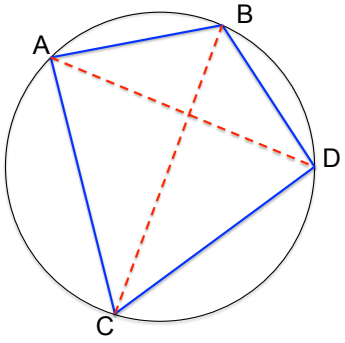

Figure 7.24: Ptolemy's theorem provides a relation among edges and diagonals in a cyclic quadrilateral.

The *Ptolemy's inequality* is an extension of this fact, and it is a more general form of Ptolemy's theorem.

Theorem 7.3.18. *Given a quadrilateral ABCD, then*

$$|\overline{AC}| \cdot |\overline{BD}| \leq |\overline{AB}| \cdot |\overline{CD}| + |\overline{BC}| \cdot |\overline{AD}|$$

where equality holds if and only if the quadrilateral is cyclic.

Recall that a convex quadrilateral ABCD is cyclic, i.e., lies in a circle, if: (i) its opposite angles are supplementary; (ii) an angle between a side and a diagonal is equal to the angle between the opposite side and the other diagonal.

In the quadrilateral that we are considering, the Ptolemy's inequality becomes:

$$ty \leq d^2 + x_1 x_2$$

from which:

$$x_2 \geq \frac{ty - d^2}{x_1}$$

Therefore, since we cannot provide explicitly the conditional distribution of x_2, we use the conditional distribution of the product ty, in order to provide an upper bound on it.

Lemma 7.3.19. *The conditional pdf of the product* ty *is the following function:*

$$f_{\mathsf{ty}|\mathsf{x}_1}(\tau|x_1) = \begin{cases} \dfrac{f(\tau/|x_1-d|,\tau)}{|x_1-d|} + 0 + \Big[I(t,\tau) \Big]_{|x_1-d|}^{\tau/|x_1-d|} & \text{if } \tau \leq |x_1-d|(x_1+d) \\ 0 + \dfrac{f(\tau/(x_1+d),\tau)}{(x_1+d)} + \Big[I(t,\tau) \Big]_{\tau/(x_1+d)}^{(x_1+d)} & \text{if } \tau \geq |x_1-d|(x_1+d) \end{cases} \tag{7.21}$$

where

$$f(t,\tau) = \left[\left(\frac{1}{2} + \frac{\sin^{-1} \frac{(\tau/t)^2 - k_2}{k_1}}{\pi} \right) \frac{2t}{k_1 \pi \sqrt{1 - \left(\frac{t^2-k_2}{k_1} \right)^2}} \right]$$

and

$$I(t,\tau) = \int \frac{4\tau}{k_1^2 \pi^2 t} \frac{1}{\sqrt{1 - \left(\frac{(\tau/t)^2 - k_2}{k_1} \right)^2} \sqrt{1 - \left(\frac{t^2-k_2}{k_1} \right)^2}} dt$$

Proof. Proof is in Appendix E. □

Figures 7.25, 7.26, 7.27 report the pdf and the cdf of the product ty for different values of d. In all cases, the analytical expression is compared with results obtained by simulations. Note that the pdf always shows a peak in $\tau = |x_1 - d|(x_1 + d)$. This case corresponds to the case in which $\alpha = 0$ and $\beta = \pi$, or vice-versa. Roughly speaking, the reason for which we have a peak at this point can be related to the fact that the distribution of the cosine of the uniform angle shows peaks in 1 and -1, that correspond to angles equal to 0 and π.

With this result, we can provide an upper bound to the distribution of x_2 using the distribution of ty. In particular, we can provide an upper bound for the conditional cdf $F_{\mathsf{x}_2|\mathsf{x}_1}(x_2|x_1)$.

Proposition 7.3.20. *The conditional cdf* $F_{\mathsf{x}_2|\mathsf{x}_1}(x_2|x_1)$ *is upper bounded by* $F_{\mathsf{ty}|\mathsf{x}_1}\left(x_1 x_2 + d^2 | x_1\right)$*, given in Prop. 7.3.19.*

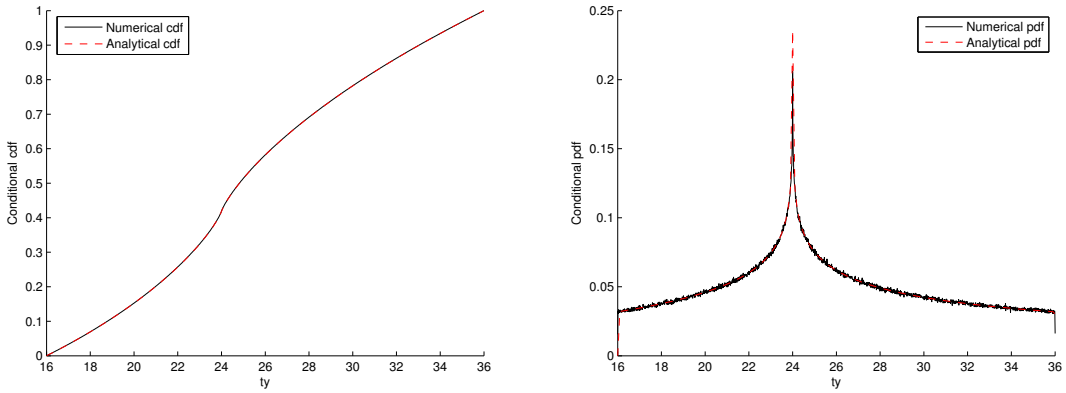

Figure 7.25: Conditional cdf (left) and pdf (right) of ty by simulation and with numerical evaluation of the integral when $x_1 = 5$ and $d = 1$.

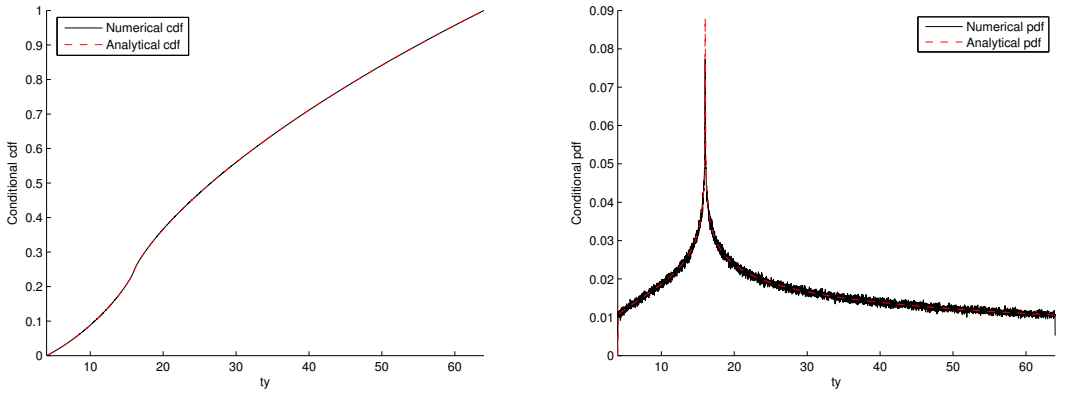

Figure 7.26: Conditional cdf (left) and pdf (right) of ty by simulation and with numerical evaluation of the integral when $x_1 = 5$ and $d = 3$.

Proof. From the Ptolemy's inequality given in Thm. 7.3.18, we know that:

$$ty \leq x_2 x_1 + d^2 \qquad \Longrightarrow \qquad x_2 \geq \frac{ty - d^2}{x_1}$$

Therefore:

$$ty \geq \tau \qquad \Longrightarrow \qquad \tau \leq ty \leq x_1 x_2 + d^2 \qquad \Longrightarrow \qquad x_2 \geq \frac{\tau - d^2}{x_1}$$

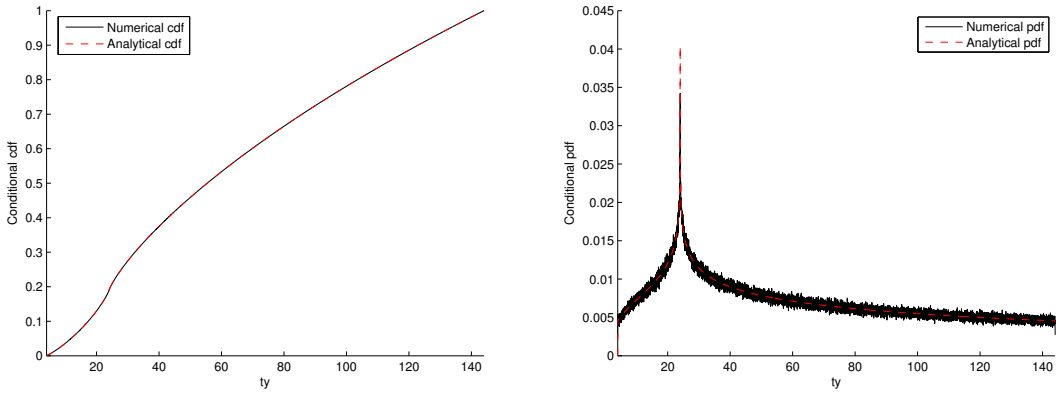

Figure 7.27: Conditional cdf (left) and pdf (right) of ty by simulation and with numerical evaluation of the integral when $x_1 = 5$ and $d = 7$.

that implies:

$$\mathbb{P}(\mathsf{ty} \geq \tau | x_1) \leq \mathbb{P}\left(\mathsf{x}_2 \geq \frac{\tau - d^2}{x_1} \middle| x_1\right) \quad \Longrightarrow \quad 1 - F_{\mathsf{ty}|\mathsf{x}_1}(\tau|x_1) \leq 1 - F_{\mathsf{x}_2|\mathsf{x}_1}\left(\frac{\tau - d^2}{x_1} \middle| x_1\right)$$

$$F_{\mathsf{x}_2|\mathsf{x}_1}\left(\frac{\tau - d^2}{x_1} \middle| x_1\right) \leq F_{\mathsf{ty}|\mathsf{x}_1}(\tau|x_1) \quad \Longrightarrow \quad F_{\mathsf{x}_2|\mathsf{x}_1}(x_2|x_1) \leq F_{\mathsf{ty}|\mathsf{x}_1}\left(x_1 x_2 + d^2 | x_1\right)$$

□

Figures 7.28-7.29-7.30 report the conditional pdf and the cdf of x_2, obtained by simulations, when $x_1 = 5$ and for different values of d. The numerical conditional cdf is compared with the analytical upper bound. Furthermore, we report also the conditional pdf of ty translated over the support of x_2. Clearly, this does not provide any bound, but it gives the idea on how far the approximation is from the real distribution. In particular, when the distance between the peaks of the two conditional pdf (x_2 and translated ty) increases, the bound becomes weaker. Note that the pdf of x_2 shows always one peak when $x_2 = x_1$, and eventually a second peak is in $2d - x1$, when this quantity is positive.

Recall that we aim at characterizing the distribution of x_2 (and its bound) in order to characterize the area of the lune (given by the area of the circle with radius x_2 minus the overlapping area of this circle with the circle of radius x_1, ref. to Figure 7.18). For the sake of completeness, Figure 7.31 reports the simulated conditional pdf and cdf (for the case $d = 1$ and $x_1 = 5$) of the area of the lune.

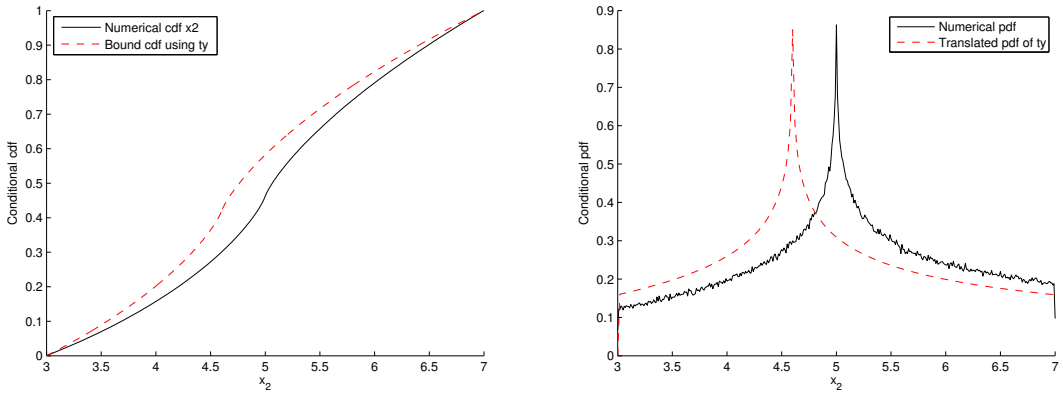

Figure 7.28: Conditional cdf (left) and pdf (right) of x_2 by simulation when $x_1 = 5$ and $d = 1$.

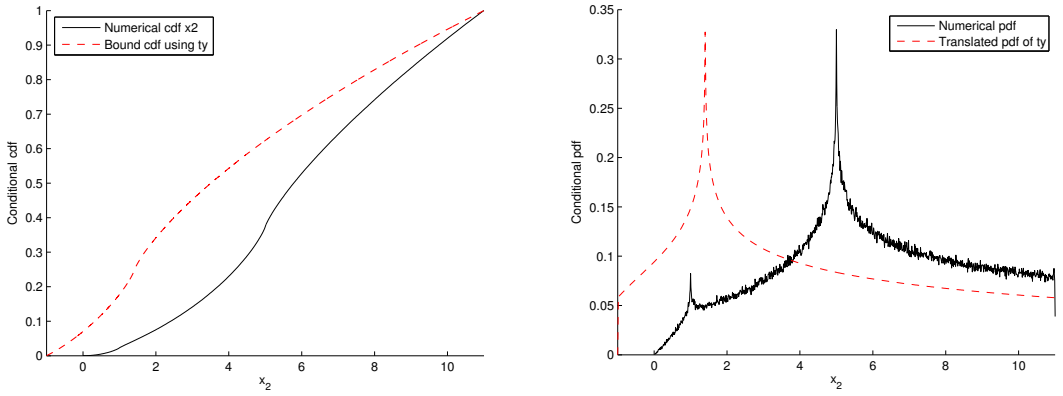

Figure 7.29: Conditional cdf (left) and pdf (right) of x_2 by simulation when $x_1 = 5$ and $d = 3$.

Finally, using the results derived so far, we can characterize the *conditional coupling probability*. This corresponds to the probability that there is no transmitter closer to RX_2 than TX_1, given (by assumption) that in the circle of radius x_1 there is no other transmitter. Namely, using the upper bound on x_2 given by the Ptolemy's inequality in Thm. 7.3.18, we provide the following upper bound for the conditional coupling probability.

Theorem 7.3.21. *The conditional coupling probability $P_{c|\mathsf{x}_1}(\lambda, x_1)$ is upper bounded by the following function:*

$$P_{c|\mathsf{x}_1}(\lambda, x_1) \leq P^U_{c|\mathsf{x}_1}(\lambda, x_1) \triangleq \int_{|x_1-d|}^{x_1+d} \int_{|x_1-d|}^{x_1+d} e^{-\lambda\Delta\left(x_1, \frac{ty-d^2}{x_1}, y\right)} f_{\mathsf{t}|\mathsf{x}_1}(t|x_1) f_{\mathsf{y}|\mathsf{x}_1}(y|x_1) dt dy \tag{7.22}$$

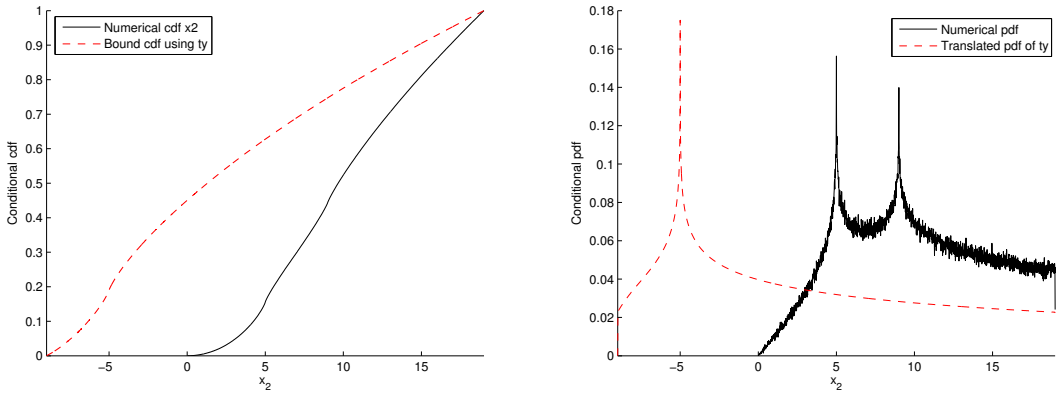

Figure 7.30: Conditional cdf (left) and pdf (right) of x_2 by simulation when $x_1 = 5$ and $d = 7$.

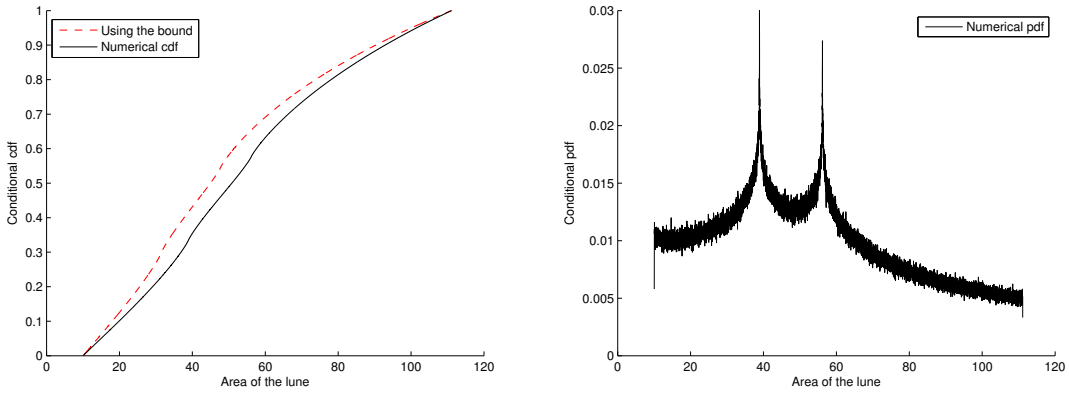

Figure 7.31: Cdf and pdf for the area of the lune when $x_1 = 5$ and $d = 1$.

where $\Delta(x_1, x_2, y)$ is defined in Prop. 7.3.12 and $f_{\mathsf{t}|\mathsf{x}_1}(t|x_1)$ and $f_{\mathsf{y}|\mathsf{x}_1}(y|x_1)$ are given in Lemma 7.3.16.

Proof. First note that from the Ptolemy's inequality, Thm. 7.3.18, and from the monotonicity property of the function $\Delta(x_1, x_2, y)$, Lemma 7.3.13, it follows that:

$$x_2 \geq \frac{ty - d^2}{x_1} \qquad \Longrightarrow \qquad \Delta(x_1, x_2, y) \geq \Delta\left(x_1, \frac{ty - d^2}{x_1}, y\right)$$

Furthermore, note that the conditional coupling probability is formally defined as:

$$P_{c|\mathsf{x}_1}(\lambda, x_1) = \mathbb{P}(\Pi_\lambda(\Delta(x_1, \mathsf{x}_2, \mathsf{y})) = 0|x_1) \tag{7.23}$$

where Π_λ is the PPP with density λ that describes the distribution of the users. In fact, the coupling probability

corresponds to the void probability defined in Prop. 7.3.2, where the compact set is the lune. It is easy to verify that increasing the compact set, the void probability increases. Therefore, decreasing the area of the lune, the coupling probability increases. This allows us to provide an upper bound for the coupling probability:

$$P_{c|\mathsf{x}_1}(\lambda, x_1) = \mathbb{P}(\Pi_\lambda(\Delta(x_1, \mathsf{x}_2, \mathsf{y})) = 0|x_1) \leq \mathbb{P}(\Pi_\lambda(\Delta(x_1, \frac{\mathsf{t}\mathsf{y} - d^2}{x_1}, \mathsf{y})) = 0|x_1)$$

Therefore, we obtain:

$$P_{c|\mathsf{x}_1}(\lambda, x_1) \leq \int_{|x_1 - d|}^{x_1 + d} \mathbb{P}(\Pi_\lambda(\Delta(x_1, \frac{\mathsf{t}\mathsf{y} - d^2}{x_1}, y)) = 0|x_1, y) f_{\mathsf{y}|\mathsf{x}_1}(y|x_1) dy$$

and, recalling that, given x_1, t and y are independent, we can write the upper bound as:

$$P_{c|\mathsf{x}_1}(\lambda, x_1) \leq \int_{|x_1 - d|}^{x_1 + d} \int_{|x_1 - d|}^{x_1 + d} \mathbb{P}(\Pi_\lambda(\Delta(x_1, \frac{ty - d^2}{x_1}, y)) = 0|x_1, y) f_{\mathsf{t}|\mathsf{x}_1}(t|x_1) f_{\mathsf{y}|\mathsf{x}_1}(y|x_1) dt dy$$

Finally, we can use the result from Prop. 7.3.2 and write that:

$$\mathbb{P}(\Pi_\lambda(\Delta(x_1, \frac{ty - d^2}{x_1}, y)) = 0|x_1, y) = e^{-\lambda \Delta\left(x_1, \frac{ty - d^2}{x_1}, y\right)}$$

□

Furthermore, the following property holds:

Corollary 7.3.22. *When λ goes to 0, the conditional coupling probability goes to 1:*

$$\lim_{\lambda \to 0} P_{c|\mathsf{x}_1}(\lambda, x_1) = 1.$$

Proof. The theorem is easy to prove. In fact, once that we have fixed x_1 (distance between RX_1 and TX_2), the area of the lune that we consider to evaluate the conditional coupling probability depends on x_2 and y. Note that, given x_1, these two distances are bounded, therefore the area of the lune is bounded as well. When λ goes to zero, the probability of having a node in the lune goes to zero, meaning that the nearest transmitter

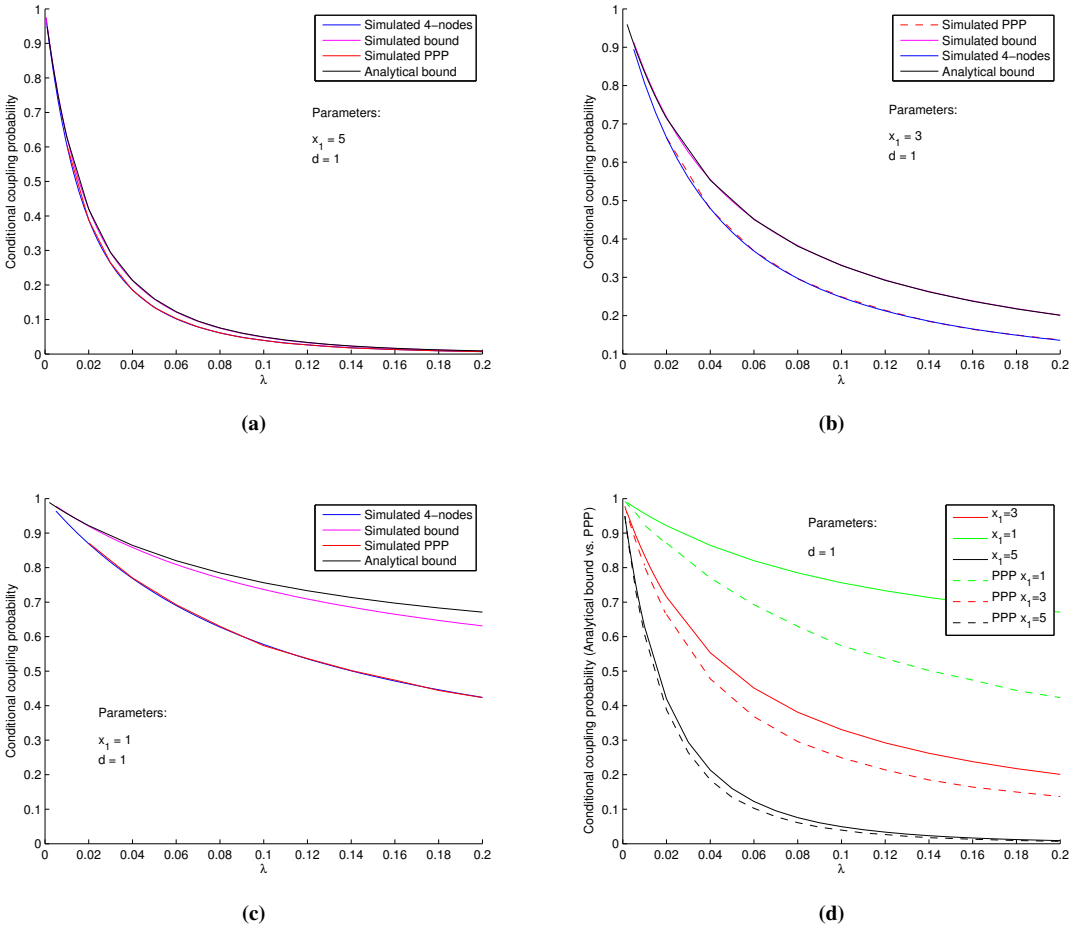

Figure 7.32: Conditional coupling probability when $d = 1$ varying x_1.

for RX_2 is TX_1 with probability one. □

In the following, we report some results that compare the analytical expression of the upper bound for the coupling probability, i.e., $P^{U}_{c|\mathrm{x}_1}(\lambda, x_1)$, with results that we have obtained through simulations. Recall that we are still assuming x_1 as fixed. Figure 7.32 reports the comparison when $d = 1$. Figure 7.32a compares the analytical bound (when $x_1 = 5$) with the same results obtained simulating 4–nodes scenarios. Furthermore, we also consider the case in which the four nodes are surrounding by nodes deployed as a Poisson point process with density λ. Figure 7.32b and Figure 7.32c report the same for $x_1 = 3$ and $x_1 = 5$. Finally Figure 7.32 compares all the three cases. As expected, increasing x_1, the bound becomes tighter. This reflects the results obtained before, where we have already noticed that for the case $x_1 = 5$ and $d = 1$

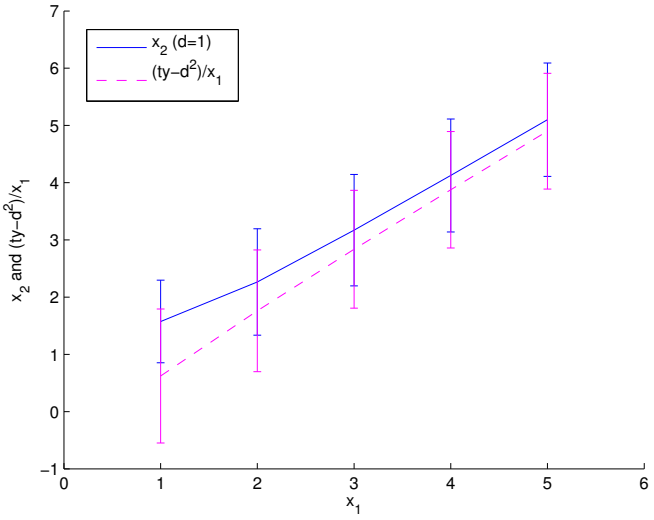

Figure 7.33: Comparison between the average value of x_2 when $d = 1$ with the average value of the bound $(ty - d^2)/x_1$.

(Figure 7.28) the bound used to approximate x_2 works better with respect to the cases in which x_1 and d get closer (Figure 7.29 and Figure 7.30). This is also emphasized in Figure 7.33 that compares the average value of x_2 when $d = 1$ with the average value of the bound $(ty - d^2)/x_1$. Increasing the difference between d and x_1, the two values get closer. Finally, as mentioned in Cor. 7.3.22, when λ goes to zero, the coupling probability goes to 1. This is clear if we keep in mind that x_1 is fixed. In fact, when λ goes to zero, the probability that there is a transmitter other than TX_1 in the lune goes to zero and therefore the two pairs of node are coupled with probability one. This is not true when we remove the condition on x_1.

We conclude this section providing some results on the unconditional coupling probability. We have already provided the expression for $f_{\mathrm{x}_1}(x_1)$, given in Eq. 7.12, that can now be used to remove the condition on x_1. In particular, as done for the conditional coupling probability, we can derive the upper bound for the coupling probability $P_c(\lambda)$.

Corollary 7.3.23. *The coupling probability $P_c(\lambda)$ is upper bounded by the following function:*

$$P_c(\lambda) \leq P_c^U(\lambda) \triangleq \int_0^\infty P_{c|\mathrm{x}_1}^U(\lambda, x_1) f_{\mathrm{x}_1}(x_1) dx_1 \tag{7.24}$$

where $P_{c|\mathrm{x}_1}^U(\lambda, x_1)$ is given in Thm. 7.3.21.

As done for the conditional coupling probability, we have also numerically evaluated the upper bound for $P_c^U(\lambda)$. The evaluation is complicated by the fact that we are numerically evaluating a triple integral. Preliminary results show that the bound might be not very good especially for some density regimes. However, we are able to provide the following fundamental result.

Theorem 7.3.24. *The value for the coupling probability when λ goes to 0 is the following constant:*

$$\lim_{\lambda \to 0} P_c(\lambda) = C_{cp} \triangleq \frac{6\pi}{3\sqrt{3} + 8\pi} \approx 0.6215.$$

Proof. Let us first note that when λ is very low, the average distance x_1 to the nearest neighbor goes to infinity. Therefore, to analytically characterize the value of the coupling probability in the low density regime, we can assume that $x_1 >> d$, then d can be neglected. If we assume that $d \to 0$, then we have that $x_1 = x_2 = y$. In this scenario, we have two circles with the same radius, whose centers are separated by a distance equal to the radius itself. Therefore, the area of the lune does depend only on the parameter x_1. In particular, using the formula provided in Prop. 7.3.12, we obtain that in this case the area of the lune is the following:

$$\Delta(x_1, x_1, x_1) = \left(\frac{\pi}{3} + \frac{\sqrt{3}}{2} \right) x_1^2$$

Furthermore, the coupling probability can be written in terms of conditional coupling probability as follows:

$$P_c(\lambda) = \int_0^\infty P_{c|\mathsf{x}_1}(\lambda, x_1) f_{\mathsf{x}_1}(x_1) dx_1 \tag{7.25}$$

Then, substituting the expression of $f_{\mathsf{x}_1}(x_1)$ given in Eq. (7.12) and the conditional coupling probability given in Eq. (7.23), we obtain:

$$P_c(\lambda) = \int_0^\infty e^{-\lambda\left(\frac{\pi}{3} + \frac{\sqrt{3}}{2}\right)x_1^2} 2\pi\lambda x_1 e^{-\lambda\pi x_1^2} dx_1 = \int_0^\infty e^{-\lambda\left(\frac{4}{3}\pi + \frac{\sqrt{3}}{2}\right)x_1^2} 2\pi\lambda x_1 dx_1$$

$$= \left[-\frac{6\pi}{3\sqrt{3} + 8\pi} e^{-\frac{3\sqrt{3}+8\pi}{6}\lambda x_1^2} \right]_0^\infty = \frac{6\pi}{3\sqrt{3} + 8\pi} \triangleq C_{cp}$$

□

Numerical simulations for the coupling probability confirms this result. Figure 7.34 reports different curves for the coupling probability varying d. The black point represents the constant C_{cp}.

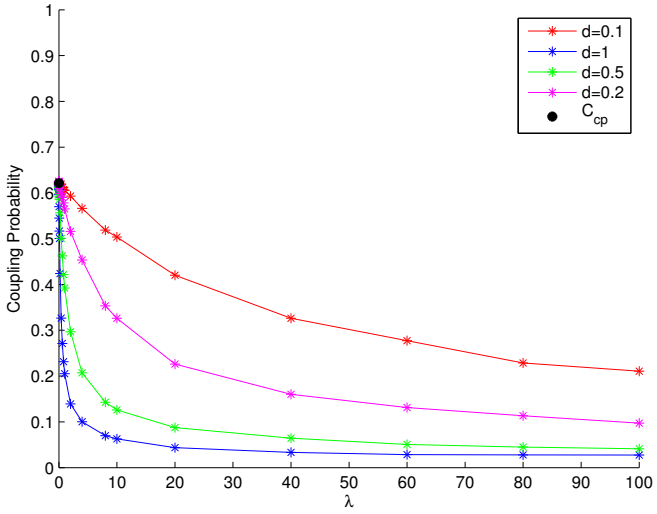

Figure 7.34: Simulated coupling probability for different values of d.

7.3.3 Best response of a node influenced by a couple

In this section, we show how we can iteratively analyze the behaviors of nodes that are connected to a chain. It is worth to recall that in any isolated sub–graph, we can find either a chain or a cycle, but not both, and not more than one. In particular, in the low density regime, we can numerically show that the probability of having a cycle goes to zero, and analytically derive that the coupling probability is 62.15%.

Let us assume that we have a network (and the associated directed influence graph) in the low density regime. The couple pairs constitute about the 62% of the nodes. The decisions of all the other nodes are influenced by the 2–player sub–games. Namely, at the equilibrium, the first node of any chain selects the best response to the 2–player sub–game, the second node selects the best response to the first node strategy and so on. In the following, we report the best response analysis of the first node connected to a couple. Figure 7.35 reports the scenario that we are considering. Players 1 and 2 form the 2–player subgame, and X_{12} and X_{21} represent the interference terms for this couple. Player 3 is the first player of the chain and is influenced by player 2 according to the term X_{23}.

As shown in Figure 6.16, the 2–player sub–game leads to one among the following cases (where the

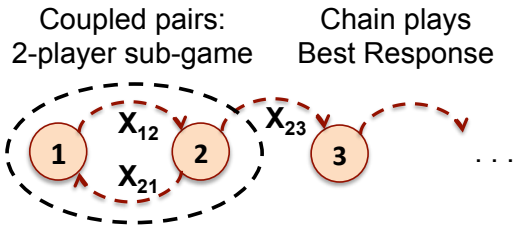

Figure 7.35: Reference scenario in the analysis of the best response of a node influenced by a couple.

first term indicates the strategy chosen by player 1 and the second term is the strategy chosen by player 2): $(0.5, 0.5)$, $(0, 1)$, $(1, 0)$, $(\beta_1^+, 0)$, $(\beta_1^-, 1)$, $(0, \beta_2^+)$, $(1, \beta_2^-)$. Therefore, the strategy P_3 of player 3 is characterized as follows:

- if $P_1 = 0.5$, then $P_3 = 0.5$
- if $P_1 = 0$
  - if $X_{23} \geq D$ then $P_3 = 1$
  - if $X_{23} < D$ then $P_3 = 0.5(1 + X_{23}/D) < 1$
- if $P_1 = 1$
  - if $X_{23} \geq D$ then $P_3 = 0$
  - if $X_{23} < D$ then $P_3 = 0.5(1 - X_{23}/D) > 0$
- if $P_1 = \beta_1^+ = 0.5(1 + \frac{X_{12}}{D})$
  - if $X_{12}X_{23} \geq D^2$ then $P_3 = 0$
  - if $X_{12}X_{23} < D^2$ then $P_3 = 0.5(1 - X_{12}X_{23}/D^2) > 0$
- if $P_1 = \beta_1^- = 0.5(1 - \frac{X_{12}}{D})$
  - if $X_{12}X_{23} \geq D^2$ then $P_3 = 1$
  - if $X_{12}X_{23} < D^2$ then $P_3 = 0.5(1 + X_{12}X_{23}/D^2) < 1$

7.4 Concluding remarks and future work

In this chapter, we extend the 2–player spectrum sharing game with interference to the more general case of N players. First, we derive partial analytical results on the characterization of the game. Moreover, we compare, through simulations, the optimal solution with the full–spread equilibrium. Then, we provide a game simulator that characterizes the quality of multiple equilibria of the game. The results of the simulations suggest that the strategy chosen by each player is mainly driven by the nearest interferer only.

In the second part of this chapter, we simplify the game model using some realistic assumption. Namely, we assume that each user selects the power allocation, considering the nearest interferer only. Furthermore, we study the coupling probability. For low density regime we provide the exact value of the coupling probability. This is a fundamental quantity in the equilibria characterization. In fact, we can identify the fraction of node that play a 2–player game.

For the low density regime, we are able to provide the exact value of the coupling probability. In these cases, we can use the results obtained from the 2–player analysis. When users are not coupled, we can simplify the interactions among them using the directed influence graph.

Publications: [107]

Chapter 8: Conclusion

The increasing demand in wireless spectrum has shown how current policies in the usage of the spectrum are often inefficient. New, more flexible models for the management of the spectrum are necessary. Furthermore, the interaction between different entities (e.g., users, networks) can be properly model resorting to non-cooperative game models. In this work, several game models have been proposed in order to model the problem of resource sharing.

In the first part of the thesis, we deeply analyze the dynamics that arise among multiple end users that try to connect to the "best" available access networks. We consider both hot–spot–based wireless networks and mesh networks. We assume that the interference between users is modeled in terms of congestion level (i.e., number of players that are choosing the same strategy). We provide several congestion games, with different end users' cost functions. We solve these games resorting to mathematical programming, comparing the equilibria with the optimal centralized solution. We further provide experimental results. In general, in these models, the equilibria reached by the players, that selfishly play their best response, are very close to the optimal solution.

Furthermore, we let the networks enter the competition, and we model this bi–level game using multi–stage games. In this game, both networks and players selfishly try to maximize their payoff. Namely, operators play first by competitively choosing their strategies (i.e., frequencies or routing patterns) to capture the highest number of end users, which, in turn, play the network selection/association games in the second stage of the game. Formal results on the existence of subgame perfect equilibria are derived for all the game instances. Even if the proposed two–stage game may not always admit any pure strategy equilibrium, it is possible to enforce approximated equilibria with a quality loss reasonably small. Finally, we show that competition among operators increases the inefficiency of the equilibria for the users.

Moreover, we propose a congestion game also for the case in which users compete for portions of the spectrum. In a cognitive network, secondary users might choose the best available spectrum opportunity on the basis of several parameters. Considering the time–varying availability of the spectrum, we provide a

repeated game that accounts for the primary users activity.

The second part of the work focuses on spectrum sharing games, where the interference between players is modeled on the basis of the geographical position of the nodes and the utility function adopted by the users is based on the Shannon capacity. Due to the complexity of the game model, we first provide a complete framework for the two–user case. We consider both the symmetric and the asymmetric case. For the symmetric case, we derive analytically the optimal solution. In contrast, for the asymmetric case, we evaluate it only numerically. Then, we deeply study the game model. We derive the Nash equilibria using the best response functions of the two users. We characterize their quality in terms of PoS and PoA. Finally, we study the stability of the equilibria. We conclude the 2–player framework, providing a stochastic characterization of the equilibria. Namely, resorting to stochastic geometry, we explicitly derive the joint probability distribution of the two interfering distances in the 2–user model. Using this result, we provide distribution probabilities over the possible strategies of the 2–player game.

Finally, we extend the model to the N–user case. We derive some analytical results, and we prove that the full–spread strategy is always a Nash equilibrium. Then, we introduce stochastic geometry as a promising approach to characterize the equilibria distribution. First, we analytically derive the coupling probability. Then, using a game simulator, we characterize the quality of multiple equilibria of the game. From the results of the simulations, we can conclude that the strategy chosen by each player is mainly driven by the nearest interferer. Therefore, using the directed–influence–graph–based approach, we can reduce and simplify the N–player game and predict the performance of large networks.

Bibliography

[1] J. D. Camp, E. W. Knightly, and W. S. Reed. Developing and deploying multihop wireless networks for low-income communities. In *Proc. Digital Communities*, 2005.

[2] Y. Zhao and G. J. Pottie. Optimal spectrum management in multiuser interference channels. *submitted to IEEE Transactions on Information Theory*, 2011.

[3] R. Etkin, A. Parekh, and D. Tse. Spectrum sharing for unlicensed bands. *IEEE Journal on Selected Areas in Communications*, 25(3):517–528, 2007.

[4] S. Hongxia, Z. Hang, R. A. Berry, and M. L. Honig. Optimal spectrum allocation in gaussian interference networks. In *Proc. Asilomar SSC*, pages 2142–2146, 2008.

[5] S. R. Bhaskaran, S. V. Hanly, N. Badruddin, and J. S. Evans. Maximizing the sum rate in symmetric networks of interfering links. *IEEE Transactions on Information Theory*, 56(9):4471–4487, 2010.

[6] I. F. Akyildiz, X. Wang, and W. Wang. Wireless mesh networks: a survey. *Computer Networks*, 47(4):445 – 487, 2005.

[7] R. Bruno, M. Conti, and E. Gregori. Mesh networks: commodity multihop ad hoc networks. *IEEE Communications Magazine*, 43(3):123 – 131, March 2005.

[8] D. Fudenberg and J. Tirole. *Game Theory*. The MIT Press, Cambridge, USA, 1991.

[9] J. Antoniou and A. Pitsillides. 4G converged environment: Modeling network selection as a game. In *Proc. ICT MOBILESUMMIT*, pages 1–5, 2007.

[10] K. Mittal, E. M. Belding, and S. Suri. A game-theoretic analysis of wireless access point selection by mobile users. *Computer Networks*, 31(10):2049–2062, 2008.

[11] J. Antoniou, V. Papadopoulou, and A. Pitsillides. A game theoretic approach for network selection. Technical report, 2008.

[12] R. W. Rosenthal. A class of games possessing pure-strategy Nash equilibria. *International Journal of Game Theory*, 2(1):65–67, 1973.

[13] S. Bosio, A. Capone, and M. Cesana. Radio planning of wireless local area networks. *ACM/IEEE Transactions on Networking*, 15(6):1414–1427, Dec. 2007.

[14] A. Raniwala, K. Gopalan, and T.-Z. Chiueh. Centralized channel assignment and routing algorithms for multi-channel wireless mesh networks. *ACM SIGMOBILE*, 8(2):50–65, Apr. 2004.

[15] E. Amaldi, A. Capone, and F. Malucelli. Radio planning and coverage optimization of 3G cellular networks. *Wireless Networks*, 14(4):435–447, Jan. 2007.

[16] P. Vidales, J. Baliosian, J. Serrat, G. Mapp, F. Stajano, and A. Hopper. Autonomic system for mobility support in 4G networks. *IEEE Journal on Selected Areas in Communication*, 23(12):2288–2304, Dec. 2005.

[17] D. Niyato and E. Hossain. A Cooperative Game Framework for Bandwidth allocation in 4g heterogeneous wireless networks. In *Proc. IEEE ICC*, volume 9, pages 4357–4362, June 2006.

[18] D. Niyato and E. Hossain. A noncooperative game-theoretic framework for radio resource management in 4g heterogeneous wireless access networks. *IEEE Transactions on Mobile Computing*, 7(3):332–345, 2008.

[19] Z. Ji and K. J. R. Liu. Dynamic spectrum sharing: A game theoretical overview. *IEEE Communications Magazine*, 45(5):88–94, 2007.

[20] D. Niyato and E. Hossain. A game-theoretic approach to competitive spectrum sharing in cognitive radio networks. In *Proc. IEEE WCNC*, pages 16–20, 2007.

[21] S. Sengupta, R. Chandramouli, S. Brahma, and M. Chatterjee. A game theoretic framework for distributed self-coexistence among IEEE 802.22 networks. In *Proc. IEEE GLOBECOM*, pages 1–6, 2008.

[22] E. Anshelevich, A. Dasgupta, J. Kleinberg, E. Tardos, T. Wexler, and T. Roughgarden. The price of stability for network design with fair cost allocation. In *Proc. IEEE FOCS*, pages 59–73, 2004.

[23] E. Koutsoupias and C.H. Papadimitriou. Worst-case equilibria. In *Proc. STACS*, pages 404–413, 1999.

[24] E. Gustafsson and A. Jonsson. Always best connected. *IEEE Wireless Communication*, 10(1):49–55, Feb. 2003.

[25] *Network Simulator 2 (NS2)*. http://www.isi.edu/nsnam/ns/.

[26] O. Ormond, J. Murphy, and G. Muntean. Utility-based intelligent network selection in beyond 3G systems. In *Proc. IEEE ICC*, pages 1831–1836, 2006.

[27] K. Premkumar. and A. Kumar. Optimum Association of Mobile Wireless Devices with a WLAN-3G Access Network. In *Proc. IEEE ICC*, pages 2002–2008, 2006.

[28] W. Shen and Q.-A. Zeng. Cost-function-based network selection strategy in integrated wireless and mobile networks. *IEEE Transactions on Vehicular Technology*, 57(6):3778–3788, 2008.

[29] Q. Song and A. Jamalipour. Network selection in an integrated wireless LAN and UMTS environment using mathematical modelling and computing techniques. *IEEE Wireless Communication*, 12(3):42–48, 2005.

[30] D. Charilas, O. Markaki, D. Nikitopoulos, and M. Theologou. Packet-switched network selection with the highest QoS in 4G networks. *Computer Networks*, 52(1):248–258, 2008.

[31] F. Bari and V. C. M. Leung. Automated network selection in a heterogeneous wireless network environment. *IEEE Network*, 21(1):34–40, 2007.

[32] M. Bernaschi, F. Cacace, G. Iannello, S. Za, and A. Pescape. Seamless internetworking of WLANs and cellular networks: architecture and performance issues in a mobile IPv6 scenario. *IEEE Wireless Communication*, 12(3):73–80, 2005.

[33] Y. Bejerano., S.-J. Han, and L. Li. Fairness and Load Balancing in Wireless LANs Using Association Control. *ACM/IEEE Transactions on Networking*, 15(3):560–573, 2007.

[34] N. Blefari-Melazzia, D. Di Sorte, M. Femminella, and G. Reali. Autonomic control and personalization of a wireless access network. *Computer Networks*, 51(10):2645–2676, 2007.

[35] Y.W. Lee and S. C. Miller. Network selection and discovery of service information in public WLAN hotspots. In *Proc. ACM WMASH*, pages 81–92, 2004.

[36] Y. Fukuda and Y. Oie. Decentralized Access Point Selection Architecture for Wireless LANs. *IEICE Transactions on Communication*, E90-B(9):2513–2523, 2007.

[37] H. Gong, K. Nahm, and J.W. Kim. Distributed Fair Access Point Selection for Multi-Rate IEEE 802.11 WLANs. *IEICE Transactions on Information and Systems*, E91-D(4):1193–1196, 2008.

[38] S. Vasudevan, K. Papagiannaki, C. Diot, J. Kurose, and D. Towsley. Facilitating access point selection in IEEE 802.11 wireless networks. In *Proc. ACM SIGCOMM*, pages 26–26, 2005.

[39] L. Chen. A distributed access point selection algorithm based on no-regret learning for wireless access networks. In *Proc. VTC*, pages 1–5, 2010.

[40] X. Fengyuan, C. C. Tan, L. Qun, Y. Guanhua, and W. Jie. Designing a practical access point association protocol. In *Proc. IEEE INFOCOM*, pages 1–9, 2010.

[41] L.-H. Yen, J.-J. Li, and C.-M. Lin. Stability and fairness of ap selection games in ieee 802.11 access networks. *IEEE Transactions on Vehicular Technology*, 60(3):1150–1160, 2011.

[42] S. Shakkottai, E. Altman, and A. Kumar. Multihoming of Users to Access Points in WLANs: A Population Game Perspective. *IEEE Journal on Selected Areas in Communication*, 25(6):1207–1215, 2007.

[43] L. Jiang, S. Parekh, and J. Walrand. Base station association game in multi–cell wireless networks (special paper). In *Proc. IEEE WCNC*, pages 1616–1621, 2008.

[44] N. Kaci, P. Maille, and J.-M. Bonnin. Performance of wireless heterogeneous networks with always–best-connected users. In *Proc. NGI*, pages 1–8, 2009.

[45] I. Milchtaich. Congestion games with player-specfic payoff functions. *Games and Economic Behavior*, 13(1):111–124, 1996.

[46] I. Malanchini, M. Cesana, and N. Gatti. On spectrum selection games in cognitive radio networks. In *Proc. IEEE GLOBECOM*, pages 1–7, 2009.

[47] K. S. Gilhousen, I. M. Jacobs, R. Padovani, A. J. Viterbi, L. A. Weaver Jr., and C. E. Wheatley III. On the capacity of a cellular CDMA system. *IEEE Transactions on Vehicular Technology*, 40(2):303–312, 1991.

[48] M. Heusse, F. Rousseau, G. Berger-Sabbatel, and A. Duda. Performance anomaly of 802.11b. In *Proc. IEEE INFOCOM*, volume 2, pages 836–843, 2003.

[49] I. Milchtaich. Weighted congestion games with separable preferences. *Games and Economic Behavior*, 67(2):750–757, 2009. on-line published.

[50] M. P. David. *Microwave Engineering*. Wiley and Sons, 4th. edition, 2004.

[51] R. Fourer, D. M. Gay, and B. W. Kernighan. *AMPL, A modeling language for mathematical programming*. 1993.

[52] *ILOG CPLEX 10.0 user's manual*. http://www.ilog.com/products/cplex/.

[53] M. Cesana, N. Gatti, and I. Malanchini. Game theoretic analysis of wireless access network selection: Models, inefficiency bounds, and algorithms. In *Proc. GAMECOMM*, 2008.

[54] R. Jain, D. Chiu, and W. Hawe. A quantitative measure of fairness and discrimination for resource allocation in shared computer systems. Technical Report TR-301, DEC Research Report, September 1984.

[55] M. Cesana, I. Malanchini, and A. Capone. Modelling network selection and resource allocation in wireless access networks with non-cooperative games. In *Proc. IEEE MASS*, pages 404–409, 2008.

[56] I. Malanchini, M. Cesana, and N. Gatti. Network selection and resource allocation games for wireless access networks. *submitted to IEEE Transactions on Networking*, 2011.

[57] D. Wu and P. Mohapatra. Qurinet: a wide-area wireless mesh testbed for research and experimental evaluations. In *Proc. COMSNETS*, pages 307–316, Piscataway, NJ, USA, 2010. IEEE Press.

[58] IEEE. Wireless LAN medium access control (MAC) and physical layer (PHY) specifications, IEEE std. 802.11, 1999.

[59] G. Athanasiou, T. Korakis, O. Ercetin, and L. Tassiulas. A cross-layer framework for association control in wireless mesh networks. *IEEE Transactions on Mobile Computing*, 8:65–80, 2008.

[60] A. J. Nicholson, Y. Chawathe, M. Y. Chen, B. D. Noble, and D. Wetherall. Improved access point selection. In *Proc. ACM MobiSys*, pages 233–245, 2006.

[61] V. Mhatre and K. Papagiannaki. Using smart triggers for improved user performance in 802.11 wireless networks. In *Proc. ACM MobiSys*, pages 246–259, 2006.

[62] H. Lee, S. Kim, O. Lee, S. Choi, and S.-J. Lee. Available bandwidth-based association in IEEE 802.11 Wireless LANs. In *Proc. ACM MSWiM*, pages 132–139, 2008.

[63] B. Kauffmann, F. Baccelli, A. Chaintreau, V. Mhatre, K. Papagiannaki, and C. Diot. Measurement-based self organization of interfering 802.11 wireless access networks. In *Proc. IEEE INFOCOM*, pages 1451–1459, 2007.

[64] IEEE. Draft amendment: ESS mesh networking, IEEE P802.11s draft 1.00, November 2006.

[65] G. Athanasiou, T. Korakis, O. Ercetin, and L. Tassiulas. Dynamic cross-layer association in 802.11-based mesh networks. In *Proc. IEEE INFOCOM*, pages 2090 –2098, May 2007.

[66] H. Wang, W.-C. Wong, W.-S. Soh, and M. Motani. Dynamic association in IEEE 802.11 based wireless mesh networks. In *Proc. ISWCS*, pages 81 –85, Sept. 2009.

[67] L. Lin, D. Raychaudhuri, H. Liu, M. Wu, and D. Li. Improving end-to-end performance of wireless mesh networks through smart association. In *Proc. IEEE WCNC*, pages 2087 –2092, April 2008.

[68] S. Makhlouf, Y. Chen, S. Emeott, and M. Baker. A network-assisted association scheme for 802.11-based mesh networks. In *Proc. IEEE WCNC*, pages 1339 –1343, April 2008.

[69] U. Ashraf, S. Abdellatif, and G. Juanole. Gateway selection in backbone wireless mesh networks. In *Proc. IEEE WCNC*, pages 2548–2553, 2009.

[70] K. Mittal, E. M. Belding, and S. Suri. Association games in IEEE 802.11 wireless local area networks. *IEEE Transactions on Wireless Communications*, 7(12):5136–5143, 2008.

[71] S. H. A. Ahmad, M. Liu, and Y. Wu. Congestion games with resource reuse and applications in spectrum sharing. In *Proc. GameNets*, 2009.

[72] H. Ackermann, H. Röglin, and B. Vöcking. Pure nash equilibria in player-specific and weighted congestion games. *Theoretical Computer Science*, 410(17):1552–1563, 2009.

[73] R. Chandra, L. Qiu, K. Jain, and M. Mahdian. Optimizing the placement of internet taps in wireless neighborhood networks. In *Proc. ICNP*, pages 271 – 282, 5-8 2004.

[74] ILOG. Cplex 10.0 user's manual. http://www.ilog.com/products/cplex/.

[75] A. Argento, M. Cesana, and I. Malanchini. On access point association in wireless mesh networks. In *Proc. WoWMoM*, pages 1–6, Montreal, Canada, 2010.

[76] A. Argento, M. Cesana, N. Gatti, and I. Malanchini. A game theoretical study of access point association in wireless mesh networks. *Computer Communications*, In Press, Corrected Proof, 2010.

[77] M. A. Khan, A. C. Toker, C. Troung, F. Sivrikaya, and S. Albayrak. Cooperative game theoretic approach to integrated bandwidth sharing and allocation. In *Proc. GAMENET*, pages 1–9, may 2009.

[78] D. Niyato and E. Hossain. Qos-aware bandwidth allocation and admission control in ieee 802.16 broadband wireless access networks: A non-cooperative game theoretic approach. *Computer Networks*, 51(7):3305–3321, 2007.

[79] L. Berlemann, G. R. Hiertz, B. H. Walke, and S. S. Mangold. Radio resource sharing games: enabling qos support in unlicensed bands. *IEEE Network*, 19(4):59–65, july-aug. 2005.

[80] I. F. Akyildiz, W.-Y. Lee, M. C. Vuran, and S. Mohanty. NeXt generation/dynamic spectrum access/cognitive radio wireless networks: A survey. *Computer Networks*, 50(13):2127 – 2159, 2006.

[81] J. Mitola III and Jr. G.Q. Maguire. Cognitive radio: making software radios more personal. *IEEE Personal Communications*, 6(4):13–18, 1999.

[82] D. Cabric, S. M. Mishra, and R. W. Brodersen. Implementation issues in spectrum sensing for cognitive radios. In *Proc. Asilomar SSC*, volume 1, pages 772–776, 2004.

[83] W.-Y. Lee and I. F. Akyildiz. Optimal spectrum sensing framework for cognitive radio networks. *IEEE Transactions on Wireless Communications*, 7(10):3845–3857, 2008.

[84] Y. Yuan, P. Bahl, R. Chandra, T. Moscibroda, and Y. Wu. Allocating dynamic time-spectrum blocks in cognitive radio networks. In *Proc. ACM MobiHoc*, pages 130–139, 2007.

[85] O. Ileri, D. Samardzija, and N. B. Mandayam. Demand responsive pricing and competitive spectrum allocation via a spectrum server. In *Proc. IEEE DySPAN*, pages 194–202, 2005.

[86] Q. Zhao, L. Tong, A. Swami, and Y. Chen. Decentralized cognitive MAC for opportunistic spectrum access in ad hoc networks: A POMDP framework. *IEEE Journal on Selected Areas in Communication*, 25(3):589–600, 2007.

[87] L. Cao and H. Zheng. Distributed spectrum allocation via local bargaining. In *Proc. IEEE SECON*, pages 475–486, 2005.

[88] I. F. Akyildiz, W.-Y. Lee, and K. R. Chowdhury. CRAHNs: Cognitive radio ad hoc networks. *Ad Hoc Networks*, 7(5):810–836, 2009.

[89] J. Ohyun and D.-H. Cho. Efficient spectrum matching based on spectrum characteristics in cognitive radio systems. In *Proc. WTS*, pages 230–235, 2008.

[90] L. Marin and L. Giupponi. Performance evaluation of spectrum decision schemes for a cognitive ad-hoc network. In *Proc. IEEE PIMRC*, pages 1–5, 2008.

[91] J. E. Suris, L. A. DaSilva, H. Zhu, and A. B. MacKenzie. Cooperative game theory for distributed spectrum sharing. In *Proc. IEEE ICC*, pages 5282–5287, 2007.

[92] A. Attar, M. R. Nakhai, and A. H. Aghvami. Cognitive radio game: A framework for efficiency, fairness and QoS guarantee. In *Proc. IEEE ICC*, pages 4170–4174, 2008.

[93] D.Tse and P. Viswanath. *Fundamentals of wireless communication*. Cambridge University Press, 2005.

[94] Z.-Q. Luo and S. Zhang. Dynamic spectrum management: Complexity and duality. *IEEE Journal of Selected Topics in Signal Processing*, 2(1):57–73, 2008. [4].

[95] E. Altman, K. Avrachenkov, and A. Garnaev. Transmission power control game with SINR as objective function. In *Network Control and Optimization*, volume 5425, pages 112–120. Springer Berlin, 2009.

[96] L. Grokop and D. N. C. Tse. Spectrum sharing between wireless networks. In *Proc. IEEE INFOCOM*, pages 201–205, 2008.

[97] M. Bennis, M. Le Treust, S. Lasaulce, M. Debbah, and J. Lilleberg. Spectrum sharing games on the interference channel. In *Proc. GameNets*, pages 515–522, Istanbul, Turkey, 2009.

[98] W. Yu, G. Ginis, and J. M. Cioffi. Distributed multiuser power control for digital subscriber lines. *IEEE Journal on Selected Areas in Communications*, 20(5):1105–1115, 2002.

[99] E. V. Belmega, B. Djeumou, and S. Lasaulce. Resource allocation games in interference relay channels. In *Proc. GameNets*, pages 575–584, Istanbul, Turkey, 2009.

[100] R. Mochaourab and E. Jorswieck. Resource allocation in protected and shared bands: uniqueness and efficiency of Nash equilibria. In *Proc. GAMECOMM*, pages 1–10, Pisa, Italy, 2009.

[101] S. Haykin. Cognitive radio: brain-empowered wireless communications. *IEEE Journal on Selected Areas in Communications*, 23(2):201–220, 2005.

[102] J. Jia and Q. Zhang. A non-cooperative power control game for secondary spectrum sharing. In *Proc. IEEE ICC*, pages 5933–5938, 2007.

[103] R. Di Taranto, H. Yomo, and P. Popovski. Two players non-cooperative iterative power control for spectrum sharing. In *Proc. IEEE PIMRC*, pages 1–5, 2008.

[104] Y. Wu and D. H. K. Tsang. Distributed power allocation algorithm for spectrum sharing cognitive radio networks with QoS guarantee. In *Proc. IEEE INFOCOM*, pages 981–989, 2009.

[105] G. Hosseinabadi, M. H. Manshaei, and J.-P. Hubaux. Spectrum sharing games of infrastructure-based cognitive radio networks. *Technical Report LCA-REPORT-2008-027*, 2008.

[106] M. Fèlegyhàzi, M. Čagalj, and J.P. Hubaux. Efficient MAC in cognitive radio systems: a game-theoretic approach. *IEEE Transactions on Wireless Communications*, 8(4):1984–1995, 2009.

[107] I. Malanchini, S. Weber, and M. Cesana. Nash equilibria for spectrum sharing of two bands among two players. In *Proc. Allerton*, Monticello (IL), 2010.

[108] P. Scheinok. The distribution functions of random variables in arithmetic domains modulo a. *American Mathematical Monthly*, pages 128–134, 1965.

[109] B. A. Murtagh and M. A. Saunders. MINOS 5.5 user's guide. *Stanford University Systems Optimization Laboratory Technical Report SOL83-20R*, 1998.

[110] M. Haenggi and R.K. Ganti. *Interference in large wireless networks*. Now Publishers Inc, 2009.

[111] M. Haenggi. On distances in uniformly random networks. *IEEE Transactions on Information Theory*, 51(10):3584–3586, 2005.

Acronyms

Appendix A: Mathematical models for the WMNAG

Hereafter, we introduce the mathematical programming formulations to find the NE for the WMNAG. First, we focus on the simplified case of a WMN featuring devices geared with single radios and operating on a single channel under the cardinality-based cost function (Section A.1). Then, we derive the formulation for the most general case of airtime-based cost metric and generic WMN topologies featuring multiple radios and multiple frequency channels (Section A.2).

A.1 Single-channel, cardinality-based cost function

To represent the WMN topology we introduce the following parameters of the model:

$$s_{lj} = \begin{cases} 1 & \text{if node } l \text{ belongs to path } j \\ 0 & \text{otherwise} \end{cases}$$

$$a_{lm} = \begin{cases} 1 & \text{if node } l \text{ and node } m \text{ interfere} \\ 0 & \text{otherwise} \end{cases}$$

$$d_{ij} = \begin{cases} 1 & \text{if STA } i \text{ can choose path } j \\ 0 & \text{otherwise} \end{cases}$$

We further introduce in our model the following variables, in order to associate each STA to a specific access point (and then to a specific routing path):

$$y_{ij} = \begin{cases} 1 & \text{if STA } i \text{ chooses path } j \\ 0 & \text{otherwise} \end{cases}$$

The constraints of the model are the following:

$$\sum_{j \in P} y_{ij} = 1 \qquad \forall i \in U \tag{A.1}$$

$$y_{ij} \leq d_{ij} \qquad \forall i \in U, \forall j \in P \tag{A.2}$$

Constraints (A.1) ensure that each STA selects only one path (i.e., access point) whereas constraints (A.2) force each STA to select a path only among the set of the available ones.

We define the optimal solution as the one that minimizes the social cost, i.e., the sum of all the STAs' costs c_{ij}. To this extent, the following objective function is used:

$$\min \sum_{i \in U} \sum_{j \in P} c_{ij} y_{ij} \tag{A.3}$$

As defined before, the cost c_{ij} is composed by two terms:

$$c_{ij} = L_j + I_j^i \tag{A.4}$$

where

$$L_j = \sum_{l \in N} s_{lj} - 1 \tag{A.5}$$

$$I_j^i = \sum_{\substack{r \in U \\ r \neq i}} \sum_{u \in P} \sum_{l \in (N \setminus A)} \sum_{m \in (N \setminus G)} s_{lj} s_{mu} a_{lm} y_{ru} \tag{A.6}$$

Constraints (A.6) refer to the case of uplink traffic, only. Indeed, it considers the set $N \setminus A$ (access points never suffer interference because they never receive) and the set $N \setminus G$ (gateways never cause interference to other nodes because they never transmit). A similar constraint can be written for the downlink traffic, as well as for mixed downlink/uplink traffic patterns.

The objective function in Eq. (A.3) is not linear, however it can be easily linearized as follows:

$$\min \sum_{i \in U} (\sum_{j \in P} \sum_{l \in N} s_{lj} y_{ij} - 1 + I_i) \tag{A.7}$$

$$I_i \geq \sum_{\substack{r \in U \\ r \neq i}} \sum_{u \in P} \sum_{l \in (N \setminus A)} \sum_{m \in (N \setminus G)} s_{lj} s_{mu} a_{lm} y_{ru} + M(y_{ij} - 1) \quad \forall i \in U, \forall j \in P \quad \text{(A.8)}$$

where M is a big number such that whenever $y_{ij} = 0$, $l_i = 0$.

Note that I_i is the *path contention cost* of STA i for the path j she has actually chosen at the solution, i.e., when $y_{ij} = 1$.

The mixed integer linear formulation with objective function (A.7) and constraints defined in (A.1), (A.2), and (A.8) can be used to characterized the global optimal solution. The very same formulation can be also used to find the best Nash equilibria of the game, by adding the following constraints:

$$M(y_{ij} + d_{ih} - 2) + \sum_{l \in N} s_{lj} + \sum_{\substack{r \in U \\ r \neq i}} \sum_{u \in P} \sum_{l \in (N \setminus A)} \sum_{m \in (N \setminus G)} s_{lj} s_{mu} a_{lm} y_{ru} \leq$$

$$\sum_{l \in N} s_{lh} + \sum_{\substack{r \in U \\ r \neq i}} \sum_{u \in P} \sum_{l \in (N \setminus A)} \sum_{m \in (N \setminus G)} s_{lh} s_{mu} a_{lm} y_{ru}$$

$$\forall i \in U, \forall j, h \in P \quad h \neq j \quad \text{(A.9)}$$

that enforce the definition of Nash equilibrium. Indeed, constraints (A.9) requires each STA to select the path with the minimum association cost, given the other players strategies, i.e., paths.

Finally, to find the worst Nash equilibrium, we replace the objective function (A.7) and constraints (A.8) with the following maximization of the social cost:

$$\max \sum_{i \in U} \sum_{j \in P} \sum_{l \in N} s_{lj} y_{ij} - 1 + I_i \quad \text{(A.10)}$$

$$I_i \leq \sum_{\substack{r \in U \\ r \neq i}} \sum_{u \in P} \sum_{l \in (N \setminus A)} \sum_{m \in (N \setminus G)} s_{lj} s_{mu} a_{lm} y_{ru} + M(1 - y_{ij}) \quad \forall i \in U, \forall j \in P \quad \text{(A.11)}$$

A.2 Multi-channel, airtime-based cost function

In this section, we present the optimization model adopted to characterize the Nash equilibria and the optimal solution of the multi-channel airtime-based game. In order to derive the mathematical formulation, we assume that:

- the wireless links in the backbone share the same bearer and can further be tuned to different orthogonal channels in the set C;
- all the access points share the same channel for the access;
- the backbone and the access network do not interfere.

The parameters used in the model are:

$$s_{jlf} = \begin{cases} 1 & \text{if device } l \text{ is receiving on channel } f \text{ along path } j \\ 0 & \text{otherwise} \end{cases}$$

$$a_{lm} = \begin{cases} 1 & \text{if devices } l \text{ and } m \text{ interfere} \\ 0 & \text{otherwise} \end{cases}$$

$$d_{ij} = \begin{cases} 1 & \text{if user } i \text{ can choose path } j \\ 0 & \text{otherwise} \end{cases}$$

- Air_access_{ij} is the airtime (in μs) for user i and the access point j;
- Air_back_{jflk} is the airtime of the wireless link between device l and device k operating on channel f and belonging to path j;
- M is a big number used for linearizing the objective function.

The decision variables are:

$$y_{ij} = \begin{cases} 1 & \text{if user } i \text{ chooses path } j \\ 0 & \text{otherwise} \end{cases}$$

- I_i^{Ch} is the total path contention cost perceived by user i.

To derive the optimal solution, the following objective function is used:

$$\min \sum_{i \in U} \left(\sum_{j \in P} \left(\sum_{n \in N} \sum_{m \in N} \sum_{f \in C} Air\_back_{jfnm} + Air\_access_{ij} \right) y_{ij} + I_i^{Ch} \right) \tag{A.12}$$

The constraints of the model are the following:

$$I_i^{Ch} \geq \sum_{\substack{r \in U \\ r \neq i}} \sum_{u \in P} \left(\sum_{l \in (N \setminus AP)} \sum_{m \in (N \setminus GW)} \sum_{k \in N} \sum_{f \in C} s_{jlf} a_{lm} y_{ru} Air\_back_{ufmk} + \right.$$
$$\left. + Air\_access_{ru} d_{rj} y_{ru} \right) + M \left(y_{ij} - 1 \right) \quad \forall i \in U, \, \forall j \in P \tag{A.13}$$

$$I_i^{Ch} \geq 0 \qquad \forall i \in U \tag{A.14}$$

$$\sum_{j \in P} y_{ij} = 1 \quad \forall i \in U \tag{A.15}$$

$$y_{ij} \leq d_{ij} \quad \forall i \in U, \, \forall j \in P \tag{A.16}$$

To obtain the best Nash equilibrium the following equilibrium constraints should be added to (A.12), (A.13), (A.14), (A.15) and (A.16):

$$M\left(y_{ij}+d_{ih}-2\right)+\sum_{n\in N}\sum_{m\in N}\sum_{f\in C}Air\_back_{jfnm}+Air\_access_{ij}+$$
$$+\sum_{\substack{r\in U\\ r\neq i}}\sum_{u\in P}\left(\sum_{l\in(N\setminus AP)}\sum_{m\in(N\setminus GW)}\sum_{k\in N}\sum_{f\in C}s_{jlf}a_{lm}Air\_back_{ufmk}+Air\_access_{ru}d_{rj}y_{ru}\right)\leq$$
$$\sum_{n\in N}\sum_{m\in N}\sum_{f\in C}Air\_back_{hfnm}+Air\_access_{ih}+$$
$$+\sum_{\substack{r\in U\\ r\neq i}}\sum_{u\in P}\left(\sum_{l\in(N\setminus AP)}\sum_{m\in(N\setminus GW)}\sum_{k\in N}\sum_{f\in C}s_{hlf}a_{lm}Air\_back_{ufmk}+Air\_access_{ru}d_{rh}y_{ru}\right)$$
$$\forall i\in U,\ \forall j,h\in P:h\neq j \tag{A.17}$$

Finally, to calculate the worst Nash equilibrium Eq. (A.12) and (A.13) should be replaced respectively by the following two equations:

$$\max\sum_{i\in U}\left(\sum_{j\in P}\left(\sum_{n\in N}\sum_{m\in N}\sum_{f\in C}Air\_back_{jfnm}+Air\_access_{ij}\right)y_{ij}+I_i^{Ch}\right) \tag{A.18}$$

and

$$I_i^{Ch}\leq\sum_{\substack{r\in U\\ r\neq i}}\sum_{u\in P}\left(\sum_{l\in(N\setminus AP)}\sum_{m\in(N\setminus GW)}\sum_{k\in N}\sum_{f\in C}s_{jlf}a_{lm}y_{ru}Air\_back_{ufmk}+\right.$$
$$\left.+Air\_access_{ru}d_{rj}y_{ru}\right)+M\left(1-y_{ij}\right)\quad\forall i\in U,\ \forall j\in P \tag{A.19}$$

Appendix B: Proof of Equivalence to a Non-Weighted Single-Choice Crowding Game

In a crowding game, players choose resources and are charged of the corresponding costs. Each resource k is characterized by a congestion level x^k, defined as the number of players that choose it, the game being non-weighted. With player-specific cost functions, the cost charged to a player i that chooses resource i is $c_i(k, x^k)$. Given this definition, the formulation of a single-choice crowding game that captures our game model is non-trivial. Assumed the SOPs to be the resources in our model, the complications are due to the fact that different players that choose a SOP can perceive different congestion levels x_i^k. Consider a scenario with three secondary users A, B, C, as shown in Figure B.1a, and suppose the SOPs to be two. If all the users choose the same SOP k, $x_A^k = x_C^k = 2$ and $x_B^k = 3$. (Note that users A and C interfere only with B, whereas B interferes with both A and B. Furthermore, the congestion accounts also for the user itself, as usual in congestion game.) Anyway, our game model can be formulated as a network crowding game and, by a mathematical trick, we reduce it to a single-choice game. In this class of games, players choose paths that connect their source to their destination. The edges of the network are the resources and the players' costs are the sum of the costs of the chosen resources. A network congestion game is generally a multiple-choice congestion game, the nodes where the players can choose being multiple. We use linear player-specific cost functions of the form $c_i(k, x^k) = a_{i,k}x^k$ where $a_{i,k}$ is a player-specific parameter. In our specific case, by opportunistically setting the parameters $a_{i,k}$s, we can produce a network congestion game that captures our game model with the property that each player makes essentially one choice. With "essentially" we mean that a player have multiple nodes wherein it can choose the next edge, but in all nodes but one there is a dominant choice independently of the other players. We report in Figure B.1b the network congestion game capturing the situation depicted in Figure B.1a. Recall that the aim of this is to construct an equivalent game that produces the same costs of the original game. The paths corresponding to each SOP are highlighted by dashed boxes. The triples over the edges denote the player-specific parameters as $(a_{A,k}, a_{B,k}, a_{C,k})$. In this case, the unique node without a dominant choice is the source. Consider player B: if it chooses the lower edge (SOP 2) in the source, then it will follow the path wherein $a_{B,2} = 0$. The same holds for player A

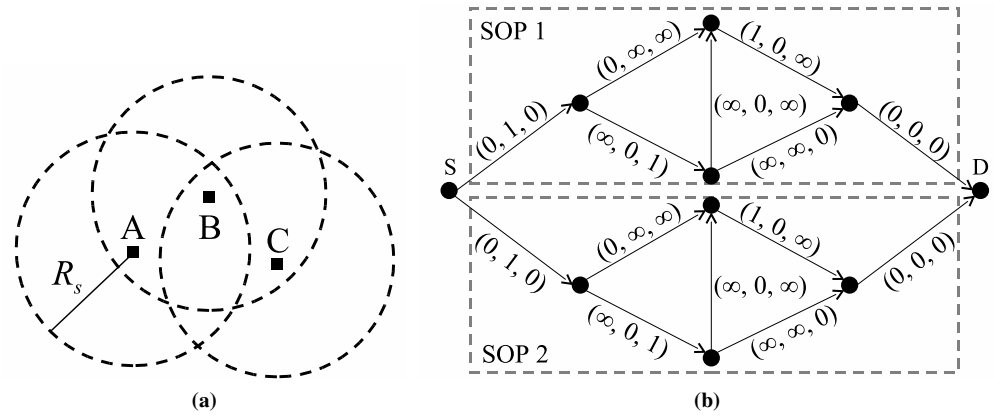

Figure B.1: (a) A topology with three secondary users. (b) Network congestion game representing the topology (a) with two SOPs ('S' denotes the source and 'D' the destination).

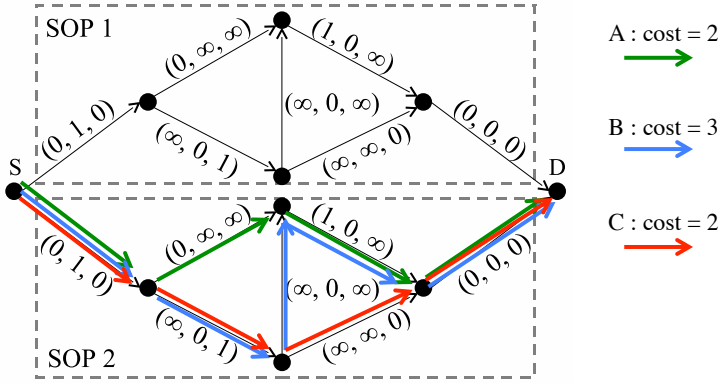

Figure B.2: Equivalent game and choices when users select SOP 2.

and C. Figure B.2 reports the case in which all users select the same SOP and the costs are the expected ones. In general, given a players' strategy profile, it can be easily shown that the costs in the game depicted in Figure B.1b are the same of the game stated in Section 5.2. Therefore, our game is essentially a non-weighted single-choice crowding game.

Appendix C: Mathematical Programming Formulation for Repeated Games

We provide here a general mathematical programming formulation that we use to find best and worst Nash equilibria and the optimal solution in our congestion games. The following model can be used (and linearized) for each one of the cost function presented in Section 5.2.3 and for the dynamic game described in Section 5.3.1. The switching cost K can be set to zero for solving the one shot game.

The parameters of the model are:

$$z_{ik} = \begin{cases} 1 & \text{if SU } i \text{ has chosen SOP } k \text{ in the previous epoch} \\ 0 & \text{otherwise} \end{cases}$$

We define the association of a user to a SOP by introducing a binary decision variable:

$$y_{ik} = \begin{cases} 1 & \text{if SU } i \text{ chooses SOP } k \\ 0 & \text{otherwise} \end{cases}$$

Finally, the constraints of the problem are:

$$\sum_{k \in B_i} y_{ik} = 1 \qquad \forall\, i \in N \tag{C.1}$$

$$y_{im}\left(c_i(m, x_i^m) + K(1 - z_{im})\right) \leq \left(c_i(k, x_i^k) + K(1 - z_{ik})\right) \qquad \forall\, i \in N, m, k \neq m \in B_i \tag{C.2}$$

Constraints (C.1) guarantee the feasibility of the assignment. Constraints (C.2) force each user to choose the strategy (SOP) which leads to the minimum cost function, that is, they ensure that, if the single user unilaterally changes her strategy, the change does not improve her own payoff (i.e. definition of Nash equi-

librium).

This formulation allows one to find equilibria that maximize/minimize the social cost. They can be found by introducing the following objective function in the formulation:

$$\min / \max \sum_{i \in N} \sum_{m \in B_i} y_{im} \left(c_i(m, x_i^m) + K(1 - z_{im}) \right) \tag{C.3}$$

Moreover, to evaluate Price–of–Stability (PoS) and Price–of–Anarchy (PoA), it is necessary to provide a model that allows one to find the optimal solution, i.e. the solution that minimizes the social cost but that could not be an equilibrium. To do this, we inhibit equilibrium constraints (C.2) and solve the model minimizing the objective function (C.3).

Appendix D: Proof of the Symmetric Optimal Solution

Hereafter, we report the proof for the optimal solution in the symmetric case. The proof is due to Jiangyuan Li[1].

We recall that the objective function is:

$$U_T(P_1,P_2)=\log\left(1+\frac{P_1D}{1+P_2X}\right)+\log\left(1+\frac{(1-P_1)D}{1+(1-P_2)X}\right)+\log\left(1+\frac{P_2D}{1+P_1X}\right)+\log\left(1+\frac{(1-P_2)D}{1+(1-P_1)X}\right) \quad \text{(D.1)}$$

Some objective values at special points are:

$$U_T(0,0)=2\log\left(1+\frac{D}{1+X}\right)$$

$$U_T(1,0)=U_T(0,1)=2\log\left(1+D\right),$$

$$U_T(0.5,0.5)=4\log\left(1+\frac{D}{2+X}\right)$$

We divide the proof in three different cases. Namely, we first consider the case in which the function is exactly along the threshold $X=\sqrt{1+D}-1$, then we consider the case in which the function is above/below this threshold.

Theorem D.1. *If $X=\sqrt{1+D}-1$, then all the maxima of the function $U_T(P_1,P_2)$ reported in Eq. (D.1) are $\{(P_1,P_2):P_1+P_2=1\}$.*

Proof. It holds that $D=X^2+2X$ and $U_T(0.5,0.5)=U_T(1,0)=U_T(0,1)=4\log(1+X)$. We can write

[1]Jiangyuan Li is a research post-doc associate in the Department of ECE at Drexel University, email: eejyli@yahoo.com.cn.

the following:

$$e^{U_T(P_1,P_2)} - e^{U_T(0.5,0.5)} = \frac{X^2(P_1+P_2-1)^2(2+X)(B_1X^4+B_2X^3+B_3X^2-6X-2)}{(1+P_2X)(1+(1-P_2)X)(1+P_1X)(1+(1-P_1)X)} \quad \text{(D.2)}$$

where $B_1 = 2P_1P_2 - P_1 - P_2$, $B_2 = P_1^2 + P_2^2 + 6P_1P_2 - 4P_1 - 4P_2 - 1$ and $B_3 = 2P_1^2 + 2P_2^2 + 6P_1P_2 - 5P_1 - 5P_2 - 4$. Since $0 \leq P_1, P_2 \leq 1$, it holds that $P_1^2 \leq P_1$ and $P_2^2 \leq P_2$. Thus, $2P_1P_2 \leq P_1^2 + P_2^2 \leq P_1 + P_2$. Then, it holds that $B_1 \leq 0$, $B_2 \leq -1$ and $B_3 \leq -4$. Finally, it follows that, if $P_1 + P_2 \neq 1$, $U_T(P_1, P_2) < U_T(0.5, 0.5)$.

On the other hand, if $P_1 + P_2 = 1$, $U_T(P_1, P_2)$ is a constant, which follows from

$$U_T(P_1, 1-P_1) = 2\log\left(1 + \frac{P_1D}{1+(1-P_1)X}\right) + 2\log\left(1 + \frac{(1-P_1)D}{1+P_1X}\right) = 2\log(1+D) \quad \text{(D.3)}$$

Therefore, all solutions are (P_1, P_2) with $P_1 + P_2 = 1$. □

Theorem D.2. *If $X > \sqrt{1+D} - 1$, then all the maxima of the function $U_T(P_1, P_2)$ reported in Eq. (D.1) are $(1, 0)$ and $(0, 1)$.*

Proof. It holds that $D < X^2 + 2X$.

First, we show that $U_T(P_1, P_2) < U_T(1, 0)$ for $P_1 + P_2 \neq 1$. Let $a = P_1/(1+P_2X)$, $b = (1-P_1)/(1+(1-P_2)X)$, $c = P_2/(1+P_1X)$ and $d = (1-P_2)/(1+(1-P_1)X)$. We need to show that for any D with $0 < D < X^2 + 2X$, it holds that:

$$\log(1+aD) + \log(1+bD) + \log(1+cD) + \log(1+dD) < 2\log(1+D) \quad \text{(D.4)}$$

which is equivalent to $g(D)D < 0$ where

$$g(D) = abcdD^3 + (abc + abd + acd + bcd)D^2 + \\ + (ab + ac + ad + bc + bd + cd - 1)D + (a + b + c + d - 2) \quad \text{(D.5)}$$

Therefore, we want to show that $g(D) < 0$ for $0 < D < X^2 + 2X$. Note that:

$$g''(D) = 6abcdD + 2(abc + abd + acd + bcd) > 0$$

This means that $g(D)$ is a strictly convex function. Therefore, it is sufficient to show that $g(0) \leq 0$ and $g(X^2 + 2X) \leq 0$ (see Figure D.1).

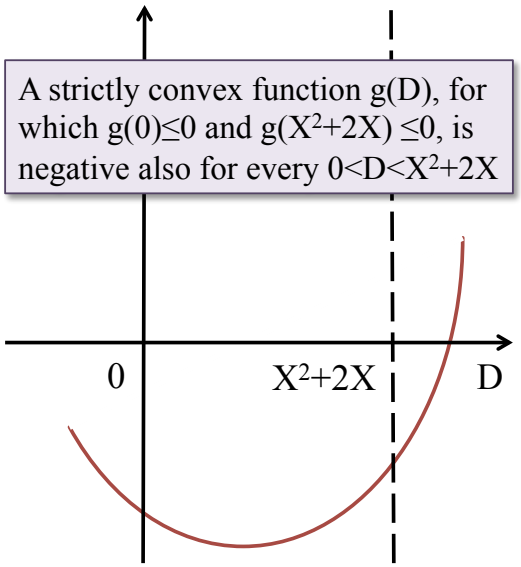

Figure D.1: Strictly convex function.

Since $a + b + c + d \leq P_1 + (1 - P_1) + P_2 + (1 - P_2) = 2$, it holds that $g(0) = a + b + c + d - 2 \leq 0$. Moreover, $g(X^2 + 2X) \leq 0$ is equivalent to

$$U_T(P_1, P_2; X = \sqrt{1 + D} - 1) \leq U_T(1, 0). \quad \text{(D.6)}$$

This has been shown in Theorem. D.1. This proves the first part.

Now, we consider the case for which $P_1 + P_2 = 1$ and we show that the optimal solution is for $P_1 = 0$ or $P_1 = 1$. This is equivalent to show that if $0 < P_1 < 1$, then $U_T(P_1, 1 - P_1) < U_T(1, 0)$. To this end, we write

$$U_T(P_1, 1-P_1) = 2\log\left(1 + \frac{P_1 D}{1 + (1-P_1)X}\right) + \\ + 2\log\left(1 + \frac{(1-P_1)D}{1 + P_1 X}\right) \quad \text{(D.7)}$$

Therefore

$$U_T(P_1, 1-P_1) - U_T(1,0) = \\ = \left(1 + \frac{P_1 D}{1 + (1-P_1)X}\right)\left(1 + \frac{(1-P_1)D}{1 + P_1 X}\right) - (1+D) = \\ = \frac{D P_1 (1-P_1)(D - X^2 - 2X)}{(1 + P_1 X)(1 + (1-P_1)X)} < 0. \quad \text{(D.8)}$$

That proves the desired result. □

Theorem D.3. *If $X < \sqrt{1+D} - 1$, then $(0.5, 0.5)$ is the unique maximum of the function $U_T(P_1, P_2)$ reported in Eq. (D.1).*

Proof. It holds that $D > X^2 + 2X$.

We want to show that $U_T(P_1, P_2) < U_T(0.5, 0.5)$ for $(P_1, P_2) \neq (0.5, 0.5)$. Let $a = P_1/(1 + P_2 X)$, $b = (1 - P_1)/(1 + (1 - P_2)X)$, $c = P_2/(1 + P_1 X)$, $d = (1 - P_2)/(1 + (1 - P_1)X)$ and $h = 1/(2 + X)$. We need to show that for any D with $D > X^2 + 2X$, it holds that

$$\log(1 + aD) + \log(1 + bD) + \log(1 + cD) + \log(1 + dD) < 4\log(1 + hD)$$

which is equivalent to $F(D)D < 0$ where

$$F(D) = (abcd - h^4)D^3 + (abc + abd + acd + bcd - 4h^3)D^2 + \\ + (ab + ac + ad + bc + bd + cd - 6h^2)D + (a + b + c + d - 4h) \quad \text{(D.9)}$$

We need to show that $F(D) < 0$ for $D > X^2 + 2X$, that is equivalent to show that $F(X^2 + 2X) \leq 0$ and $F'(D) < 0$ for $D \geq X^2 + 2X$ (see Figure D.2).

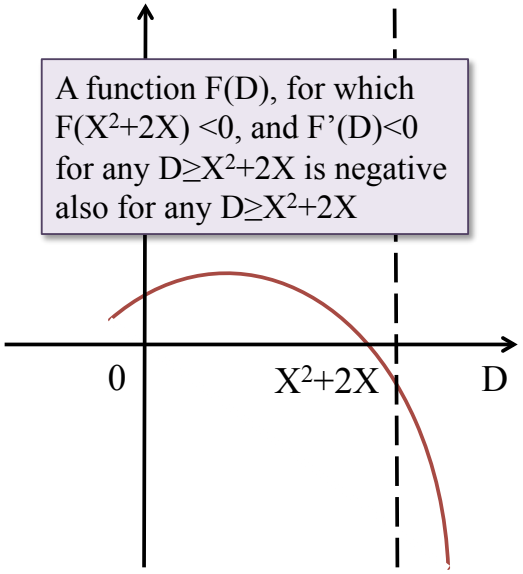

Figure D.2: Concave quadratic function.

The first part, $F(X^2 + 2X) \leq 0$, is equivalent to

$$U_T(P_1, P_2; X = \sqrt{1 + D} - 1) \leq U_T(0.5, 0.5). \quad \text{(D.10)}$$

This has been shown in Theorem. D.1.

Therefore, we want to show that $F'(D) < 0$ for $D \geq X^2 + 2X$. Note that

$$F'(D) = 3(abcd - h^4)D^2 + 2(abc + abd + acd + bcd - 4h^3)D + \\ + (ab + ac + ad + bc + bd + cd - 6h^2) \quad \text{(D.11)}$$

We first show that $abcd - h^4 < 0$. Note that:

$$abcd - h^4 = \\ = \frac{(1+X)(C_1X^2 + C_2X + C_2)}{(1+P_2X)(1+(1-P_2)X)(1+P_1X)(1+(1-P_1)X)(2+X)^4} \quad \text{(D.12)}$$

where $C_1 = (1/2)u^2(u^2-1) + (1/2)v^2(v^2-1) - u^2v^2$, $C_2 = u^2(u^2-2) + v^2(v^2-2) - 2u^2v^2$, $u = P_1 + P_2 - 1$ and $v = P_1 - P_2$. Since $-1 \leq u \leq 1$ and $-1 \leq v \leq 1$, it holds that $C_1 \leq 0$ and $C_2 \leq 0$. Thus, $C_1X^2 + C_2X + C_2 \leq 0$, but equality holds if and only if $u = v = 0$ (i.e., $P_1 = P_2 = 1/2$). Since $(P_1, P_2) \neq (0.5, 0.5)$, it holds that $C_1X^2 + C_2X + C_2 < 0$. Therefore, it follows that $abcd - h^4 < 0$.

Then, we show that $F'(X^2 + 2X) < 0$. Note that:

$$F'(X^2+2X) = \\ = \frac{A_1X^5 + A_2X^4 + A_3X^3 + A_4X^2 + A_5X + A_6}{(1+P_2X)(1+(1-P_2)X)(1+P_1X)(1+(1-P_1)X)(2+X)^2} \quad \text{(D.13)}$$

where $A_1 = (1/2)v^2(v^2-1) - 2u^2v^2 + (3/2)u^2(u^2-1)$, $A_2 = (3/2)v^2(v^2-7/3) - 8u^2v^2 + (15/2)u^2(u^2-7/5)$, $A_3 = (27/2)u^2(u^2-55/27) - 11u^2v^2 + (3/2)v^2(v^2-19/3)$, $A_4 = (17/2)u^2(u^2-65/17) - 5u^2v^2 + (1/2)v^2(v^2-25)$, $A_5 = -16u^2 - 8v^2$, $A_6 = -2u^2 - 2v^2$, $u = P_1 + P_2 - 1$ and $v = P_1 - P_2$. Since $-1 \leq u \leq 1$ and $-1 \leq v \leq 1$, it holds that $A_i \leq 0$, $i = 1, 2, 3, 4, 5, 6$. Thus, it holds that $F'(X^2+2X) \leq 0$, but equality holds if and only if $u = v = 0$ (i.e., $P_1 = P_2 = 0.5$). Since $(P_1, P_2) \neq (0.5, 0.5)$, it holds that $F'(X^2+2X) < 0$.

Finally, we show that $F'(D) < 0$ for $D > X^2+2X$. Since $abcd - h^4 < 0$, $F'(D)$ is an concave quadratic function of D. We analyze two cases:

1. $ab + ac + ad + bc + bd + cd - 6h^2 > 0$

   The equation $F'(D) = 0$ has a positive root and a negative root. Therefore, we are dealing with a concave quadratic function with a positive and a negative root. Since $F'(X^2+2X) < 0$, it holds that $F'(D) < 0$ for $D > X^2 + 2X$.

2. $ab + ac + ad + bc + bd + cd - 6h^2 \leq 0$

We first show that $abc + abd + acd + bcd - 4h^3 \leq 0$. It suffices to show that

$$3(abc + abd + acd + bcd) - 2h(ab + ac + ad + bc + bd + cd) \leq 0$$

To this end, we write

$$3(abc + abd + acd + bcd) - 2h(ab + ac + ad + bc + bd + cd) = \\ = \frac{-(r_1 X^2 + r_2 X + r_3)}{(2 + X)(1 + P_2 X)(1 + (1 - P_2)X)(1 + P_1 X)(1 + (1 - P_1)X)} \quad \text{(D.14)}$$

where $r_1 = (1/2)v^2(1 + u^2 + 3v^2)$, $r_2 = (3/2)u^2(1 - u^2) + (5/2)v^2 + (3/2)v^4$, $r_3 = 2u^2 + 2v^2$, $u = P_1 + P_2 - 1$ and $v = P_1 - P_2$. Since $-1 \leq u \leq 1$ and $-1 \leq v \leq 1$, it holds that $r_i \geq 0$, $i = 1, 2, 3$. From this it follows that $abc + abd + acd + bcd - 4h^3 \leq 0$. Thus, the equation $F'(D) = 0$ has two non-positive roots. Therefore, $F'(D) < 0$ for $D > X^2 + 2X$.

This completes the proof. □

Appendix E: Proof of the conditional pdf of the product ty

To characterize the conditional distribution of the product ty, we proceed as follows. First we can write that:

$$F_{\mathsf{ty}|\mathsf{x}_1}(\tau|x_1) = \int F_{\mathsf{y}|\mathsf{x}_1,\mathsf{t}}\left(\frac{\tau}{t}\middle| x_1, t\right) f_{\mathsf{t}|\mathsf{x}_1}(t|x_1)dt = \int F_{\mathsf{y}|x_1}\left(\frac{\tau}{t}\middle| x_1\right) f_{\mathsf{t}|\mathsf{x}_1}(t|x_1)dt$$

observing that, given x_1, y is independent on t, as proved in Lemma 7.3.14.

Substituting the expression of $F_{\mathsf{y}|\mathsf{x}_1}$ and $f_{\mathsf{t}|\mathsf{x}_1}$, derived in Lemma 7.3.16, we obtain the following integral:

$$F_{\mathsf{ty}|\mathsf{x}_1}(\tau|x_1) = \int \left(\frac{1}{2} + \frac{\sin^{-1}\frac{(\tau/t)^2-k_2}{k_1}}{\pi}\right) \frac{2t}{k_1\pi\sqrt{1-\left(\frac{t^2-k_2}{k_1}\right)^2}}dt$$

The limits of the integral are not straightforward. In order to define the limits and numerically evaluate the integral, consider Figure E.1. We can observe, that, whenever $\tau < |x_1 - d|(x_1 + d)$, t lies in the range

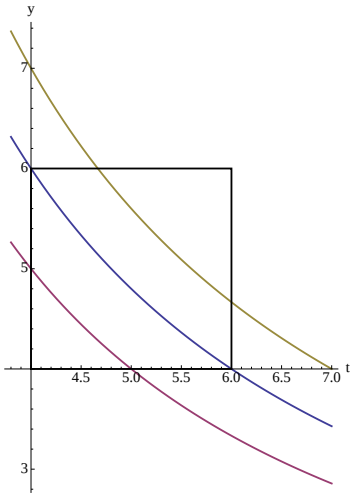

Figure E.1: Limits of the integration when $x_1 = 5$ and $d = 1$.

$\left[|x_1 - d|, \frac{\tau}{|x_1-d|}\right]$, and the cdf $F_{\mathsf{ty}|\mathsf{x}_1}(\tau|x_1)$ is given by:

$$F_{\mathsf{ty}|\mathsf{x}_1}(\tau|x_1) = \int_{|x_1-d|}^{\tau/|x_1-d|} F_{\mathsf{y}|x_1}\left(\frac{\tau}{t}\middle| x_1\right) f_{\mathsf{t}|\mathsf{x}_1}(t|x_1)dt$$

In contrast, when $\tau > (x_1 - d)(x_1 + d)$, t lies in the range $\left[\frac{\tau}{(x_1+d)}, (x_1 + d)\right]$. In this case, it is better to calculate the complementary function:

$$1 - F_{\mathsf{ty}|\mathsf{x}_1}(\tau|x_1) = \int_{\tau/(x_1+d)}^{(x_1+d)} \left(1 - F_{\mathsf{y}|x_1}\left(\frac{\tau}{t}\middle| x_1\right)\right) f_{\mathsf{t}|\mathsf{x}_1}(t|x_1)dt$$

Summarizing, we have:

$$F_{\mathsf{ty}|\mathsf{x}_1}(\tau|x_1) = \begin{cases} \int_{|x_1-d|}^{\tau/|x_1-d|} F_{\mathsf{y}|x_1}\left(\frac{\tau}{t}\middle| x_1\right) f_{\mathsf{t}|\mathsf{x}_1}(t|x_1)dt & \text{if } \tau \leq |x_1 - d|(x_1 + d) \\ 1 - \int_{\tau/(x_1+d)}^{(x_1+d)} \left(1 - F_{\mathsf{y}|x_1}\left(\frac{\tau}{t}\middle| x_1\right)\right) f_{\mathsf{t}|\mathsf{x}_1}(t|x_1)dt & \text{if } \tau \geq (x_1 - d)(x_1 + d) \end{cases}$$

We now want to characterize the conditional pdf. Therefore, we evaluate the derivative with respect to τ. When $\tau \leq |x_1 - d|(x_1 + d)$ we have that:

$$f_{\mathsf{ty}|\mathsf{x}_1}(\tau|x_1) = \frac{\partial F_{\mathsf{ty}|\mathsf{x}_1}(\tau|x_1)}{\partial \tau} = \frac{\partial}{\partial \tau} \int_{|x_1-d|}^{\tau/|x_1-d|} \left(\frac{1}{2} + \frac{\sin^{-1}\frac{(\tau/t)^2-k_2}{k_1}}{\pi}\right) \frac{2t}{k_1\pi\sqrt{1 - \left(\frac{t^2-k_2}{k_1}\right)^2}} dt$$

According to the Leibniz's rule for differentiation under the integral sign, it holds that:

$$\frac{\partial}{\partial \tau} \int_{a(\tau)}^{b(\tau)} f(t, \tau)dt = \frac{\partial b(\tau)}{\partial \tau} f(b(\tau), \tau) - \frac{\partial a(\tau)}{\partial \tau} f(a(\tau), \tau) + \int_{a(\tau)}^{b(\tau)} \frac{\partial}{\partial \tau} f(t, \tau)dt$$

where

$$f(t, \tau) = \left[\left(\frac{1}{2} + \frac{\sin^{-1}\frac{(\tau/t)^2-k_2}{k_1}}{\pi}\right) \frac{2t}{k_1\pi\sqrt{1 - \left(\frac{t^2-k_2}{k_1}\right)^2}}\right]$$

Let us first consider the last term:

$$\int \frac{\partial}{\partial \tau} f(t, \tau)dt = \int \frac{\partial}{\partial \tau} \left[\left(\frac{1}{2} + \frac{\sin^{-1}\frac{(\tau/t)^2-k_2}{k_1}}{\pi}\right) \frac{2t}{k_1\pi\sqrt{1 - \left(\frac{t^2-k_2}{k_1}\right)^2}}\right] dt =$$

$$= \int \frac{4\tau}{k_1^2\pi^2 t} \frac{1}{\sqrt{1-\left(\frac{(\tau/t)^2-k_2}{k_1}\right)^2}\sqrt{1-\left(\frac{t^2-k_2}{k_1}\right)^2}} dt$$

Note that this hold for every τ. For the sake of readability, we then define:

$$I(t,\tau) = \int \frac{4\tau}{k_1^2\pi^2 t} \frac{1}{\sqrt{1-\left(\frac{(\tau/t)^2-k_2}{k_1}\right)^2}\sqrt{1-\left(\frac{t^2-k_2}{k_1}\right)^2}} dt =$$

$$= \frac{4(k_1+k_2-t^2)(k_1-k_2+t^2)\tau\sqrt{\frac{k_1(-(k_1+k_2)t^2+\tau^2)}{(k_1+k_2-t^2)(k_1^2-k_2^2+\tau^2)}}\sqrt{-\frac{k_1((k_1-k_2)t^2+\tau^2)}{(k_1+k_2-t^2)((k_1-k_2)^2-\tau^2)}}}{k_1^3\pi^2t^2\sqrt{1-\left(\frac{(k_2-t^2)}{k_1}\right)^2}\sqrt{\frac{(k_1-k_2+t^2)(k_1^2+2k_1k_2+k_2^2-\tau^2)}{(k_1+k_2-t^2)(k_1^2-k_2^2+\tau^2)}}\sqrt{1-\left(\frac{k_2-(\frac{\tau}{t})^2}{k_1}\right)^2}} \cdot$$
$$\cdot \Phi\left[\sin^{-1}\left(\sqrt{\frac{(k_1-k_2+t^2)(k_1^2+2k_1k_2+k_2^2-\tau^2)}{(k_1+k_2-t^2)(k_1^2-k_2^2+\tau^2)}}\right), \frac{(k_1^2-k_2^2+\tau^2)^2}{k_1^4+(k_2^2-\tau^2)^2-2k_1^2(k_2^2+\tau^2)}\right]$$

where $\Phi[\phi, k^2]$ denotes the (incomplete) elliptic integral of the first kind, $F(\phi, k)$, that is defined as:

$$F(\phi,k) = \int_0^\phi \frac{d\theta}{\sqrt{1-k^2\sin^2\theta}}$$

Finally, we obtain:

$$f_{\mathsf{ty}|\mathsf{x}_1}(\tau|x_1) = \begin{cases} \frac{f(\tau/|x_1-d|,\tau)}{|x_1-d|} + 0 + \Big[I(t,\tau) \Big]_{|x_1-d|}^{\tau/|x_1-d|} & \text{if } \tau \leq |x_1-d|(x_1+d) \\ 0 + \frac{f(\tau/(x_1+d),\tau)}{(x_1+d)} + \Big[I(t,\tau) \Big]_{\tau/(x_1+d)}^{(x_1+d)} & \text{if } \tau \geq |x_1-d|(x_1+d) \end{cases}$$

Vita

Ilaria Malanchini was born in Chiari (BS), Italy, on April 6, 1983.

She received her BS and MS in Telecommunications Engineering from Politecnico di Milano (Italy) in 2005 and 2007, respectively. In January 2008, she started her Ph.D. program in Information Technology with Prof. Matteo Cesana within the ANTLab (Politecnico di Milano). At the beginning of 2010, she joined the Drexel Network Modeling Laboratory under the supervision of Dr. Steven Weber (ECE Department). In December 2011, she received her PhD in Electrical Engineering from Drexel University (Philadelphia, US). She completed her dual PhD program in March 2012, when she also received the degree from Politecnico di Milano.

In 2008, she was awarded the Meucci-Marconi Award for her MS thesis, advisor Prof. Matteo Cesana.

Her research interests focus on optimization models, mathematical programming, game theory, traffic theory and stochastic geometry, together with the application of these mathematical techniques to wireless network problems, such as network selection, resource allocation and spectrum sharing.